CARBON GEOLOGICAL SEQUESTRATION IN SALINE AQUIFERS: EFFECT OF ROCK MINEROLOGY ON WETTABILITY CHANGE TREND AND IMPLICATION FOR EFFICIENT STORAGE IN DIFFERENT AQUIFERS

by

Mumuni Amadu

Submitted in partial fulfilment of the requirements
for the degree of Doctor of Philosophy

at

Dalhousie University
Halifax, Nova Scotia
June 2016

DEDICATION

My late father, Imam Amadu Zegane, once told me that if he had the opportunity to have formal education like me, he would have counted himself among the most privileged because schools were scarce when he was young. For not getting this opportunity, he decided to send me to school to accomplish what he would have liked to do. In this regard, I deem it most appropriate to dedicate this thesis work to his scared memory. May his soul rest in perfect peace. Amen. Also, for the immense part played by my mother Adesah, Amadu, in encouraging me to have formal education particularly when I was young, this thesis is also dedicated to her. May Allah give her long life. Amen

TABLE OF CONTENTS

LIST OF TABLES

LIST OF FIGURES

ABSTRACT

In view of the accelerated increase in anthropogenic carbon dioxide in the atmosphere and the resulting climate warming, the capture and storage of this greenhouse gas in geologic media is considered a technically viable option. Consequently, the injection of carbon dioxide into a saline aquifer initially containing formation brine will lead to two-phase flow. In this regard, the wettability of the system that controls the relative mobility of fluid phases is a fundamental petrophysical parameter that deserves attention. Generally, the wettability is controlled by water-rock interaction phenomena which consists of cation exchange and surface adsorption of ions.

So far, the wettability of the system carbon dioxide-solid-brine has been studied in a manner where substrates do not reflect those of actual geologic systems that are hosts for carbon storage. Consequently, contact angles measured so far give conclusive evidence that wettability will decrease with gas injection but they do not give any clue as to the manner in which this will decrease. This is because contact angles are measured on individual minerals of rocks rather than on rock samples.

In this study, I have used two mineralogically distinct rock samples to show how contact angles will evolve given the water-rock interaction phenomena that control wettability. The two rocks are Wallace sandstone from Nova Scotia and Fontainebleau sandstone from France. The experimental methodology is based on spontaneous imbibition rise of brine of varying pH in core samples. Contact angle computations are carried out using early spontaneous imbibition dynamics theory. In addition, cation exchange reactions pertinent to the geologic system which are principal causes of formation water pH buffering, have been investigated using pulverized rock samples. Furthermore, X-Ray diffraction analysis of rock samples to support experimental results have been carried out. Results of these experiments give further conclusive evidence that cation exchange reactions can buffer formation water pH to impact expected trends in wettability evolution.

In view of the point of zero charge pH of the solid surface being fundamental to the water-rock interaction, a mathematical model has been presented that links wettability to the pH of aqueous solution.

LIST OF ABBREVIATIONS AND SYMBOLS USED

a = activity	[mol/dm^3]
A= parameter in the Leverett J function	[-]
B= parameter in the Leverett J function	[-]
C_i = concentration of species i	[mol/dm^3]
$\boldsymbol{C}$ = coulomb	[C]
D = retardation	[-]
e = electronic charge-coulomb	[C]
F = Faraday's constant	[C/mol]
F_i = fractional flow of species i	[-]
F_w = out of balance surface tension force	[N/m]
$\boldsymbol{g}$ = acceleration due to gravity	[m/s^2]
h_e = equilibrium capillary rise	[m]
I = ionic strength-mol/l	[mol/dm^3]
$J(S_w)$ = dimensionless capillary pressure function	[-]
$K^o_{H_2O}$ = Henry's law constant for water at a reference pressure	[bar mol^{-1} kg H_2O]
$K^o_{CO_2}$ = Henry's law constant for carbon dioxide at a reference pressure	[bar mol^{-1} kg CO_2]
K^+= frequency of forward wetting	[s^{-1}]
K^-= frequency of backward wetting	[s^{-1}]
K_1 = equilibrium constant for reaction 2	[mol/dm^3]
K_2 = equilibrium constant for reaction 1	[mol/dm^3]

k_B = Boltzmann's constant [J/K]

k_{rw} = relative permeability of water [fraction]

k_{rg} = relative permeability of gas [fraction]

m_i = molarity of species i [mol/dm^3]

n = number density of ions in solution [mol/m^3]

P_b = breakthrough capillary pressure [Pa]

P_c = capillary pressure [Pa]

P_{ref} = Reference pressure [bar]

P_{dc} = drainage capillary pressure [Pa]

q_t = total injection rate [m^3]

r = radius [m]

R = universal gas constant [J/mol K]

S_D = saturation of displacing phase-fraction [fraction]

S_{iw} = Irreducible water saturation-fraction [fraction]

S_w = water saturation-fraction [fraction]

t = time [s]

T = temperature [K]

$\overline{V}_{H_2O}$ = partial molar volume of water [cm^3/mol]

$\overline{V}_{CO_2}$ = partial molar volume of carbon dioxide [cm^3/mol]

$V_{H_2O}^{aq}$ = average partial molar volume of water [cm^3/mol]

x_{CO_2} = mole fraction of carbon dioxide in the aqueous phase	[fraction]
y_{H_2O} = mole fraction of carbon dioxide in the aqueous phase	[fraction]
$z^{//}$ = Acceleration	[m/s^2]
$z^{/}$ =Time derivative of distance	[m/s]
x = spontaneous imbibition rise	[m]
Greek letter meaning	**Unit**
ϕ = porosity	[fraction]
Θ = contact angle	[°]
γ^- = negative surface site	[C]
γ^+ = positive surface site	[C]
ρ = density	[kg/m^3]
μ = dynamic viscosity	[Pa·s]
μ_w = dynamic viscosity of water	[Pa·s]
μ_g = dynamic viscosity of gas	[Pa·s]
γ_{LV} = liquid-vapor interfacial tension	[N/m]
γ_{SV} = solid- vapor interfacial tension	[N/m]
γ_{SL} = solid- liquid interfacial tension	[N/m]
ρ = density	[kg/m^3]
γ_{s-br} = interfacial tension between solid and brine	[N/m]
γ_{s-vap} = interfacial tension between solid and vapor phase	[N/m]

γ_{br-vap} = interfacial tension between brine and vapor phase [N/m]

λ = pore size distribution index [-]

C_1, C_2 = fitting parameters in Leveret J function [-]

σ = surface charge density [C/m^2]

$\Phi_{H_2O}^{aq}$ = fugacity of water [Pa]

$\Phi_{co_2}^{aq}$ = fugacity of carbon dioxide- [Pa]

Θ_{Nacl} = osmotic coefficient of sodium chloride [-]

γ_{ij} = interfacial tension between phase I and phase [N/m]

ε_r = relative permittivity [-]

ε = permittivity of a medium [F/m]

ε_o = permittivity of free space [F/m]

κ = Reciprocal of the Deby length [m^{-1}]

κ_{net} = net frequency of wetting [s^{-1}]

κ_w^o = equilibrium frequency of wetting [s^{-1}]

ψ_o = surface potential [V]

ψ_s = potential of the surface layer [V]

ψ_d = potential of the diffuse layer [V]

θ = contact angle-degrees [°]

σ = surface charge density [C/m^2]

Γ = surface density of species [mol/m^2]

v = is the velocity of wetting [m/s]

ΔG = free energy change of spontaneous imbibition [J/m^2]

$\equiv SiOH$ = surface silanol

$\equiv SiO^-$ = deprotonated surface silanol on silica

$\equiv SiOH_2^+$ = protonated surface hydroxyl group (silanol) found on silica surface

$\left[\equiv SiOH_2^+\right]$ = concentration of surface protonated silinol group [mol/dm^2]

$\left[\equiv SiO^-\right]$ = concentration of deprotonated surface silanol group [mol/dm^3]

ψ_{PZC} = surface potential at the point of zero charge pH [V]

pH_{PZC} = point of zero charge p

ACKNOWLEDGEMENTS

In writing this doctoral dissertation, I sincerely acknowledge the fact that, despite my own ambitions and talents, its final completion would not have been possible without the immeasurable contributions from other individuals. In this regard, I deem it a responsibility rather than a wish to express my most heartfelt gratitude to the following people:

To Dr. Michael J. Pegg who is my principal supervisor, I greatly appreciate his immense financial contributions and academic guidance in this research work. I equally appreciate the enormous contributions and guidance of his co-supervisors, namely Dr. Robert Jamieson of the Department of Process Engineering and Applied Science and Dr. Craig Lake of the Department of Civil and Resource Engineering.

To Dr. Zoheir Farhat and his PhD student Md Islam I would like to say thanks for support in using the X-Ray diffraction analysis laboratory. Dr. Farhat was kind enough to put his laboratory at my disposal while his student helped in interpretation results.

It is equally worth appreciating the contributions of the department Engineer Mr. Matt Kuzath for his guidance in operating most of the petroleum Engineering equipment I used in my research work. I also appreciate the immense contributions from Mr. Dean Grijm (Technician) for his assistance in preparing Wallace sandstone core samples for my tests.

It is also worth appreciating the moral support given to me by my family that has kept inspiring me to date.

Dean Grijm of the Department's Machine Shop deserves my acknowledgements for his part in setting up and running the X-Ray Diffraction experiments.

CHAPTER 1 INTRODUCTION

Global warming due to anthropogenic emission of carbon dioxide (CO_2) has reached record levels in recent times and this has rendered climate change issues central to current global scientific and political debates. The Inter-Governmental Panel on Climate Change (IGPP) and the World Meteorological Organizations (WMO) are jointly responsible for coordinating and monitoring technical matters related to climate change processes. The major cause of dramatic increases in atmospheric CO_2 concentration since the industrial revolution is exponential growth trends in global energy consumption. This alarming trend has caused diversification of the global energy mix to the extent where depleting conventional energy resources (oil and gas) has caused overdependence on coal for power generation, particularly among the energy intensive economies. A 100 MW thermal power plant using coal as fuel consumes ~0.35Mt of coal/year which is equivalent to ~0.228 Mt carbon/year emitting ~0.83MT/year of anthropogenic CO_2 (Koide *at al*. 1992).

Following the Kyoto protocol (Oberthur & Ott, 1999) the need to reduce greenhouse gas presence in the atmosphere has been considered mandatory, particularly for energy intensive economies. A number of sequestration options have been proposed among which are bio-sequestration (Ramanan, 2009; Riebesell, Wolf-Gladrow, and Smetacek, 1963; Jindal, Swallow, and Kerr, 2008) and geologic sequestration (Xu, Apps, and Preuss, 2005; Gentzis, 2000) and geologic sequestration. In view of the financial and technical constraints connected with possible large-scale bio-sequestration projects, geological sequestration appears to be the most practical both from immediate and long term planning grounds. This is because the former carbon sequestration option requires huge research and technical inputs (genetic engineering research) to be highly successful (Jansson, Wullschleger, Kalluri, & Tuskan, 2010). Accordingly, the capture of anthropogenic CO_2 and the isolation of this gas in suitable geologic media have been universally acclaimed as a suitable global warming mitigation step. Geological media means saline aquifers together with depleted oil and gas reservoirs including unconventional natural gas reservoirs.

Koide *et al*. (1992) estimated the global underground storage capacity of carbon to be 320 Gt of CO_2 of which 13Gt belongs to Western European onshore alone. Reimer (1996) estimated the global storage capacity in oil and gas reservoirs to be 180 Gt of carbon. On

the basis of the same program used, they also estimated the global capacity of saline aquifers to be 100 Gt of carbon. Bachu *et al*., (1994) estimated deep saline aquifer storage capacity of Alberta to be 20 Gt of CO_2 and this alone accounts for 16% of the global storage capacity according to Koide *et al*. (1992). The consensus is that the global storage capacity of geologic formations is greater than 1,000 Gt of C with brine filled formations having the greatest potential (Gunter *et al*., 2004). Sandstones are the most abundant sedimentary porous formations (Huang, 1962) and they are the likely candidates for geologic sequestration projects.

While geologic media such as deep sandstone saline aquifers have great potential, this is no guarantee of efficient use of their available subsurface pore space to store anthropogenic CO_2. This is because injection of CO_2 into geologic media constitutes the displacement of a wetting phase fluid (formation brine) from the porous medium by a non-wetting phase fluid, which in this case is the injected CO_2. Furthermore, CO_2 is a reactive fluid and the physiochemical changes that accompany the flow of this gas in deep saline aquifers constitute significant water- rock interaction that can greatly impact the two-phase flow regime. To understand the effect of water-rock interactions accompanying two-phase flow of supercritical CO_2 and brine much research has been carried out by petroleum and chemical engineering industries. These studies have sought in different ways to understand wettability changes accompanying the two-phase flow. Consequently contact angles at conditions of temperature, pressure and salinity typical of CO_2 geologic storage have been measured on silica and mica (Chiquet *et al*., 2007). Contact angles have also been measured on silica (Jung and Wan, 2012; Espinoza and Santamaria, 2010) both of which represent some of the notable current researches aimed at addressing problems of geological storage of anthropogenic carbon. However, it is the opinion of this author that while much of the published work on CO_2-water-rock interactions have made genuine attempts at understanding wettability phenomenon related to the system CO_2-water-mineral/rock surface which is central to the two-phase flow regime, the choice of materials for experimental works have been rather biased. This is because apart from Chiquet *et al*. (2007) who used mica in addition to silica, much of the experimental data has been gathered by using silica and calcite for contact angle measurements. In this regard, the principal hypothesis of this thesis work is that these minerals do not appear to be models of the

geologic media in the strictest sense. This is because normal geologic sediments and their geologically transformed ones have accessory or authigenic minerals in addition to the principal minerals that can impact the wettability in a foreseeable manner. The principal cause of wettability or contact angle evolution in geologic systems subjected to anthropogenic CO_2 storage is the water-rock interaction reaction. Fundamental to this reaction is the surface chemistry of solids. Accordingly, all rock-forming minerals together with accessory ones have distinct surface chemistry that characterizes their point of zero charge pH. Therefore, at a given pH of aqueous solution, each of the minerals will have a different electric double layer and the resulting water-rock interaction that control contact angle evolution will be totally different for rock media and their mineral aggregates. Another obvious geologic reason is that geologic sediments undergo diagenetic transformations that are the principal causes of secondary porosity evolution (Esteban & Taberner, 2003) and the formation of accessory minerals. Consequently, carbonate rocks that are predominantly calcite have accessory minerals or diagenetic cement that will render them argillaceous (Noiriel *et al*. 2007). Therefore, under normal *in situ* geologic conditions of carbon storage in carbonate formations the resulting physiochemical reactions that will control wettability evolution will reflect that of calcite and those of the minerals that constitute diagenetic cement. Therefore, this obvious geologic fact underscores the representativeness of contact angles measured exclusively on calcite if the prime objective is to obtain information about trends in contact angle change. The situation is no different in the case of sandstone where diagenetic transformations can lead to argillaceous rock. In the geologic literature, petrologists classify sedimentary rocks by using such terminologies as argillaceous sandstone or argillaceous limestone. Finally, the surface energy of the saline aquifer rock as well as the interfacial tension/energy between water and rock are integral parts of the wettability state of the system under *in situ* geologic conditions and deserve to be given due attention in research aimed at understanding the two-phase flow regime related to geological carbon sequestration. Clearly the best way is to obtain information about the effect of total rock mineralogy on contact angle evolution is to use representative rock samples.

1.1 MOTIVATION FOR GEOLOGICAL CARBON STORAGE

The petroleum industry has a wealth of experience regarding the injection of huge volumes of fluids other than CO_2 into subsurface geologic repositories. Therefore, in choosing to geologically sequester anthropogenic carbon as a technically and economically feasible option for global warming mitigation, the question posed by environmentalists has much to do with its long-term safety in the geologic containment. The answer to this is to be found in cases related to geologic formations as natural analogues for carbon storage. In this regard, a promising natural analogue of carbon storage over geologic time frames exits in the United States of America (Fig. 1).

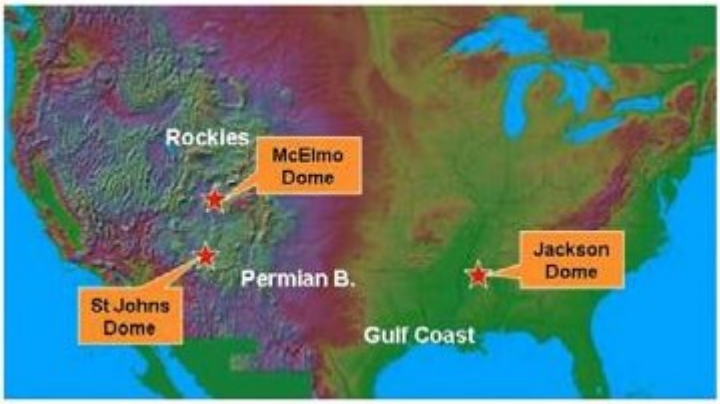

Figure 1: Location map of three carbon dioxide storage fields (Sally, Oldenburg, Hoversten, & Imbus, 2005)

As can be seen from Table 1-1, apart from the St. Johns storage site, all storage sites have depths above the minimum threshold of 800 meters. What is more, the number of years (geological time frames) of carbon storage in these formations is an additional motivation when it comes to the question of underground safety.

Table 1-1 Natural systems of carbon dioxide sink (Sally, Oldenburg, Hoversten, & Imbus, 2005)

Field	State (USA)	Original CO_2 in Place		Depth (m)	Cap rock	Years stored (Ma)
		Million. tons	Tcf			
St. Johns	AZ	730	14	500	Anhydride	0- 6 Ma
Jackson Dome	MS	100	2	4700	Carbonate	70
McElmo Dome	CO	1600	30	2300	Salt	70
All 3		2430	46			

St. Johns – Sandstone; Jackson Dome – Sandstone; McElmo Dome – Carbonate

1.2 EXISTING CONTACT ANGLE MEASUREMENT APPROACHES AND THEIR INCONSISTENCIES WITH REGARD TO IN-SITU GEOLOGIC SYSTEMS

Whenever CO_2 and brine flow in a porous medium, the wettability of the system will be governed principally by three interfacial tensions/energies. They are water-CO_2-rock- CO_2 and solid-water interfacial tensions.

The injection of CO_2 into saline aquifers will result in wettability changes due to the formation of carbonic acid under the prevailing aquifer salinity and temperature regime. The mechanism behind wettability change is related to surface charge evolution on aquifer rock surfaces. This surface charge evolution stems from ionization of surface hydroxyl groups, which produce acid and base contributions to solid-liquid interfacial tension. For conditions typical of geologic carbon sequestration, the interfacial tension between formation brine and CO_2 will remain practically constant (Chalbaud, 2009). Drainage capillary pressure data from CO_2-brine systems show positive values (Perrin and Benson, 2010) for different experimental conditions and this gives sufficient evidence to rule out direct contact of injected CO_2 with solid surfaces at all saturations. The implication is that by invoking Young's equation (Pease, 1945) to calculate contact angle, which is the thermodynamic measure of wettability, it is only changes in solid-liquid interfacial tension that control wettability evolution during CO_2 injection into saline aquifers.

Results of several studies related to CO_2-brine-silica have been published in the geological literature. These studies have generally researched the effect of CO_2 interaction with solid surfaces through the medium of brine by measuring contact angles at varying CO_2 pressures, temperatures and brine salinity (Kim *et al*., 2012). The solids used in these studies are minerals – silica, calcite and mica – extracted from potential saline aquifer rocks. The principal assertion of this work is that as good as these results are they do not represent the geological state of the saline aquifer rock medium. By this statement it is implied that experimentally the results are satisfactory but geologically they fall short of representing the true geological medium that will be eventually subjected to anthropogenic CO_2 injection. The geological argument invoked here is that the rock mass is an aggregate of minerals (Huang, 1962). Therefore, any measurement of contact angle on a solid surface that uses only components (minerals) of this aggregate (rock) will not be representative except in those cases where monometallic rocks are the targets for geosequestration and this is practically impossible. To demonstrate this point Table 1-2 shows the composition of Utsira sandstone in comparison with the minerals used in a model.

Again, this fact is supported by simulation studies on the geologic systems of the world's first commercial anthropogenic carbon geological storage in the Sleipner Field of the Norwegian sector of the North Sea (Audigane *et al.,* 2007). While the principal objective of the authors in this paper was to describe different CO_2 trapping mechanism though the formation of thermodynamically stable carbonates in water-rock interaction in the presence of dissolved CO_2, the representation of the host geologic system (saline aquifer rock) as an aggregate of minerals support the hypothesis of this thesis work. While the saline aquifer is modelled as an aggregate of minerals, the cap rock is no exception and Table 1-3 gives the mineralogical composition of a Shaley cap rock.

Generally, the idea behind carbon geosequestration is to store anthropogenic carbon in porous formations. These geologic systems are sedimentary in origin and constitute sediment deposition from different sediment sources that have been geologically transformed into indurate (solid) rocks and further modified diagenetically (Haven *et al*., 2001) by emplacement of authigenic minerals such as calcite cement, mica and glauconite.

Table 1-2 Mineralogical composition of Utsira sandstone (Audigane, Irina, Czernichowski-Lauriol, Preuss, & Xu, 2007)

Utsira sandstone composition	Vol fraction	Minerals introduced in the model	Vol %
Plagioclase	0.0301	Alibite~low	0.030
Calcite	0.0674	Calcite	0.067
Quartz	0.7633	Chalcedony	0.769
Chlorite	0.0133	Chlorite	0.013
Mica/Illite	0.0522	Muscovite	0.052
K-feldspar	0.0693	K-feldspar	0.069
Pyrite	0.0005	Not used	-
Ilmenite	0.0012	Not used	-
Apatite	0.0002	Not used	-
Zeolite	0.0022	Not used	-
Ti Oxides	0.0003	Not used	-

Table 1-3: Mineralogical composition of Nordland shale (Audigane, Irina, Czernichowski-Lauriol, Preuss, & Xu, 2007)

Nordland shale composition	Vol fraction	Minerals introduced in the model	Vol %
Plagioclase	0.132	Alibite~low	0.132
Calcite	0.010	Calcite	0.010
Quartz	0.228	Chalcedony	0.334
Chlorite	0.044	Chlorite	0.044
Mica/Illite	0.251	Muscovite	0.251
Kaolinite	0.195	Kaolinite	0.195
K-feldspar	0.023	K-feldspar	0.023
Siderite	0.011	Siderite	0.011
Smectite	0.09	Not used	-
Pyrite	0.016	Not used	-

Different minerals that constitute rocks are the rock forming minerals. They can be decomposed into different oxide minerals. This means that the pore surfaces of sedimentary

rocks that were formed from the deposition of broken down debris of previously existing minerals have oxides. This class of minerals (oxide minerals) imparts surface chemistry characteristics to pore walls that play a major role in CO_2-induced physiochemical reactions. These reactions control the wettability state of the CO_2-water-solid system during CO_2 injection into saline aquifers. Crucial to the surface chemistry of these oxide minerals is the point of zero charge pH (Nuh & Schwarz, 1989; Kosmulski, 2002) .This is the pH at which the surface charge of the oxide mineral is zero. Consequently, since each mineral (silica, carbonate, mica *etc.*) has a characteristic point of zero charge that will determine the extent of its surface charge under varying pH condition, the saline aquifer rock that was formed from different minerals cannot be represented by a single oxide mineral. In this regard, the work of Reymond and Kolenda (1999) shows explicitly that for a combination of oxide minerals the effective point of zero charge pH is what must be used as the surface chemistry characteristics. Others (Nuh and Schwarz, 1989) showed that the point of zero charge of a mixture of silica and aluminum oxide suspension depends on the weight fractions.

Contact angles measured so far for CO_2-water-solid surface systems have been based on separate mineral surfaces in high-pressure cells where CO_2 at varying pressures has been made to interact with solid surfaces through water media. Contact angles for these systems related to cases involving actual porous media are lacking even though the principal physiochemical process (pH induced solid-water interfacial tension changes) responsible for wettability changes in the systems studied are exactly the same as those that will be encountered in porous media. It is the view of the present study that there is the need for trends in contact angle variations for silica-water-CO_2 system to be better understood on the basis of proper experimental design related to actual geologic porous samples. The results of such studies can be compared to those of pure silica or mineral surfaces. This will provide reliable and precise information about the ultimate effect of CO_2 injection on the two-phase flow relative permeability. Indeed, contact angles measured on silica surfaces in previous experiments show monotonic increases with CO_2 pressure whereas observations from ongoing pilot scale CO_2 injection in the Frior sandstone formation in the US show initial increase of pH to a maximum and then a decrease following carbonate cement dissolution (Kharaka *et al*. 2006a). In terms of wettability/contact angle changes,

this represents an initial contact angle increase followed by a decrease. This field observation is clear testimony, as well as a reminder that accessory minerals such as carbonate cement, mica and glauconite, are capable of influencing contact angle or wettability changes, and that measured values on extracted minerals may not reflect these *in situ* effects.

Generally, wetting phenomena are physiochemical in origin that are governed by intermolecular forces. These forces are electrostatic, structural or solvation, and van der Waals (Oss, 2006). Therefore, in addition to van der Waals electrodynamic forces, electrostatic forces that are determined largely by the surface chemistry of the adsorbent need to be taken into consideration in developing a quantitative understating of wetting phenomena related to the water-CO_2 and rock systems where the surface of the solid has varied mineralogy (oxides) that can give rise to diverse surface functionalities. The extent of electrostatic interaction in this system will definitely be different from that of an isolated mineral from this rock.

Furthermore, in the kinetic molecular theory of wetting (Blake, 2006), the velocity of wetting has been strongly correlated with two parameters. They are the distance between adsorption surface sites of solids and the number density of absorption sites. The number density (Zhuralev & Potapov, 2006) and concentration of hydroxly groups on the surface of amorphous silica (Zhuralev, 1987). The concentration of hydroxyl groups on the surface of amorphous silicas depends on the concentration of surface functional groups that can ionize by protonation or de-protonation reactions at prevailing aqueous solution pH. Therefore, for an isolated mineral, the number density as well as the distance between adsorption sites will be different from the case of rocks that are formed geologically from the aggregation of these minerals. Also, the theory of intermolecular forces (Oss, 2006) at interfaces coupled with the Young-Dupre equation show that the contact angle for a system where phases 1 and 2 interact through the medium of phase 3, depends on the total interaction energies which consists not only of Lifshitz-van der Waals interaction but also on acid-base interactions which are contributed by all phases. In this regard, the acid-base contribution for an isolated mineral will be significantly different from the case of rocks where the total interaction energy depends on contributions from different minerals. Andre

et al., (2007) carried out a simulation studies aimed at predicting anthropogenic carbon dioxide injection into deep saline aquifers in France. In this regard, the performance of the Dogger formation carbonate was simulated. Figure 2 shows porosity and pH evolution as a function of distance from injection point. In this regard, carbon dioxide pressure is a function of distance from injection point such that its pressure decreases away from the injection point. The figure shows a clear decrease of formation brine pH towards injection point, with the potential for wettability change.

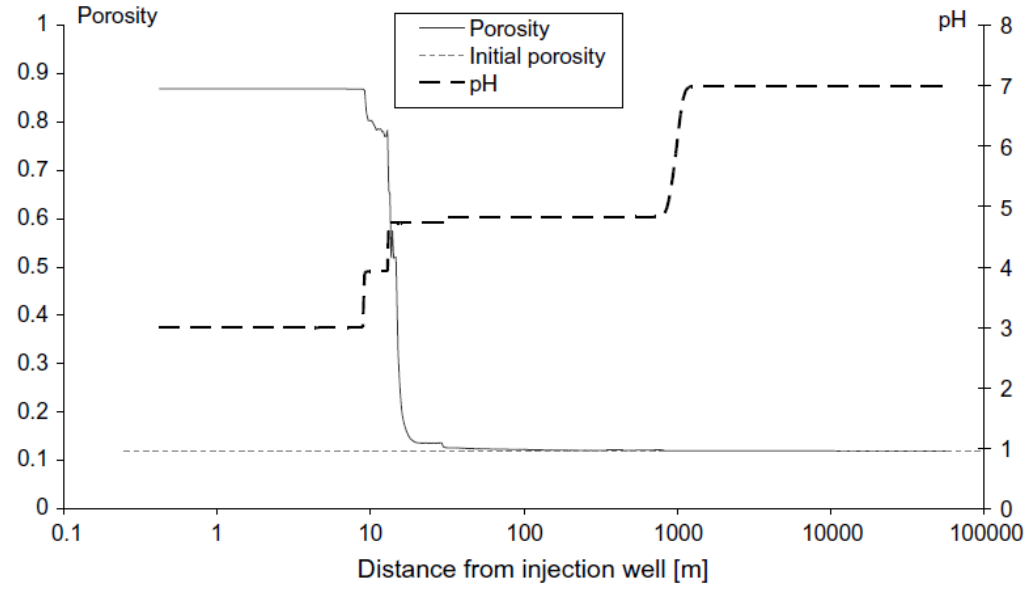

Figure 2: Porosity and pH changes as function of distance from injection point (Andre et al., 2007)

The principal cause of carbon dioxide induced wettability decrease is to be seen in its ability to dissolve in formation brine ant prevailing temperature and pressure conditions. The dissolved species is hydrated to carbonic acid (Iglauer, 2011) which dissociates to produce hydrogen ions which cause pH decrease as seen in Figure 2. It is, however, worth mentioning that pH changes in particular will depend on formation brine salinity such that the more saline formation brine is the more will be contact angle increases.

1.3 OBJECTIVES

Geological and thermodynamic arguments already invoked above show that previous research works (Chalbaud *et al*., 2009; Chiquet, *et al*., 2007; Jung and Wan, 2012) have

produced contact angles that represent those of rock forming minerals rather those of the actual geologic media (rocks) which are aggregates of these minerals. What is more, geologic systems that are to host anthropogenic carbon are sedimentary rocks that contain diagenetic minerals (Bjølykke, 1998). These are layered silicates with distinct surface chemistry characteristics and cation exchange capacities. In this regard, all indurate and lithified sedimentary rocks, clastics and precipitates have some proportions of these minerals. In a geologic system typical of CO_2-brine-solid system, there will be distinct water rock interactions involving surface complexation reactions (Koretsky, 2000) and cation exchange reactions (Laudelout *et al*., 1968) involving each mineral and the net interactions will be the one that will determine wettability evolution representative of this system. In all published works to date, formation water pH changes are the principal causes for wettability reduction in saline aquifers. Therefore, the principal hypothesis of this thesis work is that the response of formation brine to pH changes during CO_2 injection will reflect the mineralogy of the host rock. Also, the resulting solid-liquid interfacial tension which appears in Young's equation (Joanny & de Gennes, 1984) for mechanical energy balance at the three phase contact line will reflect this net interaction. Consequently, host rocks with the capacity to buffer formation water pH will resist wettability changes to some extent.

Also, all experimental works to date regarding relative permeability measurements for the system CO_2-water-rock have achieved their objectives using predetermined wettability states of core samples. In these experiments (Bennion & Bachu, 2005), mutual solubilities of phases were avoided to maintain constant wettabilities. Under actual field conditions, CO_2 at the injection front will be saturated with water vapor. This is particularly the case where the threshold depth of sequestration (800 m) is met (Bachu, 2000). Under this condition consolidated formations have absolute permeability values that render the mobility of injected carbon dioxide suitable for its phase to be water saturated. Therefore, solubility of CO_2 in formation brine is a physical possibility and change in ambient pH of formation brine will cause wettability evolution. Admittedly, the change in formation water pH will lead to wettability changes and any experimental design that make provision for carbon dioxide dissolution will replicate wettability changes similar to those encountered under field conditions.

Formation water pH changes due to dissolution of injected carbon dioxide is the principal causes of anticipated wettability evolution in geologic or saline aquifer systems. In the process engineering industries related to surface modification of ceramic materials to achieved surfaces with predetermined wettabilities (Wangab *et al.* 2010) the mathematical aspects of pH induced wettability changes of surfaces have been considered. To date, the geological sequestration community has only done a lot regarding measurement of pH induced wettability changes on mineral surfaces. The surface chemistry of the solid, rock/mineral, under different aqueous pH conditions plays a central role in surface charge development that impact solid-liquid interfacial tension/energy (Leea *et al*., 2002), and it is a major cause of wetting transition. The fundamental surface chemistry property here is the point of zero charge pH of the mineral or solid surface. In the colloid industry, this property has been determined using traditional approaches involving potentiometric methods, electroacoustic mobility of reversible particles variation with pH and direct assessment of surface charges via non- specific ion adsorption as a function of pH (Appel *et al*., 2003). Potentiometric titration method measures the adsorption of hydrogen and hydroxyl ions on amphoteric surfaces of varying ionic strength. The importance of this surface property as far as geological carbon storage is concerned is that it offers a clue as to the type of charges that will develop on rock surfaces as formation water pH reduces due to dissolved anthropogenic carbon species. This thesis will take the research work further by considering the mathematical aspects of wettability-pH relationship that integrates the point of zero charge pH parameter pertaining to minerals, specifically silica. Silica is preferred here because sandstone formations that are predominantly silica offer attractive subsurface storage volumes for anthropogenic carbon on global basis (Holloway, 2001).

Research areas in geological carbon storage can be divided into a number of areas. They are (i) research based on understanding the two-phase flow characteristics (Benion and Bachu, 2008); (ii) research aimed at understanding water rock interaction phenomenon, which impact wettability (Chiquet *et al*., 2007); (iii) research aimed at understanding the evolution of fluid-fluid interfaces in the geologic system (Chalbaud, 2009); and (iv) research aimed at understanding the long term fate of injected CO_2 (Gunter *et al*., 2004). It is the opinion of this author that because two-phase flow characteristics (relative permeability and capillary pressure) are controlled by prevailing wettability conditions, a

link can be obtained between wettability and relative permeability from drainage experiments. Apart from reported separate measurements of contact angles and relative permeability no work has so far been reported in the petroleum literature that has deduced contact angle from two-phase flow petrophysical data. On the basis of assertions so far, this thesis work will propose the following principal hypothesis: In addition, it will pursue a number of tasks. The following are the hypotheses and tasks.

1.3.1 Hypotheses

1. Different rock systems will affect wettability evolution differently due to formation water pH changes using mineralogically distinct rock samples. This is because, different mineral aggregates will interact differently with increases in hydrogen ion concentration as injected carbon dioxide dissolves in formation water. Notably, phyllosilicate minerals such as clay will have cation exchange capacities. Also, carbonate minerals from diagenetic emplacement will use added hydrogen ion for dissolution while quartz in the rock will adsorb or desorb hydrogen ion with pH changes due to the presence of surface hydroxyl functional groups. All these reactions will affect formation water pH differently. This hypothesis will be tested experimentally using different rocks samples

1.3.2 Objectives

1 To mathematically model the pH induced wettability change phenomenon while integrating the point of zero charge pH parameter and experimentally verify the model to determine this parameter. The theory of capillary imbibition at a given pH of aqueous solution leads to a relationship between contact angle and equilibrium height. In this regard, the capillary imbibition method that has not yet been used by the geological sequestration industry to verify pH induced contact angle change will be employed to test the mathematical model. Since the effective point of zero charge pH of a mineral surface is fundamentally different from that of the rock that consists of different minerals, the mathematical model will be used as the basis for proving this hypothesis by using suitable experimental data.

2 To mathematically link contact angle and/or wettability to drainage relative permeability data and to further use experimental data for determination of contact angles.

3 To propose suitable geologic media for efficient anthropogenic carbon storage.

1.4 ORGANIZATION OF THE THESIS

Chapter 1, introduced the general work with particular emphasis on carbon geosequestration and the state of contact angle measurements so far. It further defined a principal hypothesis and number of tasks.

Chapter 2 is devoted to literature pertinent to the research work in selected areas of carbon geosequestration and wettability phenomenon that are crucial for achieving the principal tasks. Accordingly, since this thesis work relies on theoretical and experimental initiatives to achieve its principal objectives, those aspects of two-phase flow that are most relevant and crucial to experimental data processing have been extensively reviewed. Thermodynamic theory required for vapor-liquid equilibrium calculations were thoroughly reviewed. Water-rock interaction theory related to cation exchange reactions, which control contact angle evolution, was also reviewed. Part of this chapter is devoted to model development regarding wettability pH relationship

Chapter 3 is devoted to the mathematical modelling aspect of the thesis work. Accordingly, an equation required for computing contact angle from drainage experiments was derived.

Chapter 4 presents experiments for validation of the mathematical models. In view of the interdisciplinary nature of this study, the experimental program involved an exhaustive measurement of spontaneous imbibition using rock samples and was further augmented by synthetic porous systems. The spontaneous imbibition experiments were largely designed to simulate the physiochemical conditions of the aquifer with regard to interfacial free energies under typical geologic conditions of saline aquifer CO_2 storage.

Since Chapter 4 is devoted to studying the effect of rock mineralogy on wettability following pH changes using spontaneous imbibition, Chapter 5 is devoted to studying the effect of rock mineralogy on wettability using drainage flow experiments. In this chapter, published literature data from landmark experiments on CO_2 displacing brine in a variety

of Canadian sedimentary basins have been utilized in addition to joint experimental data acquired in the Dalhousie University Petroleum Engineering Laboratory.

Chapter 6 gives a comparison of present studies with published works and strategies for carbon geosequestration in Nova Scotia.

Chapter 7 simply presents a summary and principal conclusion. Finally, the contributions of this study to knowledge were stated, after which recommendations for future work were made.

CHAPTER 2 BACKGROUND STUDY

2.1 PREVIOUS STUDIES OF WETTABILITY CHANGES RELATED TO CARBON GEOSEQUESTRATION

2.1.1 Carbon Dioxide Mineral Interaction under Geologic Conditions

Carbon dioxide-minerals interactions are ubiquitous in geologic systems. Two aspects can be identified, one relating to carbon dioxide-enhanced oil recovery (Holm & Josendal, 1974) and the other relating to anthropogenic carbon geological sequestration. In the case of carbon dioxide-enhanced oil recovery Rogers and Grigg (2000) have reported wettability evolution towards water wetting.

The wettability alteration phenomenon on which this thesis work is largely based has been studied by a number of workers notable among these being (Chiquet et al., 2007; Jung & Wang, 2012). In the published work of Chiquet *et al*. (2007) the effect of supercritical CO_2 in controlling wettability of rock minerals was observed. The result of their work supports the fact that CO_2 can wet the mineral surface of aquifer rocks provided the system is intermediate to water wet. In their work, the effect of supercritical CO_2 interaction on the wettability of clay minerals (mica), which is are components of seal rock layers over potential saline aquifers, and quartz were investigated. By means of contact angle measurements on these minerals, these workers arrived at a conclusion that the interaction of CO_2 with these minerals at reservoir/aquifer conditions and pressures (7-15 MPa) will cause a reduction of water wetness (Jung and Wan, 2012).

In the work of Jung and Wan (2012), wettability alteration of silica surface in CO_2-brine systems was studied under temperature, pressure and salinity conditions typical of geologic storage of carbon using silica plates. In this study, the authors arrived at a conclusion that the wettability of silica surface will be altered through interaction with supercritical CO_2. Specifically, the authors established that the wettability decreased from 7 MPa to 10 MPa and remained constant. Here, increasing pressure corresponds to increasing carbon dioxide solubility which means increases in the dissolved species of carbon dioxide. This situation corresponds to pH decreases with pressure. They also established that the wettability decreased more with increasing brine salinity.

2.1.2 Merits and Demerits of Previous Studies

The principal cause of wettability evolution due to CO_2 interaction with silica surface is physiochemical evolution of surface hydroxyl functional groups and acidic groups found on silica surface. These groups, notably the silanol formed by the dissociation and physiosorption of water molecules on the oxygen ion sites of oxide on silica surface (Mahadevan & Garofalini, 2008). Chiquet *et al*. (2007), have explained that CO_2 induced wettability change results from physiocaption of silanol group on rock surfaces. Also, dissolved carbon dioxide species will be responsible for the presence of hydrogen and bicarbonate ions (Matter & Takahashi, 2007). Another cause of wettability evolution can be seen from protonation and deprotonation reactions of silanol groups under different pH conditions. This fact obviously underscores the work of Chalbaud (2007) when the surface chemistry of silica is taken into consideration. The important parameter here is the silanol number, which is the number of silanol or surface hydroxyl groups per nanometer square, and depends on the type of silica and its impurities. For fully hydroxylated silica typical of geologic and amorphous systems, the silanol number is ~5 (nm^2) (Zhuravlev, 2006). However, studies using X-ray microanalysis and transmission electron microscopy (TEM) show inhomogeneities and other structural defects in quartz. Samples of quartz used in some studies have come from three genetic types, namely hydrothermal, pegmatitic and magmatic (Stenina *et al*., 1984). The impurities include aluminum (Al), sodium (Na) and water (H_2O) and these occupy interstitial or tetrahedral positions (Stenina *et al*., 1984). Consequently, if sandstones are predominantly the results of sediment depositions of detrital material from these genetic sources, then the presence of these impurities will affect the surface chemistry of quartz. This is because, recently Sverjensky (1994) contributed to our knowledge of point of zero charge pH calculation by showing that this fundamental surface chemistry parameter depends on the dielectric permittivity as well as the ratio of Pauling bod strength to metal-hydroxyl bond length. In this regard, the presence of impurities will affect all these parameters to impact the point of zero charge pH. Since the point of zero charge pH determines the development of surface charges and its subsequent evolution with pH, it will impact contact angle differently for a pure mineral and a mineral with impurity.

The implication here is that contact angles measured by different workers using silica or other minerals from different sources will not reflect those that will be measured on these minerals when they are in the geologic systems due to the inherent impurities in the natural geologic environments. The micro model used by Jung and Wan (2012) in their studies obviously gives contact angle changes that will be quite different from contact angles recorded by other works like Chiquet *et al.* (2007). The reason is that the latter workers used silica typical of geologic systems where anthropogenic carbon sequestration is anticipated while the micro model is constructed from amorphous silica by treating original silica at different temperatures (Wan (2012). This treatment deprives original quartz of its impurities leading to modification of its surface chemistry.

However, while the work of Chiquet *et al*. (2007) can be said to be representative of the surface chemistry state of silica under geologic conditions of carbon geosequestration (high formation brine salinity and temperatures), there still remains a shortfall in the opinion of the present study. This shortfall can be seen from the obvious fact that the mineral used was isolated from the geologic system. The system used by these workers therefore do not represent quite well the integrated geologic systems like the saline aquifer or depleted hydrocarbon reservoirs that have been formed by aggregation of minerals through sedimentation that is later affected by diagenesis in the geologic history (Lanson *et al.*, 2002). In these actual geologic systems, the pore surfaces will have different minerals with different oxide compositions leading to different silanol numbers. This fact equally underscores the works of Jung and Wan (2012) who used silica micro models for contact angle measurements. Thus, the presence of impurities in natural quartz samples has the potential to produce experimental results different from those acquired using amorphous silica in much the saw way as contact angle measured on these two types of quartz will be different from those measured using actual rock samples due to the aggregation effect of minerals in the rock sample.

2.1.3 The Need for a Fully Representative System for pH Induced Wettability Changes

Geologically, sandstone consists of ~75–85% quartz, ~10-12% feldspar on the average and a subordinate amount of accessory minerals *e.g.* diagenetic carbonate, clay and iron oxide. Table 2-1 shows the oxide compositions of different rock types. Each oxide corresponds to

the relative abundance of a particular mineral. Each of these minerals in the rock mass has its distinct surface chemistry with regard to oxide composition and will therefore have different surface charges at a given aqueous solution pH. Similarly, carbonate saline aquifers have predominantly calcite with accessory minerals such as iron oxide and clay minerals. On the basis of these mineral compositions, one would expect the pore surfaces of saline aquifer rocks interacting with carbon dioxide under geologic conditions of sequestration to have different contributions to the solid-liquid interfacial free energy, the evolution of which is the principal cause of wettability changes**.** This occurs because of the presence of different positive and negative sites directly related to protonation and deprotonation of surface sites (Sulpizi, 2012) as solution pH evolves. Therefore, the use of saline aquifer rock samples for experiments aimed at understanding wettability evolution due to carbon dioxide- water interaction reactions deserves to be considered and this is the principal goal of the present study.

Table 2-1: Oxide Compositions of Different rock types (Huang, 1962)

Constituents	Igneous (%)	Shale (%)	Sandstone (%)	Limestone (%)
SiO_2	59.14	58.14	78.33	5.19
TiO_2	1.05	0.65	0.25	0.06
Al_2O_3	15.34	15.40	4.77	0.81
Fe_2O_2	3.08	4.02	1.07	0.54
FeO	3.80	2.45	0.30	
MgO	3.49	2.44	1.16	7.89
CaO	5.08	3.11	5.50	42.57
Na_2O	3.84	1.30	0.45	0.05
K_2O	3.13	3.24	1.31	0.33
H_2O	1.15	5.00	1.63	0.77
P_2O_5	0.30	0.17	0.08	0.04
CO_2	0.10	2.63	5.03	41.54
SO_2	-	0.64	0.07	0.05
BaO	0.06	0.05	0.07	0.05
C	-	0.80	-	-
MnO	-	-	-	-
Total	99.56	100.00	100.00	99.84

2.2 SPONTANEOUS IMBIBITION

A number of multiphase flows in porous media can be distinguished. Among these, two kinds of flow related to the flow of a wetting phase, such as water, can be distinguished. They are forced imbibition and spontaneous imbibition. While in the case of the former the driving force is related to pumps, the driving energy behind spontaneous imbibition is capillary pressure gradient**.** Spontaneous imbibition is thus the flow of a wetting phase fluid into a porous medium containing a non-wetting phase under the influence of capillary pressure gradient that reflects the petrophysical characteristics of the porous medium and its chemical composition. The phenomenon of imbibition in general involves a complex interplay of capillary, gravity and viscous forces (Qasem, *et al.*, 2008). Washburn (1921) first demonstrated the phenomenon of spontaneous imbibition.

To integrate the concept of spontaneous imbibition into wettability changes related to CO_2-water-rock systems, it is noteworthy that the driving force behind this flow is the wetting state of the porous medium/capillary tube which has a strong bearing on surface/interface energy. This means that the task of integration cannot be achieved without further exploring surface or interface thermodynamic concepts related to this system. In this regard, the concept of surface free energy is essential because it determines the extent of spontaneous imbibition and its overall dynamics (Ma, *et al*.,1999). In the thermodynamic sense, the interfacial or surface free energy is an intrinsic property that characterizes an interface or surface and it is the work required to create unit surface/interfacial area between immiscible phases (Marmur, 2004). The surface or interfacial free energy has polar and dispersion components (Nguyen & John, 1978). In the case of carbon dioxide injection into saline aquifers, water rock interaction following pH evolution will electrostatically modify the solid-liquid interface which is one of the principal interfacial energies or tensions required to define the wettability of the system, globally calculated as the cosine of the macroscopic contact angle (Whyman *et al.* 2008). The following text will be devoted to the theoretical aspects of surface free energy and its relationship to spontaneous imbibition dynamics.

2.3 RELATIONSHIP OF WETTABILITY TO SURFACE AND INTERFACIAL FREE ENERGY

2.3.1 Interface Thermodynamics of Multiphase Flow in Porous Media

The surface free energy of a material is the work required to create unit surface area (Marmur, 2004). For the system carbon dioxide-water and rock surface three distinct interfacial energies come together to define the wettability state of the system. They are liquid-vapor interfacial free energy, liquid-solid interfacial free energy and vapor-solid interfacial free energy (Kwok & Neumann, 1999). For a given temperature, the magnitude of the individual interfacial free energies will be determined by polar and dispersion forces contributions. For the system mentioned above, the interfacial energy between liquid and vapor phase will be pressure dependent at a given temperature but under typical geologic conditions (for pressures above 15 MPa) the value is constant (Chalbaud *et al*., 2009) . The solid-liquid interfacial free energy will evolve under typical conditions of geologic sequestration due to water rock interaction which causes protonation of surface deprotonated species due to carbon dioxide induced acidity in formation brine. This variation of solid-liquid interfacial free energy will impact the wettability of the system through Young equation (Aksay *et al.*, 1974). Therefore water rock interaction is a major physiochemical process in carbon geosequestration that can cause wettability evolution to control the two-phase flow of injected CO_2 and formation brine. Since wettability is the sole thermodynamic attribute that governs spontaneous imbibition, the physics of how the surface free energy change of a system can be linked to spontaneous imbibition dynamics is crucial to quantifying wettability change due to CO_2 induced water rock interaction. The following sections will be devoted to this aspect.

2.3.2 Imbibition Dynamics and Free Energy of Spontaneous Imbibition for Capillary Tubes

Assuming that gravity forces are negligible compared to capillary forces then the change or reduction in free energy following spontaneous imbibition of brine/water into a cylindrical capillary is given by (Chibowski & Perea-Carpio, 2002):

$$dG = 2\pi r(\gamma_{SV} - \gamma_{SL})dx \tag{2-1}$$

in which dG is the free energy change of spontaneous imbibition [J], r is the radius of capillary tube [m], γ_{SV} is the work done to create unit solid-vapor interfacial area [Jm^{-2}], γ_{SL} is the work done to create unit solid-liquid interfacial area [Jm^{-2}] and dx is the distance advanced by the spontaneous imbibition front [m].

If the solid surface is not pre-wetted by the imbibing fluid there will be an additional surface free energy change due to the wetting of solid surface by liquid vapor. Young equation for mechanical equilibrium along the three phase contact line gives (Aksay *et al.*, 1974):

$$\gamma_{LV}\cos\theta = \gamma_{SV} - \gamma_{SL} \tag{2-2}$$

in which θ is the contact angle and all other symbols have their usual meanings.

By integrating the theory of capillary (Zhmud *et al*., 2000) flow Eq. (2-1) and Eq. (2-2) combined leads to the following equation:

$$\frac{d(x^2)}{dt} = \frac{r}{2\mu}(\gamma_{SV-}\gamma_{SL} + \gamma_{LV}cos\theta) \tag{2-3}$$

Integrating yield:

$$x^2 = \frac{r}{2\mu}(\gamma_{SV-}\gamma_{SL} + \gamma_{LV}cos\theta)t \tag{2-4}$$

This equation shows the relationship between capillary rise, interfacial free energies, cosine of contact angle and the dynamic viscosity of the imbibing liquid. Apart from capillary rise and time, all other parameters are constants at a given temperature. The next section will focus on the application of this equation for the case of the porous medium, which is assumed to consist of a bundle of parallel capillaries with different pore sizes.

2.3.3 Spontaneous Imbibition into Porous Solids

Equation (2-4) gives the distance of the imbibition front into a capillary tube of radius r. For spontaneous imbibition into a porous solid containing air, the radius in this equation is replaced by an equivalent of effective radius that takes into account the macroscopic petrophysical properties of porosity and permeability. The effective radius can also be calculated as (Salem & Chilingarian, 1999):

$$r_e = \left(\frac{8K}{\phi}\right)^{0.5} \tag{2-5}$$

In which r_e is effective or average radius [m], K is permeability [m^2] and ϕ is porosity [-]

By assuming a bundle of capillary tube model for the porous medium which regards the porous solid as consisting of bundles of parallel capillaries with different radii, the effective radius can be considered as the radius of a representative capillary of the porous medium that is subjected to spontaneous imbibition of water when the medium contains air. The equation for the porous medium becomes:

$$x^2 = \frac{1}{2\mu}\left(\frac{8K}{\phi}\right)^{0.5}\left(\gamma_S - \gamma_{SL} + \gamma_{LV}\cos\theta\right)t \tag{2-6}$$

The difference between solid surface free energy and the surface free energy of the liquid vapor interface is the film pressure. This is applicable for the case of spontaneous imbibition into capillary tubes. For spontaneous imbibition into porous solids containing air it will be assumed that the concept of film pressure is not applicable. This assumption makes it possible to remove the film pressure leading to the following equation:

$$x^2 = \frac{1}{2\mu}\left(\frac{8K}{\phi}\right)^{0.5}\left(\gamma_{LV}\cos\theta\right)t \tag{2-7}$$

This equation shows that for a given wettability state a plot of the square of imbibition penetration in the porous medium versus time will give a straight line with gradient equal to the coefficient of time. With this equation, it is, therefore, possible to determine the wettability measured by the cosine of the contact angle. This can be done by equating the gradient of the plot to the coefficient of time in this equation and solving for the cosine of the contact angle. Thus:

$$\frac{d(x^2)}{dt} = \frac{1}{2\mu}\left(\frac{8K}{\phi}\right)^{0.5}\left(\gamma_{LV}\cos\theta\right) \tag{2-8}$$

Solving for the cosine of the contact angle gives:

$$\cos\theta = \frac{2\mu}{\gamma_{LV}}\left(\frac{8K}{\phi}\right)^{-0.5}\frac{d(x^2)}{dt} \tag{2-9}$$

For spontaneous imbibition into a porous medium where distance and imbibition time are available, Eq. (2-9) provides a means of determining the cosine of the contact angle which is the universal measure of wettability (Kossen & Heertjes., 1965):

The free energy change term is connected with the surface free energy of the porous solid, considering the change in the free energy of the system per area unit as a consequence of the imbibition process. This can be calculated based on the assumption that capillary force is the only driving force for spontaneous imbibition**.** This gives surface free energy change as (Labajos-Broncano *et al.*, 2004):

$$\Delta G = \gamma_{LV} cos\theta \tag{2-10}$$

in which $\gamma_{LV}$is liquid vapor interfacial tension [N/m] and θ is the contact angle.

Substitution into Eq. (2-9) gives:

$$\gamma_{LV}\cos\theta = \Delta G = 2\mu \left[\frac{K}{\emptyset}\right]^{0.5} \frac{d(x^2)}{dt} \tag{2-11}$$

Solving for surface free energy change gives:

$$\Delta G = 2\mu \left[\frac{K}{\emptyset}\right]^{0.5} \frac{d(x^2)}{dt} \tag{2-12}$$

Equation (2-12) provides the basis for calculating free energy change accompanying spontaneous imbibition into a porous solid.

2.4 CONTACT ANGLE AND FREE ENERGY DETERMINATION FROM EARLY SPONTANEOUS IMBIBITION DYNAMICS

2.4.1 Early Spontaneous Imbibition Dynamics

Previous equations clearly provide the theoretical bases for free energy change and contact angle or wettability determination using spontaneous imbibition processes but they do not provide the fundamental bases of spontaneous imbibition dynamics theory. The spontaneous imbibition of water into a porous medium is governed by an ordinary differential equation which considers force balance among the fundamental forces of gravity, capillary and those due to viscous shear stresses in the imbibing fluid (Zhmud *et al.*, 2000).

In accordance with viscous non-compressible liquid flow along a cylindrical capillary tube the application of Newton's dynamics gives (Zhmud *et al.*, 2000):

$$[zz'' + (z')^2] = \frac{2}{r}\gamma cos\theta - \mu\frac{8}{r^2}z - \rho gzz' \qquad (2\text{-}13)$$

In which ρ is liquid density [kgm^{-3}], z is the distance advanced by the spontaneous imbibition front [m], z'' is the acceleration [ms^{-2}], z' the velocity of the imbibition front [ms^{-1}] and all other symbols have their usual meanings as before.

The first term on the right hand side of Eq. (2-13) represents capillary forces, the second term represents viscous forces and the last term represents gravity forces while the term on the left hand side represents acceleration forces.

Different solutions exist for this equation. There is the steady state solution popularly known as Lucas- Washburn equation. In this regard, if it is assumes that the sum of viscous forces and gravity forces cancel capillary forces then Eq. (2-13) reduces to:

$$\frac{2}{r}\gamma\cos\theta - \mu\frac{8}{r^2}z - \rho gzz' = 0 \qquad (2\text{-}14)$$

This is obtained by equating the left hand side of Eqn. (2-13) to zero meaning zero acceleration forces.

Two distinct solutions exist for this ordinary differential equation. The short-term asymptotic solution of Eqn. (2-14) gives (Zhmud *et al.*, 2000):

$$z(t) = \sqrt{\frac{r\gamma\cos\theta t}{2\mu}} \quad (t \to 0) \qquad (2\text{-}15)$$

This equation shows the relationship between capillary rise and time. It shows that a plot of capillary rise squared versus time will give a straight line with gradient given by the following equation: Elsewhere, Babadagli and Hatiboglu (2007), a plot of volume square versus time has been used to show a straight line plot in the early imbibition period. The gradient of the plot is given as:

$$\frac{dz^2}{dt} = \frac{r\gamma\cos\theta}{2\mu} \qquad (2\text{-}16)$$

This equation shows that the gradient of the plot can be related to the cosine of the contact angle by the following equation:

$$\cos\theta = \frac{2\mu}{r\gamma}\frac{d\left(z^2\right)}{dt} \tag{2-17}$$

By definition the cosine of the contact angle is the wettability of the system. Therefore, a capillary rise experiment can be used to determine the wettability of the system by employing height rise versus time data for the early imbibition dynamics period.

2.5 RELATIONSHIP OF FREE ENERGY CHANGE TO THE SURFACE CHEMISTRY OF ROCK SURFACES

The principal goal of this thesis work is to research wettability evolution in saline aquifers, particularly those of siliciclastic origin where CO_2 is injected for long-term containment. In this regard, by comparing CO_2 injection into saline aquifers with that of conventional water flooding of oil reservoirs for secondary oil recovery, one obvious thing is noted. In the case of the latter, the interfacial free energies of the system oil-water-rock remain practically constant. This is due to the obvious lack of water rock interaction. In the case of the former, this is not the case. This is because the dissolution of CO_2 in formation brine and its subsequent hydration into carbonic acid (Gislason *et al.*, 2010) changes formation water pH. This triggers off water rock reactions (Kharaka *et al.*, 2006b). Equation (2-2) for free energy change in spontaneous imbibition contains solid-vapor interfacial free energy and solid-liquid interfacial free energy. Consequently, the effect of water rock interaction on solid-liquid interfacial free energy and its ultimate control on both contact angle and overall free energy change deserves to be understood in the proper perspective. Pertinent to this is the dependence of the solid-liquid interfacial free energy on dispersion and polar contribution (Janczuk *et al.*, 1999). Generally, polar contributions also known as electron acceptor and donor components of surface free energy arise from protonation and deprotonation of surface hydroxyl functional groups on rock surfaces as mentioned earlier. These reactions can be represented as:

$$\equiv SiOH \leftrightarrow \equiv SiO^- + H^+$$

$$\equiv SiOH + H^+ \leftrightarrow \equiv SiOH_2^+ \quad \text{(i)}$$

In which $\equiv SiOH$ is a surface hydroxyl functional group; $\equiv SiO^-$ deprotonated surface species, $\equiv SiOH_2^+$ protonated surface species and H^+ hydrogen ion

Therefore, in order to understand the link between solid-liquid free energy changes and water rock interaction that is the principal cause of wettability evolution during carbon dioxide injection into saline aquifers, the remaining part of this chapter will be devoted to aspects of interface chemistry related to aqueous-rock systems applicable to geologic systems.

2.5.1 Concept of Point of Zero Charge (PZC) pH

For every metal oxide surface there is a characteristic pH of the ambient condition (aqueous medium) for which one of the categories of surface charge becomes zero at a given temperature and pressure (Marek, 2002). At the point of zero charge pH there is no surface charge to be neutralized by ions in the diffuse layer and any adsorbed ions existing must be associated with surface complex. This pH is, therefore, measured by knowing the pH value at which there is perfect charge balance among ions in aqueous solution with which solids have been equilibrated using titrimetric (Žalac & Kallay, 1992). In colloid chemistry, the PZC pH is fundamental to knowing the type of surface charge that an oxide surface in a solution of a given pH will develop at a given temperature.

2.5.2 Electric Double Layer in Geologic System

The electric double layer is a structure that appears on the surface of an object and it corresponds to two parallel layers of opposite charges. This surface can be a solid in or a porous surface in contact with an aqueous solution or water droplet. This structure is caused by charge transfer reaction at interfaces. The charge density gives rise to surface potential determining ions or hydrogen and hydroxyl ions. Figure 2-1 gives an illustration of the electric double layer.

There is a consensus among investigators of the double layer that the mechanism through which the double layer is formed involves two steps. They are surface hydroxylation and

dissociation of the hydroxyl formed groups under appropriate physiochemical conditions. The hydroxylation step is illustrated in Figure 2-2 and it involves surface exposed surface atoms trying to complete their coordination shell of nearest neighbors (Parks & de Bruyn, 1962). This is achieved through exposed cation pulling a hydroxyl ion or water molecule and the oxygen ion by pulling a proton from aqueous solution. This results in the covering of the surface by hydroxyl functional groups with the cation now buried below the surface. Physical evidence of the involvement of hydroxyl groups in this reaction step is amply furnished by the observation where that part of the water vapor adsorbed by metal oxide surfaces occurs as hydroxyl groups (Parks & de Bruyn, 1962).

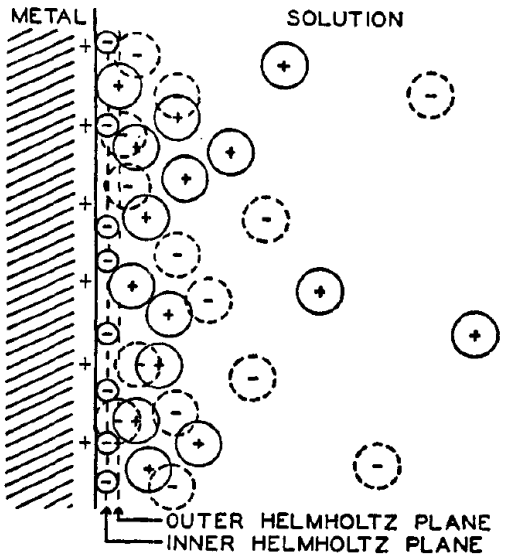

Fig. 2-1: Double layer (Grahame, 1947)

The crystal structure of a typical metal oxide such as ferric oxide serves as an example for clarifying the hydration reaction (Figure 2-2). In this crystal structure six oxygen atoms form an octahedral group around the iron atom with each oxygen atom being coordinated to four iron atoms. The hydration step therefore provides a thermodynamically favorable state for the system.

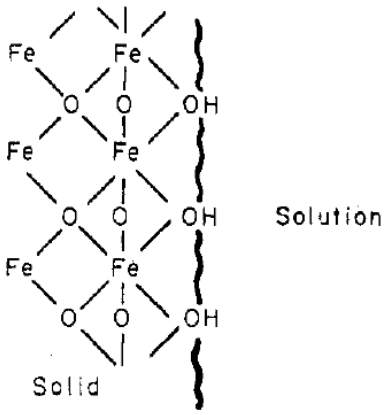

Fig. 2-2 Schematic illustration of an uncharged hydrated ferric oxide surface (Parks & de Bruyn, 1962)

2.5.3 Origin of Polar Contributions to Solid-liquid Interfacial Free Energy

Surface charge develops by two distinct surface reactions involving the adsorption of charged ions on the surface or the ionization of surface hydroxyl functional groups formed from the hydration reactions. In addition to these mechanisms of surface charge development, clay minerals also develop permanent surface charge by structural substitution (Sposito *et al*., 1999) Adsorption reaction involves protonation of surface hydroxyl functional groups while desorption reaction involves the dissociation of protons (deprotonation) from surface functional groups. Therefore, protonation and deprotonation of surface sites or functional groups leads to the development of positive and negative surface sites respectively, which constitute polar contributions to interfacial free energy.

Surface chemical reactions responsible for the formation of surface charges have been written previously for hydroxides: following Parks and Debruyn (1962) for oxides the following equations can be written:

$$\equiv MOH_2^+(surface) \leftrightarrow \equiv MOH(surface) + H^+ \quad \text{(I)}$$

$$\equiv MOH(surface) \leftrightarrow \equiv MO^-(surface) + H^+ \quad \text{(II)}$$

In which $MOH(surface)$ is a neutral surface group on the mineral surface, $MOH_2^+(surface)$ is a protonated surface group on the mineral surface, $\equiv MO^-(surface)$ is deprotonated surface group on the minerals surface and H^+ is hydrogen ion.

The symbol $\equiv MO^{-}(surface)$ means a surface deprotonated species that is attached to the crystal structure of the mineral. The meaning also applies to other species with this symbol.

In these reactions, the metal hydroxide sites are neutral or uncharged surfaces that constitute adsorption and desorption sites for protons depending on the pH conditions of aqueous solution. Adsorption reaction gives rise to positive sites while desorption reaction gives rise to negative sites. These reactions, therefore, imply amphoteric behavior of metal oxide where the surface hydroxyl group constitutes the conjugate base of the acid site $MOH_2^{+}(surface)$ or the conjugate acid of the base $\equiv MO^{-}(surface)$ (Parks, 1962). The addition of the two reactions gives:

$$\equiv MOH_2^{+}(surface) \leftrightarrow \equiv MO^{-}(surface) + 2H^{+} \qquad \text{(III)}$$

The equilibrium constant for the reaction gives:

$$\mathrm{K_1} = \frac{[\equiv \mathrm{MO^-(surface)}]}{[\equiv \mathrm{MOH_2^+(surface)}]} \left(\frac{\gamma^-}{\gamma^+}\right) [\mathrm{aH^+}]^2 \qquad \text{(IV)}$$

In which $\mathrm{K_1}$ is equilibrium constant for the reaction III [mol/l], $\equiv MO^{-}(surface)$is the concentration of deprotonated surface group [mol/l], $MOH_2^{+}(surface)$is the concentration of surfaced protonated species [mol/l], γ^{-} is the activity coefficient of negative site, $\gamma^{+}$is the activity coefficient of positive site [-], a is the activity coefficient of hydrogen ion [-] and $[H^{+}]$ is the concentration of hydrogen ion [mol/l]

The value of the equilibrium constant measures the ease of binding of protons on the metal and or mineral oxide surface. Assuming a value of unity for the ratio of activity coefficients of surface positive and negative species Eq. IV rewrites as:

$$\mathrm{K_1} = \frac{[\equiv \mathrm{MO^-(surface)}]}{[\equiv \mathrm{MOH_2^+(surface)}]} [\mathrm{aH^+}]^2 \qquad \text{(IV)}$$

This equation can be solved for any of the surface species as:

$$\equiv \mathrm{MOH_2^+(surface)} = \frac{[\equiv \mathrm{MO^-(surface)}]}{\mathrm{K_1}} [\mathrm{aH^+}]^2 \qquad \text{(VI)}$$

$$\equiv \mathrm{MO^-(surface)} = \mathrm{K_1} \frac{[\equiv \mathrm{MOH_2^+(surface)}]}{[\mathrm{aH^+}]^2} \qquad \text{(VII)}$$

Equation (VI) shows that the concentration of surface positive charge is directly proportional to hydrogen ion activity. This means that increasing the hydrogen ion concentration or decreasing ambient pH of aqueous solution will lead to an increase in surface positive charges by proton adsorption. Conversely, Eq. (VII) shows that the concentration of surface negative charge is inversely proportional to the activity of hydrogen ion. The implication is that as ambient pH decreases through hydrogen ion increases, negative site concentration reduces.

For a given mineral surface there is a pH called point of zero charge pH where the concentration of surface positive sites is equal to the concentration of surface negative sites. The equation for the ionization constant [Eq. (V)] can be written for equal surface species concentration as:

$$\mathrm{K_1} = \frac{[\equiv \mathrm{MO^-(surface)}]}{[\equiv \mathrm{MOH_2^+(surface)}]^2}[\mathrm{aH^+}]^2 = [\mathrm{aH^+}]^2 \qquad \text{(VIII)}$$

Using the chemical definition of pH Eq. VIII can be written as:

$$-logK_1 = pK_1 = log\frac{[\equiv MO^-(surface)]}{[\equiv MOH_2^+(surface)]^2} - log[aH^+]^2 = logaH^{+2} = 2pH_{PZC} \qquad \text{(IX)}$$

Thus:

$$pH_{PZC} = \frac{pK_1}{2} \qquad \text{(XI)}$$

In which pH_{PZC} is the point of zero charge pH of the solid surface and pK_1 is the negative logarithm to base 10 of the equilibrium constant $\mathrm{K_1}$. This gives the pH at the point of zero charge to be equal to half the negative logarithm of the dissociation constant.

2.5.4 Effect of pH on Surface Charge Type

At the point of zero charge pH there are equal concentrations of positive and negative charges. Above the point of zero charge pH there is an increase in pH due to decreases in hydrogen ion activity. The extent of negative site protonation is therefore decreased and the surface of metal oxide becomes predominantly negatively charged. Below the point of zero charge pH there is an increase in hydrogen ion activity and a corresponding decrease in ambient pH. The protonation reaction of surface hydroxyl groups is therefore favored and the surface of metal oxides becomes predominantly positively charged. Figure. 2-3

shows the effect of pH on adsorption density for ferric oxide in potassium nitrate solution. In the case of sandstone the dominant mineral to consider is silica (SiO_2). In this case, increasing pH above 3 which is the point of zero charge pH on the average will lead to negative charge development and decreasing pH below this point will led to positive charge development.

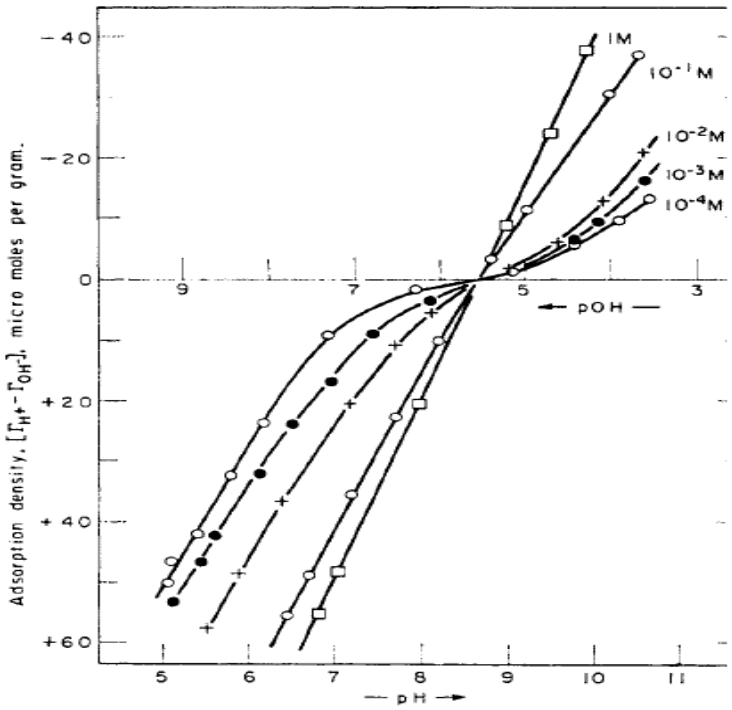

Figure 2-3: Adsorption density of potential determining ion on ferric oxide as a function of pH and ionic strength at temperature, 21°C in different concentrations of potassium nitrate (Parks & de Bruyn, 1962)

2.6 INTERMOLECULAR FORCES THEORY

When CO_2 is injected into an underground geologic storage system, a number of processes (see Fig. 2-4) of hydrodynamic, geologic, geochemical and thermodynamic origin occur. They are the following:

- Drainage two phase flow of injected carbon dioxide and resident formation brine

- Increase carbon dioxide phase pressure and decrease water phase pressure in invaded zones due to increase carbon dioxide saturation and decrease water saturation
- Interfacial interactions involving the system water, carbon dioxide and rock
- Dissolution of injected gas and hydration of dissolved gas to form carbonic acid
- Dissociation of carbonic acid
- Water rock interaction
- Wettability evolution
- Decreases in interfacial tension between carbon dioxide and brine
- Increases in interfacial tension between brine and rock surface due to water rock interaction
- Dissolution of major and minor or authigenic rock minerals due to water rock interaction (such as silica, calcite etc., siderite)
- There will be gravity segregation at low injection pressure and the extent to which this will be measured by gravity number (Ide *et al*., 2007)
- Unfavorable mobility ratio due to excessive difference between phase dynamic viscosity

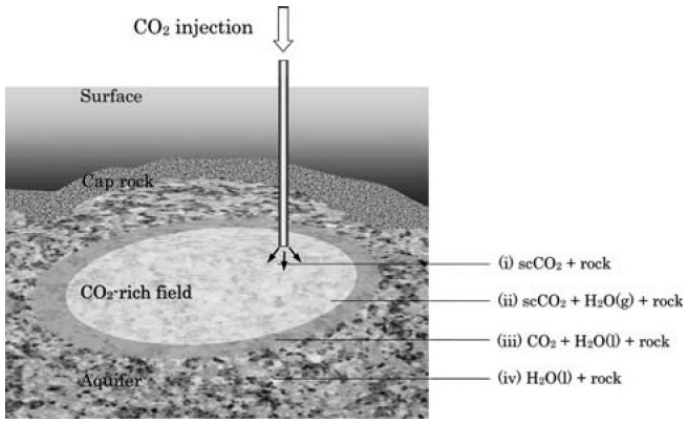

Figure 2-4 Carbon dioxide injection and water rock interactions (Lin *et al*.,, 2008)

The evolution of the wettability of the aquifer rock and its subsequent impact on the drainage two-phase flow of CO_2 and brine will depend on the interactions among some of the listed factors. Specifically, the production of hydrogen ions from carbonic acid

dissociation will cause formation water pH reduction. Thereafter, the evolution of the surface chemistry of aquifer rock will be controlled by pH evolution. The dissolution of CO_2 in formation water and the resulting density increases will impact the interfacial tension between gas and water. Similarly, the evolution of the surface chemistry of aquifer rock in response to formation water pH will impact solid-liquid interfacial tension. Consequently, interfacial interactions of the systems CO_2-water-rock will evolve with gas injection. In this regard, the surface chemistry of aquifer rock with regard to the aggregate mineralogy of the rock is a key parameter in determining the effective solid-liquid interfacial tension due to the response of different oxide mineral to pH conditions as dictated by its point of zero charge pH (Schwarz & James, 1989). In line with the interrelationship between wettability defined by the cosine of the contact angle and the three interfacial tension or interfacial free energies (Aksay, 1974) characteristic of the system carbon dioxide-water-rock, the prediction of wettability evolution under typical geologic conditions of CO_2 storage must consider a geologically realistic scenario where total solid liquid interactions contributing to wettability will reflect the aggregate surface mineralogy or nature (Elwing *et al.*, 1987) of the aquifer rock. Under geological sequestration, pressure build up can result in the interfacial tension between formation brine and supercritical carbon dioxide being nearly constant for different salinity and temperature conditions (appendices 3-1 and 4c)

2.7 RELEVANCE OF INTERMOLECULAR FORCES TO WETTING PHENOMENA RELATED TO THE SYSTEM CO_2-WATER-ROCK

2.7.1 Nature of Intermolecular Forces

At the interfaces within the system CO_2-water-rock, intermolecular forces will be manifest. The existence of forces between molecules and atoms was first put forward by van der Waals (Buckingham *et al.*, 1988). These force are electrodynamic in origin consisting of randomly oriented dipole interactions, random orienting dipole-induced dipole interactions called Debye interaction and fluctuating dipole-induced dipole or dispersion interaction described by London (Oss, 2006). Dispersion interaction is universal. The first two were later found to be similar to the third one following which the three electrodynamic forces have been jointly called Lifshitz van der Waals forces (Oss, 2006).

2.7.2 Lifshitz van der Waals forces at interfaces

The interfacial free energy is the work done to create unit interface area between phases and it is numerically equal to the interfacial tension (force/unit length) and this is a direct outcome of intermolecular forces described earlier. Accordingly, the interfacial free energy or interfacial tension can be quantified in terms of intermolecular forces. This gives for phase 1 and phase 2 (Oss, 2006):

$$\gamma_{12}^{LW} = \gamma_1^{LW} + \gamma_2^{LW} - 2\sqrt{\gamma_1^{LW}}\gamma_2^{LW} \quad (2\text{-}18)$$

in which γ_{12}^{LW} is the interfacial tension between phase 1 and phase 2, γ_1^{LW} is the surface tension of phase 1 and, γ_2^{LW} is the surface tension of phase 2, all due to Lifshitz van der Walls forces (LW).

2.8 CONTRIBUTION TO INTERFACIAL FREE ENERGY DUE TO ACID BASE INTERACTIONS

Apart from electrodynamic van der Waal forces contribution to interfacial tension, there are acid-base interactions. These contributions are known as electron acceptor and electron donor contributions respectively (Bellon-Fontaine, 1996). Compared to Lifshitz van der Waals forces the contribution due to acid-base interactions is stronger.

2.9 ORIGIN OF ACID BASE INTERACTIONS IN GEOLOGIC SYSTEMS

Rock is defined as an aggregate of minerals (Huang, 1962) and these minerals can decompose into oxide components with each oxide surface having a point of zero charge pH which is the pH at which the surface in contact with an aqueous medium will have a net zero charge. Table 2-2 shows the composition for Paleozoic Sandstone Suites of Eastern Australia while Table 2-3 shows the composition of a granitic rock. Granitic rock is worth mentioning in this thesis work because Liu.*et al*., (2003) have considered the injection of Carbon dioxide into granite and sandstones. The table shows variations in the silica content with values typically above 70%. Each oxide mineral on the surface of a pore for the case of a porous sedimentary rock and on the surface of a fracture in the case of granitic or crystalline rock has a point of zero charge pH. Above the point of zero charge pH it

develops a negative charge equivalent to an electron donor component. Below the point of zero charge pH the surface of the oxide minerals will develop a positive charge equivalent to an electron acceptor component. This is equivalent to deprotonation and protonation reactions of surface hydroxyl functional groups (Arrouvel *et al*.,, 2007) on the rock surfaces formed by the dissociation and chemisorption of water molecules on oxide surfaces. These surface functional groups have specific surface site densities (Zhuravlev, 1987) measured as number of sites per nanometer and will undergo dissociation in accordance with the pH of the aqueous medium. The presence of these hydroxyl functional groups on rock surfaces in amounts determined by their specific surface sites densities will impact the overall interaction energies or interfacial free energies of the carbon dioxide-water-rock system. Table 2-2 and 2-3 show that the silica content granite rivals that of sandstones.

Table 2-2. Oxide compositions (%) of sandstone (Bhatia, 1983)

	TS[1]	HE	HS	BS	CS
Samples	11	29	10	7	8
SiO_2	55.79	71.66	76.79	83.79	85.63
TiO_2	0.81	0.63	0.44	0.49	0.27
Al_2O_2	15.37	11.8	10.82	7.36	7.85
FeO	1.59	0.99	0.62	.055	0.53
MnO	0.22	0.08	0.05	0.02	0.01
MgO	2.57	1.43	0.99	0.98	0.37
CaO	6.65	2.54	1.16	0.18	0.10
Na_2O	4.49	2.43	2.27	1.36	0.89
K_2O	1.10	1.75	2.65	1.30	1.27
P_2O_5	0.18	0.12	0.08	0.13	0.08
S	0.36	0.03	0.04	0.02	0.02
H_2O^+	2.55	1.99	1.34	1.49	1.87
H_2O^-	0.42	0.12	0.06	0.14	0.17
CO_2	2.88	1.28	0.67	0.48	0.20
Total	94.98	96.85	97.98	97.795	99.26

TS: Tamworth Suite, HS: Hill End Suite, HS: Hodgkinson Suite, BS: Bendigo Suite, CS: Cookman Suite

As gas injection occurs CO_2 will dissolve in formation water in a manner that depends on salinity, temperature and pressure conditions. Dissolved CO_2 will hydrate into carbonic acid and dissociate in accordance with the following reaction (Gislason, 2010).

$$CO_2(gas) + H_2O(l) = H_2CO_3(aq) \quad \text{(2-XI)}$$

$$H_2CO_3(aq) = HCO_3^- + H^+ \quad \text{(2-XII)}$$

The extent of reaction (2-XI) and reaction (2-XII) will be measured by the equilibrium constants K_1 and K_2 respectively. Reaction (2-XII) is dominant at lower pH conditions.

Table 2-3: Major chemical oxide composition (wt. %) and modal mineral abundance (vol. %) in the Iidate granite (Lin *et al.*, 2008)

Oxide	Wt %	Modal mineral abundance	Volume %
SiO_2	73.99	Quartz	37.1
Al_2O	13.4	K-Feldspar	21.8
Fe_2O_3	2.05	Plagioclase	34.0
MgO	0.36	Biotite	6.3
CaO	1.8	Others	0.6
Na_2O	3.58		
K_2O	3.78		
Others	0.26		
Total	99.22		99.8

2.10 pH EVOLUTION IN SALINE AQUIFERS

As carbon dioxide is injected into geologic repositories there will be gradient of pressure and saturation from the injection point in the injection well. Normally, zones closer to the injection point have higher carbon dioxide pressure with higher concentration of carbonic acid. This causes a spatiotemporal evolution of formation water pH as shown in Fig. 2-5.

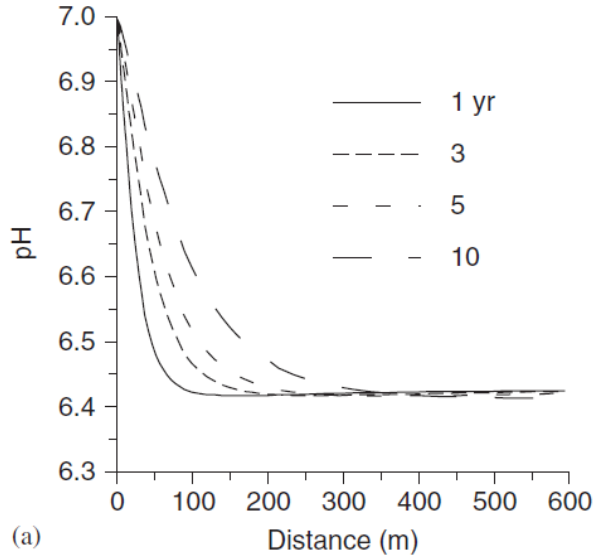

Figure 2-5. The spatiotemporal evolution of formation water pH (Xu *et al.*, 2006)

For silica surface the silanols will undergo the following reactions due to pH change (Behren & Grier, 2001). Below the point of zero charge pH of silicon dioxide

$$\equiv SiOH + H^+ = SiOH_2^+ \qquad \text{(XII)}$$

Above the point of zero charge pH

$$\equiv SiOH = SiO^- + H^+ \qquad \text{(XIII)}$$

The surface sites $\equiv S_iO^-, S_iOH_2^+$ will give rise to acid base (AB) interactions contribution to interfacial tension.

2.11 ENERGY ADDIVITY THEORY

The energy additivity theory of Fowkes holds that the interfacial tension is the sum of van der Walls electrodynamic and acid base contributions. This gives for phase 1 and phase 2 (Oss, 2006):

$$\gamma_{12} = \left(\gamma_1^{LW} + \gamma_2^{LW}\right)^2 + 2\left(\sqrt{\gamma_1^+\gamma_1^-} + \sqrt{\gamma_2^+\gamma_2^-} - \sqrt{\gamma_1^+\gamma_2^+} - \sqrt{\gamma_1^-\gamma_2^+}\right) \qquad \text{(2-19)}$$

The total interaction energy for the system carbon dioxide-water-rock where water and carbon dioxide is interacting through rock medium can be given as (Oss, 2006):

$$\Delta G_{wrCO_2}^{TOT} = \gamma_{12}^{LW} - \gamma_{13}^{LW} - \gamma_{23}^{LW} + 2\left[\left(\gamma_3^+\right)^{\frac{1}{2}}\left(\begin{array}{l}\left(\gamma_3^+\right)^{\frac{1}{2}} + \left(\gamma_2^-\right)^{\frac{1}{2}} - \left(\gamma_3^-\right)^{\frac{1}{2}} + \left(\gamma_3^-\right)^{\frac{1}{2}} \\ \left(\left(\gamma_1^+\right)^{\frac{1}{2}} + \left(\gamma_2^+\right)^{\frac{1}{2}} + \left(\gamma_3^+\right)^{\frac{1}{2}}\right) - \\ \left(\gamma_1^+\gamma_2^-\right)^{\frac{1}{2}} - \left(\gamma_1^-\gamma_2^+\right)^{\frac{1}{2}} - \left(\gamma_1^-\gamma_2^+\right)^{\frac{1}{2}}\end{array}\right)\right] \quad (2\text{-}20)$$

Subscript *r* refers to 3, 1 refers to water and 2 refers to CO_2.

In which γ_{12} is the interfacial tension between phase 1 and 2, γ_{12}^{LW} is dispersion force contribution to phase 1 and phase 2 interfacial tension, γ_{13}^{LW} is the dispersion forces contribution to phase 1 and phase 3 interfacial tension, γ_{23}^{LW} is the dispersion force contribution to interfacial tension between phase 2 and phase 3, γ_1^- is the electron donor contribution to phase 1 surface tension, γ_1^+ is the electron acceptor contribution to phase 1 surface tension, γ_2^- is the electron donor contribution to phase 2 surfacetension, γ_2^+ is electron acceptor contribution to phase 2 surface tension, γ_3^+ is the electron acceptor contribution to phase 3 surface tension and γ_3^- is the electron donor contribution to phase 3 surface tension.

By invoking the concept of mechanical equilibrium at interfaces due to interfacial forces and by integrating Dupre definition of work of adhesion, the contact angle for liquid phase 1 and solid phase 2 interacting through air is given as (Oss, 2006):

$$(1 + cos\theta)\gamma_L^{TOT} = 2\left[\left(\gamma_S^{LW}\gamma_L^{LW}\right)^{\frac{1}{2}} + \left(\gamma_S^+\gamma_L^-\right)^{\frac{1}{2}} + \left(\gamma_S^-\gamma_L^+\right)\right] \quad (2\text{-}21)$$

in which θ is the contact angle, γ_L the surface tension of liquid [N/m] and γ_S the surface tension of solid [N/m].

On the basis of this formulation Eq. (2-21) can be written by integrating the cosine of the contact angle (wettability) as (Oss, 2006):

$$(1+\cos\theta)\gamma_{CO_2-br} = \gamma_{12}^{LW} - \gamma_{13}^{LW} - \gamma_{23}^{LW} + 2\left[\left(\gamma_3^+\right)^{\frac{1}{2}}\left[\begin{array}{l}\left(\gamma_3^+\right)^{\frac{1}{2}} + \left(\gamma_2^-\right)^{\frac{1}{2}} - \left(\gamma_3^-\right)^{\frac{1}{2}}\ \ ) + \left(\gamma_3^-\right)^{\frac{1}{2}}\left(\left(\gamma_1^+\right)^{\frac{1}{2}} + \left(\gamma_2^+\right)^{\frac{1}{2}} + \left(\gamma_3^+\right)^{\frac{1}{2}}\right) - \\ \\ \left(\gamma_1^+\gamma_2^-\right)^{\frac{1}{2}} - \left(\gamma_1^-\gamma_2^+\right)^{\frac{1}{2}} - \left(\gamma_1^-\gamma_2^+\right)^{\frac{1}{2}}\end{array}\right]\right] \quad (2\text{-}22)$$

Equation (2-22) arises from the fact that interfacial tension is numerically equal to interfacial free energy and or interfacial interaction energy. This equation testifies to the eminent dependence of the wettability of the system CO_2-water-brine on acid base contributions.

2.12 DEPENDENCE OF SOLID-LIQUID INTERFACIAL TENSION ON pH FROM MOLECULAR THEORY

On the basis of molecular theory of interfacial tension the solid-liquid interfacial tension is calculated as (Oss *et al*., 1988a);

$$\gamma_{SL} = \left(\left(\gamma_S^{LW}\right) - \left(\gamma_L^{LW}\right) + 2\left(\left(\gamma_S^+\gamma_S^-\right)^{0.5} + \left(\gamma_L^+\gamma_L^-\right)^{0.5} - \left(\gamma_S^+\gamma_L^-\right)^{0.5} - \left(\gamma_S^-\gamma_L^+\right)^{0.5}\right)\right) \quad (2\text{-}23)$$

In which γ_{SL} is solid liquid interfacial tension, γ_S^{LW} is dispersion force contribution to solid-liquid interfacial tension due to solid surface, γ_L^{LW} is the dispersion forces contribution to solid-liquid interfacial tension due to water, γ_S^- is the electron donor contribution to solid-liquid interfacial tension , γ_S^+ is the electron acceptor contribution to solid-liquid interfacial tension due to solid, γ_L^+ is the electron acceptor contribution to solid-liquid interfacial tension coming from liquid and γ_L^- is electron donor contribution to interfacial tension due to water.

Under conditions typical of aquifer geologic storage the pH of formation water is closer to neutral. Therefore, for Sandstone saline aquifers that are predominantly silica (Quartz arenites, nearly 99% silica) the surface charge of silica will be negative because the point of zero charge pH of this mineral is 3. Protonated surface species will be lacking. Therefore, Eq. 3-48 can be written as:

$$\gamma_{SL} = \left(\left(\gamma_S^{LW}\right) - \left(\gamma_L^{LW}\right) + 2\left(\left(\gamma_L^+\gamma_L^-\right)^{0.5} - \left(\gamma_S^-\gamma_L^+\right)^{0.5}\right)\right) \quad (2\text{-}24)$$

Generally the electron acceptor and donor components of interfacial tension are related to the protonated and deprotonated species given in Eq. (2-23) and Eq. (2-24).These species are pH dependent through the following equation (Glover *et al*., 1994):

$$R_{pH}^- = \frac{\left[H^+\right]_{pzc}^2}{\left[H^+\right]_{pzc}^2 + \left[H^+\right]^2} \quad (2\text{-}25)$$

$$R_{pH}^+ = 1 - R_{pH}^- = \frac{\left[H^+\right]_{pH}^2}{\left[H^+\right]_{pzc}^2 + \left[H^+\right]_{pH}^2} \quad (2\text{-}26)$$

In which R_{pH}^- is the fraction of surface sites available for the adsorption of positive species [-]. R_{pH}^- is the fraction of surface sites available for the adsorption of negative species, $[H^+]_{PZC}$ is the hydrogen ion concentration of aqueous solution at the point of zero charge of rock surface [mol/l] and $[H^+]$is the concentration of hydrogen ions of aqueous solution [mol/ l]

In order to derive the pH dependence of solid-liquid interfacial tension it will be assumed here that the extent of electron donor contribution from solid will depend on the fraction of this sites available on the surface at a given pH. The following equation will be written:

$$\gamma_S^- = KR_{pH}^- = K\frac{[H^+]_{PZC}^2}{[H^+]_{PZC}^2 + [H^+]^2} \quad (2\text{-}27)$$

where K = constant of proportionality

For pH conditions typical of carbon dioxide injection (5 to 5.6-Kharaka, 2006a) Equation (2-24) can be combined with Eq. (2-25) to give:

$$\gamma_{SL} = \left[\left(\gamma_S^{LW}\right) - \left(\gamma_L^{LW}\right) + 2\left(\left(\gamma_L^+\gamma_L^-\right)^{0.5}\right) - \left\{K\left(\frac{\left[H^+\right]_{PZC}^2}{\left[H^+\right]_{PZC}^2 + \left[H^+\right]_{pH}^2}\right)\gamma_L^+\right\}^{0.5}\right] \quad (2\text{-}28)$$

Equation (2-28) clearly shows the effect of hydrogen ion inputs on solid-liquid interfacial tension. Specifically it shows that as hydrogen ion concentration increases due to CO_2 dissolution the expression involving hydrogen ions and the electron acceptor contribution

to solid-liquid interfacial tension from liquid will decrease due to protonation reaction explained earlier. This increase is supported by the published work of Chatelier *et al*., 1995)

2.13 IMPLICATION FOR DIFFERENT SALINE AQUIFER ROCKS

Saline aquifer rocks can be divided into two categories based on the ability of minerals found in the rocks to buffer formation water pH. Normally, carbonate cement and mica minerals found in sandstones saline aquifers will tend to buffer formation water pH through hydrogen ion reaction with carbonate cement minerals (iron and magnesium carbonate) and through cation exchange reactions respectively. Any of these reactions has the capacity to deplete added hydrogen ions from carbonic acid dissociation leading to pH buffering. Wallace sandstone is a typical example of this type with 82% silica and significant amount of glauconite and mica.

The other types of siliciclastic saline aquifers are the predominantly monomineralic types which have close to 99% quartz (Ruffet *et al*., 1991). This aquifer will not be capable of formation water pH buffering and wettability changes during carbon dioxide injection into these aquifers will depend on variations of the three interfacial tensions found in Young's equation. In the case of those with formation water pH buffering capability the change in wettability will depend on changes in solid-carbon dioxide and liquid-carbon dioxide interfacial tensions.

The third type of saline aquifer rock deserves to be distinguished because it is monomineralic in calcite. These are the carbonate formations. In these saline aquifers there is abundant calcite to react with added hydrogen ion to the extent that pH increases can occur after some time and this can lead to decreases in sold-water interfacial tension leading to eminent wettability change. It is, however, important to mention that in those siliciclastic saline aquifers where there are formation water pH buffering mechanisms the minerals responsible for these (iron and magnesium carbonates) occur as accessory or subordinate minerals. This means that excess of hydrogen ion concentration following high gas saturation can lead to this pH buffering mechanism to be lost.

2.14 KINETIC MOLECULAR THORY OF WETTING

In the kinetic molecular theory of wetting molecular processes occur within the intermediate vicinity of the moving wetting-phase where solid, liquid and a second immiscible fluid meet. For wetting to occur the molecules of one fluid phase must displace those of the other and the formulation of the direct link between molecular activity and macroscopic flow within the liquid is the major preoccupation of this theory. Generally, the extent of wetting is governed by solid-liquid interaction (Blake & Coninck, 2002). The stronger this interaction the faster the wetting and the smaller the equilibrium contact angle and *vice versa*. For liquid displacing gas from the surface of a solid there is a dynamic contact angle that is a function of the moving line velocity.

According to the kinetic molecular theory of wetting, the velocity of wetting is determined by the frequency κ and length λ of individual molecular displacement along the wetting line. These displacements are assumed to occur to and from with a net frequency given by (Blake & Coninck, 2002):

$$\mathrm{K}_{net} = \mathrm{K}^{+} - \mathrm{K}^{-} \tag{2-29}$$

In which $\mathrm{K}_{net}$is the net frequency of wetting, $\mathrm{K}^{+}$is the frequency of forward wetting and $\mathrm{K}^{-}$is the frequency of backward wetting.

At equilibrium, the frequency of forward wetting is equal to the frequency of backward wetting making the net frequency equal to zero. Equation (2-29) is then written as:

$$\mathrm{K}_{net} = 0 = \mathrm{K}^{+} - \mathrm{K}^{-} \tag{2-30}$$

Hence:

$$\mathrm{K}^{+} = \mathrm{K}^{-} = \mathrm{K}_{w}^{o} \tag{2-31}$$

Where K_{w}^{o} is the equilibrium frequency of wetting.

This refers to the partial wetting domain where the contact angle is greater than zero. For wetting to be effective work must be expended to overcome energy barriers related to the displacement of molecules. This work is directly linked to the out of balance surface tension force given as Blake (2006):

$$F_w = \gamma_{LV} cos(\theta^o - \theta) \tag{2-32a}$$

where F_w is the out of balance surface tension force, $\boldsymbol{\gamma_{LV}}$is the vapor-liquid interfacial tension, $\boldsymbol{\theta^o}$equilibrium contact angle [degrees] and $\boldsymbol{\theta}$ dynamic contact angle.

By discounting viscous effects, the work done by this driving force is used entirely within the three-phase zone and any channel where dissipation is required.

By integrating this theory with the right activated rate theory (Frenkel, 1946) and (Glastone, 1941) of transport in liquids the following equation has been presented:

$$v = 2\mathrm{K}_w^o \lambda \sinh\left[\frac{\gamma_{LV}}{2nk_BT}(cos\theta^o - cos\theta)\right] \quad (2\text{-}32b)$$

Where $\boldsymbol{v}$ is the velocity of wetting [ms^{-1}], n is the number of absorption sites per unit area on solid, k_B is Boltzmann constant [JK^{-1}] and T is absolute temperature [K]. All other symbols have been defined before. The equilibrium frequency of wetting is related to the activation free energy of wetting ΔG_w as:

$$\kappa_w^o = \frac{k_BT}{h} exp\left(\frac{-\Delta G_w}{Nk_BT}\right) \quad (2\text{-}33)$$

where h [J/s] is Planck's constant and N is a Avogadro's number.

This equation shows that at a given condition defined by temperature, the lower the free energy change of spontaneous imbibition the lower the equilibrium frequency of wetting. This means reduced water rock interaction and reduced wettability

2.15 IMPLICATIONS FOR ROCK MEDIA

The equation for wetting velocity contains the number of adsorption sites per unit area of the solid undergoing wetting or de-wetting. This number directly reflects the surface hydroxyl functional groups on solid surfaces that have been formed by protonation or deprotonation related to surface ionization in response to change in aqueous solution pH. Therefore, in rocks where we have mineral aggregates together with authigenic minerals within the matrix and on pore surfaces, the number of adsorption sites per unit surface area will be totally different from the case of an isolated mineral such as quartz, calcite of muscovite. This justifies the choice of a rock medium for contact angle measurements related to the CO_2-water-rock system.

2.16 PROTONATION AND CATION EXCHNAGE REACTIONS MERITS

2.16.1 Pertinent Geochemical Recations

The preceding sections have eventually outlined the theoretical basis for pH induced wettability evolution during carbon geosequestration. While pH induced availability of surface deprotonated species is the principal cause of solid-liquid interfacial tension changes giving rise to wettability change, other reactions can also be proton sinks depending on the chemical composition of aquifer or reservoir rock. In this reagard, it is possible to distinguish between two extremes of sandstones. They are quartz arenites consisting predominatly of quartz grains (99%) in addition to quatrz cement (Huang, 1962). The other class of sandstone contains diagentic or authigenic minerals such as mica ($(K,Na)_2 X_n AlSi_3O_{10}(OH,F)_2 \;\; X = Al^{+3}, Mg^{+2,}, F^{+2}, F^{+3}$, (Davidson and Vickers, 1972)) and glauconite ($(K)_2(Fe_{1-x}, Mg_x)_2 Al_6(SiO_{10})_3(OH)_{12}$, (Chapelle, 1983)). These authigenic minerals are capable of cation exchange reactions which forms the basis for potassium leaching reactions. Therefore, the pertinet geochmeical reactions following carbon dioxide injection into saline aquifers can be represented by the followin reactions:

Dissolution and hydration reactions of carbon dioxide is given as:

$$CO_2(g) \leftrightarrow CO_2(aq) \leftrightarrow H^+ + CHO_3^- \qquad \text{(XV)}$$

In which $CO_2(g)$ is gaseous carbon dioxide, $CO_2(aq)$aqueous carbon dioxide, $CHO_3^-$is bicarbonate ion and H^+ is hydrogen ion.

Surface Protonation reaction given as (Sverjensky & Sahai, 1996):

$$\equiv SiO^- + H^+ \leftrightarrow \equiv SiOH \qquad \text{(XVI)}$$

The velocity or rate of this reaction is mass action dependent (Connors, 1990) and it depends on the concentration of hydrogen ion in solution. As hydrogen ion activity increases due to pH decreases of aqueous solution the forward reaction is favored in accordance with Le Chatelier's law and this creates neutral surface species ($\equiv SiOH$).

Cation exchange reaction given as (Chapelle and Knobel, 1983):

$$A^+BR = AR + B^+ \qquad \text{(XVII)}$$

In which A^+ and B^- are the exchangeable monovalent cations and refers to the insoluble non diffusible non-ionic portion of the substrate.

In terms of two phase flow of injected carbon dioxide and resident formation brine, what is required for higher sweep efficiency is lower wettability of the system water-CO_2-rock (silica). If this is to be achieved then reaction XVI is more favorable compared to reaction XVII when it come to proton or hydrogen ion consumption because this reaction will result in wettability decrease. To see which reaction is preffered or has the highest rate requires kinetic consideration and the following sections will be devoted to that.

2.17 TWO-PHASE FLOW HYDRODYNAMIC THEORY

The concept of fractional flow and the frontal advance theory of Buckley and Leveret are fundamental to petroleum reservoir engineering aspects related to enhanced oil recovery related to multiphase flow in porous media. If two or more phases flow in a porous medium, the fraction of the total flux that is assigned to a given phase at any point is the fractional flow. For efficient water flood recovery by forced imbibition, an efficient flood requires the mobility of injected water to be low and that of the displaced oil to be high. This implies a high wettability of the reservoir rock with regard to injected water. For two-phase flow of a displacing and a displaced phase in a porous medium the application of mass balance gives the following generalized differential equation (Pope, 1980):

$$\frac{\partial S_D}{\partial t} + \frac{q}{A\phi}\frac{df_D}{dS_D}\frac{\partial S_D}{\partial x} = 0 \qquad (2\text{-}34)$$

In which S_D is the displacing phase saturation, f_D the displacing phase fractional flow, q is the total injection rate, A is the cross sectional area of injection, ϕ is the porosity, t is time and x is distance

By noting that the space derivative of the displacing phase saturation is negative this equation reduces to:

$$\frac{\partial S_D}{\partial t} - \frac{q}{A\phi}\frac{df_D}{dS_D}\frac{\partial S_D}{\partial x} = 0 \qquad (2\text{-}35)$$

The solution for the velocity of saturation gives:

$$\left(\frac{dx}{dt}\right)_{S_D} = \frac{q}{A\phi}\frac{df_D}{dS_{D\,|S_D}} \tag{2-36}$$

where:

$\frac{df_D}{dS_{D\,|S_D}}$ is the displacing phase saturation derivative of fractional flow evaluated at a saturation of interest.

For any displacement experiment the displacing phase saturation in the porous medium will increase from the initial irreducible saturation to one less the residual saturation of the displaced phase (Archer & Wall, 1986), page 105. Between these two saturations there exist two zones. They are the stabilized zone and the drag zone. The stabilized or zone is formed by the saturation distribution between the initial irreducible saturation and a frontal saturation which is formed depending on the wettability of the porous medium with regard to the displacing phase. Between the frontal saturation and one less residual saturation of the displaced phase the drag zone is formed (Smith *et al*., 1992), page 11-13

Generally, the higher the frontal saturation for a given water flooding for oil recovery the higher the fractional flow and the less wetting the system is to the injected water. By applying mass balance criterion the construction of a sharp front eliminates what is known in the petroleum literature as the double saturation phenomenon (Smith *et al*., 1992). Based on this theory a Welge tangent (Binninga & Celia, 1999) can be drawn from the initial displacing phase saturation to a point where it makes tangent with the fractional flow curve (see Figure. 2-6). With this approach the velocity of the shock front evaluated at the frontal saturation gives:

$$\left(\frac{dx}{dt}\right)_{S_{Df}} = \frac{q}{A\phi}\left(\frac{df_D}{dS_D}\right)_{S_{Df}} \tag{2-37}$$

In which the fractional flow derivative is evaluated at a saturation corresponding to the frontal saturation S_{Df} of the displacing fluid.

Depending on the wettability of the displacing phase the frontal saturation corresponds to a given fractional flow. The higher this value, the higher the mobility of the displacing phase and *vice versa*.

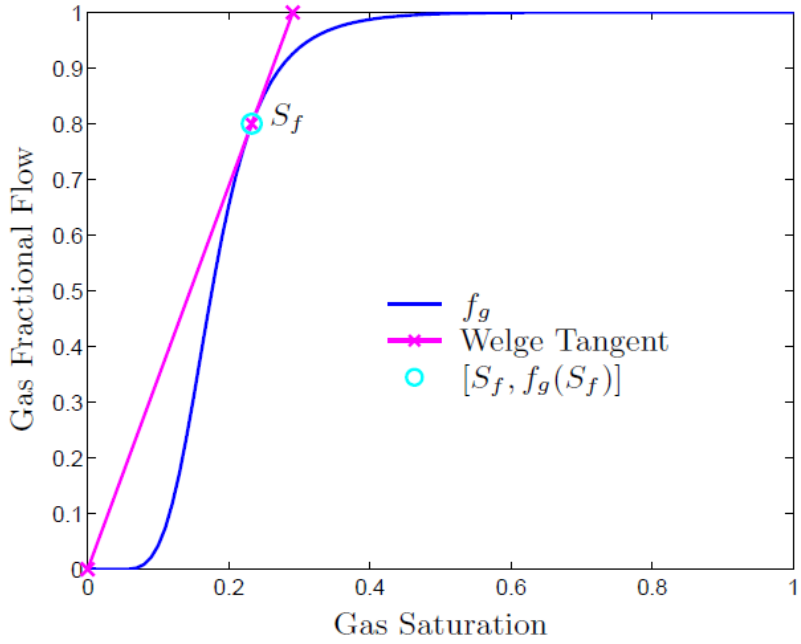

Figure 2-6: Fractional flow curve with Welge tangent (Garcia & Pruess, 2003)

2.18 APPLICATION TO DRAINAGE FLOW

Drainage flow occurs in the porous medium where a non-wetting phase such as gas is injected to displace a wetting phase such as water from the porous medium as encountered in the geological sequestration of carbon. For gas injection under this condition the frontal advance theory for calculating the velocity of the frontal saturation gives (Smith *et al*., 1992):

$$\left(\frac{dx}{dt}\right)_{S_{gf}} = \frac{q}{A\phi}\left(\frac{df_g}{dS_g}\right)_{S_{gf}} \tag{2-38}$$

where S_{fg} is frontal saturation and f_g is the fractional flow of gas

The generalized fractional flow equation including aquifer dipping angle and capillary pressure written for gas injection gives (Sater *et al.,* 2008)

$$f_g = \frac{1 + \frac{k_w}{q_t \mu_w}\left[\frac{\partial P_c}{\partial x} - g\Delta\rho \sin\alpha\right]}{1 + \frac{k_{rw}}{k_{rg}} * \frac{\mu_g}{\mu_w}} \tag{2-39}$$

In which f_g is the fractional flow of gas [-]; q_t is the total flux [ms^{-1}], μ_g is the dynamic viscosity of gas [cp], μ_w is the dynamic viscosity of water [cp], $\frac{\partial P_c}{\partial x}$ is the capillary pressure gradient [psi/ft], k_{rg} is the relative permeability of gas [-], k_{rw} is the relative permeability of water [-], $\Delta\rho$ is density change between fluid phases [lbm/ft^3] and α is the dipping angle of reservoir [^{o}]

Assuming negligible capillary effect and a horizontal system this equation becomes:

$$f_g = \frac{1}{1+\frac{k_{rw}}{k_{rg}} * \frac{\mu_g}{\mu_w}} \tag{2-40}$$

Phase relative permeabilities are functions of phase situations as:

$$k_{rg} = k_{rg}(S_g) \tag{2-41a}$$

$$k_{rw} = k_{rw}(S_w) \tag{2-41b}$$

Substitution into Eqn. (2-40) gives (Gunter et al., 2004)

$$f_g = \frac{1}{1+\frac{k_{rw(S_w)}}{k_{rg(S_g)}} * \frac{\mu_g}{\mu_w}} \tag{2-42}$$

Equation (2-42) shows that, given relative permeability as a function of phase saturations the fractional flow for injected carbon dioxide can be constructed as a function of gas saturation. Since the fractional flow curves reflect the wettability of the system for multi-phase flow in porous media, it provides a practical and theoretical means for evaluating gas

sweep efficiency which requires low gas mobility evidenced by low frontal saturation velocity.

2.19 DRAWING OF THE FRACTIONAL FLOW CURVE COUPLING GEOCHEMISTRY

For relative permeability measurements at varying temperatures conducted in the present work, CO_2 was equilibrated with brine and injected under supercritical conditions. To draw the Welge tangent, the partial miscibility or solubility of CO_2 and water at experimental conditions must be taken into consideration. Generally, the physics of the system is totally described by coupled fractional flow and geochemical flows (Noh *et al*., 2007). This calls for the consideration of total carbon flux in addition to water flux in the overall material balance equation of the system. Consequently, the conservation equation assuming no dispersive effect is given as (Noh *et al*., 2007):

$$\frac{\partial C_i}{\partial t} + \frac{\partial F_i}{\partial x} = 0, i = 1 \ldots . n_c \tag{2-43}$$

where:

$$C_i = x_i(1 - S) + y_i S,\ 1 \ldots . n_c \tag{2-44}$$

And

$$F_i = x_i(1 - f) + y_i f,\ 1 \ldots . n_c \tag{2-45}$$

In which C_i is concentration of component, F_i is fractional flow of component I, x_i refers to liquid phase, y_i refers to gas phase, S is saturation, n_c is the number of components

For the case under consideration where we have only carbon dioxide species Eqn. (2-38) can be written as:

$$\frac{\partial \mathrm{CO_2}}{\partial \mathrm{t}} + \frac{\partial \mathrm{CO_2}}{\partial \mathrm{x}} = 0, \mathrm{i} = 1 = \mathrm{CO_2} \tag{2-46a}$$

$$\frac{\partial \mathrm{S_g}}{\partial \mathrm{t}} + \frac{\partial \mathrm{f_g}}{\partial \mathrm{x}} = 0 \tag{2-46b}$$

Under this condition, the solution to Eq. (2-46) is a wave of varying fluxes and concentrations. In this case a mixed wave is generated where the velocity of the specific shock or the fastest shock is given as (Noh *et al*., 2007)

$$v\Delta C = \frac{f_g^- - \frac{c_{CO_{2,a}}}{c_{CO_{2,a}} - c_{CO_{2,g}}}}{S_g^- - \frac{c_{CO_{2,a}}}{c_{CO_{2,a}} - c_{CO_{2,g}}}} \tag{2-47}$$

In which $v\Delta C$ is the velocity of the specific shock; f_g is the fractional flow of gas, C_{ia} is the solubility of carbon dioxide in aqueous phase, C_{ig} is the concentration of carbon dioxide in the vapor phase and S_g^- gas saturation upstream the shock.

Since the computation of the fastest shock velocity involves the use of two distinct points, Eqn. (5-22) shows that the tangent used for velocity computation which is the Welge tangent passes through the points $\left(\frac{C_{i,a}}{C_{i,a} - C_{i,g}}, \frac{C_{i,a}}{C_{i,a} - C_{i,g}}, S_g^-, f_g^- \right)$

Equation (2-47) can be written as:

$$v\Delta C = \frac{f_g^- - D}{S_g^- - D} \tag{2-48a}$$

In chromatographic terms the point involving concentrations $\left(\frac{C_{i,a}}{C_{i,a} - C_{i,g}}, \frac{C_{i,a}}{C_{i,a} - C_{i,g}} \right)$ is called the retardation (Lee *et al*., 1974) D.

Consequently, because of partial miscibility, that is solubility of CO2 phase in brine and that of brine phase in CO_2 phase prior to injection, the tangent to the fractional flow curve is drawn from the point $\left(\frac{C_{i,a}}{C_{i,a} - C_{i,g}}, \frac{C_{i,a}}{C_{i,a} - C_{i,g}} \right)$. (2-48b)

The foregoing text shows that in order to calculate the specific shock velocity as well as draw the Welge tangent in an experimental work, the solubility of CO_2 at experimental conditions is required. This approach requires thermodynamic concepts involving vapor-

liquid computations for the system carbon dioxide-brine under experimental conditions. The following section will be devoted to that.

2.20 THERMODYNAMIC CONCEPTS: VAPOR-LIQUID EQUILIBRIUM THEORY

2.20.1 Water solubility in supercritical carbon dioxide

The mutual solubility of supercritical carbon dioxide and brine under reservoir conditions are calculated as (Hassanzadeh *et al*., 2008):

$$y_{H_2O} = \frac{K^o_{H_2O} a_{H_2O}}{\Phi_{H_2O} P_{tot}} \exp\left(\frac{\left(P - P^o\right)\bar{V}_{H_2O}}{RT} \right) \tag{2-49}$$

$$x_{CO_2} = \frac{\Phi_{CO_2}\left(1 - y_{H_2O}\right)P_{tot}}{55.508\gamma^{/}_{x} K^0_{CO_2(g)}} \exp\left(\frac{\left(P - P^0\right)\bar{V}_{CO_2}}{RT} \right) \tag{2-50}$$

Where:

$$logK^o_{CO_2(g)} = 1.189 + 1.304 * 10^2 T - 5.55 * 10^{-5} T^2 \tag{2-51a}$$

$$logK^o_{H_2O} = 2.209 + 3.097 * 10^{-2} T - 1.098 * 10^{-2} T^2 + 2.048 * 10^{-7} T^3 \tag{2-51b}$$

In which $K^o_{CO_2}$ is Henry's law constant for carbon dioxide solubility at reference pressure [bar mol^{-1} kg H_2O] and $K^o_{H_2O}$ is Henry's law constant for water at a reference pressure [bar mol^{-1} kh H_2O], y_{H_2O} is the mole fraction of water in carbon dioxide phase, x_{CO_2} is the mole fraction of carbon dioxide in liquid phase, T is absolute temperature [K], R is universal gas constant [J/K], $\bar{V}_{H_2O}$ is partial molar volume of water [cc/mol], $\bar{V}_{CO_2}$ partial molar volume of carbon dioxide [cc/mol], P_{tot} is total pressure [bar], P is pressure of interest [bar], P^o is reference pressure, Φ phase fugacity, $\gamma^{/}_{x}$ is an activity coefficient for carbon dioxide.

The fugacity of water is calculated as (Portier & Rochelle, 2005)

$$\Phi_{H_2O}^{aq} = \Phi_{H_2O} = a_{H_2O} P_{H_2O}^{sat} \exp\left[\frac{V_{H_2O}^{aq}\left(P - P_{H_2O}^{sat}\right)}{RT}\right] \quad (2\text{-}52)$$

In which a_{H_2O} is water activity, Φ_{CO_2} is the fugacity of carbon dioxide [Pa], Φ_{H_2O} is the fugacity of water [Pa], x_{CO_2} is the mole fraction of carbon dioxide in aqueous phase [-], y_{H_2O} is the mole fraction of water in carbon dioxide phase [-], $\ln a_{H_2O} = -0.0360 I \Theta_{NaCl}$, $V_{H_2O}^{aq}$ is the average partial molar volume of water [cm^3/mol], $P_{H_2O}^{sat}$ is the saturation vapor pressure of water [bar-], R is the universal gas constant [bar per mol Kelvin], T is the temperature [K] and l the ionic strength[mol/dm^3]

I is the ionic strength defined as (Helgeson, 1969):

$$I = \frac{1}{2}\sum_i z_i^2 m_i \quad (2\text{- }53)$$

In which z_i is the valence on an ion, m_i is the molarity of an ion [mol/dm3] and Θ_{Nacl} is the osmatic coefficient of sodium chloride

The saturation vapor pressure of water as a function of temperature and salinity is given as (Benson & Krause Jr., 1984):

$$P_{wv} = \left(1 - 5.370 * 10^{-4} S\right) \exp \left\langle \begin{array}{l} 18.1973\left(1 - \dfrac{373.16}{T}\right) + \\ 3.1813 * 10^{-7}\left\{1 - \exp\left[26.1205\left(1 - \dfrac{T}{373.16}\right)\right]\right\} \\ -1.8726 * 10^{-2}\left\{1 - \exp\left[8.03945\left(1 - \dfrac{373.16}{T}\right)\right]\right\} + \\ 5.02802 \ln\left(\dfrac{373.16}{T}\right) \end{array} \right\rangle \quad (2\text{-}54)$$

In which P_w is the saturation vapor pressure of water [bar], S is salinity in parts per million and T is the temperature in Kelvin

Henry's law constant is calculated as (Spycher and Press, 2010)

$$K\left(T, P_{ref}\right) = K^{o}\left(T, P_{ref}\right) \exp\left(\frac{\left(P - P_{ref}\right)\bar{V}}{RK_T}\right) \quad (2\text{-}55)$$

T_K is temperature [K] and P_{ref} is the reference pressure [bar]

Henry's law constant $K_i^o\left(T, P_{ref}\right)$ (bar/mol) for phases at temperatures from 12 to 109°C and pressures between 1 and 600 bar are calculated as (Spycher and Preuss, 2010)

$$logK^{o}_{CO_2(g)} = 1.189 + 1.304 * 10^{2} t - 5.55 * 10^{-5} t^{2} \quad (2\text{-}56a)$$

$$logK^{o}_{H_2O} = 2.209 + 3.097 * 10^{-2} t - 1.098 * 10^{-2} t^{2} + 2.048 * 10^{-7} T^{3} \quad (2\text{-}56b)$$

t = temperature [°C]

The solubility of carbon dioxide in brine is calculated using the following equation (Portier and Rochelle, 2005)

$$m_{CO_2} = K^o\left(T, P_{ref}\right)\frac{\varphi_{CO_2} x_{co_2}}{\gamma^{/} K^H_{CO_2}\left(T, P^{sat}_{H_2O}\right)}\exp\left[\left(\frac{\overline{V}^{\infty}_{CO_2}}{RT}\right)\left(P - P^{sat}_{H_2O}\right)\right] \qquad (2\text{-}56c)$$

In which $\gamma^{/}$ is the salting out effect of carbon dioxide in sodium chloride solution [-], m_{CO_2} is the solubility of carbon dioxide in brine [mol/dm^3] and $\overline{V}^{\infty}_{CO_2}$ is the partial molar volume of carbon dioxide at infinite dilution [mol/dm^3]

The average partial molar volume (cm^3/mol) of phases over the pressure range is calculated as:

$$\overline{V} = a + b\left(T_K - 373.15\right),\ \ b = 0\ \ for\ T_K < 373.15\ \ K \qquad (2\text{-}57)$$

T_K = temperature [K]

For lower temperatures from 12-109°C and pressures from 1-600 bar the average partial molar volume are calculated as (Spycher and Preuss, 2010).

$$\overline{V}_{CO_2} = 32.6\ \ cm^3\ /\ mol$$
$$\overline{V}_{H_2O} = 18.1\ \ cm^3\ /\ mol \qquad (2\text{-}58)$$

The density of supercritical carbon dioxide is calculated using a virial equation of state as (Ihmels & Gmehling, 2001):

$$P = \rho[R + B\rho + C\rho^2 + D\rho^3 + E\rho^4 + F\rho^5] \qquad (2\text{-}59)$$

where:

$$B = a_1 - \frac{a_2}{T} - \frac{a_3}{T^2} - \frac{a_4}{T^3} - \frac{a^5}{T^4}$$

$$C = a_6 + \frac{a_7}{T} + \frac{a_8}{T^2}$$

$$D = a_9 - \frac{a_{10}}{T} \qquad (2\text{-}60)$$

$$E = a_{11} + \frac{a_{12}}{T}$$

$$F = \frac{a_{13}}{T}$$

where: ρ is the density*, R* the universal gas constant—MPa L/mol F (0.008314472), and T is the absolute temperature.

2.21 PROBLEMS WITH RESEARCH ON PAST CONTACT ANGLE MEASUREMENTS FOR THE SYSTEMS WATER-CARBON DIOXIDE ROCK

Problems with contact angle measurement of the above mentioned system can be realized by integrating the geological definition of rock with Eqs. (2-19) – (2-22) where contact angle will be determined by all acid base contributions in the system in addition to van der Walls contributions. Measurements so far have involved isolated minerals of rock (calcite, silica, shale). These minerals are carefully selected to provide wettability change with pH carbonate saline aquifers, sandstone aquifers and caprocks respectively. Therefore, in the systems where these experiments were carried out acid base contributions to contact angles were coming only from the minerals used in the experiments as well as from the fluid-fluid (carbon dioxide–brine) interfaces. The principal objective of carbon geosequstration is to geologically sequester carbon in rock media where we have a host of minerals forming the rock. Different oxide compositions and diagenetic minerals characterize rock media. All these minerals have different surface chemistry and will therefore give multiple acid base contributions. Consequently, to provide experimental data of contact angle representative of the geologic conditions of carbon sequestration there is the need fill the research gap by using rock samples in experiments where the acid base contributions from respective minerals with different surface chemistry will reflect in the contact angle data.

2.22 MODEL DEVELOPMENT

2.22.1 Problem Analysis and Mathematical Development

The solubility of CO_2 depends on its phase pressure, salinity of formation fluid and temperature. Assuming there are no pH buffering reaction mechanisms such as carbonate cement dissolution (Ross *et al*., 1982 or silicate hydrolysis (Emberley *et al.* 2004) the concentration of carbonic acid and hydrogen ions are expected to increase with continuous injection of CO_2. Thus during CO_2 injection, the pH of formation water will decrease. This decrease in formation water pH will reflect the ionization of surface functional groups such as hydroxyl groups found on silica surfaces (Vezenov *et al*., 1997) thereby affecting the electric double layer forces. It therefore stands to reason that the injection of CO_2 into a saline aquifer causes pH changes which will perturb the original electrical double layer and affect the stability of the thin water film that will form in a system involving carbon dioxide-brine and solid minerals surface. The contact angle of the system will therefore evolve in accordance with pH changes caused by carbon dioxide injection.

Petroleum reservoir rocks consist of aggregates of minerals. These rock-forming minerals are quartz, feldspar, plagioclase, *etc*. The mineralogical composition of reservoir rocks is normally determined first by obtaining information about the oxide compositions of the rock (Huang, Petrology, 1962) and then using this information to deduce fractions of normative minerals in the rock. The oxides are then calculated to the normative minerals, which correspond to the rock-forming minerals. In most cases, the structure of a crystal surface terminates in bivalent anions such as the oxygen anion (Boehm, 1971). According to Boehm, the dissociation and chemisorption of water molecules on oxide sites of minerals on reservoir or aquifer rocks gives rise to hydroxyl functional groups such as silanols and alunols and the surface chemistry of the rocks under different pH environments is largely controlled by these functional groups. Most oxide surfaces show hydroxylation under normal conditions when water (either liquid or vapour) has access to it (Boehm, 1971).

Generally the wettability of the system involving CO_2, brine and saline aquifer rock surface, reflects fluid phase mobilities that are closely linked to fractional flow and displacement efficiencies (Anderson, 1987). For higher sweep efficiency the mobility of the resident brine must be higher than the mobility of injected gas. This corresponds to

higher fractional flows for water and lower fractional flow for injected gas. Normally the more wetting the saline aquifer is to the resident brine the poorer the sweep efficiency of the injection. For the system, carbon dioxide, brine and saline aquifer rock, the mineralogy of the rock as well as the surface chemistry status with regard to the point of zero charge pH determines wettability evolution during carbon dioxide injection into saline aquifers. This is because, the point of zero charge pH of the rock surface determines the nature of surface charge density and surface potential as well as trends in their variations on either side of the point of zero charge pH. Table 2-4 shows the point of zero charge pH values of typical silicate minerals encountered in sedimentary rocks.

Table 2-4: Point of zero charge pH of some silicate minerals (Sverjenky, 1994)

Silicate mineral	Point of zero charge pH
Silica	2.9
Muscovite	7.6
Phlogopite	7.6
Anorthite	7.14
Albite	6.95

For the system comprising a siliciclastic saline aquifer such as sandstone, formation water and supercritical CO_2, the point of zero charge pH of the rock surface (predominantly silica) is on the average 3 (Reymond & Kolenda, 1999). The pH of normal formation brine is approximately 6.5–7 (Magot *et al*., 2000). Above the point of zero charge pH the surface of a metal oxide will develop negative charges due to deprotonation reactions with corresponding negative surface potentials. Below the point of zero charge pH positive charges will develop with corresponding positive surface potentials (Illes *et al*., 2006). For typical saline aquifers, such as those of sandstone, the point of zero charge pH is in the range 3–3.5. This means that for normal formation water with a pH value close to 7 the surface of these aquifer rocks will be negatively charged. As pH decreases following carbon dioxide injection the negative charges will begin to decrease due to decreasing pH until at a pH of 3 when the net surface charge is zero. The process of decreasing pH from

that of average formation water (pH in the range 6.5–7) to the point of zero charge pH causes an increase in solid-liquid interfacial tension (Chatelier *et al*., 1995). According to Ross *et al.*, (1982), the minimum pH for a natural ideal carbon dioxide system related to natural gas reservoirs due to solubility trapping is 5. Therefore, investigation of wettability evolution and its implications for injected gas and resident formation brine fluid phase mobilities and sweep efficiencies is warranted.

2.23 RELATING WETTABILITY TO pH

The relationship between surface charge density and surface charge potential reads (Atkinson *et al*., 1967):

$$\frac{e\psi}{k_B} = \sigma\sqrt{\frac{2\pi}{\epsilon n k_B T}} \tag{2-61}$$

In which Ψ is the surface potential of minerals surface [V] and n is the ion density [mol /m^3], e is the electronic charge [C], k_B is Boltzmann constant [J/K], σ is surface charge density [C/m^2], ε is dielectric permittivity **[**F/m**]**.

In the following section this equation will be exploited for deriving the pH wettability relationship.

In the literature, the effect of surface modification of silica by amine group on wettability has been studied. In this regard, the relationship between contact angle change and aqueous solution pH change is given as (Carre *et al.,* 2003):

$$\frac{d\cos\theta}{dpH} = -\frac{2.303RT\sigma}{F\gamma_{LV}} \tag{2-62}$$

In which θ is the contact angle [degrees], R is the universal gas constant [J/K/mol] F is Faradays constant [C/mol], γ_{LV} is liquid-vapor interfacial tension **[**N/m**]**.

In order to derive pH cosine of contact angle or wettability relationship these basic equations will be used.

From Eq. (2-61) the following can be written:

$$\sigma = 2.303\left(pH_{pzc} - pH\right)\left(\frac{2\pi}{\varepsilon n k_B T}\right)^{-0.5} \tag{2-63}$$

The Nernst equation gives (Bowden *et al*., 1977):

$$\psi = -2.303\frac{k_B T}{e}\Delta pH = -2.303\frac{k_B T(pH - pH_{PZC})}{e} = \frac{2.303 k_B T}{e}(pH_{PZC} - pH) \tag{2-64}$$

The change in cosine of contact angle from Eq. (2-62) gives:

$$\frac{d\cos\theta}{dpH} = -\frac{2.303RT\sigma}{F\gamma_{LV}} \tag{2-65}$$

Substitution for surface charge density from Eq. (2-63) into Eq. (2-65) gives:

$$dcos\theta = -2.302^2\frac{RT}{F\gamma_{LV}}\left(\frac{2\pi}{\epsilon n k_B T}\right)^{-0.5}(pH_{PZC} - pH)dpH \tag{2-66}$$

Under normal conditions of carbon geosequestration there is pH reduction from average formation water pH to a lower value closer to the point of zero charge pH of silica surface in the case of silisiclastic saline aquifers. The integration limits are the initial pH of formation water to the pH of interest and the wettability at initial formation water pH (pH_o) to the wettability at a given pH of interest. Application of these limits leads to:

$$\int_{(cos\theta)_o}^{cos\theta} dcos\theta = -\int_{pH_o}^{pH} 2.303^2\frac{RT}{F\gamma_{LV}}\left(\frac{2\pi}{\epsilon n k_B T}\right)^{-0.5}(pH_{PZC} - pH)dpH \tag{2-67}$$

In which $\cos\theta_o$ is the cosine of the initial contact angle initial pH [-] and $\cos\theta$ is the cosine of the final contact angle at a given pH[-]

The final integration gives:

$$cos(\theta) = cos(\theta)_o - \frac{2.303}{F\gamma_{LV}}\left(\frac{2\pi}{\epsilon n k_B T}\right)^{-0.5}\left[pH_{PZC}pH - \frac{pH^2}{2}\right]_{pH_o}^{pH} \tag{2-68}$$

Expanding the term in the square bracket on the right hand side of the equation gives:

$$cos(\theta) = cos(\theta)_o + \frac{2.303^2}{F\gamma_{LV}}\left(\frac{2\pi}{\epsilon n k_B T}\right)^{-0.5}[0.5pH^2 - pH_{PZC}pH + (pH_{PZC}pH_o - 0.5pH_o^2)] \quad (2\text{-}69)$$

This equation can be written as:

$$cos(\theta) = cos(\theta)_o + \zeta[0.5pH^2 - pH_{PZC}pH + (pH_{PZC}pH_o - 0.5pH_o^2)] \quad (2\text{-}70)$$

Where:

$$\zeta = \frac{2.303}{F\gamma_{LV}}\left(\frac{2\pi}{\epsilon n k_B T}\right)^{-0.5} \quad (2\text{-}71)$$

2.23.1 Implication of pH Induced Wettability Evolution Equation

While pursuing the principal objective of testing the hypothesis that trends in contact angle change following pH decreases of formation brine during carbon dioxide injection will be different for rocks and minerals, it is worth noting at this point before the experimental set up what the mathematical model has to say. In this regard, the most single parameter in Eq. (2-70) is the point of zero charge pH of minerals/rocks surfaces. Thus, for rock media with different mineral aggregate, the point of zero charge pH of interest is the effective value. For a mineral surface, the point of zero charpe pH is that specific to the mineral surface. Equation (2-70) can now be written differently for a mineral and for rock as:

For a mineral:

$$\cos(\theta) = \cos(\theta)_o + \zeta\left[0.5pH^2 - pH_{PZCm}pH + \left(pH_{PZCm}pH_o - 0.5pH_o^2\right)\right] \quad (2\text{-}70a)$$

For rock:

$$\cos(\theta) = \cos(\theta)_o + \zeta\left[0.5pH^2 - pH_{PZCr}pH + \left(pH_{PZCr}pH_o - 0.5pH_o^2\right)\right] \quad (2\text{-}70b)$$

In which pH_{PZCm} is the point of zero charge pH of a mineral surface and pH_{PZCr} is the effective point of zero charge pH of rock surface which takes into accont the proprtions of different components. Consequetly, the first step in testing the hypothesis has been explicitly provided by the mathematical model.

2.23.2 Comparison of Wettability Change Trend for Minerals and Rocks

To purse the principal hypothesis that pH induced wettability change will be different for minerals and rocks this section will consider the pH derivative of wettability. Thus, the following equations can be written after combining Eq. (2-62) and Eq. (2-63):

$$d\cos\theta = \frac{2.303^2 RT}{F\gamma_{LV}}\left(\frac{2\pi}{\varepsilon n k_B T}\right)\left(pH - pH_{pzc}\right)dpH \tag{2-72}$$

This can be written for a mineral and rock as:

$$d\cos\theta = \frac{2.303^2 RT}{F\gamma_{LV}}\left(\frac{2\pi}{\varepsilon n k_B T}\right)\left(pH - pH_{pzcm}\right)dpH \tag{2-73}$$

$$d\cos\theta = \frac{2.303^2 RT}{F\gamma_{LV}}\left(\frac{2\pi}{\varepsilon n k_B T}\right)\left(pH - pH_{pzcr}\right)dpH \tag{2-74a}$$

All equations show that wettability change at a given pH depends on the point of zero charge pH of solid (rock/minerals) surface. To give a detailed interpreation for wettability change requires knowledeg of point of zero charge pH for rocks and minerals. Assuming sandstones which consists predominatly of quartz and other subordinate amount of mineral components, the general finding is that a system that has pure quartz will have a lower point of zero charge of pH and when there is a mixture the point of zero charge pH is higher (Schwarz *et al*. 1984). In the strictest sense, rock is a combination of minerals due to magmatic differentiation for ingeous rocks (Kemp *et al*., 2007) and partly due to diagenesis for sedimentary rocks (Miller Jr., 1966). In this regard, one would expect the point of zero charge to be different in each case. Petrologically, limestone consists predominatly of calcite and some subordinate amount of minerals accounted for due to diagenesis. Therefore, the point of zero charge pH must reflect this system. The point of zero charge pH of quartz is 3 on the average (Kosmulski, 2002) and that of calcite is between 8 and 9 on the average (Somasundaran and Agar, 1967). Therefore, if sandstone is regarded as a saline aquifer then, the effective point of zero charge of this system must be different for the case where it consists entirely of quartz. This statement also applies to limetsone as a saline aquifer. Figure (2-7) shows zeta potential measurements for Tuscarora sandstone

and Columbus Limestone (Sasowsky *et al*., 2000). To deduce the point of zero charge pH from a plot of zeta potential versus pH, the curve is extrapolated to the horizontal axis where zeta potential is zero. In this regard, Figure (2-7) shows that extrapotaion of the curves to the horizontal axis gives point of zero charge pH values greater than the case where each consisted of 100% of its predominant mineral.

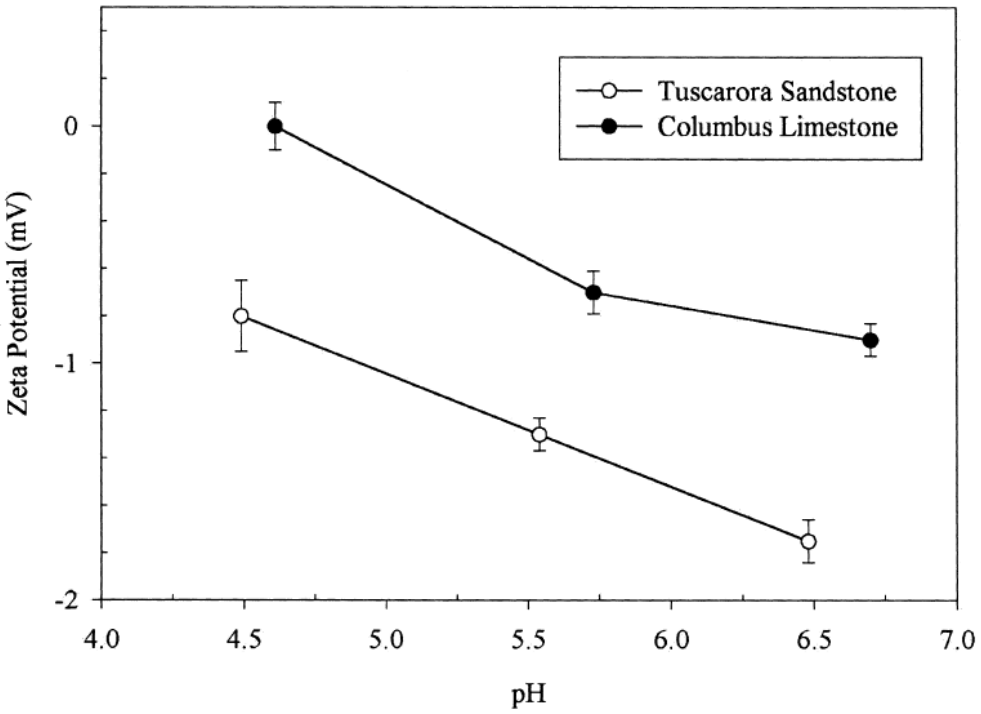

Figure 2-7: Zeta potential versus pH for sandstone and limestone rock samples (Sasowsky *et al*., 2000).

With this in mind trend in wettability change for a mineral and rock can be explained as follows:

2.23.3 Interpretation for Non-Cation Exchange Reaction Scenario

By referring to Eq. (2-73) the point of zero charge pH of a pure solid (quartz or calcite) is smaller compared to the case where it is regarded as rock (sandstone or limestone). The implication is that wettability changes for a given pH of aqueous solution where there is no cation exchange reaction will be bigger. On the contrary, the equation for rock (2-74a), shows that wettability change under the same condition of no-cation exchange reaction will

be smaller. The obvious reason is that the effective point of zero charge pH of the system is bigger compared to its pure state defined by Eq. (2-73)

2.23.4 Interpretation for Cation Exchange Reaction Scenario

The effect of cation exchange reactions typical of rock/ sedimentary rocks with argillaceous and or phyllisilicate minerals is to deplete solution protons added by dissolution of carbon dioxide or acidification of formation brine in this case. This is possible because, hydrogen ion in solution are exchanged for framework cation of phyllosilicate minerals (Yadav *et al*., 2000). This can cause pH change to be resisted and this means buffering. In this regard, since formation brine pH buffering can ony be caused in rock medium, the implication for the rock system is that the following equation can be written

$$d\cos\theta = \frac{2.303^2 RT}{F\gamma_{LV}}\left(\frac{2\pi}{\varepsilon n k_B T}\right)\left(pH - pH_{pzcr}\right)dpH \approx 0 \quad \text{(2-74b)}$$

For $dpH \approx 0$ due to buffering.

The overall implication is that for rock systems, wettability changes less compared to mineral systems.

2.24 THEORETICAL BASIS OF WETTBILITY EVOLUTION

Under field conditions typical of geological carbon storage the principal cause of wettability evolution is change in solid-liquid interfacial tension. This parameter is pH dependent in accordance with the following equation (Chatelier, *et al*.,1995)

$$\gamma_{SL} = \gamma_{SL}^{0} + \gamma_{SL}^{ion}\left(pH\right) \quad \text{(2-75)}$$

In which γ_{SL} is the solid-liquid interfacial tension, γ_{SL}^{0} is the component of solid-liquid interfacial tension at the point of zero charge pH and $\gamma_{SL}^{ion}\left(pH\right)$ is the free energy per unit area required to form surface charges from surface ionizeable hydroxyl group relative to the point of zero charge pH

In petroleum engineering and allied disciplines, the theory of wettability quantifies this petrophysical parameter in terms of interfacial tensions between phases as (Liu *et al*., 2010):

$$\cos\theta = \frac{\gamma_{SV} - \gamma_{SL}}{\gamma_{LV}} \tag{2-74b}$$

In which θ is contact angle, γ_{SV} is solid-vapor interfacial tension, γ_{SL} is solid-liquid interfacial tension and γ_{LV} is liquid-vapor interfacial tension

Generally, as pH decreases due to gas injection the pH dependent component increases (Fritz, *et al*., 2000). At a given pressure when the solubility of carbon dioxide in brine is constant the density difference between brine and carbon dioxide is constant so the interfacial tension between them is also constant. Solid-vapor interfacial tension is constant. That means increases in solid-liquid interfacial tension will lead to wettability decrease in accordance with Eq. (2-75).

2.25 POSSIBLE TRENDS IN pH INDUCED WETTABILITY EVOLUTION

With regard to the point of zero charge pH and formation water pH three possible cases can be distinguished during carbon dioxide injection into saline aquifers. They are the following:

2.25.1 Case 1: Point of Zero Charge pH is Equal to or Near Formation Water pH

Case one is when the formation water pH is equal or close to the point of zero charge of the aquifer rock mineral surface. In the sedimentary basin, increase in salinity results in pH decrease (Hanor, 1994). In basins characterized by salt diapirism such as in the North Sea and the United States Gulf Coast it is possible for pH to decrease from 7 to 3 (Hanor, 1994). Where the target aquifer is sandstone such as the geologic repository for the Sleipner carbon dioxide injection project the point of zero charge pH will be that of silica which is on the average 3 (Kosmulski, 2004). In this case Eq. (2-70):

$$cos(\theta) = cos(\theta)_o + \zeta[0.5pH^2 - pH_{PZC}pH + (pH_{PZC}pH_o - 0.5pH_o^2)] \tag{2-75}$$

This gives:

$$cos(\theta) = cos(\theta)_o + \zeta[0.5pH^2 - pH_{PZC}pH] \quad (2\text{-}76)$$

This equation shows that for cases where the formation water pH is equal to or near the point of zero charge pH of rock surface, the wettability at a given pH during CO_2 injection following pH decrease will depend on the point of zero charge pH. The bigger this value the lower will be the wettability and vice versa and this will be encountered in cases where there is no pH buffering reaction due to carbonate cement dissolution or silicate hydrolysis (Guntera *et al.,* 2000). Since pH will normally decrease with carbon dioxide injection these types of aquifers are presumably the best because the low water wettability will ensure high relative permeability of this phase and low relative permeability of the injected gas phase that will enhance favorable mobility ratio for enhanced sweep efficiency.

Generally, the equation also shows that the wettability of such a system is generally very low with regard to water as pH decreases because the system is already near of close to its minimum wetting state with regard to pH. This corresponds to electrocapillary maximum in electrowetting systems corresponding to maximum solid-liquid interfacial tension (Shao, *et al*., 2010)**.**

2.25.2 Case 2: Point of Zero Charge pH is less than Formation Water pH

In this case Eqn. (2-70) is recalled as:

$$cos(\theta) = cos(\theta)_o + \zeta[0.5pH^2 - pH_{PZC}pH + (pH_{PZC}pH_o - 0.5pH_o^2)] \quad (2\text{-}70)$$

This situation is what is normally encountered for cases of carbon dioxide geosequestration in normal formation waters where salinities are not ultra-high. The salinities here are generally between 7 and 8 with a mean value of 7.4 (Petalas & Diamantis, 1999):

Under this condition, the second term in the bracket on the right hand side of this equation is less than the first term. This gives a net positive, which together with the negative sign in front of the bracket will produce a positive figure. There are three positive terms on the right hand side of this equation and this means that under this condition the water wettability at a given pH is more than that of the case where the formation water initial pH is closer to the point of zero charge pH during carbon dioxide injection. Under these

conditions too, wettability will decrease with decrease pH and this is a generalized interpretation. This will enhance sweep efficiency of gas injection**.**

2.25.3 Case 3: Point of Zero Charge is Greater than Formation Water pH

This situation could arise where carbon dioxide is injected into formation waters hosted by non-conventional saline aquifers such as fractured or brecciated basalts (McGrail, *et al*., 2006). Petrologically, this type of aquifer consists predominantly of olivine with end members being fosterite and fayalite. The point of zero charge of these minerals is around 8: Fosterite–8.8) (Sverjensky & Sahai, 1996).

In this case the second term in the bracket on the right hand side of this equation becomes more than that of the first term. This gives a net negative which together with the negative in front of the bracket will give a positive term. In this case the difference is not so high so water wettability at a given pH during carbon dioxide injection will, therefore, be higher or simply put pH decrease following gas injection will lead to wettability increase.

2.25.4 Implication for Different Saline Aquifer Rocks

Saline aquifer rocks can be divided into two categories based on the ability of minerals found in the rocks to buffer formation water pH. Normally carbonate cement and mica minerals found in sandstones saline aquifers will tend to buffer formation water pH through hydrogen ion reaction with carbonate cement minerals (iron and magnesium carbonate) and through cation exchange reactions respectively. Any of these reactions has the capacity to deplete added hydrogen ions from carbonic acid dissociation leading to pH buffering. Wallace sandstone is a typical example of this type with 82% silica (Quarry, 2001) and significant amount of glauconite and mica.

The other types of siliciclastic saline aquifers are the predominantly monomineralic types which have close to 99 percent quartz (Ruffet *et al*, 1991) . This aquifer will not be capable of formation water pH buffering and wettability changes during carbon dioxide injection into these aquifers will depend on variations of the three interfacial tensions found in Yong's equation. In the case of those with formation water pH buffering capability the change in wettability will depend on changes in solid-gas and liquid gas interfacial tensions.

The third type of saline aquifer rock deserves to be distinguished because they are monomineralic in calcite. These are the carbonate formations. In these saline aquifers there is abundant calcite to react with added hydrogen ion to the extent that pH increases can occur after some time and this can lead to decreases in sold-water interfacial tension leading to eminent wettability change. It is, however, important to mention that in those siliciclastic saline aquifers where there are formation water pH buffering mechanisms the minerals responsible for these (iron and magnesium carbonates) occur as accessory or subordinate minerals. This means that excess of hydrogen ion concentration following high gas saturation can lead to this pH buffering mechanism to be lost.

2.26 PRESENT RESEARCH TOPIC

To provide contact angle data for the system CO_2-water-rock, the present work will utilize rock samples from potential geologic repositories with promising global storage capacities. To also replicate past works, the present work will choose two mineralogically distinct sandstones. They are Wallace sandstone with variable chemistry and Fontainebleau sandstone with 99% quartz.

The present work will also pursue its theoretical objective by carrying out a mathematical model of the pH induced wettability change on minerals surfaces.

2.27 SUMMARY AND CONCLUSIONS

The principal objective of this thesis work is to research wettability evolution accompanying anthropogenic CO_2 into saline aquifers due to water rock interaction phenomena. In this chapter, the theoretical foundations underlying notably, free energy change of spontaneous imbibition processes that are intimately linked to wettability have been thoroughly reviewed to aid understanding of wettability evolution. Accordingly, the cause of wettability evolution in such systems, namely solid-liquid interfacial energy evolution due to pH changes been clearly explained in the context of the surface chemistry of reservoir rocks. The theoretical basis for the computation of contact angle and free energy change of spontaneous imbibition has also been thoroughly established. What is more, the net effect of pH changes following CO_2 injection is seen in wettability changes

which result from changes in solid-liquid interfacial tension. Accordingly, the relationship of solid-liquid interfacial energy to the pH of aqueous media and the point of zero charge pH of the solid surface has also been established. Also, thermodynamic and fractional flow theories required to deal with cases of mutual phase solubility have been established. Cation exchange reactions and surface adsorption reactions are two geochemical reactions pertinent to water rock interactions. The theoretical basis of cation exchange reaction has been reviewed.

Prior to the injection of CO_2 into a saline aquifer, the interfacial tension or energy between reservoir/aquifer rock surface and water has a fixed value determined by the state of formation water salinity,temperature and pH. As CO_2 is injected, the dissolution of this gas will alter formation water pH. From intermolecular forces theory of surface and or interfacial tension, the interfacial tension can be regarded as being the sum of the contributions from Lifshitz-van Der Waals and polar contributions which have electrosataic origin (Oss *et al*., 1988a). pH alteration following carbon dioxide injection will modify the surface charge of rocks. This interfacial charge development will cause change in the contributions of the acid and base components of solid-liquid interfacial tesnion. From Young's equation, the contact angle which is the thermodynmaic measure of the wettability of the system; aquifer rock surface-water-carbon dioxide is controlled by three major interfacial tensions/energies related to the interfaces of the system. They are, solid-gas interfacial tension, water-gas interfacial tension and solid-water interfacial tension. Under conditions typical of geological carbon sequstration where pressures are in excess of 15 MPa with hypersaline formation brine, the interfacial tension of liquid-gas as well as solid gas will be practically constant (appendiec 3-1 and 4C)**.** Therefore, the major interfacial tension that will control water wettability of aquifer rock surface is the solid-liquid interfacial tension which evolves in response to carbon dioxide dissolution and acidity increases. The predominant cause of system wettabililty change related to carbon geosequestration is, therefore, pH variation. This chapter of the thesis work has shown theoretically the dependence of wettability on pH. In addition to this major task, it has also shown the parallel phenomenon related to electrostatic induced wettability modification by drawing an example from the electocapillary phenomenon in the colloid industry**.**

For the sake of anthropogenic carbon storage in siliciclastic saline aquifers, two types can be identified.They are the quatz rich (quartz arenite) and high to moderate quartz containing saline aquifer rocks (Mcbride, 1963; Suttner *et al*., 1981). The latter type often has significant amount of authigenic minerals like mica and glauconite among others, that have the potentential to buffer formation water pH during carbon dioxide injection. This, therefore, has the potential effect of oppossing wettability change despite carbon dioxide dissolution. The next chapter of this thesis work will be devoted first to testing experimentally the pH wettability relationship derived in in this chapter and second to determining the response of different saline aquifer rocks to pH induced wettability evolution. The later task will employ two mineralogically distinct saline aquifer rock types. The extent of pH buffering reactions for these types of rocks will also be experimentally investigated.

With this goal in mind, the principal motivation with regard to experimantal design is that the major cause of contact angle or wettability changes under *in situ* geologic conditions of carbon dioxide injection is change in solid-liquid interfacial tension induced by ionization of surfcace hroxyl groups in response to formation water pH changes. Therefore, any experimantal set up that can lead to realization of this major physiochemical reaction while pH is varied will provide similar experimental conditions for study. Consequently, the spontaneous imbibition flow into porous or capillary tubes where capillary presure gradient is the major driving force will be exploited for achieving the exeperimental objectives. In this set up, synthetic formation brine of varying pH will be made to imbibe into samples of porous media filled with air as the non wetting phase fluid.

The motivation for the choice of the spontaneous imbibition method stems from the fact that dewetting of a mineral surface by carbon dioxide-brine-solid interaction is caused principally by water rock reaction that becomes effective when the pH of brine changes. In this regard, it is not carbon dioxide direct interaction with solid surface that causes dewetting. In the end, previous researchers measured contact angles that evolved due to pH changes and this pH change is caused by the formation of carbonic acid in brine and its subsequent dissolution that increases hydrogen ion activity. Therefore, any means that can be used to replicate pH change in the presence of a mineral/rock surface while information

about contact angle is deduced will lead to realization of experimental goals similar to those of previous researchers. In this reagrd, acidifying experimental brine to a given pH level for the spontaneous imbibition experiments is like having carbon dioxide at a given pressure to effect dissolution for the production of carbonic acid which dissociates to establish a corresponding pH level in the case of previous researcher.

To test the Hypothesis that rocks with different mineral aggregates will have difference response to pH changes and wettability evolution in saline aquifer following carbon dioxide injection, samples of siliciclastic rocks of different varying authigenic mineral (clay mineral) concentration will be used for cation exchnage reaction experiments.

In the published work of Carre *et al.,* (2003), a parabolic fit was obtained for an experimental data involving a chemically modified silica surface. In this regard, a plot of the cosine of the contact angle (wettability) and the pH of aqueous solution (Figure 5) and that of contact angle and pH of aqueous solution (Figure 4) agree with the model in the present work. It is worth mentioning here that while the experimental data fit gave a parabolic trend with an excellent regression, there was no prior model. By integrating Nernst equation of electrochemistry and surface charge density theory with the equation given by Carre *et al.,* (2003), Eq. (3-2), the parabolic trend has been explicitly and mathematically proven.

This chapter has therefore, fully established all theoretical concepts required for achieving its principal objectives. What is more, it has invoked the concepts of intermolecular forces as encountered in the system CO_2-water and rock in addition to invoking the fundamental tenets of the molecular kinetic theory of wetting to establish the fact that contact angles measured so far for these systems which are models of what is expected in the actual geologic medium of CO_2 storage lack the overall acid base interactions of the entire system.

CHAPTER 3

3. DERIVATION OF CONTACT ANGLE UNDER DRANAGE FLOW CONDITIONS

3.1 Relationship of Wettability to Multi-Phase Flow in Porous Media

Wettability is a fundamental petrophysical parameter related to multi-phase flow in porous media and it determines the flow and distribution of phases in time and space. Therefore, multi-phase porous media fluid flow data related to imbibition and drainage contain indirect information about wettability or contact angle. The objective of this section is to derive an equation for calculating contact angle from drainage flow data. This will provide the opportunity for calculating contact angles from drainage relative permeability data from mineralogically distinct rock samples as part to the approach to testing the principal hypothesis.

Leveret introduced the universal capillary pressure function which links capillary pressure to a J function, which depends on saturation and the average pore throat radius of the sediment. This equation gives (Nam and Kaviany, 2003; Krause *et al*., 2009):

$$P_c = \gamma_{gl} \cos\theta \sqrt{\frac{\phi}{K}} J(S_w) \tag{3- 1}$$

in which $P_c, \gamma_{gl} \cos\theta, \sqrt{\frac{\phi}{K}}, J(S_w)$ are capillary pressure (Pascal), interfacial tension between CO_2 and water, contact angle for the system, reciprocal of average pore diameter (m) and Leveret J function (dimensionless) respectively.

To calculate capillary pressure, the proper form of the Leveret function must be used. This is given as (Silin *et al*., 2009):

$$J(S_w) = A\left(\frac{1}{S_e^{c_1}} - 1\right) + B\left(\frac{1}{S_e^{c_2}} - 1\right)^{1/c_2} \tag{3-2}$$

in which

$$S_e = \frac{S_w - S_{iw}}{1 - S_{iw}} \tag{3-3}$$

In which A, B, c_1, c_2 are fitting parameters, S_w is water saturation [fraction] and S_i is irreducible water saturation [fraction]

This equation is written with the curve fitting parameters as (Nam & Kaviany, 2003):

$$J(S_w) = 0.0038\left(\frac{1}{S^{c_1}} - 1\right) + 0.28\left(\frac{1}{S^{c_2}} - 1\right)^{1/c_2} \tag{3-4}$$

Equation (3-1) can now be written as:

$$\gamma_{gl}\cos\theta = \frac{P_c}{\sqrt{\frac{\phi}{K}}J(S_w)} \tag{3-5}$$

The relationship between capillary pressure, breakthrough capillary pressure and effective saturation is given as (Kewen, 2004):

$$P_{dc} = P_b\left(\frac{S_w - Siw}{1 - S_{iw}}\right)^{-1/\lambda} \tag{3-6}$$

in which P_{dc} is drainage capillary pressure, P_b breakthrough capillary pressure and S_{iw} is irreducible water saturation, S_w is water saturation in drainage flow experiments and λ is the pore size distribution index.

Substitution Eq. (3-6) into Eqn. (3-5) gives:

$$\gamma_{gl}\cos\theta = \frac{P_b\left(\frac{S_w - S_{iw}}{1 - S_{iw}}\right)^{-1/\lambda}}{\sqrt{\frac{\phi}{K}}J(S_w)} \tag{3-7}$$

The thermodynamic significance of Eqn. (3-7) can be realized by reference to the definition of interfacial tension and the cosine of the contact angle. The interfacial tension between brine and water is the force per unit length measured at the interface or the thermodynamic work done required to create unit interfacial area (Rosen & Kunjappu, 2012) while the cosine of the contact angle is the wettability (Checco *et al*., 2003) of the system carbon dioxide, water and rock. The unit of interfacial tension is force per unit length while the

cosine of contact angle is dimensionless. In the molecular kinetic theory of wetting (Blake & Coninck, 2002; Petrove & Petrove, 1992) the product of these two thermodynamic quantities represents a driving wetting force in the partial wetting domain. Under constant wettability conditions the product must be constant for the system while under varying conditions of contact angle or interfacial tension or both the product must change accordingly. This equation will be used later in this work together with the proper form of Leveret J function as given by Eqn. (3-4) for testing pH buffering capacity of different sandstones, using drainage relative permeability data. It will also be used to calculate contact angle for constant wettability conditions.

3.2 DERIVATION OF PORE SIZE DISTRIBUTION INDEX FROM DRAINAGE RELATIVE PERMEABILITY DATA

The utility of Eq. (3-7) lies in its ability to calculate the product of the interfacial tension and wettability which measures wetting tendency. To be able to do that, information about the macroscopic parameter of pore size distribution must be known. The following approach gives details for determining this parameter from drianage relative permeability data:

The relationship between water drainage relative permeability, effective water saturation and the pores size distribution index is given as (Oostrom & Lenhard, 1998;Flett *et al*., 2004):

$$k_{rw} = S_e^{\eta} \tag{3-8}$$

In which k_{rw} is water drainage relative permeability, S_e is effective saturation Eq. (3-3) and $\eta = \frac{2}{\lambda} + 3$

Taking logarithm of both sides and plotting logarithm of water relative permeability versus logarithm of effcetive saturation gives a straight line where the gradient can be solved for lamda and the absolute value used. Thus, lamda is equal to:

$$\frac{2+3\lambda}{\lambda} = \frac{d\log krw}{d\log Se} \tag{3-9}$$

Equation (3-8) enables calculation of the pore sized distribution index given the definition of effective water saturation and the gradient of the plot.

Purcel also presented the following equation for water drainage relative permeability (Li & Horne, 2002):

$$k_{rw} = S_e^{\frac{2+\lambda}{\lambda}} \tag{3-10}$$

In the literature, experimental evidence shows that Brook-Corey equation (3-8) calculates water relative permeability lower than experimental values while Purcell's model calculates water relative permeability that matches experimental data. What is more, Eq. (3-10) can be treated similar to Eq. (3-8) to obtain information about the pore size distribution index. In the present work, Eq. (3-10) was used to generate information about this parameter. Also, given water relative permeability versus effective saturation data this parameter can be calculated for every saturation and the average value computed. Thus,

$$\lambda = \frac{2logS_e}{logk_{rw} - logS_e} \tag{3-11}$$

3.3 CALCULATION OF CONTACT ANGLE FROM CAPILLARY RISE

If a capillary tube is dipped into a beaker containing water, capillary imbibition results in an equilibrium height above the level of water in the beaker that can be linked to contact angle, gravitational constant, density of imbining fluid, surface tension of imbining fluid and capillary radius as:

$$\cos\theta = \frac{\rho g r}{2\gamma_{LV}} h_e \tag{3-12}$$

In which θ is contact angle, ρ is density of imbining fluid, g is gravitaional constant, r is capillary radius, h_e is equilbrium constant and γ_{LV} is the liquid-vapor interfacial tension, here taken to be equal to the surface tension of imbibing fluid.

CHAPTER 4 EXPERIMENTAL PROGRAM

The objective of this chapter is to test the wettability-pH relationship derived in Chapter 2. This chapter outlines the design of suitable experimental programmes for testing concepts relating to possible formation water pH buffering due to the presence of diagenetic minerals and effect on contact angle evolution.

One cause of wettability decrease in the system carbon dioxide-brine-solid/rock is the water rock interaction reaction which leads to increases in solid-liquid interfacial tension as explained in Chapter 2. The goal of the experimental set up is to realize water rock reaction by causing brine at a given pH to imbibe spontaneously into an air filled porous filled system. In this way, water rock interaction caused by proton adsorption at ionized surface sites in the porous system will cause wettability evolution similar to that in actual geologic systems.

4.0 EXPERIMENTAL PROGAMS AND OBJECTIVES

4.0.1 Capillary Imbibition Experiments

The mathematical model (Eq. 2-70) developed in this thesis resulted in a parabolic relationship between wettability and aqueous solution pH. The objective of this experimental design is to test this equation by varying the pH of water imbibing into a capillary tube at room temperature. Wettability will be quantified by contact angle calculation using a capillary rise equation.

4.0.2 Rock Imbibition Experiments with Wallace Sandstone Core Samples

Wallace sandstone contains 82% silica (Quarry, 2001) and significant amounts of glauconite and mica. The objective of this experiment is to show the potential for these authigenic minerals to buffer formation water pH and to also resist wettability changes during CO_2 injection. This experiment will therefore test the principal hypothesis of this study.

4.0.3 Rock Imbibition Experiments with Fontainebleau Sandstone Core Samples

Compared to Wallace sandstone from Wallace, Nova Scotia, Fontainebleau sandstone has 99 percent silica (Timothy, *et al.*, 2006) (see Table 1) with quartz cement. It is, therefore, an extreme case compared to Wallace sandstone. It is, therefore, expected that lack of

significant amount of diagenetic minerals will cause significant pH changes in saline aquifers hosted by this rock during CO_2 injection and will lead to pronounced wettability change. This experiment will further test the principal hypothesis.

4.0.4 Sand Pack Experiments

This system is mineralogically similar to that used elsewhere (Kim *et al*., 2012) but structurally different due to its role as a porous medium rather than a simple mineral surface on which contact angle can be measured. Spontaneous imbibition contact angle determinations from these experiments will represent those of silica-water systems where pH induced surface reactions can produce contact angle changes similar to those of simple mineral surfaces. In the present study, there is material limitation with regard to Fontainebleau sandstone core sample. The objective of this experiment is to be able to conduct more experiments with a representative porous medium similar to that of Fontainebleau sandstone. The sand pack consisting of silica will enable realization of this goal since Fontainebleau is 99% silica. To achieve this objective sand grains will be loaded into custom built imbibition tubes to produce porous system with the desired composition.

4.0.5 Investigation of Cation Exchange Reaction

These experiments are design to test the potential of authigenic minerals to influence pH induced wettability change in CO_2-Brine-silica systems. These constitute the third experimental design that will test the principal hypothesis of this work. This experiment will be conducted by milling samples of Wallace sandstone and Fontainebleau sandstone. Known weights of powdered samples will then be added to acidified brine and pH versus time of aqueous solution will be recorded to detect cation exchange reactions if any.

4.1 MATERIALS AND EQUIPMENT

4.1.1 Geologic Materials

To systematically achieve the theoretical objective of this study, two sandstone core samples with distinct variation in mineralogy were used. One was Wallace sandstone. This is glauconitic sandstone that occurs in the late Jurassic to early cretaceous unit of the Scotian Group. The geological motivation for the choice of this sandstone is that the Scotian Group contains thick units **(**Appendix 4D) of this glauconitic sandstone that are potential targets for carbon geosequestration. Appendix 4E gives the chemical composition

of this sandstone as given by the Mineral Processing Laboratory of Dalhousie University. Color wise, it is greyish green with distinct shiny minerals. All cores used were drilled from one chunk of rock procured from the Wallace Quarry in Nova Scotia. The cores were drilled with water as the lubricating fluid and later cut into the required length and diameter using a different machine with oil as lubricating fluid. They were thoroughly cleaned to remove chemicals and oil stains using a combination of toluene and alcohol. The average value of porosity measured was 12% and that of permeability was 0.7 mD. These values, particularly porosity, compare quite well with those deduced in this laboratory in oil recovery experiments (appendix 4O) using these sandstone core samples. The cores had diameter equal to 38 mm and length equal to 76 mm.

The other sandstone is Fontainebleau from the Dogger Formation in France. This sandstone is quartz arenite with 99 percent quartz and quartz cement (Lindquist & Venkatarangan, 2000). It is Eocene of age and looks dull white in appearance. The samples were purchased from Vinci Technology in France. They had already been used in previous core flooding tests involving oil recovery. The cores were therefore cleaned for use in this study. After thorough cleaning the porosities of the cores were determined using the imbibition method.

4.1.2 Characterization

Petrophysical characterization of core samples was achieved using two approaches that are standard in the petroleum industry. The porosity of the core samples was determined using the imbibition method. In this method, the core samples were initially cleaned to remove stains due to fluid used in drilling. The cores were weighed empty and then put in a beaker of brine which was left in a vacuum chamber **(**Stable vacuum oven model 281A) for saturation overnight. The saturated core was then retrieved and weighed. The difference between the wet weight and the dry weight gave the mass of brine occupying the pore space. The volume of brine was obtained by dividing this mass by the density of brine at experimental conditions. Porosity was calculated by dividing the volume of brine by the bulk volume of core sample.

Permeability was determined using the Bench top relative permeability core flooding equipment manufactured by Vinci Technology of France (Figure 4-2). A plot for pressure drop versus flow rate for Fontainebleau sandstone test is seen in appendix 4F

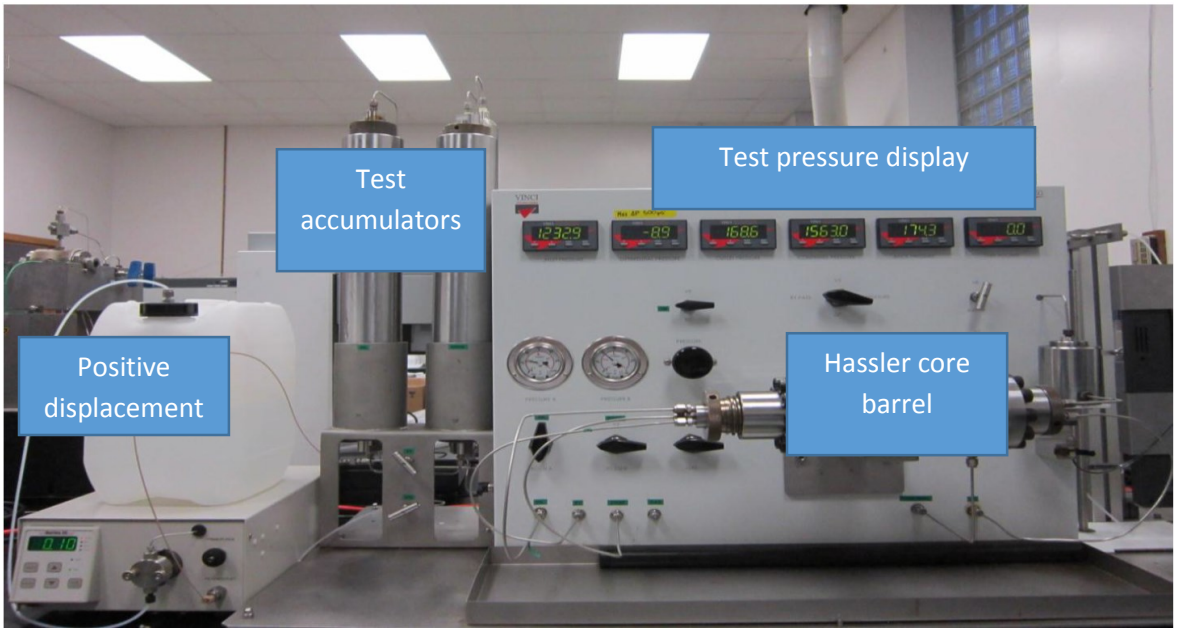

Figure 4-1b: Bench Top Core Flooding Equipment with 2 accumulators and Hassler Core Barrel

The system is operated using a positive displacement pump and testing is digitally monitored using a programmed installed on a computer.

4.1.3 Brine pH Measurement

The pH was measured with a double junction probe (pH TESTR 30) capable of measuring to two decimal places with an error of 0.01 pH. Adjustment of the pH of aqueous solution was achieved by using nitric acid.

4.1.4 Brine Preparation and Core Sample Characterization

Experimental brine was prepared using laboratory grade sodium chloride and calcium chloride manufacture by Sigma Aldrich. The chemicals were used without further purifications. The brines were degassed and store at room temperature before spontaneous imbibition experiments. Dominant ions of formation brine sample belonging to the Carboniferous of Sydney Basin (Cape Breton) (Martel *et al*., 2001) were used. This consisted of dissolving 21.3 g of calcium chloride dihydrate and 110 g of sodium chloride in 1-dm^3 of distilled water. These correspond to the weight of individual solids found in this basin brine. This gives total dissolved solute of 132300 mg/l

4.1.5 Contact Angle and Free Energy Change Computation

The equations for calculating contact angle and free energy change of spontaneous imbibition contain petrophysical parameters (porosity and permeability), the dynamic viscosity of the imbibing fluid and the interfacial tension between the imbibing fluid and air content of the porous medium. The calculations of contact angle and free energy change assumed that the addition of acid did not change the interfacial tension between brine and air to a measurable extent. This is seen from appendix 4M for hydrochloric acid for values of pH typical of those used in these experiments.

4.2 EXPERIMENTAL PROCEDURES UNDER AMBIENT CONDITIONS

4.2.1 Capillary and Rock Imbibition Experimental Procedures

All spontaneous imbibition experiments involving capillary tube, Wallace and Fontainebleau Sandstone core samples, and sand packs porous systems were performed at room temperature. In the capillary tube experiments, pH control of aqueous solution was achieved using dilute nitric acid. The use of dilute nitric acid stems from the fact that in the pH induced wettability change it is the protonation of solid surface deprotonated sites that results in solid-liquid interfacial tension change leading to wettability change. This acid will dissociate to produce hydrogen ions for this reaction.

The capillary tube was glued to the side of a scale to make it easier to read height rise of the meniscus. The experimental set-up is seen in Fig. 4-2 and Fig. 4-3. Figure 4-5 gives the schematics of the set-up. To avoid evaporation of water from the surface of water in the beaker a thin film of mineral oil was poured on the water. To begin the experiment the capillary tube with scale is dipped into the beaker with part of the system below water level. The equilibrium height was then read with the surface of water as the zero level. This procedure was used for different pH of the aqueous solution.

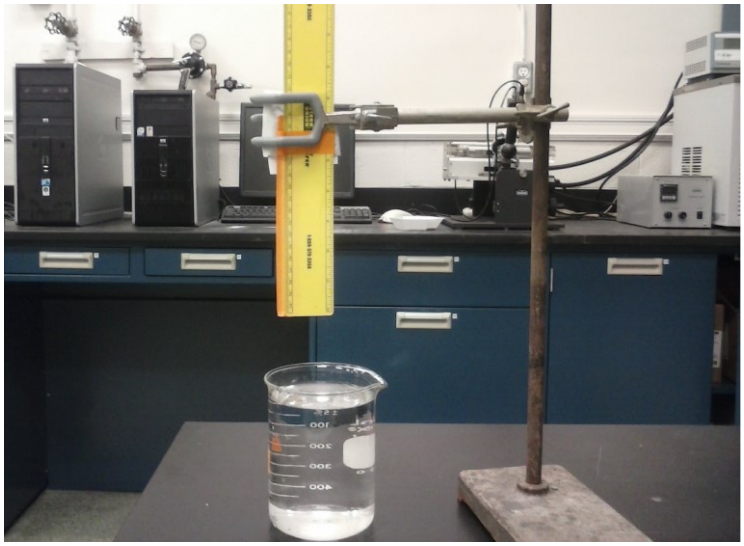

Figure 4-2: Set up for capillary rise experiment

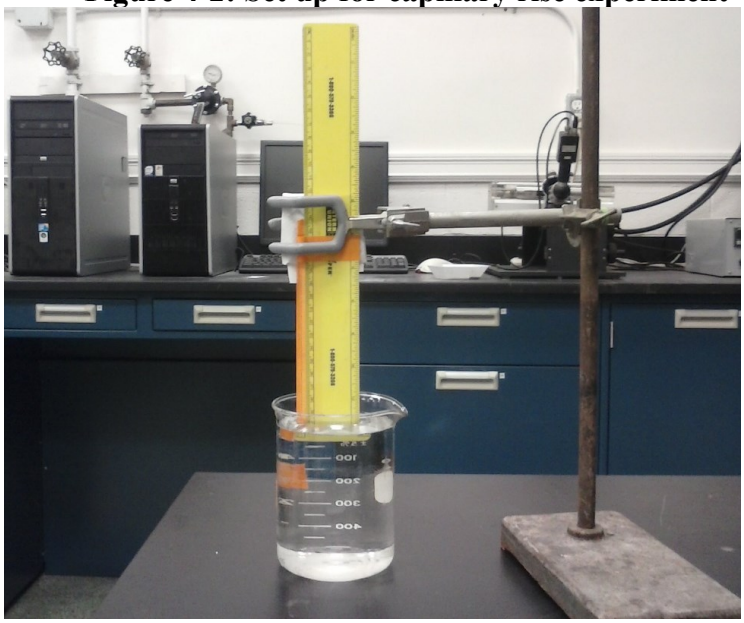

Figure 4-3: Capillary rise experiments in progress

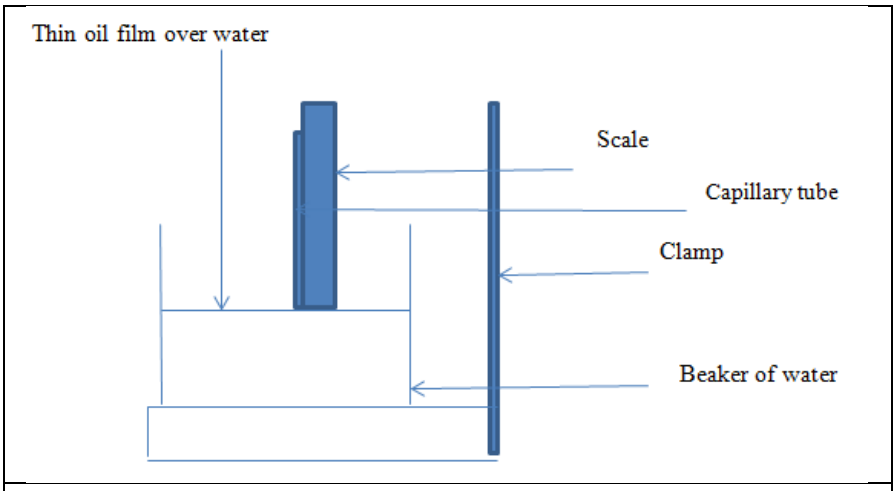

Figure 4-4: Schematic of capillary imbibition set-up

4.2.2 Rock Imbibition Experimental Procedure

Spontaneous imbibition into an air filled core was achieved by maintaining constant contact with the core bottom surface with a beaker of brine at a given pH. To avoid pH changes due to evaporation from the surface of the beaker, a thin film of light oil was poured on the surface of the water in the beaker. Height rise was read from a scale attached to the rock. Spontaneous imbibition time was measured using a stopwatch. Figures 4-5 through 4-7 show the set-ups while Figures 4-6 and 4-7 show experimental images. Figure 4-8 shows the schematic of the set up.

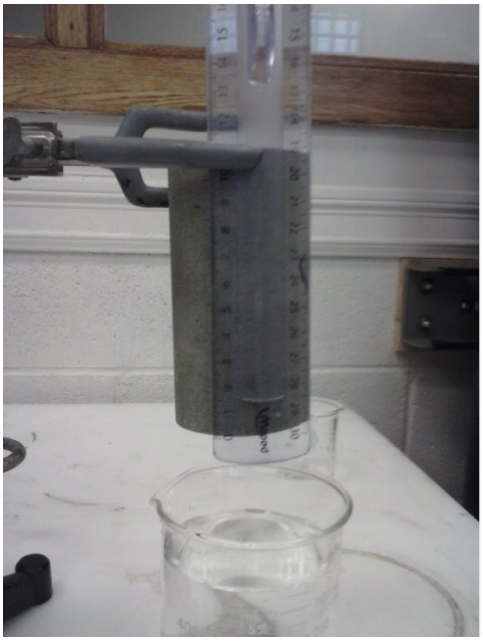

Figure 4-5: Experimental set-up before imbibition

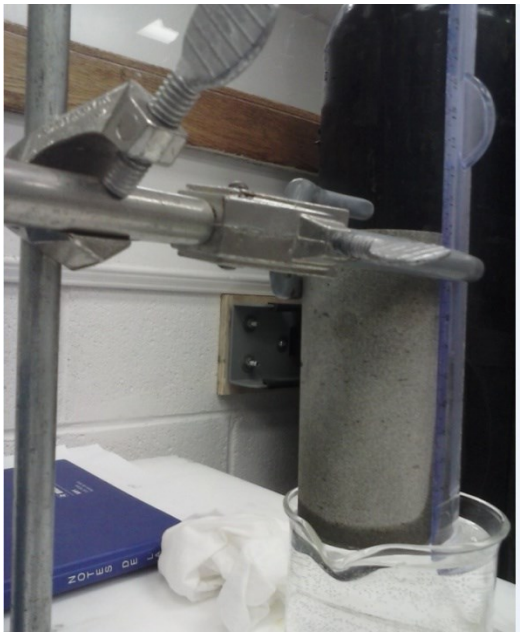

Figure 4- 6: Imbibition front after 52 minutes of rock imbibition

Figure 4-7: Imbibition front after 52 minutes of rock imbibition

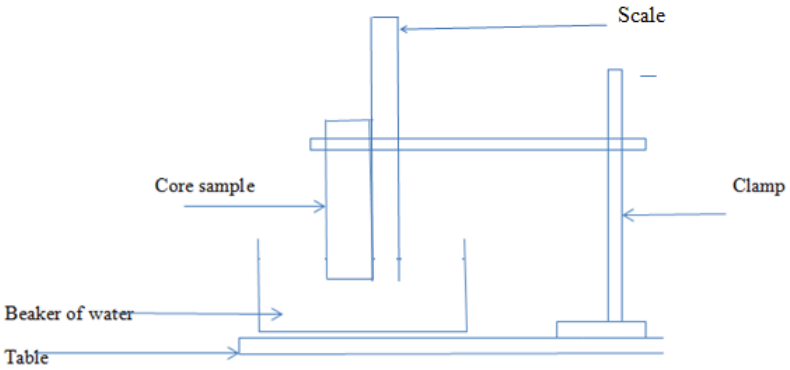

Figure 4-8: Schematic of experimental set up

4.2.3 Sand Pack Imbibition Experimental Procedure

Sand grains were scooped from Dalhousie University Civil Engineering aggregate pit and dried. Normally, sand deposits are mined from sand deposits and they would normally contain some amount of clay minerals. Sand pack porous systems were produced by loading dried sand into custom built imbibition tubes. The custom built imbibition tubes (28 mm Φ × 200 mm long) were made in-house. Figure 4-9 shows these tubes with graduation while Figure 4-10 shows the experimental set up. Figure 4-11 shows the schematics of the set up. To obtain consistent porosity and permeability the loaded tubes

were taped in a consistent number to ensure equal compaction. Spontaneous imbibition of experimental brine of varying pH were conducted and imbibition rise versus time data were acquired.

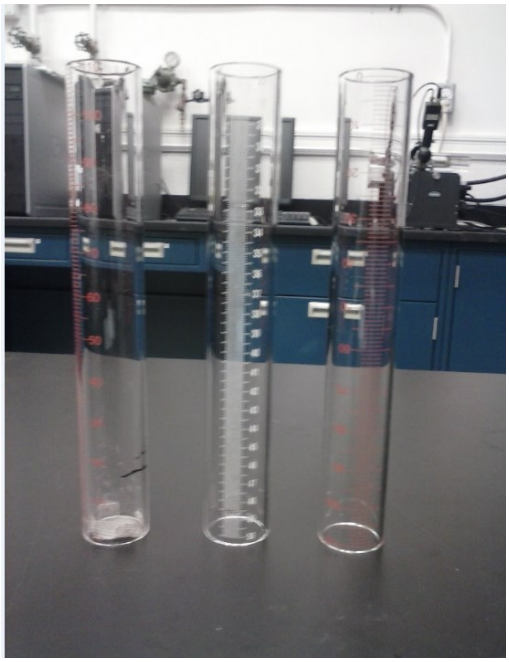

Figure 4-9: Custom built imbibition tubes

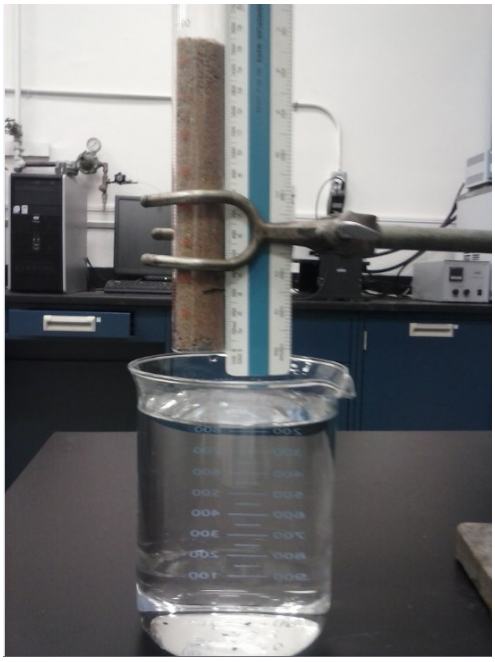

Figure 4-10: Experimental set-up for sand pack imbibition experiment

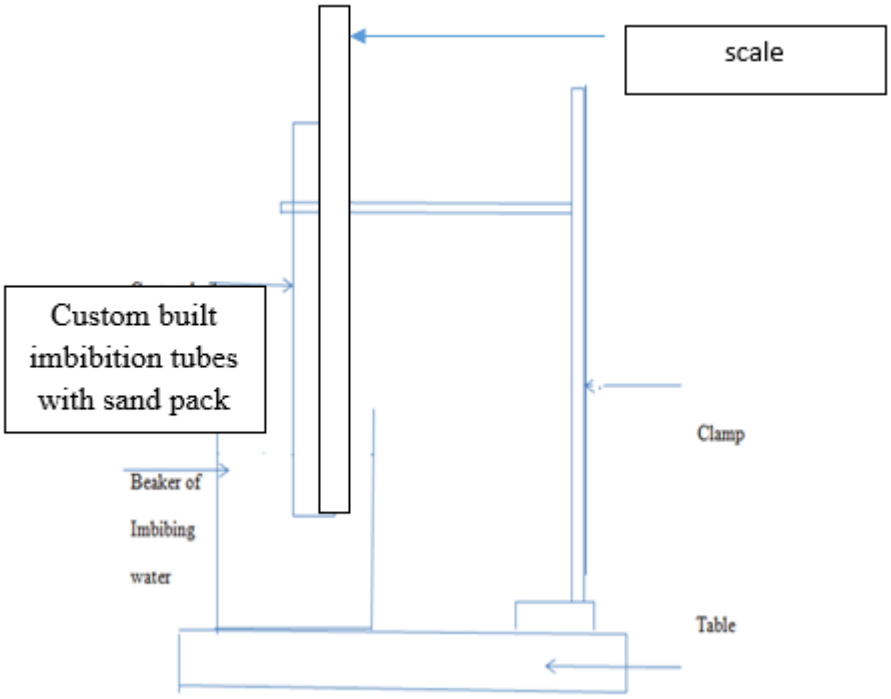

Figure 4-11: Schematic of sand pack imbibition experiment

4.3 CAPILLARY IMBIBITION EXPERIMENTAL RESULTS AND DISCUSSION

The capillary tubes used in this experiment had a diameter of 0.6 mm. Synthetic brine used in spontaneous imbibition experiments were also used for these experiments. Contact angles at varying pH of imbibing brine were calculated using Eq. (3-9).

Figures 4-12, 4-13 and 4-14 give plots of wettability versus pH with regression coefficients of 0.97, 0.94 and 0.91 respectively while Figure 4-15 gives a plot of contact angle versus pH with regression of 0.91.

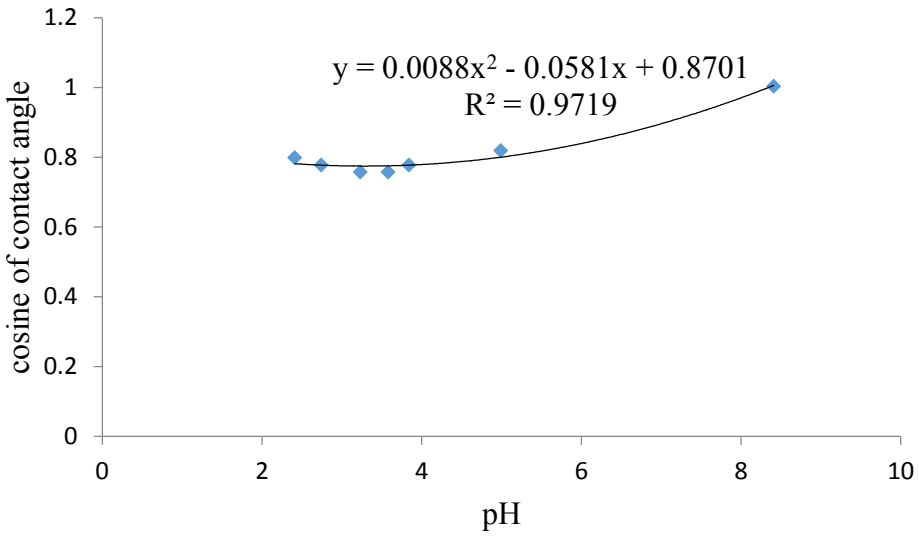

Figure 4-12: A plot of wettability versus pH of brine for experiment 1(from appendix 4.3.1)

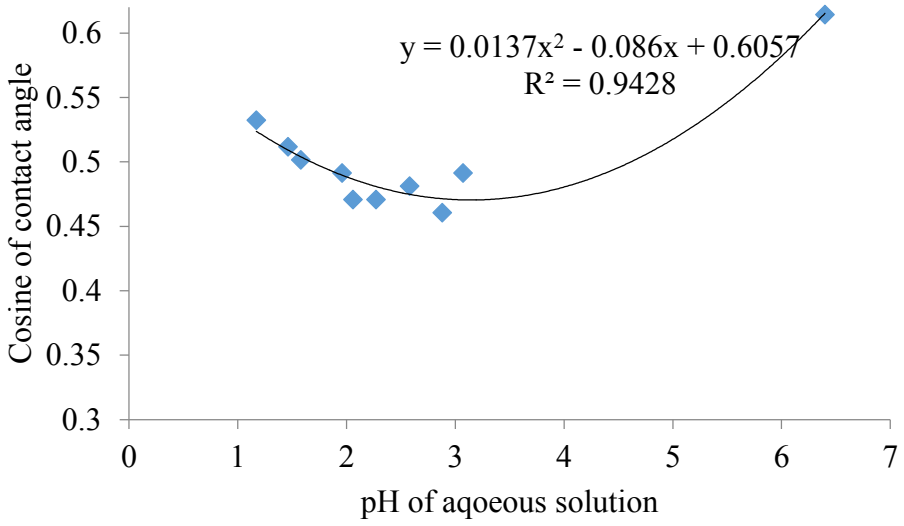

Figure 4-13: A plot of wettability versus pH of brine for experiment 2 (from appendix 4.3.2) replot

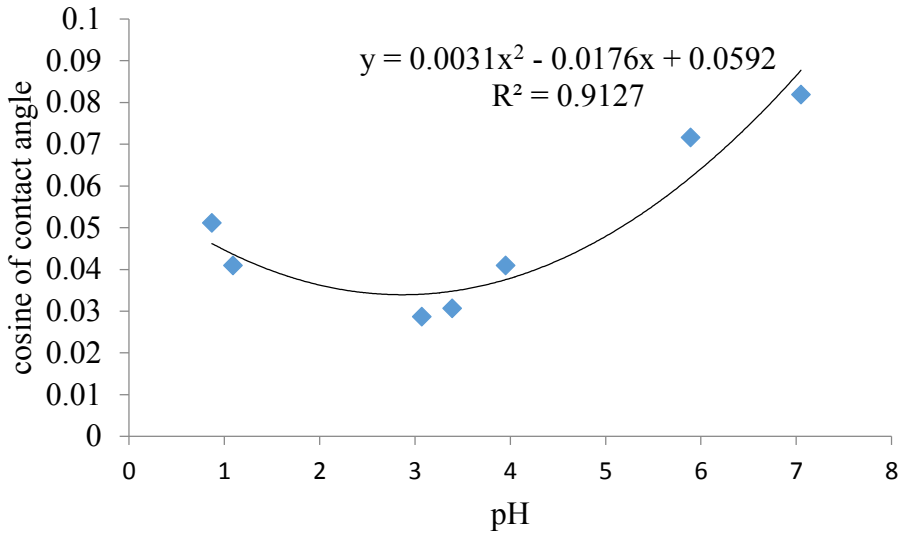

Figure 4-14: A plot of wettability versus pH of brine for experiment 3 (from appendix 4.3.3)

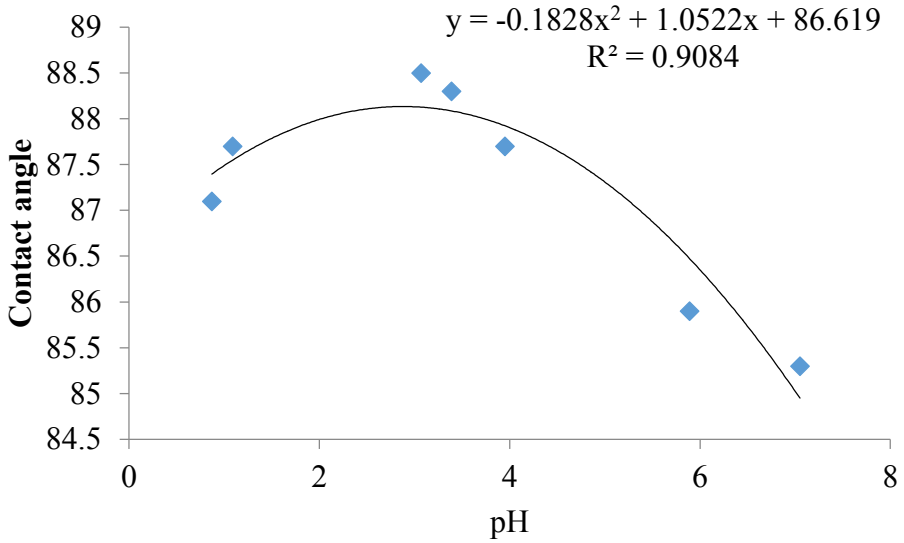

Figure 4-15: A plot of contact angle versus pH of brine for experiment 3 (from appendix 4.3.3)

Figure 4-16 shows a plot of contact angle versus pH where the pH of aqueous solution was adjusted using sodium hydroxide solution. The regression for this plot is the highest with a value equal to 0.99.

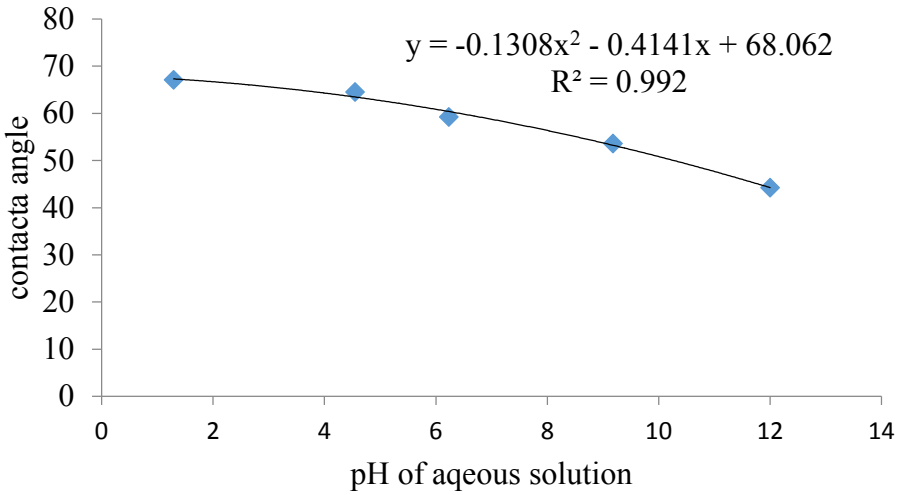

Figure 4-16: Plot of contact angle versus pH using data from appendix 4.3.3.1

Elsewhere (appendix 4-3, Appendix 4.4.2 and Appendix 4N) the graph of contact angle versus pH is similar to those obtained in this study

4.3.1 Validation of the wettability-pH parabolic equation

The equation (2-70) derived in this study that predicts a quadratic relationship between pH and wettability has a coefficient that depends on a number of physical constants. These are listed in Table 4-1. These physical constants were used in appendix 4.4.1. The extent of validity of this equation depends on computation of the coefficients of the quadratic fits using these input parameters. The step-by-step computation given in appendix 4.4.1 using inputs parameters shows that calculated coefficients are quite close to those of the quadratic fits.

Table 4-1 Parameters for input Calculations

Physical Constant	Value
Universal gas constant (R)	8300 J/K/mol
Boltzmann constant (k_B)	$3.8*10^{-27}$ J/K
Temperature (K)	273 K
Faraday constant (F)	96485 C/m
Dielectric constant of brine (ε)	75.44 F/m
Interfacial tension (γ_{LV})	0.073 N/m

The validation of the equation gives the following equations with coefficients:

For experiment 1 (Figure 4-12) substitutions of coefficients gives the quadratic equation as:

$$y = 0.010x^2 - 0.04x + 0.32 \quad (4\text{-}1)$$

From the parabolic fit to experimental data (Figure 4-12) the experimental equation gives:

$$y = 0.0088x^2 - 0.0581x + 0.87012 \quad (4\text{-}2)$$

The coefficients of these equations are appreciably closer

For Figure 4-13, substitution of coefficients gives the quadratic equation as

$$y = 0.010x^2 - 0.04x + 0.51 \quad (4\text{-}3)$$

Parabolic fit to experimental data gives:

$$y = 0.0137x^2 - 0.086x + 0.6057 \quad (4\text{-}4)$$

The coefficients of these equations are also appreciably closer to fitted ones

4.3.2 Calculation of Point of Zero Charge pH of Borosilicate Glass

Theoretically, at the point of zero charge pH of the solid surface the gradient of the plot of wettability versus pH must be zero because this is the minimum wettability. To obtain this pH for the solid surface, the quadratic equations that fit the data are differentiated and equated to zero. The pH, when the resulting equation is solved, is equal to the point of zero charge pH. Using this approach the following are the point of zero charge pH of borosilicate glass surface for the three experiments: Exp #1 = 3.30, Exp #2 = 3.14; and Exp #3 = 2.84, which gives an average = 3.1. Carre *et al*., (2003) obtained 3 for glass in a similar plot.

(Bourikas *et al*., 2003), used different techniques to obtain the point of zero charge pH of quartz. The following were their values for five different methods: 3.1, 3.3, 3.0, 2.9, and 3.2, which gives an average = 3.1. Theoretically derived point of zero charge pH from Figure 4-16 gives 1.58 which is within values expected for glass Marek, 2002-Table 1). Obviously, this value is lower than those deduced from previous plots. It is also lower than

those deduced from the cited reference above. This requires explanation. Actually the experimental data for plotting Figure 4-16 was acquired after using all the available capillary tubes in the first set of experiments where the pH of aqueous solution was reduced using nitric acid acid. Examination of the figures show that ultra-low pH conditions were reached at the end of each experiment. Generally, silicate dissolution is motivated by two principal causes. In the sedimentary basin, silica dissolution due to temperature motivation has been implicated for basin subsidence (Walderhaug *et al*., 2001). Another cause of silica dissolution is pH motivation. This can be extremely high pH (Bauer and Berger, 1998) or extremely low pH.The implication is that silica dissolution by low pH mediation (Knauss and Wolery, 1998; Muhammad *et al*., 2011) was encountered under these pH conditions encountered at the end of the pH reduction experiments. The implication is that surface etching due to dissolution introduced what is known in the wettability literature as a roughness induced wettability (Netz and Andelman, 1997; Herminghaus, 2000; Rupp *et al*., 2004). To see why the resulting point of zero charge pH will be lower than those encountered earlier requires recalling that the quadratic equation (2-70) predicts a higher wettability for a given pH where the point of zero charge pH of solid surface is higher and *vice versa* .In this regard, Figure 4-16 gives contact angles clearly higher, particularly when compared to literature values (Appendix 4.4.2 (iso)). This explains the lower value deduced for Figure 4-16. Also, while it is not within the scope of this thesis work to introduce crystal theory related to the point of zero charge pH it is sufficient to mention that the point of zero charge pH of a mineral surface has been deduced by integrating crystal chemistry. In this regard, Sverjensky, (1994) has contributed to point of zero charge pH determination by adding electrostatic solvation theory to crystal chemistry. Therefore, etching of silica by dissolution will have the effect on crystal that will also affect the point of zero charge pH as found in this work. The reason is that dissolution produces surface with mineral crystals that have weak metal to oxygen bond.

Information from the capillary glass tube manufacturer indicates it is borosilicate or fused glass. This type of glass is preferred in the laboratory because of its very low thermal expansivity and high boiling point (Barz *et al*, 2009)**.** Barz *et al*. (2009) measured the zeta potential of borosilicate or fused glass as a function of aqueous solution pH for different ionic strength. By normalizing the zeta potential with the negative logarithm of the ionic

strength there was a collapse of data onto a single curve. The result could be fitted with a curve and the extrapolation of this curve to zero zeta potential that corresponds to the isoelectric point also known as the point of zero charge pH for static conditions gave a range of pH values between 1.7 and 2. Appendix 4.4.2 (iso) shows the result. In addition to this (Scales *et al*., 1992) reported values of the isoelectric point of borosilicate glass to be between 2.6 and 2.8. The average for these literature values gives 2.4. The difference between this and that obtained using spontaneous imbibition is 0.6. In comparison, it can the value of 3 obtained in this study is appropriate. Regarding surfaces and interfacial electrical phenomena, the isoelectric point which is the elctrokinetic equivalent of the point of zero charge pH of a solid surface (Kosmulski, 2009) has been determined using contact angle and or wettability versus pH plots (Cuddy *et al*., 2013; Barthels-Labrousse, 2002; Trevino *et al*.; 2011). Appendix 4.4.2 (iso) shows plots similar to those of this study with scatter

4.3.3 Conclusion

One utility of the wettability versus pH equation in this study lies in its applicability to the deduction of the point of zero charge pH of a solid surface. In this study the quadratic fits give average values of the point of zero charge pH of borosilicate glass from which the capillary tubes are made to be 3. Appendix 4G and appendix 4H show values for silica to be in close agreement. This is quite within the range of values reported for silica glass, which comes from quartz with the same value of point of zero charge pH. The value also agrees with the average value obtained by (Bourikas *et al*., 20030.

Results of the experimental work show close agreement with theory. In addition, calculation of the coefficients of the quadratic fits for two experiments using fundamental physical constants show close agreement.

The wettability pH relationship (2-70) was derived in Chapter 2 assuming constant fluid-fluid and solid gas interfacial tension and varying solid-liquid interfacial tension. The simulated experiments where water at varying pH imbibes into a capillary tube containing air shows variation of contact angles with pH. The following are the principal conclusions from these experiments.

1. The wettability-pH equation is parabolic. Fitting of capillary imbibition experimental data with a quadratic trend shows that variation of wettability with the pH of experimental brine is appreciably described by this equation.
2. Results of wettability versus pH measurement using capillary imbibition can be used to obtain information about the point of zero charge pH of quartz and this has helped to achieve the task related to the point of zero charge pH of a solid surface.
3. The average value of 3.1 for the point of zero charge pH of borosilicate glass is quite close to that obtained in a published work involving contact angle versus pH plot for bare glass.
4. Under geological conditions of carbon dioxide sequestration in siliciclastic saline aquifers, wettability will change due to pH changes of formation water.

4.4 ROCK SPONTANEOUS IMBIBITION EXPERIMENTAL RESULTS AND DISCUSSION

In this work contact angle and free energy change of spontaneous imbibition were computed using the following equations previously derived:

$$\cos(\theta) = \frac{2\mu}{\gamma_{LV}} \frac{dz^2}{dt} \left(\frac{K}{\emptyset}\right)^{-0.5} \quad (2\text{-}17)$$

$$\Delta G = \frac{dz^2}{dt} 2\mu \left(\frac{K}{\emptyset}\right)^{-0.5} \quad (2\text{-}12)$$

where ΔG is the change in free energy of spontaneous imbibition (J/m^2), γ_{gL} air-water interfacial tension (N/m), g gravity (m^2/s), μ dynamic viscosity of liquid (Pa.s), K absolute permeability (m^2), ϕ porosity (fraction), $\frac{dx^2}{dt}$ is the gradient of height squared *vs.* time plot (m^2/s) and θ contact angle respectively.

pH of experimental brine was adjusted using nitric acid as before. Interfacial tension values for calculations were obtained using the concept of interfacial tension gradient by considering salinity effect. In this regard, the net effect for this calcium chloride and sodium chloride brine was taken as the sum due to individual surface tension gradients (Weissenborn &Pugh, 1996).

4.4.1 Discussion

Table 4-2a gives a summary of calculated contact angle and free energy change of spontaneous imbibition using Wallace Sandstone core samples with synthetic brine. The thermodynamic free energy change in spontaneous imbibition measures the work done related to molecular displacement of air by imbibing brine. The computations are carried out using information from Figures 4-17 to 4-21a. All experiments give very good linear correlation coefficient in accordance with spontaneous imbibition dynamics theory. The average value of the contact angles for different pH of aqueous solutions gives 89.71 degrees while the average value for free energy change gives 0.00034 kJ/m^2. The average contact angle of 89.71 compares quite well with all values for these experiments. The average value of 0.00034 for the free energy changes for all experiments also compares quite well with those of individual free energy changes except that for the experiment with pH equal to 9.77.

Table 4-2a: Experiment with synthetic brine using Wallace sandstone

pH	Gradient [10^{-8} m^2/s]	Contact angle [°]	Free energy change [J/m^2]	R^2
1.79	4	89.68	0.00037	0.99
3.00	3	89.76	0.00028	0.99
5.11	4	89.68	0.00037	0.99
6.77	5	89.61	0.00047	0.99
9.77	2	89.84	0.00019	0.99

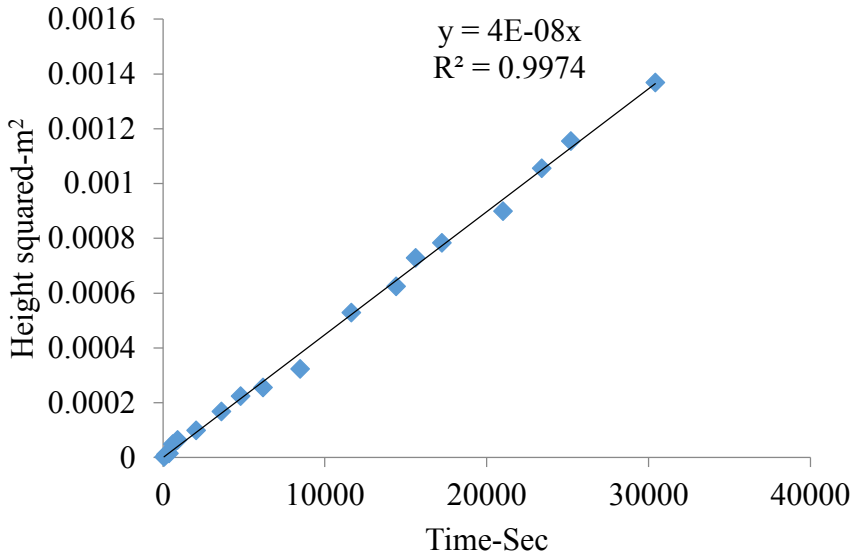

Figure 4-17: Plot of height squared versus time for early spontaneous imbibition dynamics for pH equal to 1.79 (from appendix 4.4.1.1) (Wallace Sandstone)

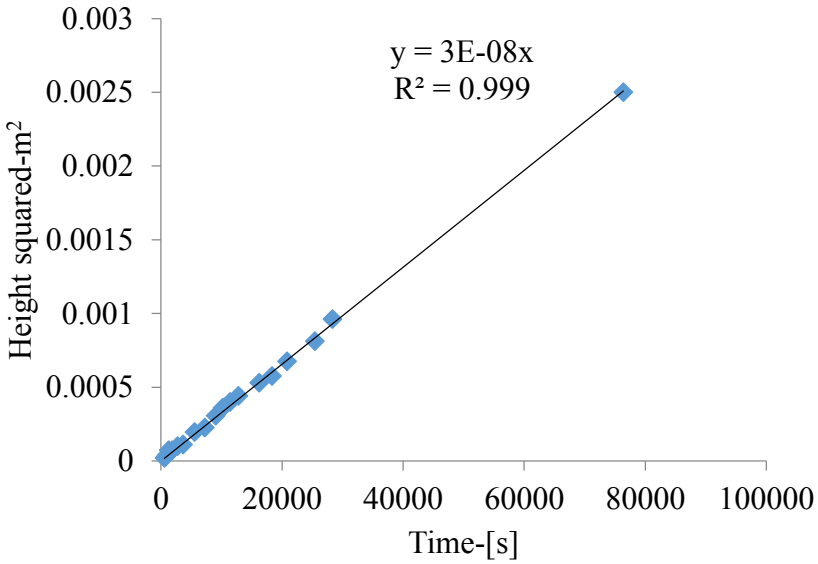

Figure 4-18: A plot of height rise squared versus time for early spontaneous imbibition dynamics for pH equal to 3.05 (from appendix 4.4.1.2) (Wallace Sandstone)

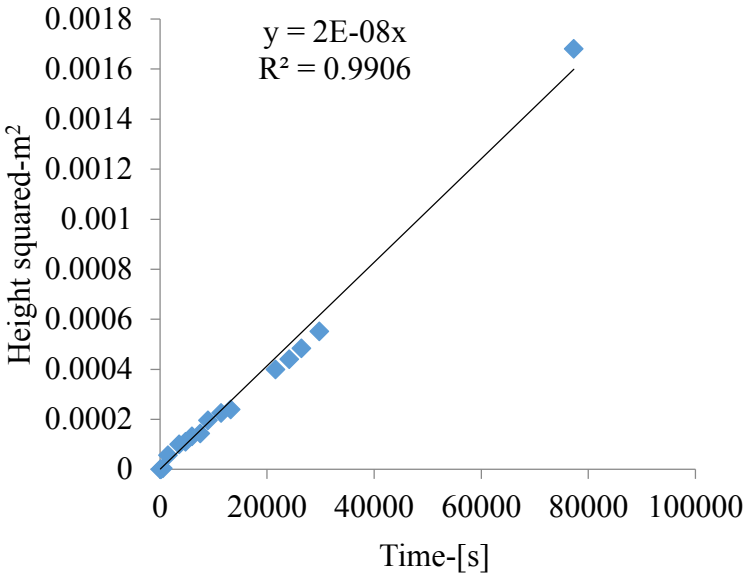

Figure 4-19: A plot of height rise squared versus time for early spontaneous imbibition dynamics for pH equal to 5.11 (from appendix 4.4.1.3) (Wallace Sandstone)

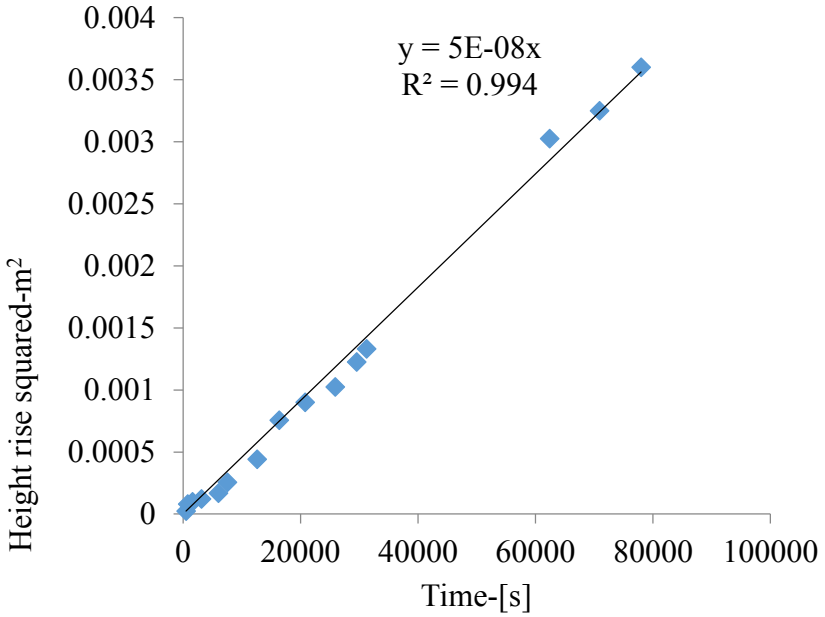

Figure 4-20: A plot of height rise squared versus time for early spontaneous imbibition dynamics for pH equal to 6.77 (from appendix 4.5.1.4) (Wallace Sandstone)

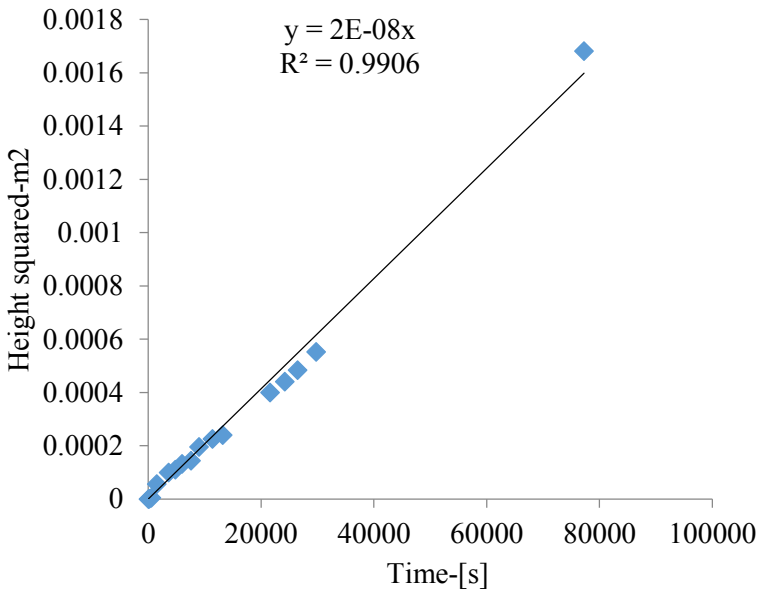

Figure 4-21a: A plot of height rise squared versus time for early spontaneous imbibition dynamics for pH equal to 9.77 (from appendix 4.5.1.5) (Wallace Sandstone)

Table 4-2b represents repeated experimental results for Wallace sandstone, this time with pH values ranging from 3.5 to 6.6. The average value of contact angles for all pH in this case is 89.53 degrees while the average value of free energy changes is 0.00055 J/m^2. These averages compare quite well with those of Table 4-2a for the same rock sample. In all cases, one interesting and distinct observation as far as the principal objective of this thesis work is concerned is that for this rock type, pH changes results in almost insignificant contact angle changes. Data for this Table are deduced from Figure 4-21b

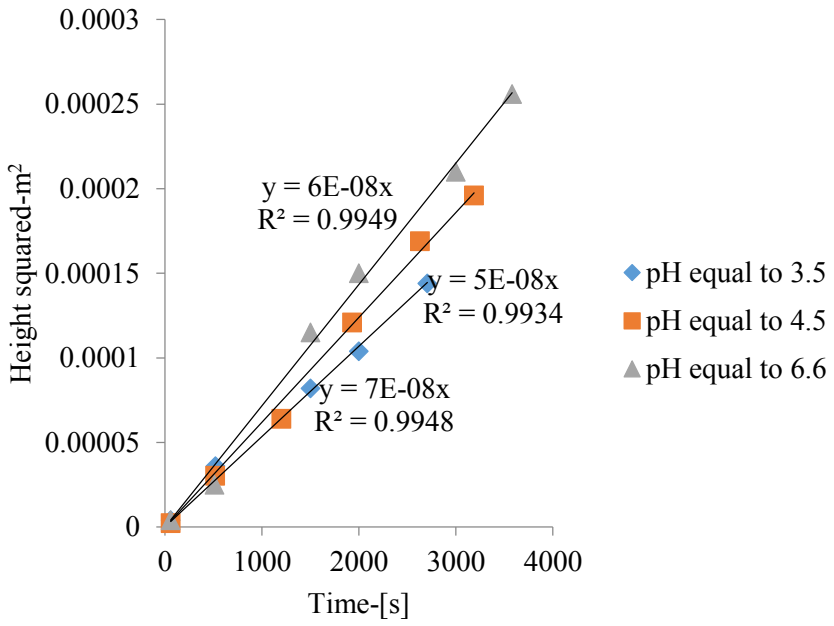

Figure 4-21b: Combined plots for repeated Wallace sandstone experiment using brine (from appendix 4.8.5 through 4.8.7)

Table 4-2b: Repeated experiment with synthetic brine using Wallace sandstone

pH	Gradient [10^8 m^2/s]	Contact angle [°]	Free energy change { J/m^2}	R^2
3.5	5	89.61	0.00047	0.99
4.5	6	89.53	0.00056	0.99
6.6	7	89.45	0.00066	0.99

Table 4-2c presents experimental results for tap water using Wallace sandstone core samples. Data in Table 4-2b were derived by plots similar to those presented before, using experimental data from appendix 4.4.1.6. Here, it makes sense to compare contact angles for two pH values. In this regard, at pH equal to 3 for the original experiment (Table 4-2a) the calculated contact angle is 89.76. The repeated contact angle for pH equal to 3.5 (Table-4-2b), gives 89.61. The result for tap water (Table 4-2c) gives 89.53. The average for brine experiments gives 89.69 compared to experiment for tap water, 89.53. The difference between the two is 0.16. This result is to be expected if the surface complexation model (Wang & Shengche, 1997) is invoked here. In this regard, deprotonation of surface hydroxyl group as explained in Chapter 2 will produce surface charge species in accordance with the following equation:

$$\equiv SiOH \leftrightarrow \equiv SiO^- + H^- \tag{4-5}$$

Protonation will also produce the following reaction:

$$\equiv SiOH \leftrightarrow \equiv SiOH_2^+ \tag{4-6}$$

At the same time ionization of dissolved salt species will produce the following reactions:

$$NaCl \leftrightarrow Na^+ + Cl^-$$
$$CaCl_2 \leftrightarrow Ca^+ + 2Cl^- \tag{4-7}$$

On the basis of these reactions one would expect contact angle for brine experiment to be bigger than that for tap water because of the double adsorption phenomenon which drives the surface of solid more towards zero charge density compared to tap water where there is only hydrogen ion adsorption. Calculated contact angles for pH 1.79 for both cases also show the same trend. In the published work Jung and Wan (2012) increasing brine salinity leads to contact angle increases at a given temperature.

Table 4-2c: Experiment with tap water using Wallace sandstone

pH	Gradient [10^8 m^2/s]	Contact angle [°]	Free energy change {J/m^2}	R^2
1.79	5	89.61	0.00050	0.99
3.00	6	89.53	0.00060	0.99
7.66	2	89.84	0.00020	0.99

At a pH of 1.79 the calculated contact angle for Table 4-2a is 89.68 while that for tap water experiments (Table 4-2c) is 89.61. At this low pH surface roughness comes into play due to proton mediated dissolution mechanism. The contact angle calculated in this case will not reflect the physics of spontaneous imbibition exploited for contact angle calculation.

At a pH of 6.7 for the original experiment (Table 4-2a) the contact angle is 89.61 while that for tap water at near pH 7.66 (Table 4-2c) is 89.84. At the pH values, the surface of silica is predominantly deprotonated with negative surface species representing deprotonated silanol species (first equation). This will prompt the following complexation reactions:

$$\equiv SiOH + Na^+ + Cl^- \leftrightarrow \equiv SiO^- Na^+ + H^+$$
$$\equiv SiOH + Ca^+ + 2Cl_2^- \leftrightarrow SiO^- Ca^+ + H^+ \quad (4\text{-}7)$$

Each of these surface complexation reactions will result in increases of solid-liquid interfacial tension in accordance with the energy additivity concept because there will be adsorption of ions on solid surface due to the presence of surface charges resulting from protonation or deprotonation reactions. However, the presence of brine will reduce interfacial tension while for the case of tap water the interfacial tension will be higher. On the basis of the formula for contact angle computation (Chapter 3) we expect a higher value of contact angle calculation for tap water experiment compared to brine experiment and this is the case.

Another factor is accounted for by the obvious effect of salt on interfacial phenomenon (Cacace, *et al*., 1997). Generally, interfacial tension of water decreases with salt concentration and this partly accounts for the calculated contact angles and free energies.

It is clear that average values for contact angles and free energy changes for all pH values of the experiments show that pH changes do not significantly impact water wettability of the rock. This observation is quite contradictory to the mathematical theory of this thesis work and deserves to be explained in a realistic manner. In this regard, the only way changes in pH will not lead to changes in wettability despite the established theoretical relationship between pH and wettability which has been accepted in published works is when there is a pH buffering mechanism in the system. This can happen if there are minerals capable of consuming the added hydrogen ion in chemical reactions. Typical minerals can be siderite (iron carbonate), calcite (calcium carbonate cement) and micaceous minerals such as muscovite or glauconite. The carbonate minerals can react with excess acidity and this helps to buffer aqueous solution pH while the micas and glauconites can take part in cation (hydrogen ion) exchange with the solution by exchanging potassium from their framework for solution hydrogen ions. These are the likely causes of wettability not changing despite pH changes. Therefore, experimental design for determining the possibility of these reactions is absolutely necessary in order to arrive at meaningful conclusions and this will be planned in the latter part of this chapter.

Table 4-3 gives a summary result of experiments with Fontainebleau sandstone using synthetic brine. The Table is deduced from Figure 4-22 and Figure 4-23. The table shows that at pH equal to 2.8 the contact angle is 88.42 and when the pH is increased to 5.34 the contact angle is 84.48 implying wettability increase. A pH of 2.8 is quite closer to 3 and for Fontainebleau sandstone experiment to produce a result quite different from that of Wallace sandstone means that this sandstone is sensitive to pH changes with regard to acid induced wettability alteration. This is because; the experimental brines are the same for all cases. One thing distinct and also interesting while comparing the results of Fontainebleau sandstone to those of Wallace sandstones is that in the case of the former, a change of pH from 2.80 to 5.34 (a change of pH unit of 2.54) causes a measurable contact angle change (3.94). With regard to results for Wallace sandstone, a change in pH from 3.00 to 5.11 causes contact angle to change from 89.76 to 89.68 resulting in insignificant contact angle change (0.06 ^{o}).

Table 4-3: Experiment with synthetic brine using Fontainebleau sandstone

pH	Gradient [10^7 m^2/s]	Contact angle [°]	Free energy change J/m^2	R^2
2.80	2	88.42	0.0019	0.99
5.34	7	84.48	0.0065	0.99

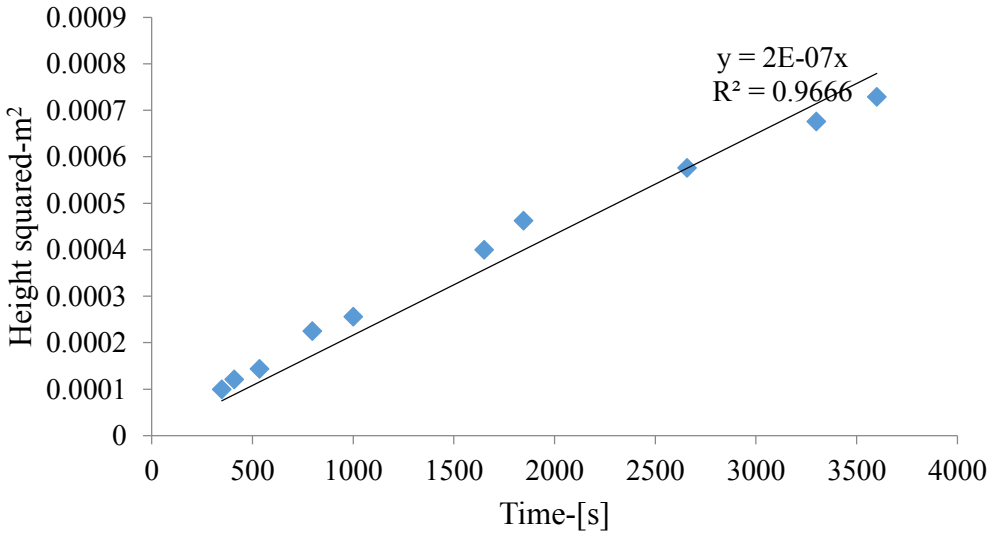

Figure 4-22: A plot of height rise squared versus time for early spontaneous imbibition dynamics for pH equal to 2.80 (from appendix 4.4.1) (Fontainebleau Sandstone)

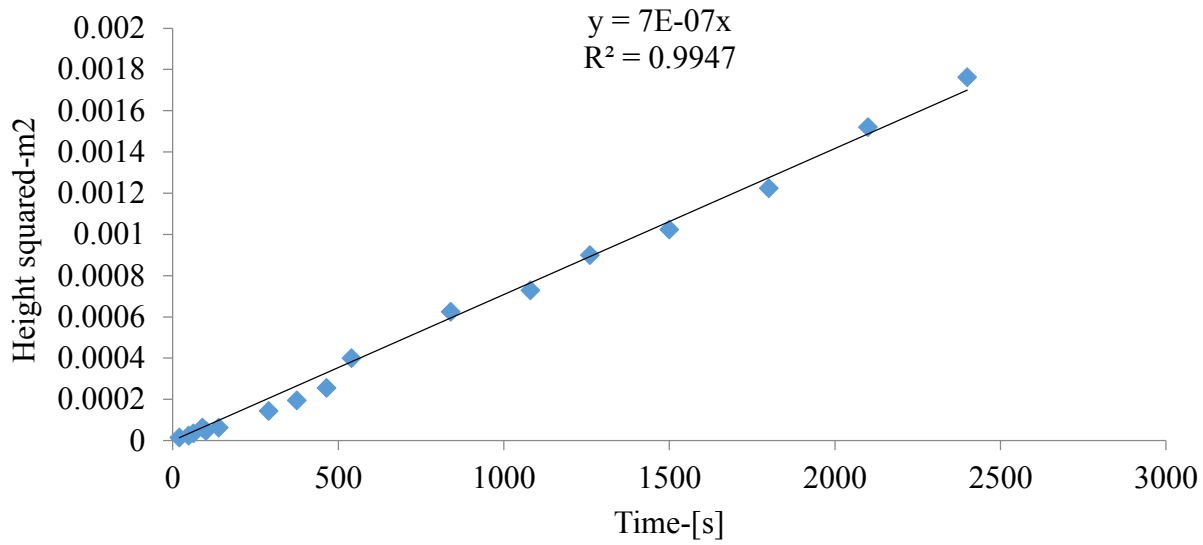

Figure 4-23: A plot of height rise squared versus time for early spontaneous imbibition dynamics for pH equal to 5.34 (from appendix 4.4.2) (Fontainebleau Sandstone

The experimental results for Fontainebleau sandstone show the theoretical and experimental expectations of this thesis work. In other words, wettability decreases with decreasing pH of aqueous solution. Therefore, the likely explanation for these experimental results with regard to Fontainebleau sandstone core samples is that there was insignificant or no pH buffering mechanism as expected in the case of Wallace sandstone core experiments.

For both rock types, pH decreases result in contact angle increases but this increase is remarkable for Fontainebleau sandstone compared to Wallace sandstone. In all rock types, the principal cause for contact angle changes due to pH change will be a reaction involving the adsorption of hydrogen ions to negative surface species produced from deprotonation reactions of surface silanol species Eq. (4-5). At pH above 3 the surface of silica will be negatively charge. As acidity occurs by addition of hydrogen ions, the adsorption of these ions will cause changes in solid-liquid interfacial tension, which in terms of Young's equation will cause contact angle variation. Therefore, where the added hydrogen ion is consumed by some kind of reaction this will represent pH buffering. This means that there

are always less hydrogen ions to cause significant change in solid-liquid interfacial tension to give rise to significant contact angle changes.

4.4. 2 Comparison of Experimental Findings with Results of Published Work on Water Rock Reaction in the presence of Supercritical Carbon Dioxide

The experimental findings of the spontaneous imbibition involving aquifer rocks (Wallace sandstone) with pH buffering capability and monomineralic rocks (Fontainebleau sandstone) with non-pH buffering capability have been supported by the research work of (Newell *et al*., 2008). In this published work the authors used water-rock reaction studies in reaction cells to measure pH *vs.* time for different mixtures and interactions of aqueous solution in the presence of supercritical carbon dioxide at a temperature and pressure (75^{o}C, 200 bar) typical of carbon geosequestration. Appendix 4I shows their result for a monomineralic rock with no pH buffering capability. This appendix (4I) shows change in pH of aqueous solution as it interacts with supercritical CO_2 in the absence of carbonate buffering minerals. In the present work, pH changes of aqueous solution is similar to that of Newell *et al*., (2008) in the presence of supercritical CO_2 and indicates wettability decreases and this has been observed for the case of Fontainebleau sandstone where there is significant change and for the case of Wallace sandstone where rock mineralogy is the cause of slight wettability changes.

Figure 4-23a shows a plot of height square versus time for Wallace Sandstone and Fontainebleau sandstone experiments. Plots show that even though the pH values are quite closer the gradient of the plots differ markedly. In the case of Fontainebleau sandstone, the higher gradient at this pH (2.8) quite closer to that of Wallace Sandstones (3) means that there is a marked change in contact angle, since the equation for contact angle computation is directly linked to the gradient of the plot.

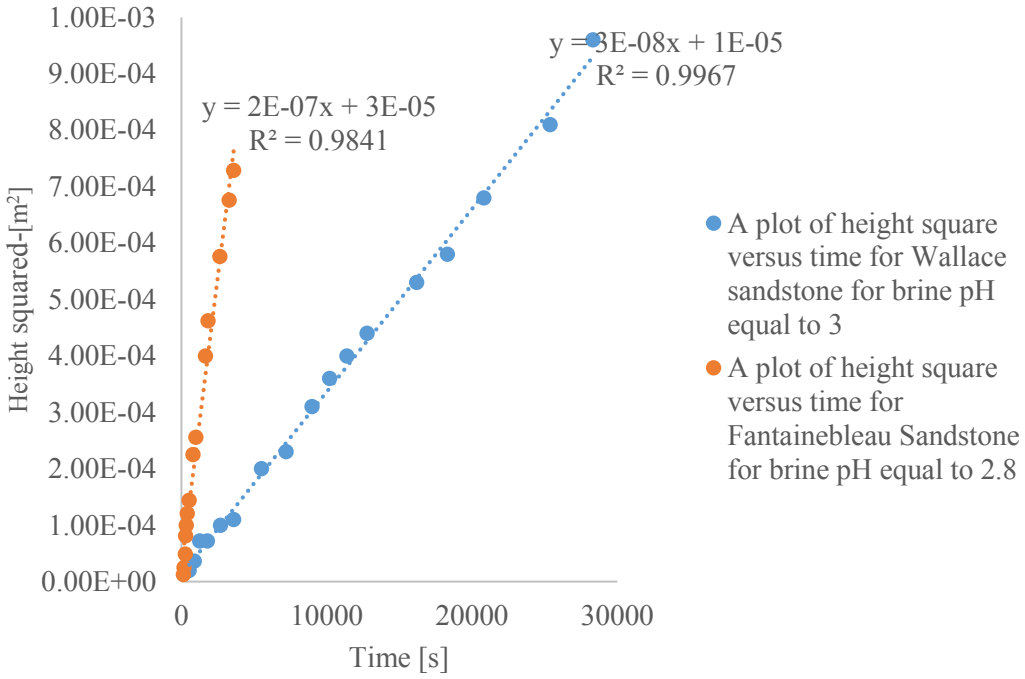

Figure 4-23a: A plot of height rise square versus time for experiments on Wallace Sandstone and Fontainebleau sandstone at pH equal to 3 and 2.8 respectively.

Figure 4-23 b shows a plot of height squared versus time for Wallace sandstone experiment using tap water without pH adjustment. The pH of tap water was read at ambient temperature as 7.40. This experiments was used as a baseline experiment. The gradient of the plot is $2*10^{-7}$ m^2/s. Table 4-2a shows an experimental data with pH equal to 6.77 which is closer to this pH. The gradient of the plot is $5*10^{-8}$ m/s. Table 4-2b also shows another experimental data for pH equal to 6.6 for repeated Wallace sandstone experiment. This pH is close to 7.40 and the gradient of the plots is $7*10^{-8}$. With this gradient the calculated contact angle for the base line experiment is 88.50 while corresponding values at approximately the same pH in table 4-2a and 4-2b are 89.61° and 89.45° respectively. This corresponds to1.11° and 0.95° difference respectively. This slight variation is to be expected from wettability theory related to surface charge. In this regard, at pH near neutral a saline solution with ions will cause surface complexation by adsorption of opposite ions at opposite surface sites of solids. This reduces surface charge density and would lead to wettability reduction and contact angle increase. Therefore, the nearly one degree difference in contact angle is expected. Thus, a saline solution will result in lower

wettability and higher contact angle. Furthermore, the close values of contact angles for Wallace sandstone experiments with brine and pH adjustment compared to that of the base line experiment testifies to the fact that the ambient wettability of this sandstone is maintained even with pH changes and this further supports it possible pH buffering capability

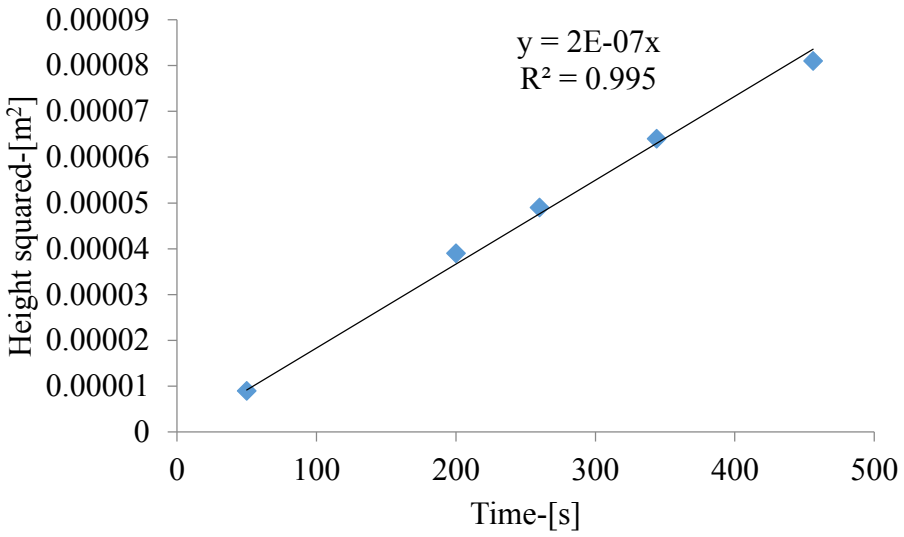

Figure 4-23b: A plot of height squared versus time for Wallace sandstone experiment using tap water (appendix 4.4.2a)

Figure 4-23c shows a similar plot for oil (kerosene) experiment (as a base line wettability) using Wallace Sandstone core samples. The ambient pH is 7.3. The gradient of the plot is equal to that of Figure 4-23b. The contact angle is, therefore, the same. The result of this experiments further supports the pH buffering capability of Wallace Sandstone. This is because base line experimental data give computed contact angle similar to those of pH control experiments.

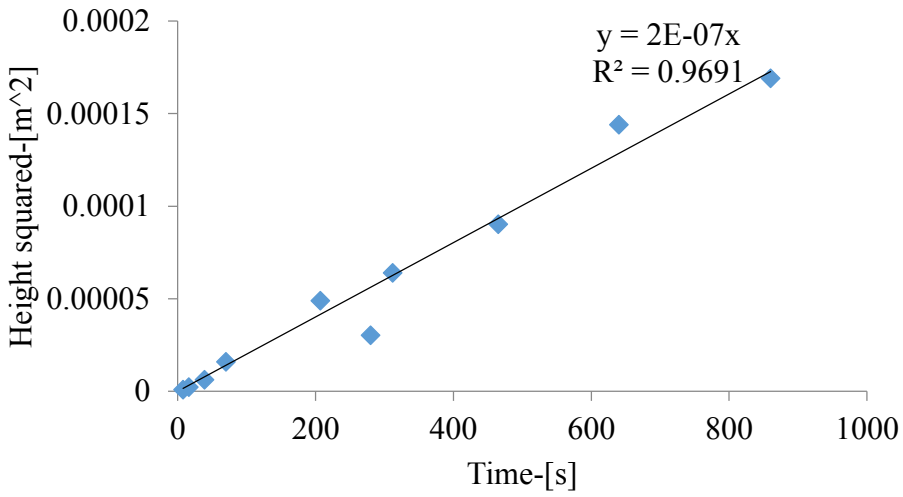

Figure 4-23c: A plot of height squared versus time for Wallace sandstone using kerosene (appendix 4.4.2b)

4.4.3 Interpretation of Experimental Results in the Light of Mathematical Model

In Chapter 2, trends of wettability or contact angle changes for rocks and minerals were mathematically revealed. The conclusion of this chapter with regard to pH induced wettability change is that for minerals, wettability changes will be more pronounced following pH change compared to rocks. This is because, pH decrease is the main cause for wettability decrease and this has been accepted in published works cited so far. In minerals there are no diagenetic minerals to cause pH buffering. This means there will be marked pH decreases. In the case of rocks, the presence of diagenetic minerals such as clays and or phyllosilicates will cause pH changes to be less severe. The experimental findings of this chapter for Wallace sandstone and Fontainebleau sandstone support the models. In this regard, Table 4-2a through 4-2c show that Wallace sandstone shows approximately constant contact angle or wettability while Table 4-3 for Fontainebleau sandstone shows that there is significant change in contact angle for a pH change from 2.8 to 5.34. Although both systems are rocks geologically Fontainebleau sandstone is a quartz arenite with approximately 99% quartz content with insignificant buffering capability. In the case of Wallace sandstone it makes sense to conclude that as brine of a given pH imbibes spontaneously through the core there is the tendency for pH to be buffered causing contact angles to change slightly. This tendency could be caused by cation exchange reaction.

4.4.4 Conclusion

The principal objective of this experimental program was to test the principal hypothesis of this work. That is, contact angle or wettability evolution during CO_2 injection into saline aquifers will be controlled by rock mineralogy such that where host rock mineralogy offers the possibility for pH buffering reactions, wettability evolution will be different from the case of a saline aquifer rock devoid of this. The following are the conclusions of these experiments:

1. For those sandstone aquifers where there are authigenic minerals capable of buffering formation water pH, the wettability of the system will show slight variations.
2. For sandstone saline aquifers that have very high silica content and insignificant authigenic minerals for pH buffering, the wettability of the system show significant changes with decreases in formation water pH. Generally, there will be significant decrease in water wettability with changes in formation water pH.
3. The salinity of the saline aquifer affects wettability evolution such that aquifers with high salinities will offer the greatest opportunity for significant wettability decreases with formation water pH decrease.
4. Conclusion 4, therefore, supports the decision of the geological community to sequester anthropogenic carbon in deep saline aquifers with hyper-saline conditions.
5. The overall result of the experimental program support the principal hypothesis of this study

4.4.5 Experimental Results for Sand Pack Imbibition and Discussion

Due to the limited availability regarding Fontainebleau core samples, only two experiments were conducted for rock imbibition. Since this sandstone has a high proportion of sand, one way to arrive at a more conclusive result is to conduct imbibition experiments on a porous system with composition that approximates to that of this sandstone. Consequently, a synthetic porous system where sand is predominant is the ideal one. This system was obtained by loading sand grains into a custom-built imbibition tube described earlier. Spontaneous imbibition tests were then conducted similar to those of rock imbibition test.

Table 4.4 shows the summary results for the gradient of the plots from Figs. 4-24, 4-26, 4-28, and 4-29. The good regression of the plots support the early spontaneous imbibition theory which is the requirement for contact angle computation. The physical implication of using sand packs that have predetermined loading into the custom-built imbibition tubes is that the porosity and permeability of all sand packs are presumably the same. Constant porosity and permeabilities were achieved by gently tapping loaded tubes in a consistent manner. The theoretical basis for contact angle computation shows that this parameter can be linked to the gradient of the plot. The extent of wettability change due to varying pH of aqueous solution can, therefore, be correlated with the gradient of the plot and this means that the higher the gradient of the plot the higher the wettability (lower contact angle) and *vice versa*. On the basis of this, one would expect that since wettability decreases with pH, the gradient of the straight-line plot must equally decrease with pH decreases. This trend is clearly observed in Table 4-4 up to pH = 4.56. Below this pH or at a pH = 3.34 the gradient of the plot shows an increase. At a pH of 1.96 it decreases again.

Table 4-4: Summary of Experimental Results (Sand pack)

pH	Gradient of plot [m^2/s]	R^2
6.95	0.0013	0.98
4.56	0.0002	0.95
3.34	0.0004	0.99
1.96	0.0001	0.96

In the context of the mathematical model of this study, this trend can be explained by considering the quadratic relationship between pH and wettability. This quadratic trend shows a minimum value at the point of zero charge pH of the mineral surface. In the case of sand pack, this is between 2.5 to 4.5. This means that in these experiments the point of zero charge of the surface of the minerals of the sand pack is 4.56. Therefore below this pH of the aqueous solution the wettability will increase and this must be shown by an increase in the gradient of the straight-line plot at pH value equal to 3.34. Table 4-4 clearly shows this trend. However, in accordance with the theory that the wettability and therefore, the gradient of the straight-line plot must increase monotonically for pH values below 4.56 there is a clear violation at pH equal to 1.96. At this pH value of the aqueous solution, the gradient of the plot decreases, meaning an eminent decrease in wettability. In order to explain this trend in wettability, knowledge of silicate dissolution theory is required which

is beyond the scope of this thesis work. The fact, however, still remains that these porous systems with predominantly high silica content similar to Fontainebleau sandstone core sample show consistent wettability decrease with pH decrease which support the principal hypothesis that porous systems which lack pH buffering mechanisms will respond to eminent wettability decreases with formation water pH decreases following carbon dioxide injection.

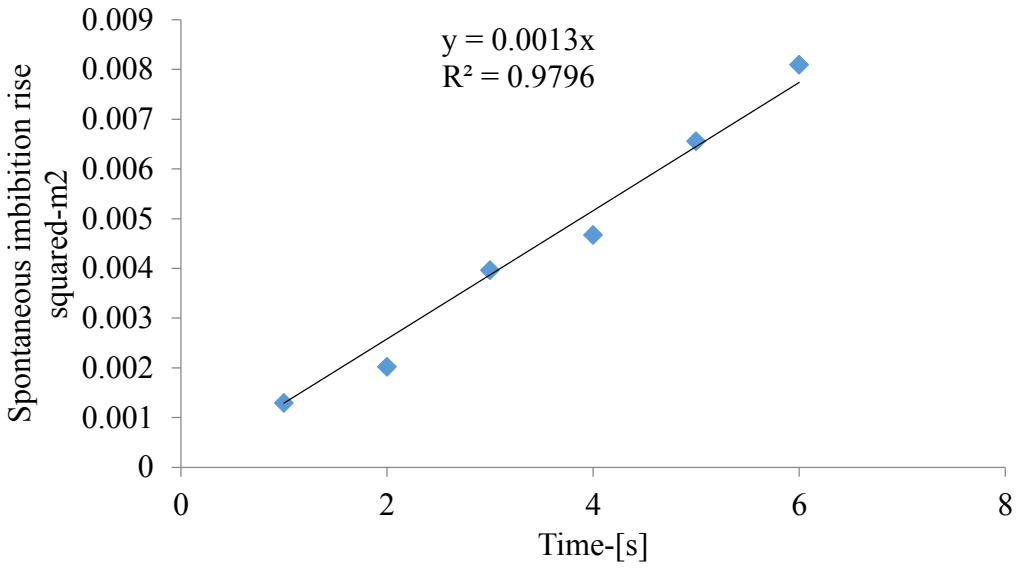

Figure 4-24: Spontaneous imbibition rise squared versus pH for pH equal to 6.95 (from appendix 4.7.1)

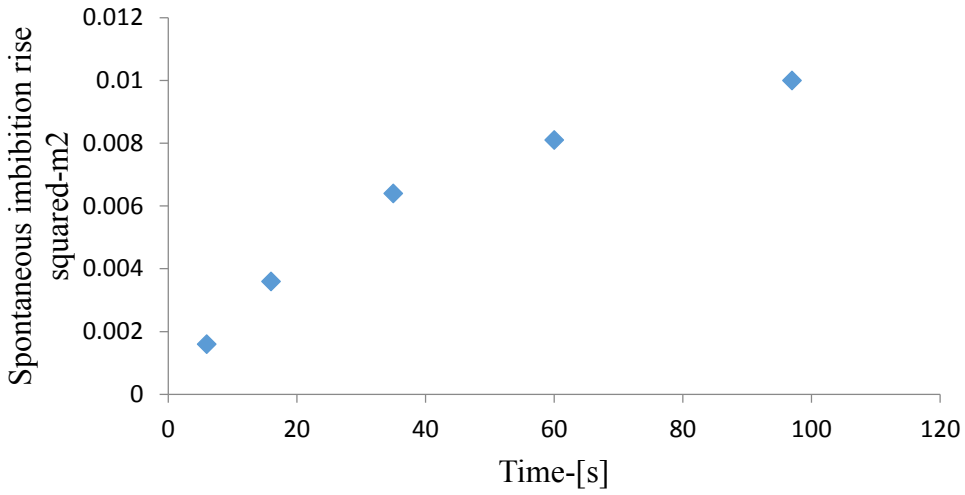

Figure 4-25: Spontaneous imbibition rise squared versus pH for pH equal to 4.56 (from appendix 4.7.2)

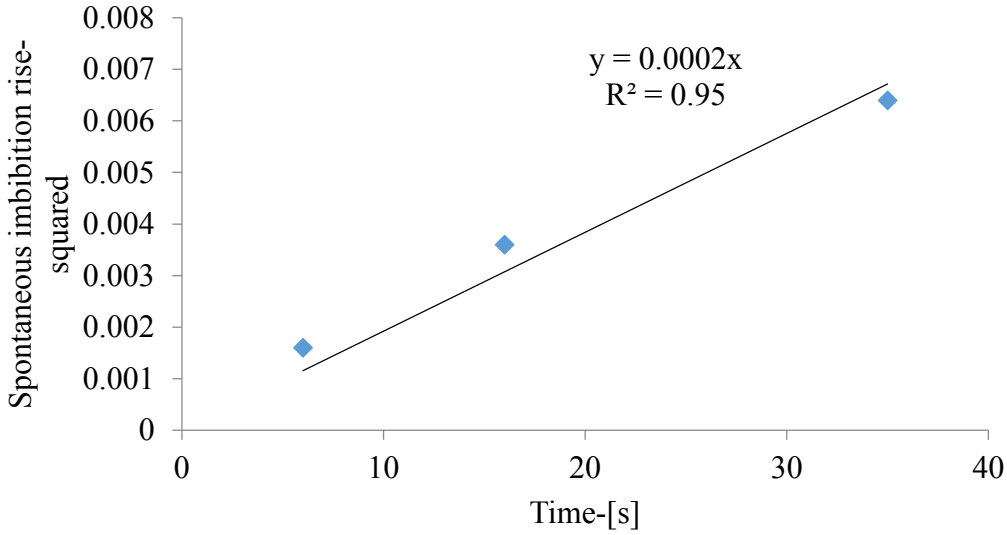

Figure 4-26: Spontaneous imbibition rise squared versus pH for pH equal to 4.56 plotted for the linear section of the data (from appendix 4.7.2)

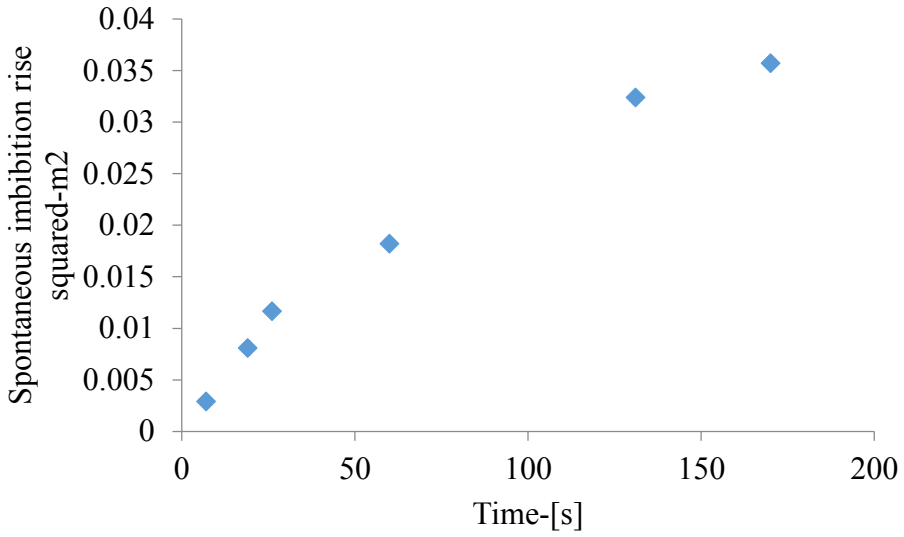

Figure 4-27: Spontaneous imbibition rise squared versus pH for pH equal to 3.34 (from appendix 4.7.3)

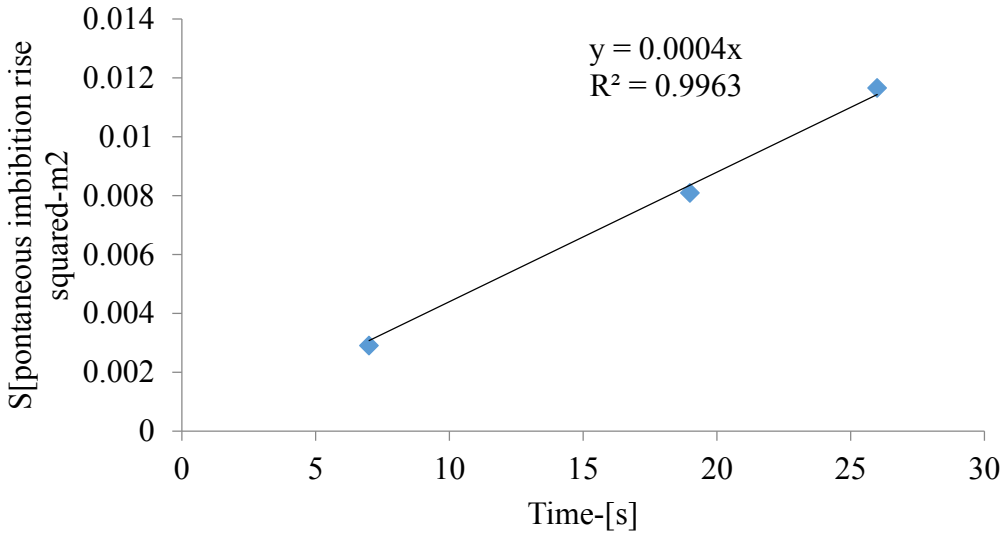

Figure 4-28: Spontaneous imbibition rise squared versus pH for pH equal to 3.34 plotted for the linear part of the data (from appendix 4.7.3)

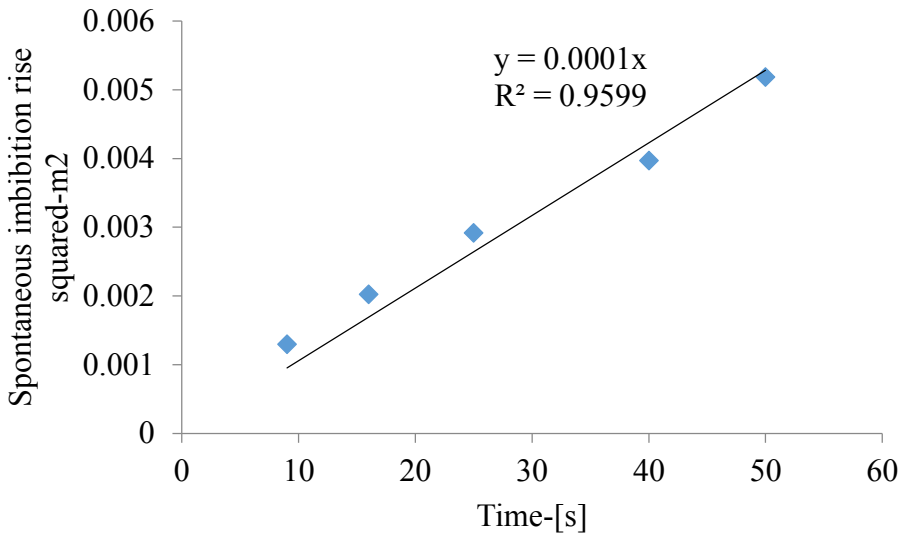

Figure 4-29: Spontaneous imbibition rise squared versus pH for pH equal to 1.96 (from appendix 4.7.4)

4.4.6 Relative Errors of Straight Line Plots

In all plots of height rise squared versus time the principal parameter for contact angle computation are the gradients of the plots. Therefore, the accuracy of calculated contact angle depends much on this parameter. The other parameters are assumed to be accurately measured. In this regard, errors are assumed to be due mostly to height rise and time readings and all errors will be integrated in the gradients of the plots. To determine uncertainty, a graphical method of error analysis was used. In this regard, all figures with regression coefficients less than 0.95 were subjected to graphical error analysis. Appendices J and K series starting from page (272-277) contain the details of approach. The plots for Wallace Sandstone experiments had regression coefficients 0.99. Figure 4.22 for Fontainebleau Sandstone has a relative error of 0.17 while Figures 4.26 and 4.29 for sand pack experiments have relative errors 0.17 and 0.08 respectively. These uncertainties are quite minimal and give credence to computed contact angles.

4.4.7 Introducing Scaled Wettability Concept Plot

The equation (2-17) for calculating the contact angle as derived before is:

$$\cos(\theta) = \frac{2\mu}{\gamma_{LV}} \frac{dx^2}{dt} \left(\frac{K}{\emptyset}\right)^{-0.5}$$

In this equation, the variables are cosine of contact angle and the gradient of the straight-line plot. All other parameters are constant. The equation can be rewritten as:

$$\cos\theta = C\frac{dx^2}{dt}$$

where:

$$C = \frac{2\mu}{\gamma_{LG}}\left(\frac{\theta}{K}\right)^{-0.5}$$

Diving both sides of the second equation by C gives:

$$\frac{\cos\theta}{C} = \frac{C}{C}\frac{dx^2}{dt} = \frac{dx^2}{dt}$$

Henceforth, the ratio of the cosine of the contact angle and the gradient of the plot shall be called a scaled wettability, which can be plotted for every experiment. The following Figure 4-30 shows a plot of scaled wettability for four sand packed experiments with a quadratic fit which is appreciable.

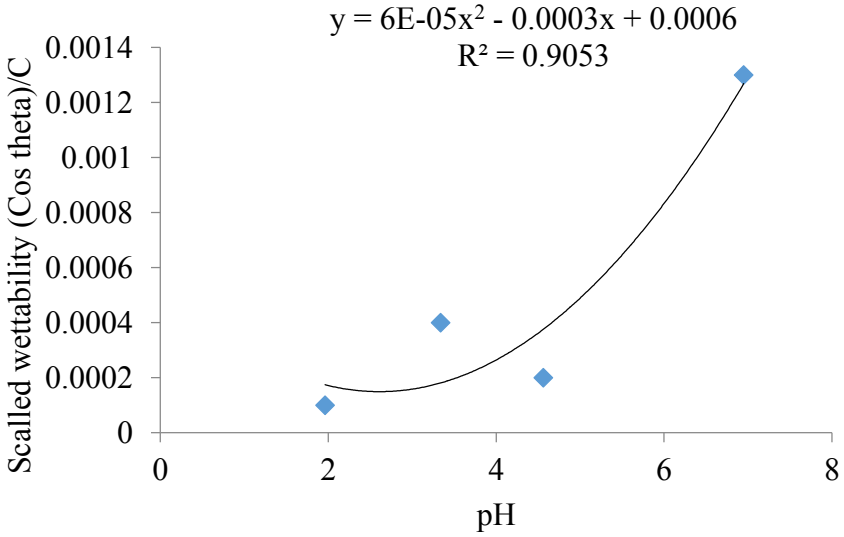

Figure 4-30: Scaled wettability versus pH for four experiments

On the basis of the wettability-pH relationship derived in Chapter 3, the point of zero charge pH of the sand pack porous system can be deduced as the pH of the aqueous solution

where the wettability is a minimum. From Fig. 4-30 this can be deduced as a pH equal to 2.5. According to Schwarz *et al*., (1984) the value for clean quartz is 3.08 which is quite close to this value.

Bourikas *et al.,* (2003) used different techniques to obtain the point of zero charge pH of quartz. The following were their values for five different methods: 3.1, 3.3, 3.0, 2.9, and 3.2 which gives an Average = 3.14.

Parks (1962) reports the point of zero charge pH of quartz as 1.5-3.5. The value of 2.5 obtained in the present work falls within those of published works as seen from the cited references.

To see the theoretical justification of this plot requires knowing the surface chemical reactions that will occur as water with varying pH conditions imbibe spontaneously into the porous sand pack. Here, the homogeneity of the sand pack requires that the parameter crucial to wettability evolution that controls the spontaneous imbibition be considered. This is the point of zero charge pH of quartz. At pH values above the point of zero charge pH there is deprotonation of the surface hydroxyl functional group (silanol) and the surface of quartz will have negative sites. As aqueous solution pH decreases there will be proton adsorption at negative sites and this will drive the surface towards neutrality. At the point of zero charge pH the wettability will be a minimum. Therefore, in accordance with the pH dependence of wettability, plot of wettability versus pH must show a minimum from which the point of zero charge pH can be deduced. Although the number of data points are limited application of the theory leads to a value of this parameter that agrees with those found in published works

4.4.8 Determining the Effective Point of Zero Charge pH of Wallace Sandstone

Figure 4-31below shows a plot of contact angle versus aqueous solution pH using the data for brine imbibition into Wallace sandstone core samples (Table 4-2a). The plot has been fitted with the parabolic model of this work. By using the approach for capillary imbibition plots the point of zero charge pH of Wallace sandstone surface at the turning point is 3.56.

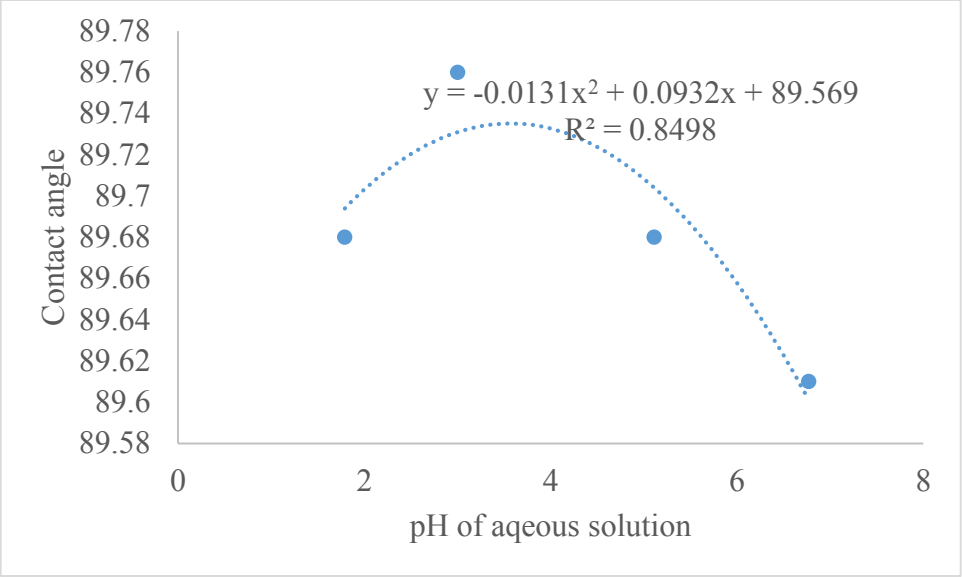

Figure 4-31 Plot of contact angle versus aqueous solution pH

As explained earlier, one utility of the wettability pH relationship in this study is seen in the theoretical determination of the point of zero charge pH of as a solid surface from experimental data. Although the data used for plotting is insufficient, the application of this theory makes it easier to test the principal hypothesis of this thesis work that different rock systems will respond differently to pH change and wettability evolution. Geochemically, Wallace sandstone is different from the porous sand pack which is 100% quartz. Wallace sandstone has only 82 percent of silica in addition to other non-silica minerals. Therefore, in line with the fact that the effective point of zero charge pH of a solid surface will be controlled by the point of zero charge pH of its components, one would expect to see a difference between the values of this parameter deduced for Wallace sandstone and a porous sand pack. The application of this theory clearly shows that there is a difference.

This plot lends credence to that fact that using only quartz as a representative mineral of a potential sandstone saline aquifer is not enough. In the literature, the point of zero charge pH of pure silica has been reported with ranges. In this study, comparison of the value of 3.56 for Wallace sandstone and 2.5 for pure quartz from sand pack porous systems shows a difference. To see if this makes sense the work of Reymond and Kolenda (1999) regarding the point of zero charge pH of a mixture of silica and alumina as an impurity fraction deserves to be consulted. This is clearly shown in appendix 4-6. From this figure,

the point of zero charge pH of pure silica is lower than the case where it contains an impurity. This means as the percentage of silica decreases in the rock, the effective point of zero charge pH of the system increases. This finding supports the experimental work of the present study in which Wallace sandstone with 82 percent quartz plus glauconite, mica (sericite) and other subordinate minerals has a point of zero charge pH of 3.56 while the porous silica pack has a point of zero charge pH equal to 2.5.

Furthermore, Schwarz *et al*. (1984), studied the point of zero charge pH of silica and alumina suspension. They arrived at the following two formulas:

$$pH_{pzc}(mixture) = 4.1 - 3.08 f_{Si_2O_2}$$

$$pH_{pzc}(mixture) = 7.18 + 3.08 f_{Al_2O_3}$$

In which $pH_{pzc}(mixture)$ is the point of zero charge pH of silica-alumina mixture, $f_{Si_2O_2}$ is the weight fraction of silica in the mixture and $f_{Al_2O_3}$ is the weight fraction of alumina in the mixture.

On the basis of this formula one would expect the point of zero charge pH of Wallace sandstone to be higher than that of a sand pack porous system and that is what the theoretical and experimental approach of this thesis has shown.

In addition, Shen *et al*., (1999) studied the effect of magnetite impurity on the point of zero charge pH of silica. Appendix 4-7 sums up their findings. The figure shows that as the impurities increase the point of zero charge pH increases. In this case, a sand pack porous samples is considered pure while Wallace sandstone is considered as sand containing impurities and would have a higher point of zero charge pH and this is supported by the work of Schwarz *et al*. (1984). This supports values of the parameter deduced in the present study.

Summarily, in view of the fact that all plots of contact angle/wettability versus pH have shapes and trends similar to those reported in literature, this study has used a novel method based on spontaneous imbibition to determine the point of zero charge pH of silica and rock sample. The only limitation here is the data but, theoretically and objectively, the

approach serves to compare values of what will be called here as silica doped and pure silica point of zero charge pH.

4.4.9 Conclusion

The objective of the sand pack spontaneous imbibition experiment is to show that for clean sands where there are no minerals capable of buffering aqueous or formation water pH, water wettability of the saline aquifer will decrease significantly in accordance with the hypothesis of this study and in accordance with the experimental observations of published literature works regarding CO_2-brine-silica systems. The results of these experiments using spontaneous imbibition measurements support literature works regarding wettability decreases during CO_2 injection into saline aquifers. The following sum up the conclusions of these experiments.

1. Experimental results of the sand packed porous systems which are the synthetic analogues of geological systems typical of Fontainebleau (ultra-high silica content) support the hypothesis that consistent wettability decreases are possible under geological carbon sequestration in saline aquifers where pH buffering mechanisms are lacking.
2. Experimental findings further lend credence to the results of contact angle and wettability trends observed for Fontainebleau sandstone core samples and provide a conclusive evidence that under conditions typical of geological carbon sequestration in such systems, consistent wettability decreases will enhance injection gas sweep efficiency by increasing water mobility and decreasing that of injected CO_2.
3. Experimental results of sand packed porous systems have further provided the basis for determining the point of zero charge pH of silica surface and this value falls within those determined from capillary imbibition experiments. The value also falls within those reported in the literature. This serves to augment the achievement of the objective related to this surface chemistry parameter.
4. The point of zero charge pH of a solid surface is a fundamental surface chemistry parameter that controls the evolution of the electric double layer. Accordingly, this parameter is central to the presence of the electron donor and electron acceptor

components of solid-liquid interfacial tension, which is the principal cause of the pH induced wettability evolution. To date, different methods have been used to determine this parameter. The present study has used a novel approach based on spontaneous imbibition flow into a porous system to determine this parameter.

5. Application of the pH dependent wettability equation derived in this study for the determination of the point of zero charge pH of the porous sand pack and Wallace sandstone gives credence to the principal hypothesis that different rock systems will experience different trends in wettability change. The reason is that the principal cause of pH wettability evolution in saline aquifers under geologic carbon storage is decrease in surface charge due to pH decrease and the development of this surface charge as well as its evolution in time and space depends on the point of zero charge pH of the solid surface. Obviously, this will be different for rock medium that is considered as an aggregate of minerals.
6. By referring to Eq. (2-70) the cosine of contact angle should be bigger (smaller contact angle) where the point of zero charge pH of rock surface is bigger for a given pH and *vice versa*. In this thesis work, experiments have been conducted on rock samples having nearly 100 % silica (Fontainebleau sandstone) and that having a smaller percentage of silica (Wallace sandstone-82%). Normally, the effective point of zero charge pH of the former will be smaller meaning significant changes in contact angle at a given pH of formation brine. For the latter sandstone, the effective point of zero charge pH will be bigger meaning less changes in contact angle at given pH. This is what has been established in the experimental findings involving rock samples with different mineralogy.

4.5 TESTING OF HYPOTHESIS USING CATION EXCHANGE REACTION EXPERIMENTS

The experimental objective of this section is to investigate the extent of cation exchange reaction mechanism for Wallace Sandstone and Fontainebleau sandstone core samples.

4.6 SAMPLES CHARACTERIZATION

Cation exchange reaction in geologic systems is typical of minerals with cation exchange capacities (Carrol, 1959). Some minerals capable of action exchange reactions are glauconite and mica (Chapelle & Knoble, 1983). The hypothesis is that, if mica and glauconite are present in samples, exchange of solution protons produced from the dissociation of nitric acid for potassium in the octahedral frame work of these phyllosilicates will cause pH buffering to resist wettability change. To arrive at a conclusive evidence regarding experimental findings from imbibition experiments, the presence of these minerals in samples must be experimentally confirmed and this requires the detection of glauconite and mica. Also, apart from cation exchange reactions, which are capable of pH buffering, dissolution of authigenic calcite cause the consumption of hydrogen ion and this has the potential to buffer pH. In this regard, the detection of carbonate minerals is a necessity.

4.6.1 Materials and equipment

The anticipated source of mica for this experiment is sandstone core sample pulverized to 150 μm. The sandstone core samples were Wallace sandstone and Fontainebleau sandstone. The former is greyish green and the presence of glauconite is a possibility. Apart from this, visible specs of minerals can be seen which resemble muscovite mica. The latter is dull white in appearance and is well-sorted sandstone with 99% percent quartz and quartz cement. This sample, therefore, has a very small proportion of micaceous minerals.

4.6.2 Carbonate Analysis

The objective was to detect authigenic minerals in the form of carbonate cement (calcium carbonate (calcite), magnesium carbonate (dolomite) or iron carbonate (siderite) in Wallace sandstone. Total carbon analysis was done using Eltra CS 2000 Carbon Sulfur Determination PC Controlled equipment at the Minerals Engineering Centre (MEC) of Dalhousie University. Results of this analysis are seen in Table 4-7.

In all, two samples were submitted for carbonate analysis aimed at obtaining conclusive evidence for calcite or siderite composition of Wallace sandstone. The results show that, carbonate presence is not conclusive because of the low values of the analytical results for both samples (Wallace sample 1 and Wallace sample 2).

Table 4-5: Results of carbon analysis for carbonate presence

	Weight percent %	
Sample	C (total)	C (Organic)
CO2 sample	0.049	0.044
WSS # 1	0.044	0.046
WSS # 2	0.046	0.051

Table 4-5 gives conclusive evidence that carbonates are not present in this sandstone sample.

4.6.3 X-ray Powder Diffraction Analysis

The purpose of this characterization is to detect mica and glauconite in rock samples using X-ray powder diffraction analysis. The Bruker X-ray diffraction system with copper tube was used with 40 keV with an X-ray wave length of 1.54Å.

Appendix 4J shows results obtained from analysis of powdered Wallace sandstone sample. Appendix 4K (Tomita *et al.,* 1988) shows X-ray diffraction results for mica where the peak occurs at 5.3 Angstrom. Normally micas show high intensity at interatomic spacing of 5Å. Appendix 4L (Porrenga, 1968) shows results for glauconite powder from literature sources. This gives peaks coinciding with twice the diffraction angle at 10, 18, and 28. Appendix 4K also shows the same trend. Comparison of these diffraction patterns to the analysis done using Wallace sandstone powder shows that at twice the diffraction angle equal to 28 there is a peak corresponding to glauconite.

4.7 CATION EXCHANGE EXPERIMENT

So far, the experimental detection of minerals capable of cation exchange reaction (mica and glauconite) in Wallace sandstone is a motivation for the principal hypothesis that cation exchange reactions in rock imbibition experiments are the principal cause for brine pH buffering which hindered significant wettability decrease despite measurable pH decreases. The objective of cation exchange experiments in this case is to observe trends in pH changes similar to those observed for the two rock types. To achieve this objective, the following experimental design will be adopted:

i. Mix weighed samples of pulverized rock in experimental brine of a given initial pH in a beaker
ii. Measure the initial pH of the mixture
iii. Cover the beaker to prevent evaporation induced pH changes
iv. Measure the pH of the mixture with time
v. Determine initial potassium concentration of mixtures prior to experiment
vi. Determine final potassium concentration of mixtures after experiment to confirm cation exchange reaction and potassium release from phyllosilicates.

Elsewhere, (Karima *et al*., 2012) potassium has been leached from glauconite using acidified mixture

The following sum up these steps:

2.2 g each of the pulverized samples were first weighed and put in 100 cc of the synthetic brine of initial pH 1.7. The mixture was vigorously stirred to obtain a uniform mixture. After a uniform mixture was obtained the initial pH corresponding to time zero was measured using the pH probe (EUTECH) manufactured by EUTECH which measures pH to two decimal places. A stopwatch was started after the first pH reading and the pH of the aqueous solution was measured every two minutes interval. This procedure was repeated for both sandstone samples but with 10 g of the pulverized samples. In all cases, experiments were conducted at room temperature similar to those of rock imbibition experiments.

Detection of potassium concentration increases in aqueous solution by comparison of initial and final potassium concentration of mixtures taken from the cation exchange reaction was achieved using The Varian Vista-Pno Simultaneous ICP-OE equipment at the MEC.

4.7.1 Synthetic Brine

Synthetic brine was prepared with 43.5 g of sodium chloride and 12.6 g of calcium chloride dehydrate as prepared before. The reagents are all 99 percent purity purchased from Sigma Aldrich and they were used without further purification. The balance, EC4000 d 0.1g manufactured by Symmetry and distributed by Cole Parmer was used. The initial pH of the synthetic brine for an experiment was obtained by reducing the pH of the synthetic brine

using aqueous nitric acid (99%) purity purchased from Sigma Aldrich and used without further purification. The initial experimental pH in this study was 1.79 and 5.35.

4.8 RESULTS AND DISCUSSION

Figure 4-34 shows plots of aqueous solution pH *vs.* time for experiments with Wallace Sandstone and Fontainebleau sandstone powder for an initial solution pH of 5.37 using10 g of each sample. The Figure. (4-34) shows that, at any time, the curve for Wallace sandstone lies above that for Fontainebleau sandstone. This means that, at any time, solution pH for Wallace sandstone experiment is higher than that for Fontainebleau sandstone. This is to be expected because of the anticipated pH buffering mechanism as suggested by results of spontaneous imbibition experiments for this sandstone (Wallace), from Nova Scotia and confirmed by the presence of mica and glauconite deduced from X-Ray analysis. The curve for Fontainebleau lies below that for Wallace sandstone for possible lack of pH buffering reactions due to significant cation exchange reaction.

The two curves start at pH values higher that the initial pH. This is because after mixing aqueous solution with 10 g of powder, the mixture was vigorously stirred in order to obtain a uniform mixture before pH reading. During the stirring time (3 minutes) there was some obvious pH buffering mechanism going on in all cases and this led to pH values higher than the initial pH of aqueous solution.

The curve for Fontainebleau sandstone shows that there is a certain level of pH buffering mechanism which could be caused by carbonates or micas but since this sandstone is quartz arenite with 99 % quartz the concentration of minerals capable of pH buffering reactions is negligible. This is due to the significant presence of quartz cementation at the detriment of other accessory or authigenic minerals (Haddad *et al*., 2006).

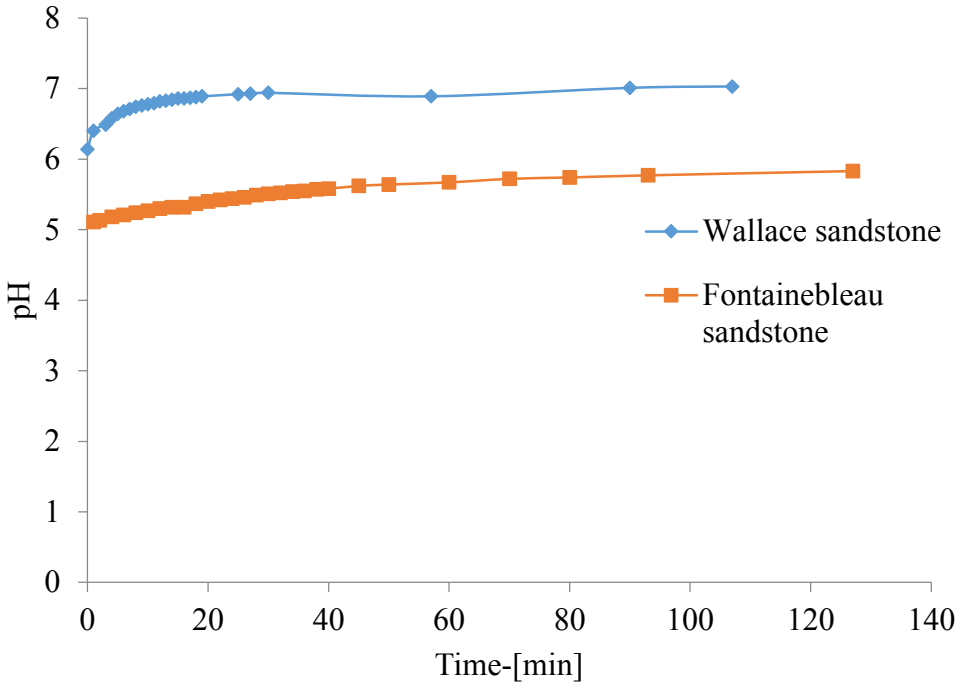

Figure 4-34: Measured pH versus time 10 g of each sample in aqueous solution (NaCl: 43.5gm/l+CaCl: 12.6 g/dm^3) with an initial pH of 5.37 (from appendix 4.6.1)

The initial pH of the experimental brine after acidification was 5.37. When powdered samples of different rock types were added and stirred the initial pH of each mixture was read and the curve for each one starts at the respective initial pH value.

Figure 4-35 shows plots of transient hydrogen ion concentration versus time for a 10 gram sample of each rock for an initial pH of 5.37. Hydrogen ion concentrations were computed from transient pH values using the chemical definition of pH. Accordingly, the curve for Fontainebleau lies above that for Wallace because of the high transient hydrogen ion concentration compared to that of Wallace sandstone. Both curves do not start at the same point because when samples of each rock is mixed with acidified brine the initial pH of the aqueous solution after stirring to achieve an initial pH will be different because of difference in the extent of pH buffering

Figure 4-36 and Figure 4-37 show similar plots for both sandstones using 10 g with an initial aqueous solution pH of 1.76. Similar trends are observed in these plots.

The initial pH of the experimental brine after acidification was 1.76. When powdered samples of different rock types were added and stirred the initial pH of each mixture was read and the curve for each one starts at the respective initial pH value.

Figure 4-38 and Figure 4-39 show similar plots for the case of 2 g of each sample powder for an initial solution pH of 1.76. In these plots the figures for Fontainebleau sandstone experiments do not start from their initial pH values after sample addition to acidified brine and stirring to obtain an initial pH. There was no special reason. In all cases, experimental results confirm the presence of strong pH buffering reactions for Wallace sandstone and almost negligible pH buffering mechanism for Fontainebleau sandstone reactions.

X-Ray diffraction analysis for Wallace sandstone show the presence of glauconite and mica. These micaceous minerals are capable of cation exchange reaction by exchanging frame work potassium (Saleem, 1993) for solution cation which is hydrogen ions in this case. This cation exchange reaction has been used as the basis of potassium leaching from glauconitic sandstones and mica bearing rocks. In this regard Yadav *et al.* (2000) have reported potassium dissolution reaction from glauconitic sandstones using dilute solutions of hydrochloric acid, nitric acid and sulfuric acid similar to that used in this study. They reported that the kinetics of leaching reaction can be described by a chemical model during the initial stage and diffusive model during the latter stage. Osman & Suter (2000) have also reported strong cation exchange capacity (CEC) of muscovite. In the ground water community Chapelle and Knobel (1983) have reported the potential for potassium contribution to ground water from glauconite in Maryland aquifer. These researches involving cation exchange reactions between micaceous minerals and aqueous solutions give possible clues that, the experimental observations in this thesis work involving cation exchange experimental work is likely due to potassium release from muscovite or glauconite. In these experiments, the possibility of pH buffering due to carbonate presence in all Wallace sandstone samples is negligible due to the negative result for carbonate analysis as seen in Table 4-7.

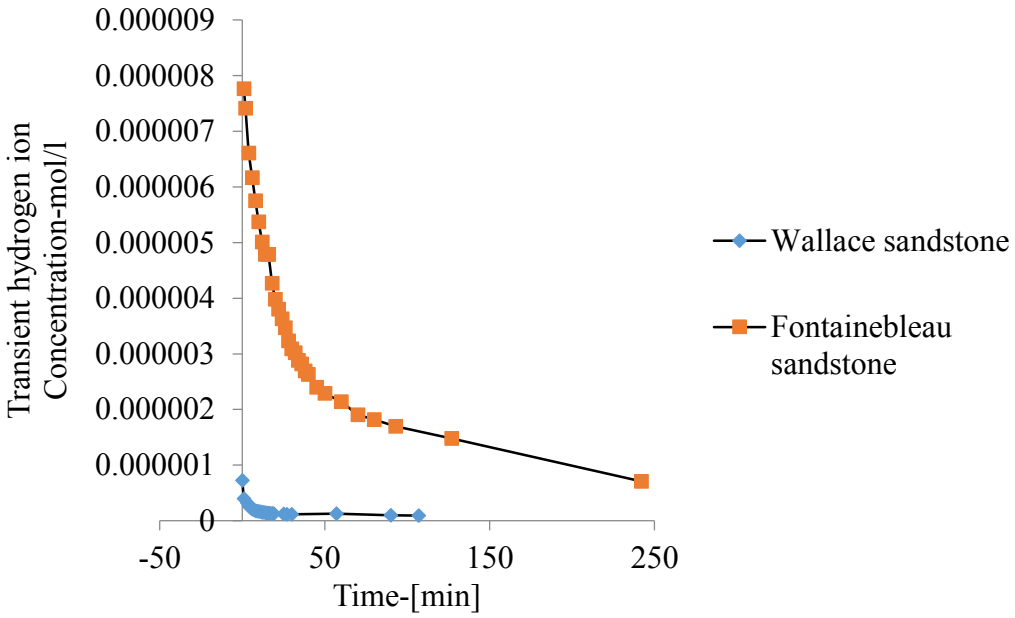

Figure 4-35: Transient hydrogen ion concentration versus time pH 5.37 (from appendix 4.6.2)

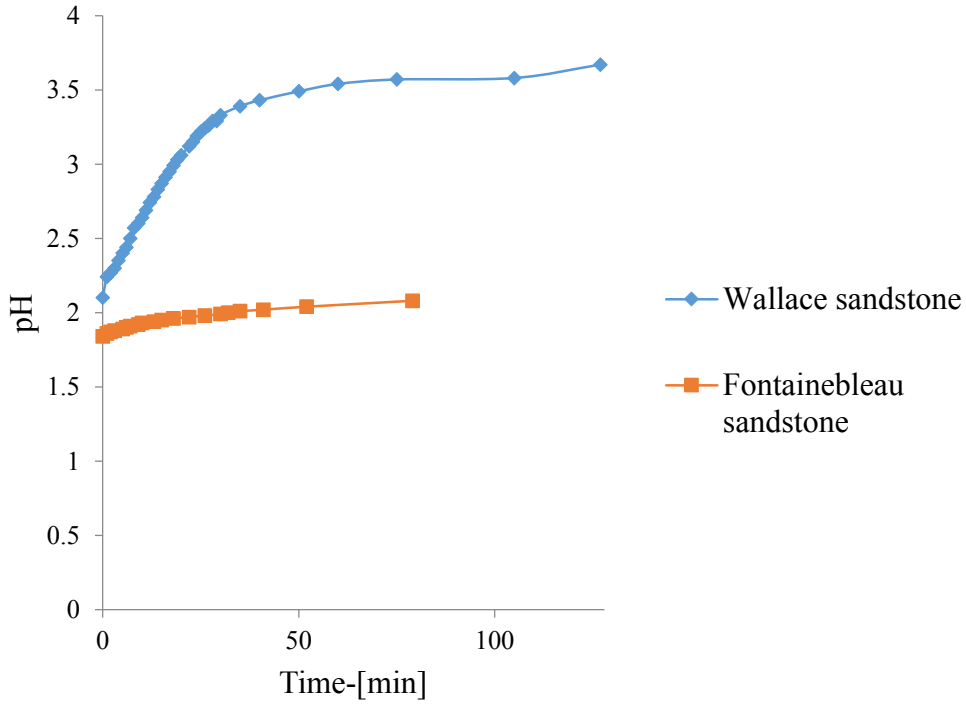

Figure 4-36: Measured pH versus time 10 g of each sample in aqueous solution (NaCl: 43.5 g/dm^3+CaCl: 12.6 g/dm^3) with an initial pH of 1.76 (Wallace sandstone-blue, Fontainebleau-red) (from appendix 4.6.3)

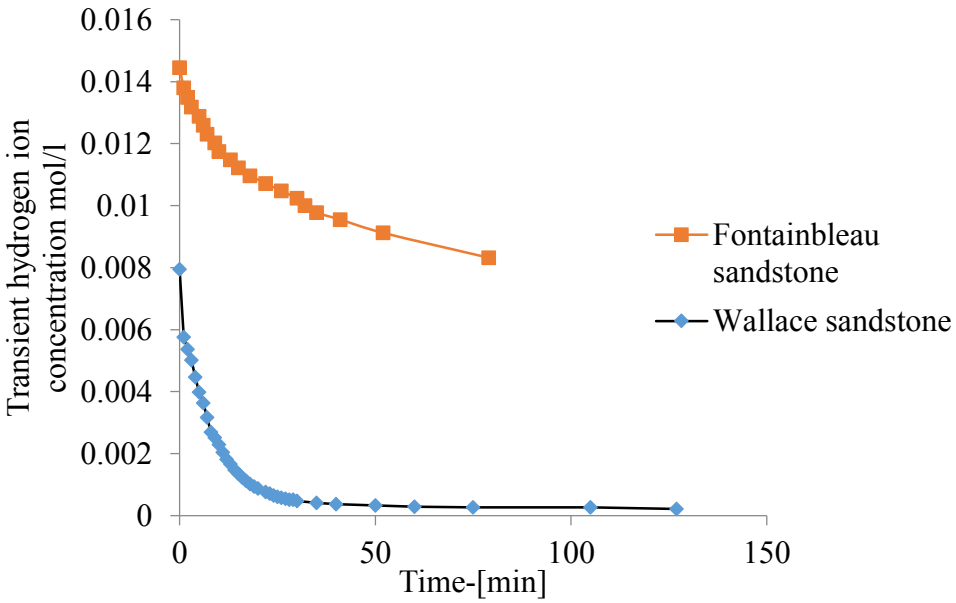

Figure 4-37: Transient hydrogen ion concentration versus time for equal to pH 1.76 (from appendix 4.6.4) using 10 g of sample

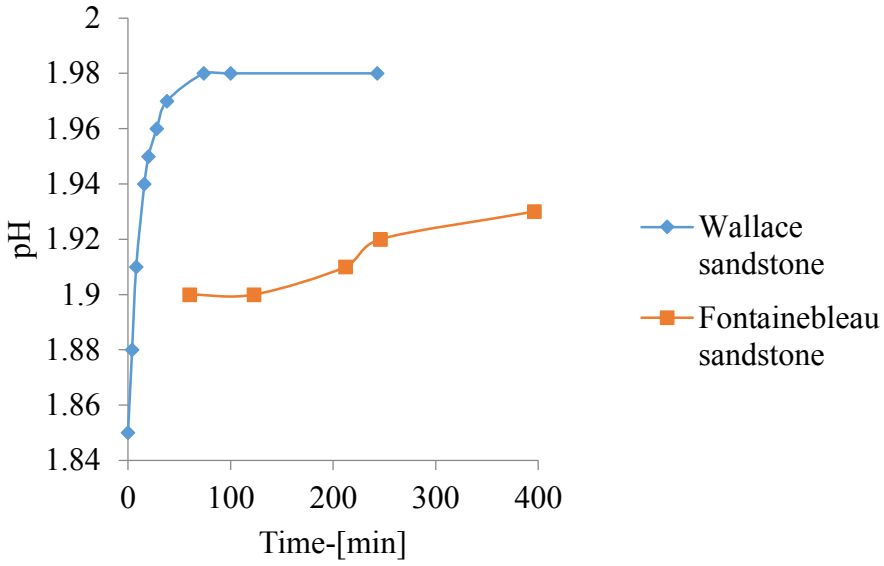

Figure 4-38: Measured pH versus time 2.2 g of each sample in aqueous solution (NaCl: 43.5 g/dm^3 + CaCl: 12.6 g/dm^3) with an initial pH of 1.76 (from appendix 4.6.5)

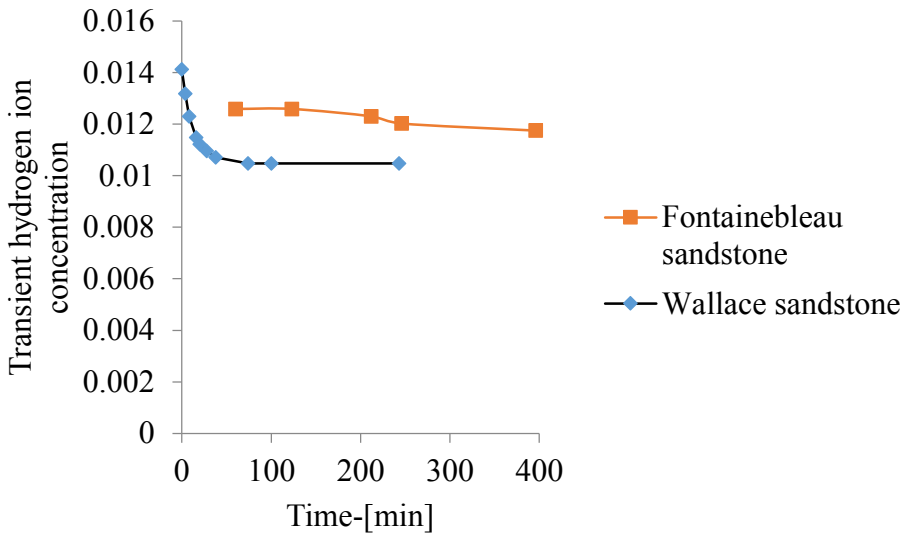

Figure 4-39: Transient hydrogen ion concentration versus time pH 1.76 for 2.2 g of samples in aqueous solution (from appendix 4.6.6)

Figure 4-40 shows combined plots of transient solution pH versus time for Wallace sandstone samples for different initial solution pH. The trend is similar to those revealed by previous plots

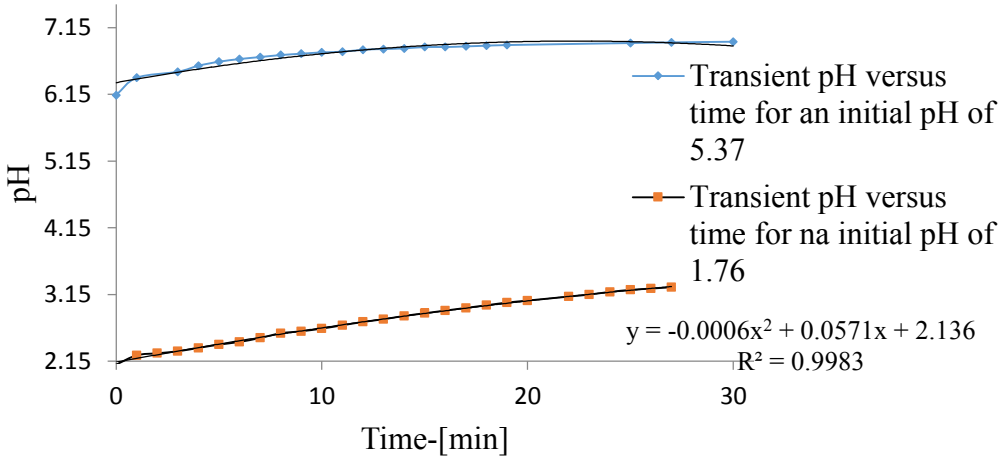

Figure 4-40: Combined plot of transient pH of aqueous solution versus time for Wallace sandstone at different initial pH of aqueous solution

Table 4-6 shows results of potassium analysis for Wallace Sandstone and Fontainebleau Sandstone. With the presence of micaceous and glauconitic phyllosilicates the release of potassium into solution is inevitable. In this regard, Table 4-8 confirms the anticipation.

Table 4-6: Results of potassium analysis

Sample	Potassium concentration mg/l
Acidified brine	3.39
Acidified brine with pulverised Wallace sandstone sample	28.5, 27.5
Acidified brine with pulverised Fontainebleau sandstone sample	9.6

From Table 4-6, initial acidified brine analysis gave 3.39 milligram of potassium per liter. This was taken as the base line value. Acidified brine with Wallace sandstone pulverized sample gave 29.5 mg of potassium/dm^3. A repeated analysis gave 27.5 mg/l. The result for pulverized Fontainebleau sandstone sample gave 9.6 mg/dm^3. This confirms the earlier anticipation that this sandstone has insignificant proportion of minerals capable of cation exchange reaction.

The result of potassium analysis is therefore quite conclusive that potassium release from minerals in all samples into brine and the taking of hydrogen ion in return was the likely cause of aqueous water pH buffering mechanism. This reaction was more pronounced in the case of Wallace sandstone and that led to enhanced pH buffering during spontaneous imbibition experiments with this sandstone core samples. Results of potassium analyses in the case of Fontainebleau is very low and this points to almost negligible pH buffering mechanism for experiments with this sandstone leading to eminent wettability decreases with decrease in aqueous water pH. Since potassium presence is conclusive this element could be coming from two likely sources of minerals. They are invariably glauconite, muscovite or Biotite detected by X-Ray diffraction analysis. The oxide analysis of Wallace sandstone (Appendix 4 E) contains potassium oxide (%) which reflects the relative amount of phyllosilicate minerals put together

4.8.1 Discussion Based on Individual pH Experiments

The relationship between hydrogen ion concentration on solid surface and that in the bulk solution with regard to the solid- aqueous solution interaction is given as (Chan *et al*., 1975):

$$[H_i]_S = [H_o] e^{\left(\frac{Z_i \psi_o}{k_B T}\right)} \qquad (4\text{-}8)$$

In which $\left[H^+\right]_S$ is the concentration of Hydrogen on solid, $\left[H^+\right]_0$ is the concentration of Hydrogen ions in solution z_i is the charge on this ion, ψ is the potential on solid surface, T is the temperature, R is the universal gas constant and k_B is Boltzmann constant.

At a pH of 5.37 the point of zero charge pH of glauconite (4) is exceeded. Its surface will develop a negative charge. This pH is lower than the point of zero charge pH of muscovite (6.3) therefore its surface will develop a positive charge. At a pH of 5.37, hydrogen ions will be repelled from the surface of glauconite. The only mechanism of hydrogen ion depletion is by exchange with framework cation (potassium).

At a pH of 1.76 the surfaces of muscovite and glauconite are positively charge because the pH value is below their individual point of zero charge pH. Consequently, exchange reactions will be by cations exchange between solution pH and potassium ions from the octahedral framework of glauconite and muscovite. Generally, cation exchange reactions are faster (Srasra *et al*., 2000) and this causes faster change of pH in the case of cation exchange reactions using Wallace sandstone. Cation exchange reaction was not conducted on sand pack samples for the obvious reason that it lacks authigenic minerals to cause this reaction.

4.8.2 Conclusion

Cation exchange reaction experiments in this thesis work were conducted in order to explain the pH buffering reactions observed in Wallace sandstone spontaneous imbibition experiments and to further hold on to the principal hypothesis that cation exchange reaction has the potential to impact wettability trends during geological sequestration of anthropogenic carbon. These reactions were principally responsible for depleting hydrogen ion input from nitric acid dissociation, an effect that buffered brine pH and prevented significant wettability decrease as encountered in the case of Wallace sandstone. Accordingly, results for Fontainebleau sandstone pulverized sample showed less pH buffering reaction. From X-Ray powder diffraction analysis of Wallace sandstone and carbonate analysis coupled with trends in experimental findings for the two rock types, the following conclusions can be drawn:

1. Diagenetic minerals such as mica and glauconite are capable of buffering formation water pH by hydrogen ion consumption through cation exchange reaction potassium ion input from their octahedral frame work structure
2. For sandstones that possess high proportions of these minerals, water wettability of minerals surface will be preserved and formation water pH decreases will be controlled
3. Experimental findings strongly support the hypothesis of the present work that, the most realistic way to obtain an idea about contact angle evolution trends during geological sequestration of anthropogenic carbon is to conduct measurement on rock samples rather than on individual minerals which constitute rocks.

4.9 SPONTANEOUS IMBIBITION STUDIES ON POTENTIAL CAP ROCK MATERIALS

4.9.1 Experimental objective

Apart from saline aquifers that have proven global storage capacity for anthropogenic carbon dioxide storage, depleted oil and gas reservoirs (Stevens *et al.,* 2001) are also suitable candidates due to their already availability and geologic periods of proven cap rock security. The geological implication with regard to their depth of occurrence is that potential cap rocks are likely to be carbonaceous shales with high proportions of carbon (Calvert & Pedersen, 1992). These carbonaceous shales have point of zero charge pH close to that of normal formation waters under normal geologic conditions of carbon sequestration

As carbon dioxide is injected into depleted oil and gas reservoirs accidental fracturing of the storage medium can cause fracture propagation into the cap rock (Detournay, 2004). Under that condition, carbon dioxide will invade the cap rock and its mobility is a major environmental concern because of its potential for potable groundwater pollution at lower horizons. Therefore, investigation of how wettability will evolve and how it will impact both carbon dioxide and resident brine mobility is the prime objective of this section

Under typical conditions of carbon dioxide geological storage, pH decreases will be caused by injected carbon dioxide dissolution and its subsequent hydration to carbonic acid which

dissociates to produce hydrogen ions. pH of aqueous formation brine will therefore decrease as injection goes on. To simulate this experimentally, brine with decreasing pH will be made to imbibe simultaneously into porous sample made of sampled rock powder. The initial pH of formation brine typically encountered under geological carbon storage is near neutral (Andre *et al*., 2007). Consequently, the pH of experimental brine will be reduced below neutral to replicate carbon dioxide dissolution.

4.9.2 Rock Samples and Characterization

Because of the difficulty of getting actual shale samples to represent shale cap rock, slate samples were used for two reasons. One is geological and it has to do with the fact that at depths typical of depleted oil and gas reservoirs shales are likely to undergo low grade metamorphism to produce slates (Hower *et al*., 1976)**.** The other reason is associated with its availability in down town Halifax where a lot of excavation in connection with construction works are going on**.** Slate samples for this study was from a low grade metamorphic shale (Hicks *et al*., 1999) of the Meguma Group of Canada. The samples were taken from a construction site in down town Halifax. Figure 4.9.1 shows this. The motivation for opting for a low metamorphosed shale (slate) stems from the fact that, elsewhere (Debecker & Vervoort, 2013) , the behaviour of cap rocks of similar lithologies under low grade metamorphic conditions have been studied. The composition of this rock sample obtained from construction sites in down town Halifax is assumed to be similar to that obtained by Erslev (1998), appendix 4.9.1 in the present work. This is because the author studied the mineralogy of this group.

Figure 4.9.1: Samples of Meguma Slate from a construction site in down town Halifax (Queens Street, between 1358-1478)

4.9.3 Sample Preparation

The samples were crushed in a mold using a piston and two size range fractions were sieved for the experiment based on the size of the wire gauze used to cap the bottom of the custom built imbibition tubes used in this experiment. This procedure was taken because the custom build imbibition tubes have open ends and this requires using a wire mesh to cap one end in order to contain particles or grains meant for the porous pack. This prevented particles from falling into the beaker containing the spontaneously imbibing brine.

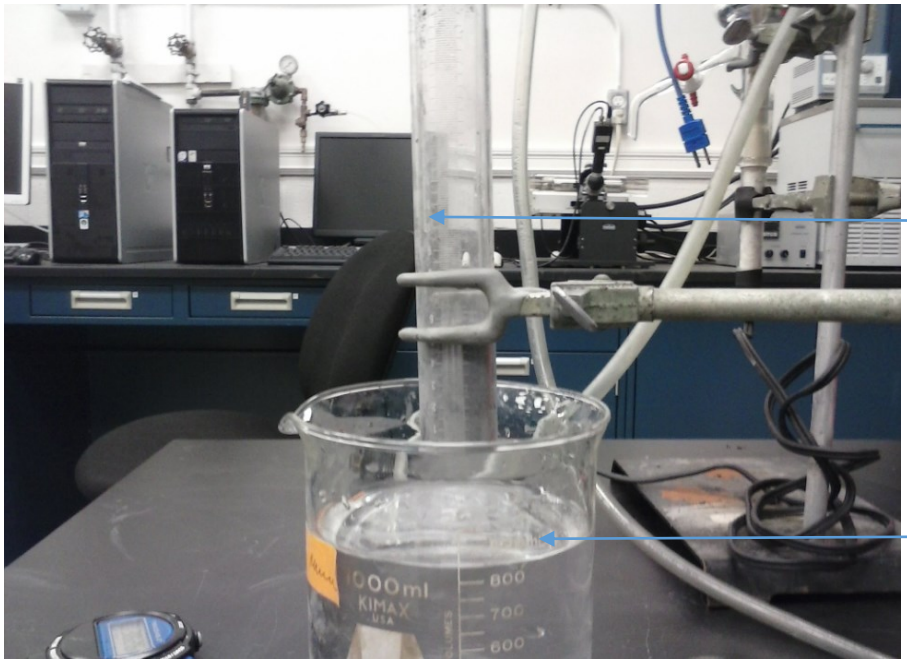

Figure 4.9.2: Experimental set up for spontaneous imbibition

4.10 RESULTS AND DISCUSSION

Theoretically, imbibing brine interacts with rock surface and provides the opportunity for water rock interaction which leads to protonation or deprotonation of surface sites and this is the principal cause of solid-liquid interfacial tension changes (Chatelier, *et al*., 1995) leading to contact angle change. The experimental methodology of this study, therefore, replicates those of actual geological conditions of sequestration and the results will be discussed as follows:

Figures 4.9.3 through 4.9.10 show plots of height rise squared versus time with very good regression coefficients showing close agreement between experimental results and the theory of early spontaneous imbibition dynamics presented in Chapter 2. Experimental data for the plots are found in appendices starting from 4.9.3 to 4.9.4. In all cases, the regression coefficient are above 0.95.

Experimental plots for pH equal 6.95 (size: 300-335 micrometers)

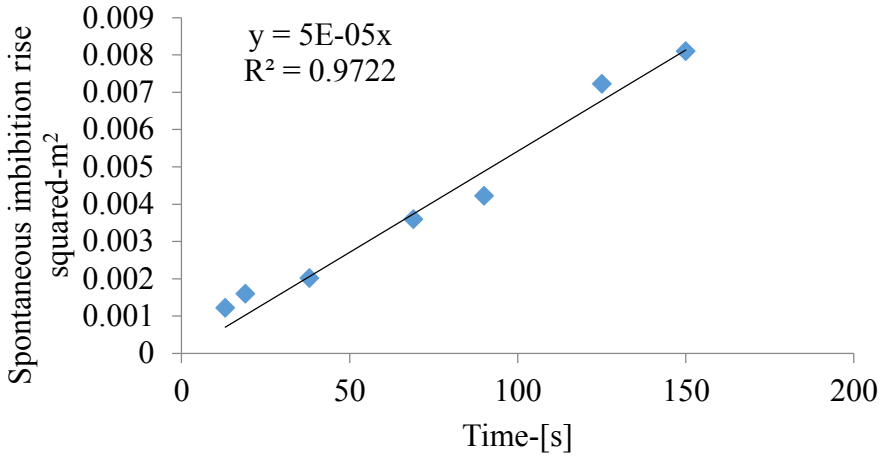

Figure-4.9.3: Experimental plot for pH equal to 6.95

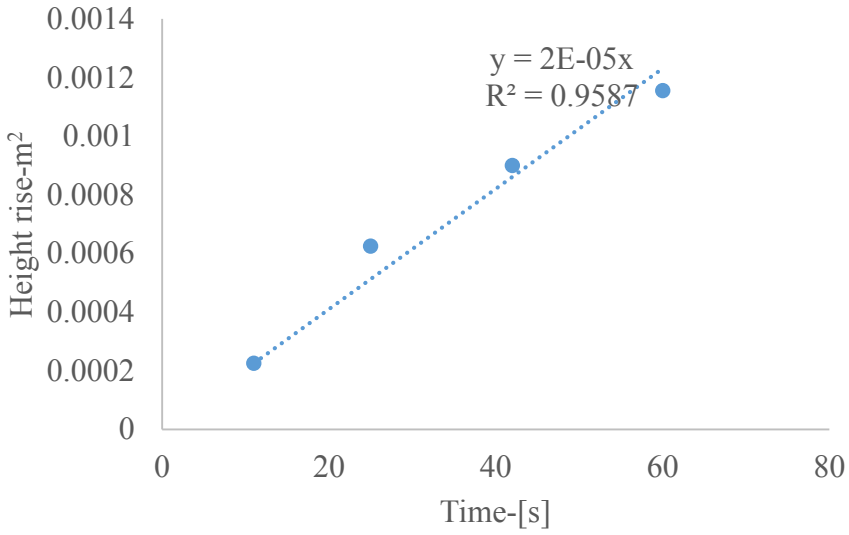

Figure 4.9.4: Experimental plot for pH equal to 6.95 repeated

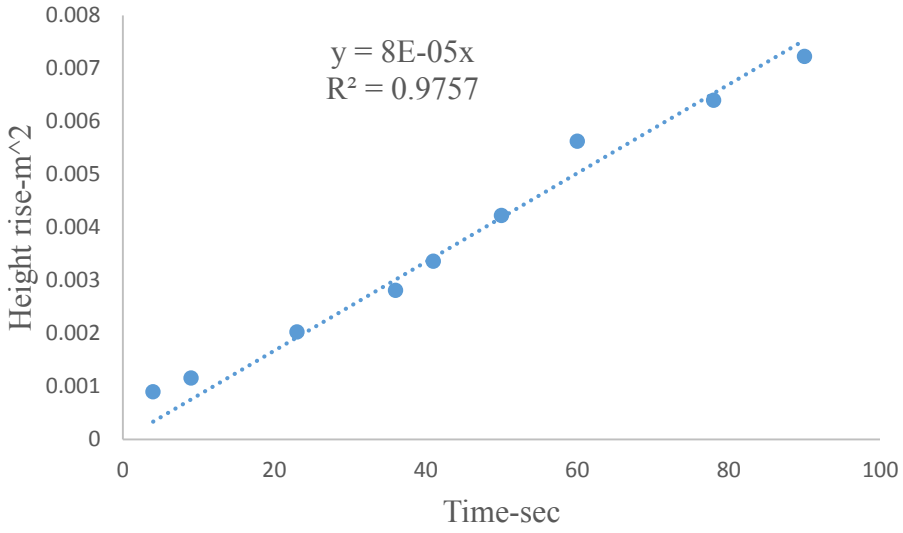

Figure 4.9.5: Experimental plot for pH equal to 5.05

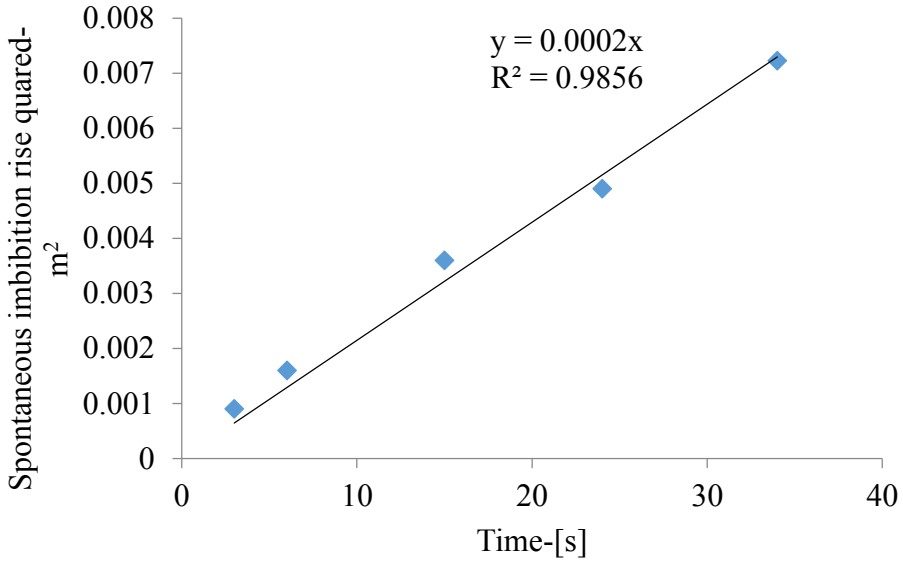

Figure 4.9.6: Experimental plot for pH equal to 5.05 repeated

Experimental results for sizes (106-163) micrometer range for pH equal to 6.95

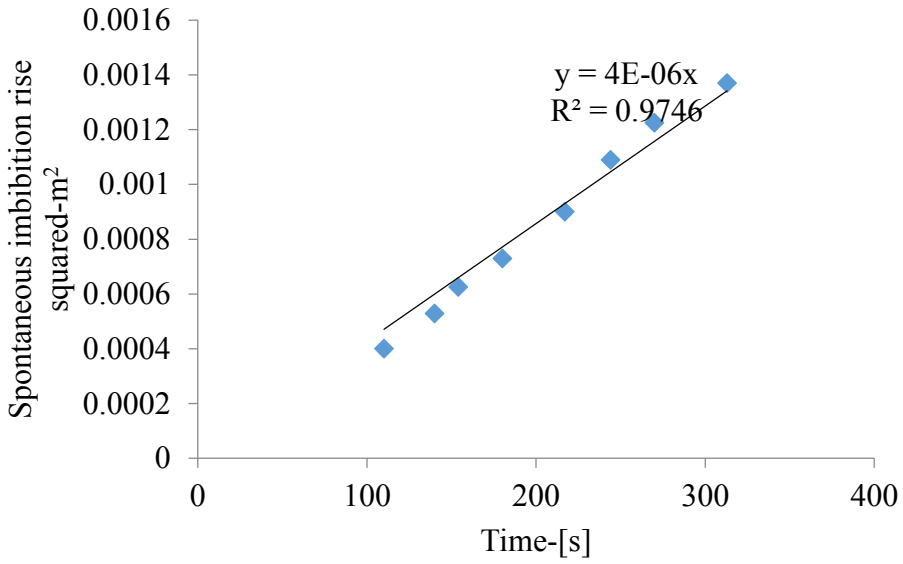

Figure 4.9.7: Experimental plot for pH equal to 6.95

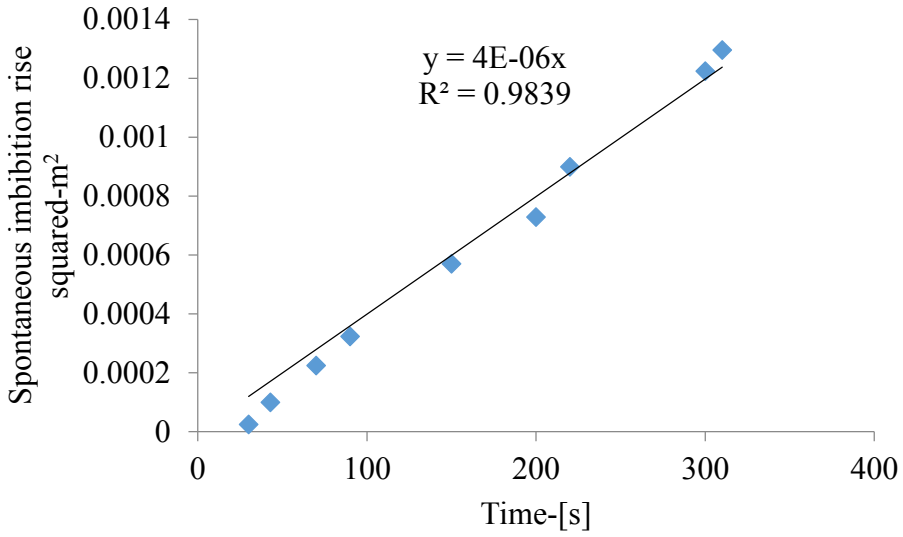

Figure 4.9.8: Experimental plot for pH equal to 6.95 repeated

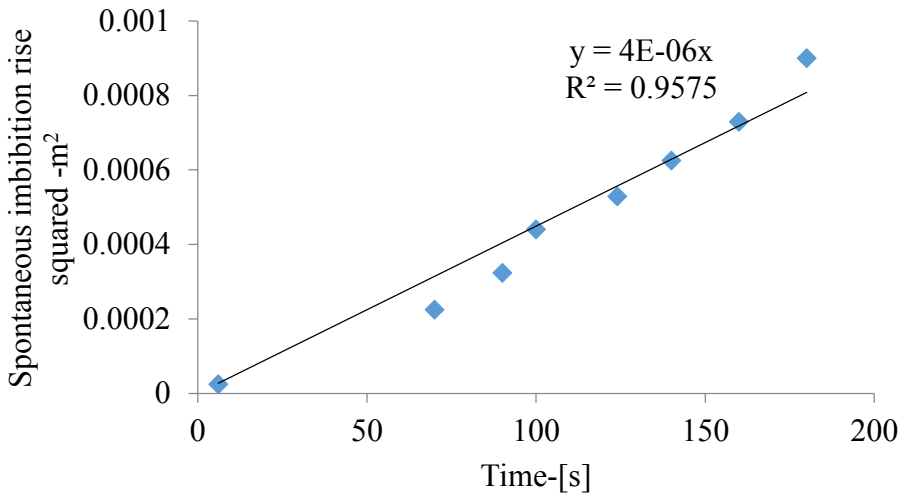

Figure 4.9.9: Experimental plot for pH equal to 5.12

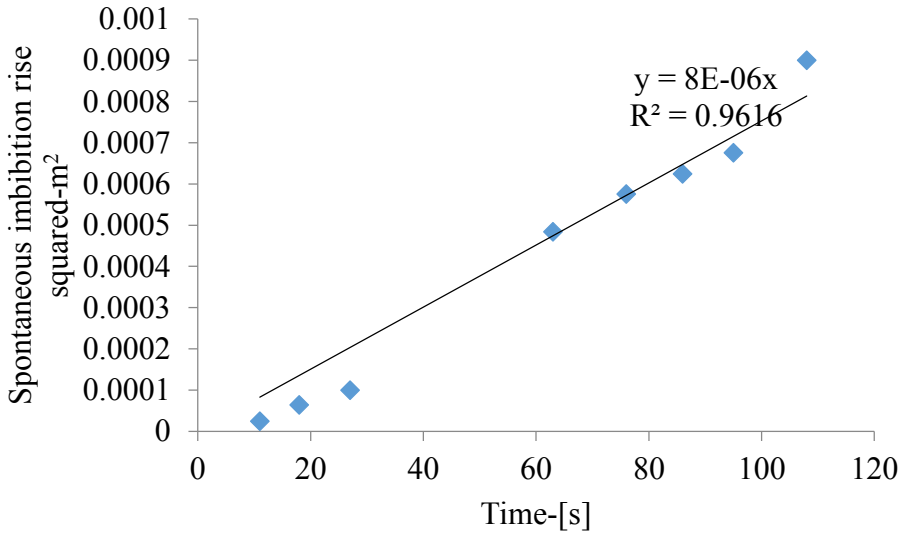

Figure 4.9.10: Experimental plot for pH equal to 5.12 repeated

In these experiments, information about contact angle change was deduced from change in gradient similar to that of sand pack experiments. This means the porous packs were compacted in a predetermined manner to ensure consistent porosity and permeability. This means that if the gradient increases, wettability increases and *vice versa*. Table 4-7 sums up the gradients and regression coefficients from graphical plots of experimental results. In all sizes ranges, the results show that as pH decreases the gradient of the plot increases

and that means wettability increase. However, for the size range of 106-163 micrometers, the first experimental result showed a lower value of gradient at pH equal to 5.12 compared to that at 6.95. The repeated experiment, however, produced a gradient value that follows the expected trend when compared to the gradient at pH equal to 6.95

Table 4-7: Deduced parameters of experimental plots

Size range micrometer	pH	Experiment Gradient m^2/s	Regression coefficient	Repeated gradient	Regression coefficient
300-335	6.95	$5*10^{-5}$	0.97	$2*10^{-5}$	0.958
	5.15	$8*10^{-5}$	0.98	0.0002	0.99
106-163	6.95	$5*10^{-6}$	0.97	$4*10^{-6}$	0.98
	5.05	$4*10^{-6}$	0.98	$8*10^{-6}$	0.96

From the point of view of surface charge chemistry and minerology it is possible to discuss the experimental trend in wettability evolution for slate. The Meguma slate is carbonaceous (O'Brien & Charles, 1985) with silica content similar to that reported elsewhere (Wang & Wang, 1995). , appendix 4.9.2. The point of zero charge pH reported in this work (Wang & Wang, 1995), is near 7.8. This agrees quite well with the point of zero charge pH of carbonaceous shales reported by Pikaray *et al*., (2005). In this regard, appendix 4.9.2 in this work shows that carbonaceous shales with silica content closer to that of Meguma slate have point of zero charge pH closer to 7.8. The implication with regard to surface charge development as pH decreases is that there will be protonation of the surface silanol groups leading to increases in surface change density. In the wettability literature, increasing surface charge density leads to increases in wettability (Bodhak *et al*., 2009) and decreasing surface charge density leads to an opposite effect. This trend in surface charge increase and type of surface charge is what is expected from the concept of the point of zero charge pH of solid surface. Generally, the point of zero charge pH is the pH of the aqueous solution at which the net charge is zero (Parks & Bruyn, 1962). Increasing the pH above the point of zero charge leads to increase in surface charge density which will be negative with negative potential and decreasing the pH below the point leads to increase in surface charge density which will be positive with positive potential (Naidu *et al*., 1994-Figure 1). This means decreasing pH towards this point will decrease surface charge and lead to wettability decrease. In the case of the present study, the assumed point of zero charge pH value for

slate surface means that at a pH of 6.95 the surface charge was positive. As the pH decreased to 5.05-5.12, the surface charge was increasing and that means wettability increase. Therefore, increases in gradient as pH of experimental brine decrease is what is theoretically expected from wettability theory related to surface charge density (Naidu *et al*., 1994). Trends in wettability observed in this study is quite comparable to that of the work of Takahashi and Kovscek, (2010-Figure 10) who found that wettability increased at pH values below the point of zero charge pH of siliceous shales. In this regard, a mineral with the point of zero charge pH equal to or above the pH of normal formation brine is calcite. This mineral has a point of zero charge pH between 8 and 9 (Somasundaran & Agar, 1967). This means that for experimental conditions with regard to pH using calcite, wettability will increase as pH reduces under normal geological conditions. This observation has been reported by the work of Wang *et al*., (2013).

Due to wettability evolution trends observed in these experiments it becomes necessary to consider the mineralogy of rock or slate in relationship to the surface chemistry, particularly the point of zero charge pH. Rock is an aggregate of minerals (United States Patent No. US 3666506 A, 1972) James Jr, and it is expected that its effective surface chemistry characteristics such as the point of zero charge pH will reflect the compositions of individual minerals (Schwarz *et al*., 1984). Slate consists predominantly of clay or micas depending on the degree metamorphism but sometimes with significant proportions of quartz and subordinate amounts of calcite pyrites and hematite (King, 2005-2016). On the basis of this aggregation of minerals one would expect that the effective point of zero charge pH would be controlled by those of mica which is 6.6 (Sverjensky, 1994) and quartz which is averagely 3. The estimate from Sverjensky (1994), is from crystal chemistry. An estimate based on surface charge variation with pH gives a value around 7.5 (Butt *et al*., 2003). Thus, based on the work of Schwartz *et al.* (1984), the point of zero charge pH of slate is expected to have a value between 3 and 7.5. Therefore, the initial pH of the experimental brine used in the present study was likely below the effective point of zero charge pH to cause positive charge development. Consequently, at any pH from 5.05-5.12 the surface charge density increased from that at pH equal to 6.95 and wettability increase was therefore expected (Bodhak, *et al*., 2009). There is, therefore, a good agreement between established theory and the experimental observations of the present study. Finally,

this trend in wettability variation for pH of aqueous solution below the point of zero charge pH of slate means that there will be enhance water wettability with pH in the event of gas breakthrough to prevent extensive migration of Carbon dioxide through the cap rock.

4.10.1 Relative Error Calculation

In these plots uncertainties were determined using graphical error analysis, for plots with regression coefficient below 0.95. Details of approach are found in appendices J and K series (page 272-277). Accordingly, relative errors were derived for Figures 4.94, 4.99 and 4.9.10. Values are 0.098, 0.06 and 0.12 respectively. These uncertainties are quite minimal compared to actual values.

4.10.2 Conclusion

In the petroleum literature, predominant cap rock lithologies are fine grained rocks (shales) and evaporates. If injected anthropogenic carbon dioxide is to be contained in the geologic repository then its stratigraphic trapping capability by cap rocks must be guaranteed. This guarantee can be viewed in two aspects. One is its ability to provide a high breakthrough capillary pressure to contain the column of injected gas. The other is related to the relative mobility of carbon dioxide in the cap rock in the event of breakthrough. What is more, the petroleum literature has been so much obsessed with traditional shales as cap rocks to the detriment of their low grade metamorphosed equivalents which are slates. It is the view of the present study that this should not be the case because there are low grade metamorphosed shales or slates in the sedimentary column that can be potential cap rocks related to geological sequestration of anthropogenic carbon dioxide. In all cases, wettability evolution of the system shale/slate rock-brine-carbon dioxide has not been reported. This study has conducted an experiment to determine pH induced wettability evolution in slate and the following sum up the conclusion of this study:

1 Increases in surface charge density will result in wettability increases in accordance with wettability literature
2 Regarding the net point of zero charge pH of slate surface, trend in wettability changes as observed in this study is supported by experimental observation in literature published works related to minerals with similar or closer point of zero charge pH

3 The geological implication is that in the event of carbon dioxide leakage into slate cap rock unit its relative mobility will be low because water wettability of the system will be low due to its enhance wetness with pH decrease

4 In the event of carbon dioxide breakthrough into slate wettability increase will increase capillary forces and this will make water displacement difficult

5 Comparison of wettability evolution in slate cap rocks with those of quartz arenite sandstones show that within pH values of formation brine under geological carbon storage, low water wetness with low displacing capillary pressures will be encountered for sandstones while the opposite will be encountered for cap rocks

CHAPTER 5 CONTACT ANGLE COMPUTATION FROM DRAINAGE EXPERIMENTAL DATA

5.1 INTRODUCTION

The principal motivation of this thesis work is the dependence of contact angle for the system CO_2-brine-rock not only on one mineral of the system as pointed out in previous chapters but rather on the mineral aggregate of the system. Accordingly, Chapter 4 was devoted to proving the effect of rock mineralogy on contact angle where the pH of formation water decreases following CO_2 injection. This task was achieved using the spontaneous imbibition flow. Wettability is a fundamental physiochemical phenomenon related to multiphase flow in porous media (Fatt and Klikoff Jr.,1959) and encountered for both imbibition (spontaneous and force imbibition flows) and drainage flow (Hinkley & Davis, 1986). The water rock interaction, manifest in CO_2-transport in saline aquifers is geochemical in origin and thermodynamically linked to interfacial phenomenon by virtue of wettability (Gray, 1991;Hassanizadeh and Gray, 1993; Leij, 1997) and kinetically, by virtue of the proton mediated dissolution of silicate minerals (Banwart & Steven, 2000). On the other hand, problems of two-phase flow within the system are better viewed within the scope of hydrodynamics strongly linked to the modified Darcy equation for multiphase flow in porous media. The hydrodynamic theories are connected to fractional flow and the frontal advance concept of Buckley and Leveret (Doster & Hilfer, 2011).

In line with the hypothesis that cation exchange reaction of glauconitic and micaceous minerals in sandstones will tend to maintain ambient wettability in glauconitic sandstones during CO_2 sequestration, the principal objective of this chapter is to conduct experiments under conditions where carbon dioxide solubility will occur with increasing gas saturation. In this regard, proton consumption due to this reaction will tend to maintain constant wettability and any method used to compute any wettability related parameter must reveal a constant trend. Also, in the petroleum literature, landmark experiments on CO_2-brine drainage experiments exist that have been conducted at controlled predetermined wettabilities. Therefore, contact angles computed using these data acquired on sandstones of varying glauconite and clay mineral compositions will reflect rock types.

5.2 EXPERIMENTAL CONDITIONS

5.2.1 Ambient wettability variation

In all experiments reported in the literature about capillary pressure and relative permeability measurements (Akbarababi *et al*, 2013; Bennion and Bachu, 2006) maintaining an ambient wettability has always been one of the prime objectives. In these experiments, core samples are saturated with brine-saturated CO_2 at reservoir conditions to ensure that no more CO_2 dissolves during flooding. This prevents further water-rock interaction due to the presence of dissolved species of CO_2 which are the principal causes of ambient wettability evolution. The core is then flooded with CO_2 saturated with brine vapor to avoid the salting out effect.

Results of spontaneous imbibition experiments in Chapter 4 have already demonstrated the ability of Wallace sandstone to buffer pH experimental brine. In line with the potential pH buffering mechanism of Wallace sandstones as established from spontaneous imbibition measurements and cation exchange reactions, this chapter presents the design of an experimental set-up with wettability conditions totally different from those reported in the literature. Accordingly, the ability of Wallace sandstone to buffer brine pH will be tested by ensuring transient wettability change over space. This will be done by saturating the core samples with non-CO_2 saturated brine. The solubility of CO_2 in brine depends on salinity, temperature and pressure. This test design will ensure that as CO_2 pressure builds up in the core at constant salinity and temperature, the pressure dependence of solubility (increasing solubility with pressure, decreasing solubility with salinity and temperature) will reduce wettability with time. In this case, if indeed Wallace sandstone is capable of buffering formation water pH as proven by spontaneous imbibition experiments in Chapter 4, then increasing solubility with pressure must not cause any measurable pH change and this must lead to ambient wettability preservation.

5.3 EXPERIMENTAL PROGRAM

5.3.1 Equipment

The equipment used in this experiment (Figure 5-A) is the Core Flooding System manufacture by Vinci Technology of France. The schematics is similar to that of Figure 5-1 (Poston *et al*., 1970).

This system is fully equipped with differential pressure transducers to be able to measure pressure drop across flowing phases during testing. Its pressure rating is 68.95 MPa. Apart from the pressure drop measuring capability it can measure and digitally display axial and radial stresses under reservoir testing conditions. It has Hastelloy accumulators that enable the system to hold the test fluids under reservoir condition of temperature. Temperature during testing can be controlled to a maximum of 300^{o}C. During testing, the core sample is contained in a core holder where confining and axial stresses under reservoir conditions. The injection system is equipped with two pumps, with one as a standby pump during testing. The separator system is designed to separate two producing fluids. Testing is monitored digitally on a computer screen where pressure history data is stored.

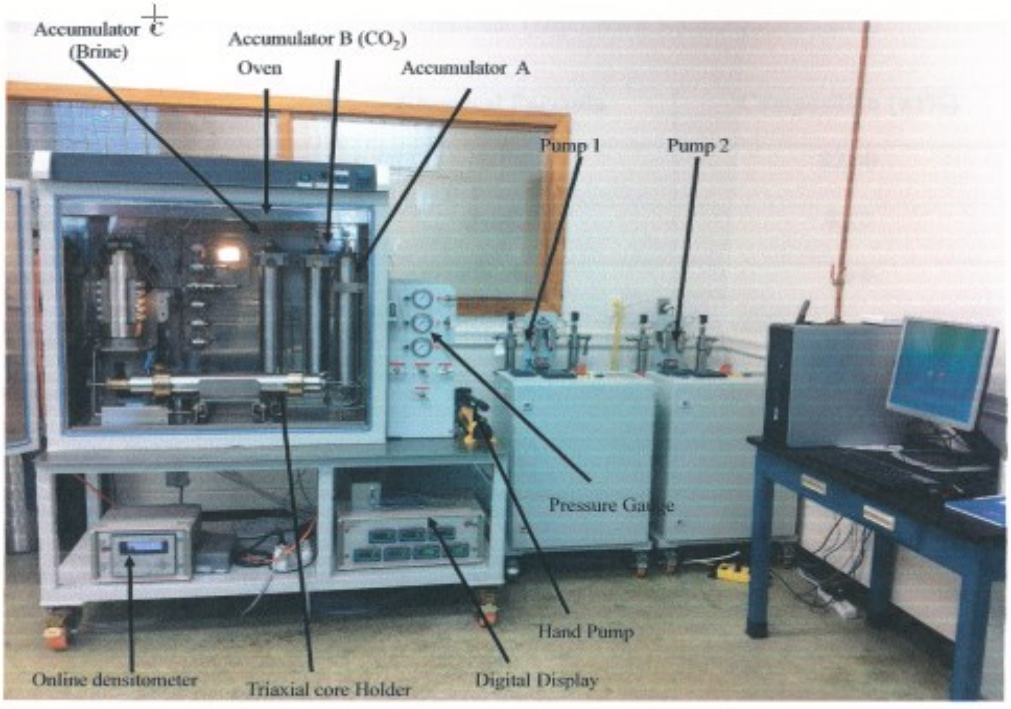

Figure 5-A: Test chamber with separators, core holder and accumulators

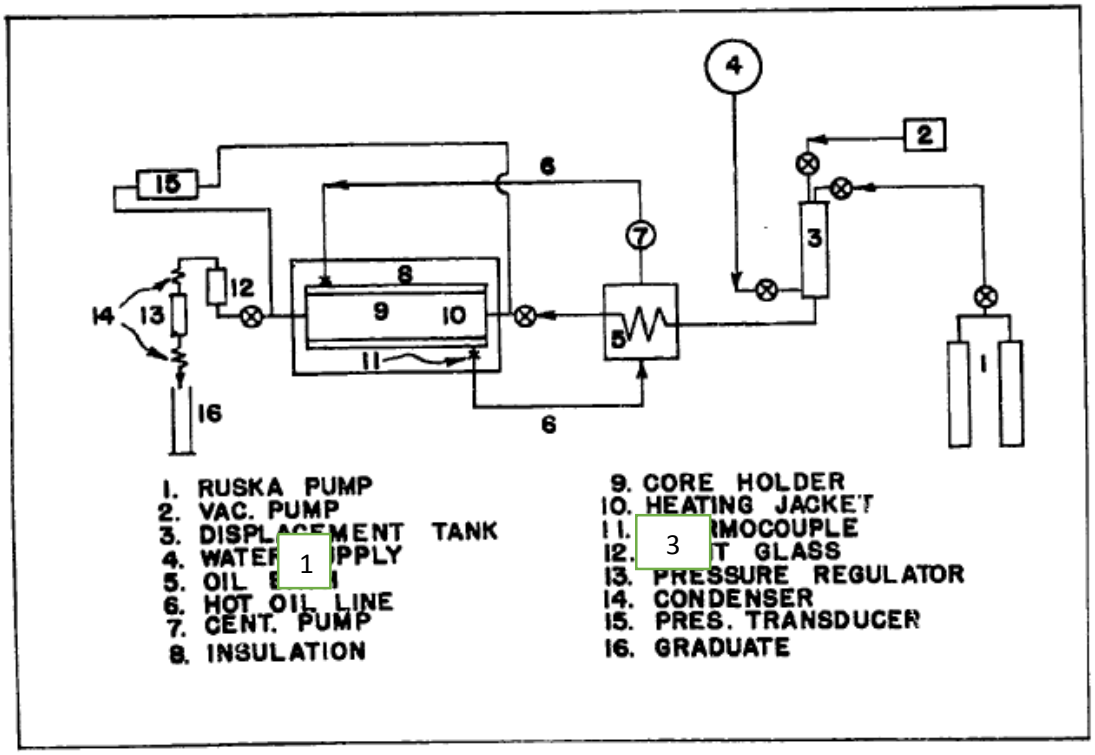

Figure 5-1: Schematics of Testing Equipment (Poston *et al*., 1970)

5.3.2 Injection plan

In view of test material availability limitations this test was carried out with dual purpose. One was to obtain relative permeability data under supercritical conditions for a separate project report (Nwajiaku, 2011) and the other was to test the theory that Wallace sandstone is capable of formation water pH buffering. In this experiment, three test temperatures were selected to ensure supercritical conditions of CO_2. They were 55ºC, 65ºC and 75ºC. Since the objective of this test was to verify the theory that Wallace sandstone has formation water pH buffering capability, the major goal in the experimental set-up was to create appropriate *in situ* hydraulic and stress conditions for flow. This had to do with selecting an appropriate pore pressure (pump pressure) and confining or overburden stress. The overburden pressure was 20.68 MPa and the pump pressure for injection was 11.03 MPa. Test**s** were, therefore, carried out under supercritical conditions**.** Since confining pressure was greater than pump pressure, flow along the core axis was possible. This set-up also provided the opportunity for obtaining relative permeability data under *in situ* supercritical conditions. The reason is that the selected test temperatures and test pressure are within CO_2 critical conditions. Also, by using a mean global value for an overburden pressure of

0.023 MPa per meter (1 psi/ft) (Christian, 1973), the overburden pressure corresponds to a depth of 915 meters which is above the critical depth of 800 meters (Bachu, 2002).

5.3.3 Test Procedure

The test procedure used here is similar to that reported elsewhere (Bennion & Bachu, 2007) involving the following steps:

i. Mount core sample in the Hassler core barrel in a horizontal manner
ii. Evacuate sample to remove trap gas
iii. Apply net reservoir overburden pressure
iv. Pre-saturate sample with 100% formation brine
v. Increase pore pressure to desired reservoir value while maintaining net overburden pressure and displace formation brine in core by replacing it with CO_2 saturated brine
vi. Heat to reservoir temperature while maintaining pore pressure and overburden pressure
vii. Saturate carbon dioxide with water vapor at operating temperature (55 ^oC, 65 ^oC and 75 ^oC and pressure (11.03 MPa)
viii. Conduct unsteady state relative permeability test by injecting water saturated CO_2 to displace brine in the core sample until irreducible water is achieved

5.3.4 Materials

The core samples have the same dimensions as those used for spontaneous imbibition experiment, 76 length diameter and 38 mm diameter

Brine used in this experiment has the same composition as that used for spontaneous imbibition experiments. This consists of 110 grams of sodium chloride and 23. 1 grams of calcium chloride dissolved in one liter of deionized water.

5.4 COMPUTATIONAL RESULTS

5.4.1 Thermodynamic Calculations

Thermodynamic parameters were computed using equations (2-49) through (2-60) from Chapter 2. Constants required for calculating the density of CO_2 using the virial equation of state was obtained from appendix (5-8). The fugacity coefficient for $CO_2$was deduced from appendix (5-9). To determine the salting out effect of CO_2-brine system the equivalent sodium chloride concentration concept was employed using appendix (5-10). This was achieved by using the concentrations of solutes in brine.

5.4.2 Fractional Flow plots

Fractional flow plots were carried out using two-phase flow theory presented in Chapter 2. Appendices 5-1, 5-2 and 5-3 show calculation results for Wallace sandstone while appendices 5-4, 5-5 and 5-6 show results for Ellersely Sandstone, Cardium Sandstone and Basal Cambrian Sandstone respectively. In this regard, fractional flow plots for Wallace sandstone were obtained by integrating the retardation factors calculated from solubility theory causing Welge tangents to be drawn from the retardation point to make contact with the fractional flow curve. For experiments using literature source data, tangents were drawn from the origin of the fractional flow curve in accordance with theory.

5.4.3 Calculated Flooding Properties

Flooding properties were calculated based on hydrodynamic theories reviewed in Chapter 2. Thus, the specific shock velocity was calculated using Eq. (2-48a). The retardation factor was calculated using Eq. (2-48b). In the case of experimental data at constant wettability conditions obtained from literature sources, the retardation was zero due to non-solubility of CO_2.

5.4.4 Wetting Force Computation

The right hand side of Eq. (3-20) measures the product of gas water interfacial tension and the cosine of the contact angle. In the case of the present experimental set up CO_2 solubility does not maintain constant wettability conditions. The average value, however, can be calculated. This parameter is calculated here as a wetting force. Petrophysical data namely, porosity and permeability for calculation were taken from the cited references in Tables 7 and 8.

5.5 FRACTIONAL FLOW PLOTS OBTAINED BY PROCESSING OF LITERATURE SOURCE DATA

The theory for the derivation of fractional flow curves for drainage experiments at constant wettability conditions has been presented in Chapter 2. The theories governing the drawing of Welge tangent for the case coupling geochemistry and for that without solubility or constant wettability condition has also been presented

5.6 RESULTS AND DISCUSSION

The first column of Table 5-1 indicates experimental temperatures. The second column gives results of water vapor pressure calculated using the required thermodynamic equation (2-54) from Chapter 2. Calculated results show consistency because the vapor pressure of water at a constant salinity must increase with temperature.

Table 5-1: Calculated vapor pressures at experimental Conditions

Temp. [K]	P_{vw} **check** bar
328	0.155
338	0.243
348	0.378

Table 5-1 shows results of calculated vapor-liquid thermodynamic properties. The second column shows calculated CO_2 density using the virial equation of state (Eq. 5-35) (with calculation results in appendix 5-7 using Maple). Results are realistic because the density of CO_2 will decrease with temperature at constant pressure. The third column gives the mole fraction of CO_2 in the vapor phase. As the temperature increases, the vapor phase of water increases leading to a reduction in the vapor phase of CO_2. This is in accordance with the calculated results. The forth column shows calculated vapor phase fraction of CO_2 which reflects a decreasing trend with temperature. The fifth column shows the calculated solubility of CO_2 using Eqn. (2-56c)**.** It shows solubility decrease of CO_2 with temperature at constant salinity of brine. Column 6 shows the calculated retardation factors using Eqn.

(2-48b). This data (column 6) is required for construction of gas fractional flow versus gas saturation curves.

Table 5-2: Calculated vapor-liquid equilibrium properties at experimental conditions

Temp C	Density of CO_2 in vap phase [kg/dm^3]	mole fraction of CO_2 in vapor phase	concentration of CO_2 in vapor phase-M	Concentration of CO_2 in liquid phase con-mol/l	Retardation D
55	0.437	0.99541	9.932	0.947	-0.105
65	0.433	0.99535	9.841	0.831	-0.092
75	0.43	0.99524	9.773	0.764	-0.085

Table 5-3 shows the calculated thermodynamic parameters required for the derivation of the results of Table 5-2. Table 5-4 gives combined results of Table 5-2 and Table 5-3. The fugacity of carbon dioxide (column 6 of Table 5-4) was extracted from appendix 5-9. The salting out effect for carbon dioxide (column 7 of Table 5-4) was deduced from a published work (Helgeson, 1969) by integrating the concept of equivalent sodium chloride concentration of formation brine (appendix 5-10).

Table 5-3: Calculated thermodynamic properties of liquid-vapor phases at experimental conditions

Temp C	Temp K	Equilibrium constant for water at reference point	Activity of water	Fugacity of water-Pa	Total pressure bar	Mole fraction of water in the vapor phase
55	328	0.157137	0.74425	0.236786574	110.453	0.004352
65	338	0.249108	0.74617	0.372000692	110.545	0.004396
75	348	0.382406	0.748308	0.55948168	110.675	0.004491

Table 5-4: Calculated thermodynamic properties together with final carbon dioxide concentration

Tem K	Equilibrium constant of carbon dioxide at reference pressure bar/mol	Mole fraction of water in the vapor phase	Mole fraction of carbon dioxide in the vapor phase	Total pressu re-bar	Fugacity of Carbon dioxide	Salting out effect	Final concentrat ion of CO_2
328	54.95	0.00435	0.99565	110.4 53	0.68	1.689	0.94687
338	64.57	0.00440	0.9956	110.5 45	0.7	1.677	0.83104
348	72.44	0.00449	0.99551	110.6 75	0.72	1.665	0.76427

Table 5-5 gives specific shock velocities for Wallace sandstone experiments. Data for computation were extracted from Figures 5-3 through Fig. 5-5 (gas fractional flow versus gas saturation graphs).

Table 5-5: Calculated flooding properties of Wallace sandstone at experimental conditions

	Temperature-C		
	55	65	75
Specific shock velocity less retardation [-]	7.14	16.67	14.29
Specific shock velocity with retardation [-]	3.3	5.18	5.14
Average gas saturation at breakthrough	0.148	0.118	0.125

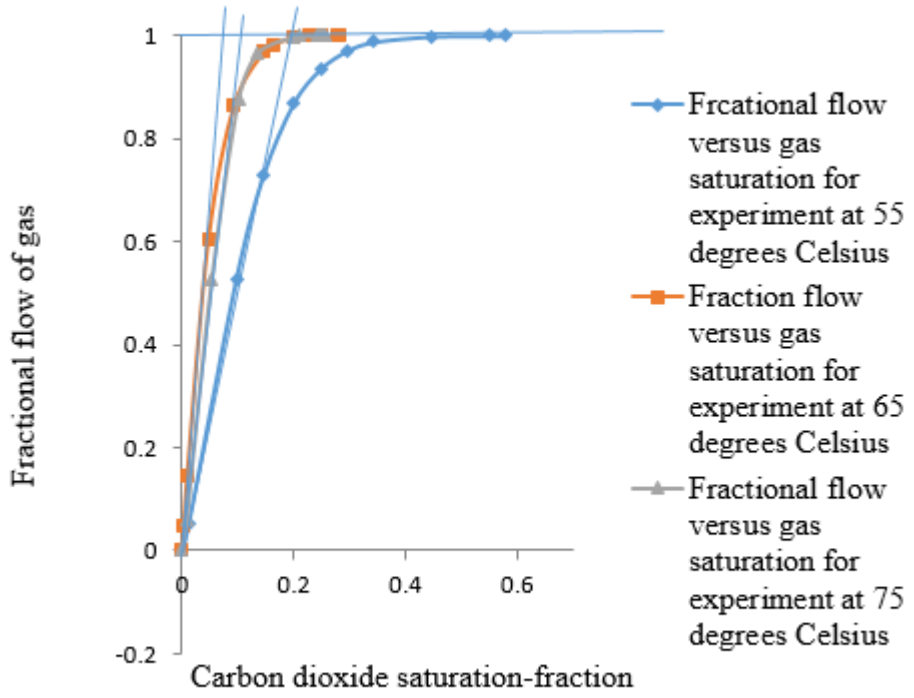

Figure 5-2: Plots of fractional flow versus carbon dioxide saturation for Wallace sandstone assuming no retardation effect in all experiments

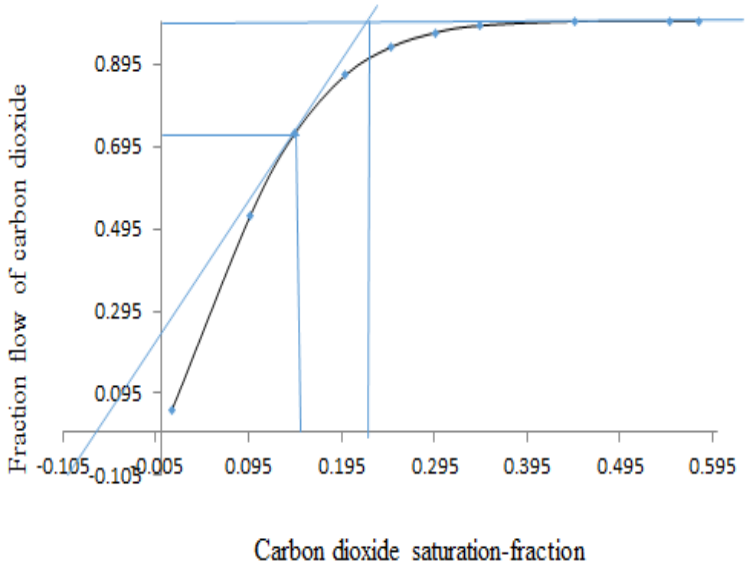

Figure 5-3: Plot of fractional flow versus gas saturation with retardation effect for experiment at 55^{o}C

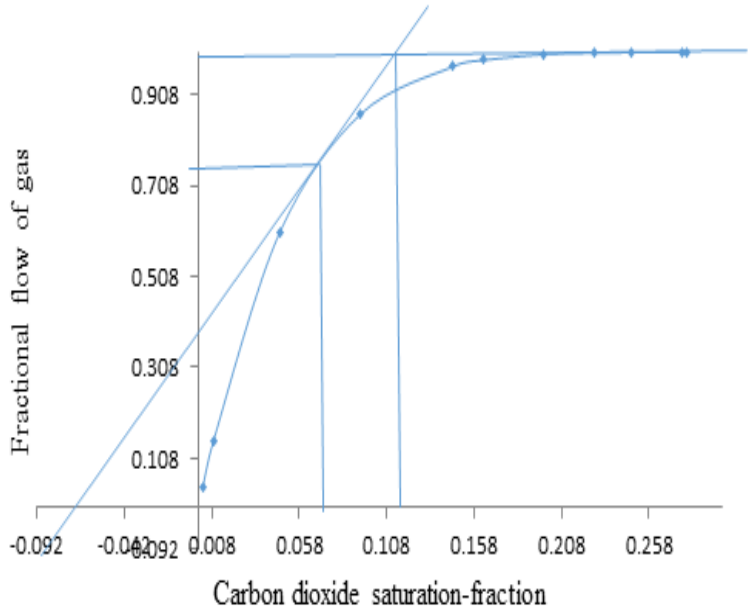

Figure 5-4: Plot of fractional flow versus gas saturation with retardation effect for experiment at 65°C

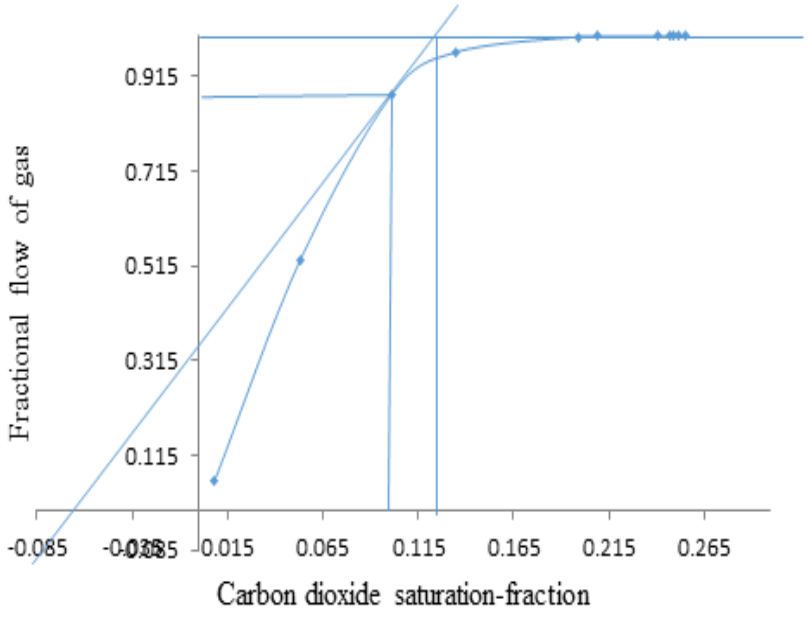

Figure 5-5: Plot of fractional flow versus gas saturation with retardation effect for experiment at 75 °C

Table 5-6a gives calculated flooding properties (specific shock velocity, average gas saturation at breakthrough and average contact angle of the system) using Welge tangent approach. Data for these calculations were extracted from Fig. 5-6 through Fig. 5-8.

Table 5-6a: Calculated flooding properties by processing literature data

	Sample		
	C S	ES	BCS
Specific shock velocity-[-]	2.52	3.66	1.91
Average gas saturation -[-] at breakthough	0.41	0.274	0.53
Average wetting force-N/m	0.006	0.014	0.036
Temperature [°C]	43	40	75

CS= Cardium sandstone, ES = Ellerslie sandstone, BCS = Basal Cambrian sandstone

To understand calculated trends in Table 5-6 requires integrating knowledge of geology and mineralogy of the geologic setting from which core samples were obtained in Alberta for drainage test involving CO_2 displacing brine. The following section will be devoted to that.

5.7 MINERALOGY OF INDIVIDUAL SANDSTONES

Plots of fractional flow versus gas saturation using literature data from Alberta sandstones show differences in gas saturation at breakthrough which is a good indicator of water displacement efficiency. To understand the differences requires knowledge of individual rock mineralogy. Generally, the glauconitic sandstones of Alberta basin are medium to fine grained litharenites with averagely 87% quartz, 2% percent potassium feldspar, 1 percent plagioclase (albite), 5% glauconite (annite), 2%kaolinite, 1% calcite, 1% dolomite and 1% siderite (Gunter, *et al.,,* 2000; Sherwin, 1996).

With regard to Cardium sandstone, diagenetic emplacement of calcite and siderite has been confirmed by carbon and oxygen isotopic data (Machemer & Hutcheon, 1988). In contrast to Cardium sandstone unit of the lower Cretaceous of Alberta, there exists a quartzose sandstone unit, which overlies the Lower Jurassic units with mature and super maturity (Hopkins, 1981). Being quartzose or arenite in nature this unit has a very high proportion of sand, generally above 90 to 99 percent with quartz cement (Huang, 1962), compared

with Cardium sandstone. Modal analysis of rock samples from the Basal Cambrian Unit of the Cretaceous strata point to quartz arenite with at least 95% silica and quartz cement overgrowth (Weides et al., 2014) with muscovite, chlorite, biotite and zircon as accessory minerals.

In the Cretaceous unit of the Scotian Shelf Wallace sandstone is found to be similarly glauconitic from oxide analysis (MEC) and from X-Ray powder Diffraction analysis (present work) with 82% silica and 1.13% potassium oxide, which has a bearing on glauconite composition. In addition to glauconite, another phyllosilicate is muscovite, which appears as visible shiny specs uniformly distributed throughout the rock sample.

Thin section analysis of the Cretaceous sandstones of Alberta reveal digenetic cements comprising kaolinite, illite and montmorillonite (Carrigy & Mellon, 1964). These occur mostly associated with quartzose sandstone implying subordinate proportions whereas in Wallace sandstones glauconite and muscovite occur as significant proportions seen from oxide analysis.

Generally, the geology described so far shows that the sandstones in Alberta basin are litharenites with averagely high silica content compered to Wallace sandstone. On the basis of digenetic emplacement the sandstones can further be distinguished with varying degrees of authigenic clays, which are capable of formation water pH buffering. Consequently, the Basal Cambrian sandstone has a very high silica composition (95%) closer to a monomineralic rock. Cardium sandstone also has silica composition that falls with the range determined for Basal Cambrian sandstone. In contrast to these two sandstone units the Ellerslie unit of the lower Cretaceous of Alberta has been found to contain some amount of digenetic calcite in addition to authigenic clays (Edie & Andrichuk, 2005). Therefore, the effect of rock mineralogy on wettability must reflect more for the case of Ellerslie sandstone. In this regard, Table 5-6b shows that the two sandstone units with high proportions of silica have calculated contact angles quite different from that of Ellerslie sandstone.

Table 5-6b: Calculated average contac angle for different rock types

Sandstone	Average contact angle ^{0}	General quartz content (%)	Reference
Ellerslie	65.17	45-70	(Williams, 1963)
Cardium	69.98	90	(Nightingale, *et al*., 2009)
Basal Cambrian	87.84	65-95	(Talmana, Ernie, Andrew, David, & Stefan, 2013)

This is to be expected because of the increased formation water pH buffering that will be experienced. In this regard, the calculated contact angle using Eq. (3-7) for Basal Cambrian sandstone shows the highest value (87.94 degrees) at an experimental temperature of 75^{o}C, followed by the value for Cardium (69.98^o) at an experimental temperature of 43^{o}C. The value for Ellerslie sandstone from Table 5-6b is the lowest (65.14^o) at an experimental temperature of 40^{o}C. Although all experiments were not carried out at the same temperature, the results of Ellerslie and Cardium can be compared because of the very small temperature difference. In this case, it becomes clear the diverse mineralogy of Ellerslie sandstone affords it a greater formation water pH buffering capacity similar to those of Wallace sandstone in spontaneous imbibition experiments. Apparently, experiment for Basal Cambrian sandstone was conducted at higher a temperature but the high percentage of silica that is pH sensitive with regard to wettability change justifies the high contact angle, meaning a greater decrease in water wettability for this sandstone. At this point it is worth mentioning that average contact angles for Wallace sandstones were physically not meaningful because of solubility changes with CO_2 pressure in the core. Therefore, while experiments for the three sandstones (Ellerslie, Cardium and Basal Cambrian sandstone) were carried out at predetermined wettability conditions by saturating cores with CO_2-saturated brines and injecting brine saturated carbon dioxide to avoid miscibility and wettability changes, experiments for Wallace sandstone core samples were

carried out by injecting water saturated CO_2 into brine not saturated with CO_2. The resulting gas solubility in brine and wettability evolution does not permit calculation of average contact angles for these experiments.

Appendix 5-11 and Appendix 5-12 give data and references for fluid and interfacial properties which are also references from which drainage experimental data were processed in accordance with the theory of the present work. Appendix 5-14 show detailed procedure for contact angle computation.

Tables 5-7, 5-8 and 5-9 show Excel calculation results for drainage flow properties for experiments at 55ºC, 66ºC and 75ºC. Geologically, Wallace sandstone contains glauconite and mica (muscovite). As carbon dioxide dissolves to produce hydrogen ions, cation exchange reactions similar to that shown experimentally in Chapter 4 will be present. Therefore, pH buffering reactions will cause wettability of the system to show slight variation. This is quite the case for this study. Accordingly, the average value of the product cosine of the contact angle, which is wettability and the interracial tension between carbon dioxide and water will show slight variation with water saturation. The average values of this parameter henceforth referred to as wetting force are 0.0158 mN/m, 0.0126 mN/m and 0.0027 mN/m for experiments at at 55ºC, 65ºC and 75ºC respectively. All these average values at each experimental temperature are closer to the values calculated at individual saturations. Therefore, these slight variations in wettability (wetting force) are similar to those observed for spontaneous imbibition experiments.

Table 5-7: Results for Experiments at 55°C (Wallace Sandstone)

Water saturation	Water relative permeability	Carbon dioxide relative permeability	$\sigma \cos\theta$
0.988	0.96	0.001	0.0239
0.903	0.703	0.025	0.0182
0.855	0.574	0.046	0.0182
0.801	0.444	0.076	0.0186
0.752	0.343	0.108	0.0190
0.704	0.255	0.146	0.0190
0.656	0.18	0.19	0.0179
0.553	0.064	0.305	0.0073
0.451	0.007	0.452	0.0001

Table 5-8: Results for Experiments at 65°C (Wallace Sandstone)

Water saturation	Water relative permeability	Carbon dioxide relative permeability	$\sigma \cos\theta$
0.997	0.98	0.002	0.0268
0.991	0.94	0.007	0.0219
0.953	0.703	0.04	0.0174
0.907	0.458	0.079	0.0167
0.854	0.245	0.124	0.0157
0.837	0.189	0.139	0.0145
0.802	0.098	0.168	0.0089
0.773	0.045	0.193	0.0028
0.752	0.02	0.21	0.0005
0.723	0.002	0.235	0.0001

Table 5-9: Results for Experiments at 75 ºC (Wallace Sandstone)

Water saturation	Water relative permeability	Carbon dioxide relative permeability	$\sigma \cos\theta$
0.992	0.94	0	0.0075
0.947	0.637	0.016	0.0071
0.899	0.38	0.057	0.0065
0.865	0.235	0.103	0.0016
0.801	0.059	0.222	0.0008
0.791	0.041	0.247	0.0001
0.759	0.007	0.327	0.0001
0.753	0.004	0.342	0.0
0.751	0.003	0.349	0.0

Normally, the average saturation of the displacing phase at breakthrough is a good measure of injection sweep efficiency (Al Bahlani & Babadagli, 2008) and wettability (Standnes & Austad, 2003). The more wetting the system is with regard to the injected fluid the higher the injection sweep efficiency because of decreased relative mobility of the injected phase and increase relative mobility of the displaced phase. In this study CO_2 is the injection phase while brine is the displaced or wetting phase. The average gas saturation in the systems at breakthrough is 0.148, 0.118 and 0.125 for experiments at 55ºC, 56ºC and 75ºC respectively. These results are quite in line with wettability theory.

Generally, water wettability reduction for the system CO_2-water rock is due to acidity increases. At a constant salinity the solubility of CO_2 will decrease with temperature. This has been clearly shown from thermodynamic calculations (Table 5-2). Therefore, at 55ºC the solubility CO_2 will be higher. The activity of hydrogen ions will be higher compared to activity values at 65ºC and 75ºC due to solubility reduction as observed in Table 2. Under these conditions, the system is more wetting with regard to resident brine as solubility decreases due to temperature increases. This implies a reduction in relative mobility of CO_2 at lower temperatures and a corresponding increase in water relative mobility. The sweep efficiency for gas injection is, therefore, higher at 55ºC decreasing with temperature increase. This explains the observed average gas saturation at breakthrough. However, the result at 75ºC defies this trend. The likely explanation here is that at higher temperatures, the temperature effect on fluid properties plays a major role.

The specific shock velocities also show similar trends. Generally, the more wetting the system is with regard to the injected fluid the lower will the specific shock velocity be at a given temperature. The Table, therefore, shows increases in specific shock velocity from 3.3 at 55^{o}C to 5.18 at 65^{o}C. Once again, the high temperature effect causes this trend to be disobeyed at 75^{o}C. Specific shock velocity calculated without the effect of retardation is physically not meaningful due to the partial miscibility condition (Noh *et al*., 2007)

A molecular dynamic simulation of a system of water molecules has been carried out by Stillinger and Rahman (1972) and the effective pair potential theory was used for calculation. The results showed a breakdown of hydrogen-bond order and a rapid increase in the freedom of molecular motion that accompany temperature rise. This hydrogen bond rupture could be the cause for radical changes in molecular interactions that can impact interfacial tension adding to the already existing effect on dynamic viscosity to cause deviations from expected trends at a higher temperature.

Tables 5-10 through 5-12 (for Ellersely, Cardium and Basal Cambrian Sandstones respectively) show cosines of the contact angles calculated using the mathematical model of this study designed to achieve the objective of deriving contact angle from flow data. As explained earlier, core-flooding procedures involving CO_2-brine systems normally replicate predetermined wettability conditions. Therefore, based on the equation, the product of the cosine of the contact angle and the interfacial tension between gas and water will be constant. This means that at all saturations this product or wetting force will be constant due to non-mutual solubility of phases and therefore constant pH environment. Accordingly, results of computation of contact angles using pertinent data confirms this trend. What is more, calculated contact angles are quite convincing and fall within those normally encountered in petroleum engineering practice. In the system oil-water-silica (sandstone oil reservoir), contact angles have normally been reported ranging from 0 to 40 degrees averagely. This trend is revealed by a published work in Appendix 5-13. This is due to lack of water rock interaction in these systems which impact solid-liquid interfacial tension to cause wettability evolution similar to that encountered in the carbon dioxide-water -rock system.

Wettability is an important factor affecting fluid behavior in the subsurface, including oil, gas, and supercritical CO_2 in deep geological reservoirs. For example, CO_2 is generally assumed to behave as a non-wetting fluid, which favors safe storage. However, in view of geochemical heterogeneity in geologic systems, mixed wettability conditions are possibilities. What is more, recent experiments suggest that with time, the wettability of super-critical CO_2 may change from non-wetting to partially wetting due to changes in electrostatic interactions which impact solid-liquid interfacial tension. These changes are caused by chemical reactions between dissolved CO_2 and subsurface geologic environment. Bandara *et al*. (2016) used multiphase pairwise force smoothed particle hydrodynamics model to study complex pore-scale processes involved in geological carbon storage which integrates the effect of spatial and temporal wettability variations on long-term distribution of the gas in porous media. They concluded that the wettability of the porous media changes from brine-wet to partial-wet or CO_2 wet. Contact angles calculated in the present work fall within partial or CO_2 wetting case as anticipated in the cited work of Bandara *et al*. (2016). In this work, the authors agreed that an angle of 90 degrees falls within partial wetting domain. Iglauer *et al*., (2015) also give a range of intermediate wettability from 80^o-100^o. This means Contact angle calculated for Basal Cambrian Sandstone falls within intermediate and or partial wetting domain while that for Cardium Sandstone comes quite closer.

Table 5-10: Results of contact angle calculation for Ellerslie Sandstone

Gas saturation-fraction	Relative permeability of gas	Relative permeability of water	$\sigma\cos\theta$	$\cos\theta$	θ
0.034	0.0008	0.8052	0.015345	0.4729	65.17
0.051	0.0018	0.7159	0.015217	0.4689	65.17
0.068	0.0034	0.632	0.015114	0.4658	65.17
0.085	0.0055	0.5535	0.015054	0.4639	65.17
0.102	0.0082	0.4127	0.015031	0.4632	65.17
0.119	0.0115	0.4127	0.015038	0.4634	65.17
0.136	0.0153	0.4127	0.015065	0.4643	65.17
0.153	0.0199	0.293	0.015106	0.4655	65.17
0.17	0.025	0.2411	0.015154	0.4670	65.17
0.188	0.0309	0.1943	0.015207	0.4686	65.17
0.205	0.0374	0.1528	0.015254	0.4700	65.17
0.222	0.0446	0.1164	0.015296	0.4714	65.17
0.239	0.0525	0.0851	0.01533	0.4724	65.17
0.256	0.0612	0.0588	0.015355	0.4732	65.17
0.273	0.0706	0.0375	0.015372	0.4737	65.17
0.29	0.0807	0.0211	0.015382	0.4740	65.17
0.307	0.0916	0.0095	0.015386	0.4742	65.17
0.324	0.1032	0.0025	0.015388	0.4742	65.17
0.341	0.1156	0	0.015386	0.4742	65.17

Table 5-11: Results contact angle calculation for Cardium Sandstone

Water saturation-fraction	Gas saturation fraction	Gas relative permeability krg	Water relative permeability krw	$\sigma \cos\theta$	$\cos\theta$	θ
1	0	0	1	----	----	
0.969	0.031	0.0002	0.9715	0.007279509	0.3676	68.43
0.938	0.062	0.0008	0.7539	0.006741623	0.3404	70.10
0.907	0.093	0.0019	0.6468	0.006608104	0.3337	70.51
0.876	0.124	0.0038	0.5499	0.006632401	0.3349	70.43
0.845	0.155	0.0068	0.4628	0.006743913	0.3406	70.10
0.814	0.186	0.011	0.3849	0.006911005	0.3490	69.57
0.783	0.217	0.0166	0.3159	0.007112985	0.3592	68.9
0.752	0.248	0.0239	0.2552	0.007329379	0.3701	68.27
0.72	0.28	0.0329	0.2025	0.007538148	0.3807	67.62
0.689	0.311	0.0438	0.1573	0.007680552	0.3879	67.18
0.658	0.342	0.0569	0.1191	0.007691089	0.3884	67.15
0.627	0.373	0.0723	0.0874	0.007459738	0.3767	67.87
0.596	0.404	0.0902	0.0616	0.006846098	0.3457	69.78
0.565	0.435	0.1107	0.0413	0.00573911	0.2898	73.15
0.534	0.466	0.134	0.0259	0.004190601	0.2116	77.78
0.503	0.497	0.1602	0.0148	0.002516858	0.1271	82.7
0.472	0.528	0.1896	0.0074	0.001155291	0.0583	88.69
0.401	0.599	0.2222	0.003	1.52049E-05	0.0007	89.96
0.41	0.59	0.2582	0.0008	4.31021E-05	0.0021	89.88
0.379	0.621	0.2978	0		AVE	69.98

Table 5-12: Results of contact angler calculation for Basal Cambrian sandstone

Gas relative permeability	Gas saturation-fraction	Water saturation-fraction	Water relative permeability	$\sigma\cos\theta$	$\cos\theta$	θ
0.0003	0.035	0.965	0.9105	6.16E-06	0.0002	87.84
0.00005	0.071	0.929	0.9105	4.68E-06	0.0001	87.84
0.0008	0.106	0.894	0.8248	4.28E-06	0.0001	87.84
0.0012	0.106	0.894	0.743	4.28E-06	0.0001	87.84
0.0019	0.141	0.859	0.665	4.21E-06	0.0001	87.84
0.0029	0.177	0.823	0.5911	4.31E-06	0.0001	87.84
0.0047	0.212	0.788	0.5211	4.51E-06	0.0001	87.84
0.0076	0.247	0.753	0.4552	4.77E-06	0.0001	87.84
0.0123	0.282	0.718	0.3933	5.06E-06	0.0001	87.84
0.0194	0.318	0.682	0.3356	5.3E-06	0.0001	87.84
0.0299	0.353	0.647	0.2821	5.38E-06	0.0002	87.84
0.0449	0.388	0.612	0.2328	5.15E-06	0.0002	87.84
0.0657	0.424	0.576	0.1879	4.41E-06	0.0002	87.84
0.094	0.459	0.541	0.1474	3.16E-06	0.0001	87.84
0.1315	0.494	0.506	0.1114	1.69E-06	0.0001	87.84
0.1805	0.529	0.471	0.08	5.8E-07	0.0000	0.00
0.1805	0.565	0.435	0.0535	9.98E-08	0.0000	0.00
0.2433	0.6	0.4	0.0318	7.45E-09	0.000	0.00
0.3228	0.635	0.365	0.0154	1.44E-10	0.0000	0.00
0.4221	0.671	0.329	0.0045	1.13E-13	0.0000	0.00
0.5554	0.706	0.294	0	4.4E-164	0.0000	0.00

Figure 5-2 shows the fractional flow versus water saturation for Wallace sandstone and the Welge tangents drawn without the effect of retardation. Figures 5-3 through 5-5 show gas fractional flows versus gas saturation and corresponding Welge tangent drawn by taking into consideration retardation effect derived from thermodynamic calculations. Accordingly, the average gas saturations at breakthrough were determined using the frontal advance theory of Buckley and Leveret (Pande *et al*., 1987). Results of fractional flow are found in Appendices 5-1 – 5-3

Figure 5-6 through 5-8 show fractional flow versus gas saturation derived from excel sheet calculations (Appendices 5-4 – 5-6). Data for these plots were obtained by processing drainage flow data in accordance with two-phase flow theory. Pertinent parameters deduced from fractional plots are found in Tables 5 and Table 6 respectively.

Plots of fractional flow *vs.* gas saturation using literature data from Alberta sandstones show differences in gas saturation at breakthrough which is a good indicator of water displacement efficiency and the geological reason has already been discussed. Accordingly, specific shock velocities reflect the gradients of Welge tangents such that the higher the specific shock velocity the less wetting the system is and the higher the calculated contact angle.

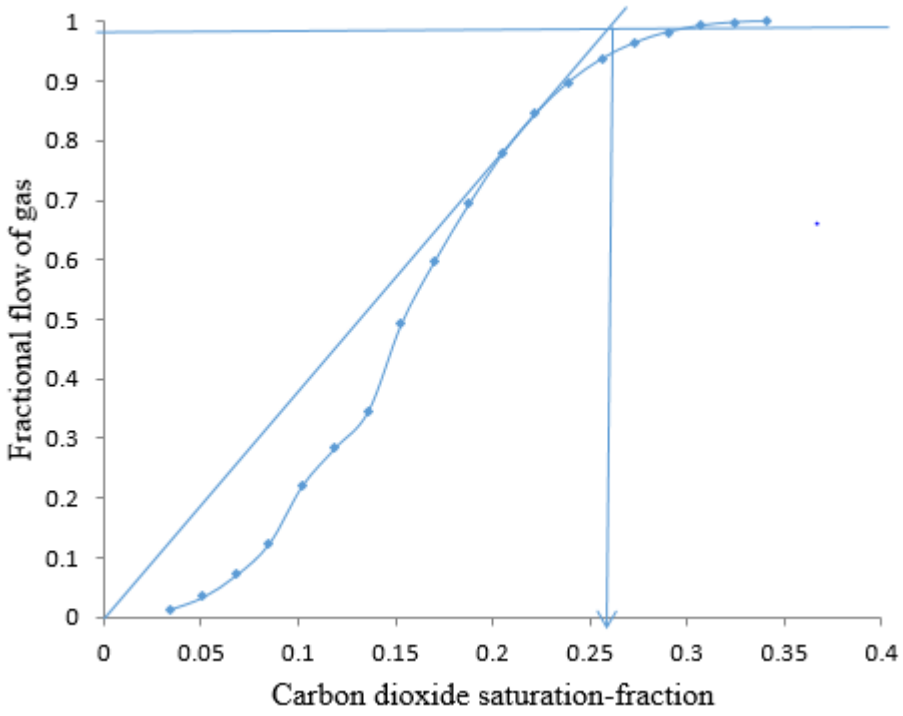

Figure 5-6: Plots for Ellerslie sandstone

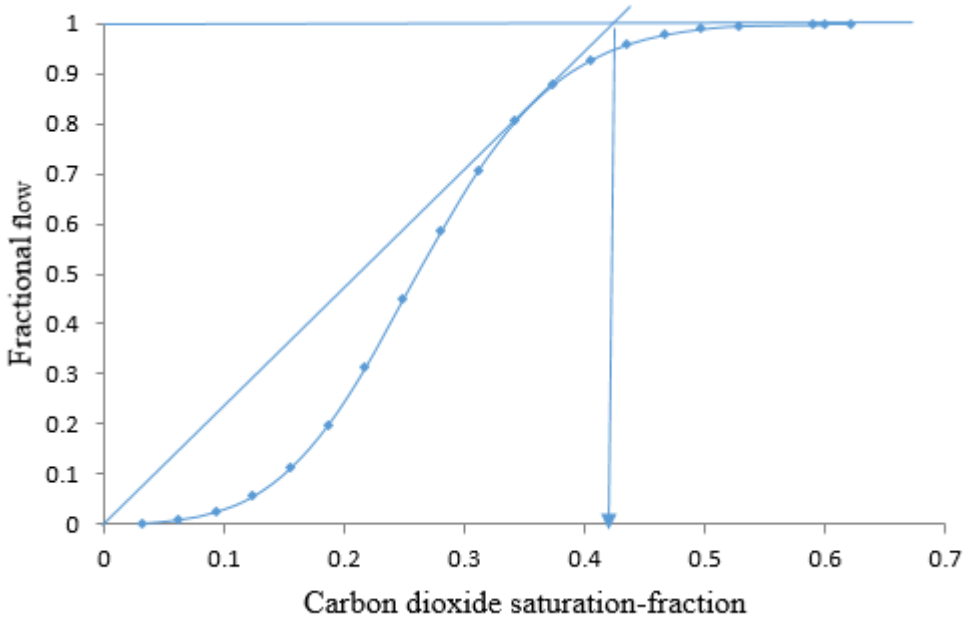

Figure 5-7: Plot for Cardium sandstone

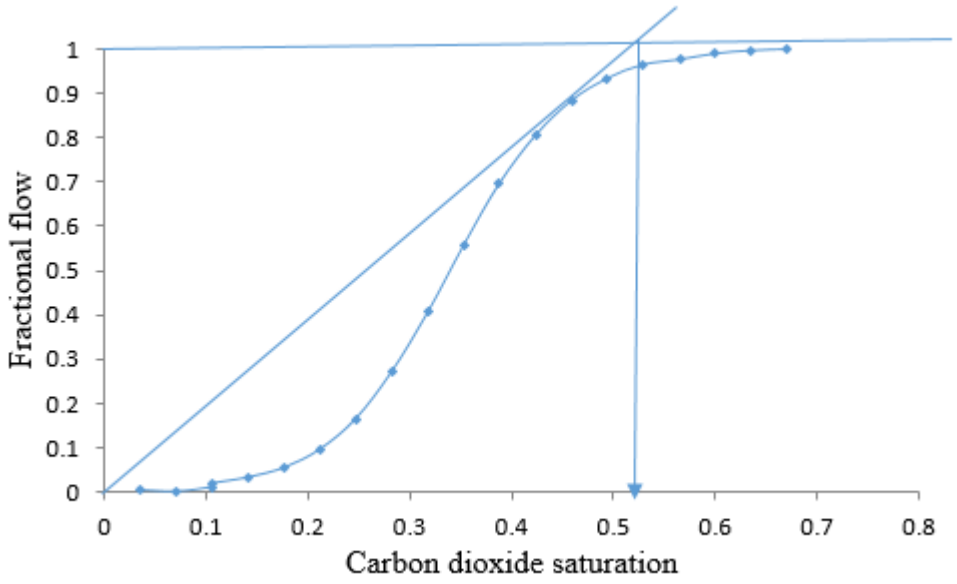

Figure 5-8: Plot for basal Cambrian sandstone

5.8 RELATIONSHIP OF THE PRINCIPAL HYPOTHESIS OF THIS WORK TO PUBLISHED DATA

The principal hypothesis of this thesis work is founded on the premises that trends in contact angle changes associated with the pH induced wettability change of the system-carbon dioxide-brine-solid/rock surface will reflect the mineralogy of the system. Accordingly, this hypothesis has been established using spontaneous imbibition flow. In addition, contact angles have been calculated from literature published data related to drainage flow using a mathematical model. This approach is quite complementary because in the petroleum literature, porous media multiphase flow are distinguished as drainage or imbibition.

On the basis of the hypothesis, saline aquifer rocks with less pH buffering mechanism will experience more reduction in water wetness. This means that in these systems it must be easier to move water and this should lead to less irreducible water saturation. On the contrary, saline aquifers with less pH buffering capability should have less reduction in water wetness leading to more irreducible water saturation. To see that the hypothesis has been supported by literature published data requires extracting irreducible water saturation related to Table 5-6b from the appropriate literature. In this regard, according to Bachu and Bennion (2008) Table 3, the irreducible water saturation for Basal Cambrian sandstone, the most quartz arenite (high silica content) with the greatest wettability decreases (contact angle equal to 87.84^{o}) is 0.294. From Table 5-6b, the next less wetting is the one with a contact angle of 73.6^{o} and this is Cardium sandstone. This sandstone has irreducible water saturation of 0.379. The most resistant to pH change in this case is Ellersely sandstone with (with significant digenetic clays and authigenic calcite) an irreducible water situation of 0.659. The mineralogy of these rocks have already been discussed in section 5.7. In the light of these observations and computations it is appropriate to say that when previous researchers measured contact angles on minerals other rock samples they were trying to interpret wettability changes not actually representative of actual geologic media where carbon dioxide will eventually be stored. Consequently, the principal hypothesis is strongly supported

5.8.1 Conclusion

In the petroleum literature two types of porous media flow can be distinguished. They are drainage flow where a non-wetting phase displaces a wetting phase from the porous medium and imbibition flow, forced or spontaneous where a wetting phase displaces a non-wetting phase from the porous medium. In each of these flow types, the wettability of a solid surface with regard to the invading fluid plays a major role in the distribution of phase saturations. Therefore, the effect of rock mineralogy, which is central to the rock-fluid interaction phenomenon responsible for the acid induced wettability evolution during CO_2 flooding must be practically demonstrable for this type of porous media fluid flow. In Chapter 4, the effect of rock mineralogy on acid induced wettability evolution was experimentally demonstrated using Wallace sandstone (multi-mineral rock), Fontainebleau (quartz arenite) and sand pack. In this chapter, the effect of multi-minerology on acid induced wettability evolution as well as pH buffering has been demonstrated using core flooding data involving drainage flow (CO_2 displacing brine) in Wallace sandstone core samples. Also, the effect of monomineralogy on acid induced wettability evolution has been demonstrated using drainage flow data in quartz arenite sandstone core samples, data being taken from literature sources. The following conclusions can be drawn. One thing, however, deserves to be mentioned and that concerns data from literatures sources. Although viscosity ratios and petrophysical parameters for different tests were not the same, the equation presented for contact angle calculation gives results that reflect the geology and mineralogy of individual rocks. The reason is that wettability evolution for the system water- CO_2-rock is due to water rock interaction phenomena, which depends on rock mineralogy. This has the effect on solid-liquid interfacial tension to cause wettability changes. Therefore, the extent to which water rock interaction will occur will depend more on rock mineralogy. The following sum up the conclusion of this chapter:

1. Wallace sandstone contains glauconite and mica which are capable of formation water pH buffering by cation exchange reactions. These reactions have the effect of causing slight pH and wettability changes and this is responsible for nearly constant values of the wetting force parameter calculated at different saturations in the drainage flow for all experimental temperatures

2. By integrating fractional flow and thermodynamic concepts with geochemistry, the effect of partial miscibility through gas solubility in brine has been used to show that partial miscibility has a retardation factor which has the effect of reducing the specific shock velocity leading to increased gas saturation at breakthrough in CO_2 injection.
3. The slight change in the wetting force parameter with different saturations in Wallace sandstone experiments is a clear indication of the pH buffering capacity of this rock similar to that observed in spontaneous imbibition experiments in Chapter 4
4. Regarding literature source data used for contact angle calculations, experiments were carried out on quartz arenite with (predominantly quartz) varied subordinate amount of authigenic minerals. In this regard, Basal Cambrian sandstone has the greatest proportion of quartz and the contact angle calculated for this rock reflects the fact the effect of acidity causes significant change in soli-liquid interfacial tension which is responsible for a larger contact angle
5. Next to Basal Cambrian sandstone with a higher proportion of quartz is Cardium and the significant proportion of authigenic clays present in this rock sample leads to a smaller change in solid-liquid interfacial tension causing a lower contact angle to be calculated compared to that of Basal Cambrian sandstone sample
6. The sample with authigenic calcite in addition to authigenic clay minerals comes from Ellerslie sandstone. Accordingly, the effect of acidity on solid-liquid interfacial tension is less because of stronger pH buffering mechanism. The lowest contact angle has been calculated for this case
7. The work of this chapter has demonstrated the effect of rock mineralogy on acid induced wettability similar to that observed in Chapter 4 using drainage experimental data. Therefore, this chapter has successfully tested the hypothesis that rock mineralogy will control wettability evolution during CO_2injection into saline aquifers
8. The equation presented in chapter three for pursuing the ultimate objective of calculating contact angle from flow data has proved to be useful. This is because it calculates contact angles that reflect those of water rock interaction systems and

comparison to those of published data for oil-water systems belonging to the same mineralogy supports the validity of the equation.

9. The work of this chapter has led to the achievement of the objective defined earlier.

CHAPTER 6 COMPARISON OF PRESENT STUDY WITH PUBLISHHED WORKS AND IMPLICATION FOR THE GEOLOGICAL COMMUNITY

6.1 The Principal View of this Study on Water-Rock Interaction

Puah *et al,* (2010) studied the effect of surface charge on the wettability of coated Titania surface. Based on kinetic molecular theory analysis of their results, they concluded that, surface charge control both static and dynamic wettability of Titania surface. Jasper *et al* (2006) argued that the interaction between CO_2 and surface hydroxyl functional groups causes physiochemical caption of these groups responsible for wettability resulting in contact angle decrease. However, on the basis of infrared spectroscopy of direct CO_2-silica interaction Trip and Combes (1998) concluded that this physiocaption mechanism is weak. Vihnyakov *et al,* (2008) reported that, supercritical CO_2 could react with surface hydroxyl groups through the mechanism of hydrogen bonding.

The main chemical groups on silica surface are silanols and silicic acid groups and the hydrophobicity of this surface depends on the surface density of these hydrophilic groups (Jung & Wan, 2012). At near neutral pH of formation brine, silica surface is negatively charged because the pH at the point of zero charge of silica is 3. The principal reaction reads (Jung & Wan, 2012):

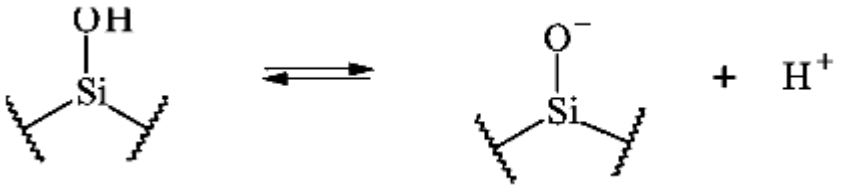

(6-1)

The species on the left is a neutral surface hydroxyl group and the first species on the right is a deprotonated surface hydroxyl group.

In the system silica-CO_2-brine, the dissolution of CO_2 produces acidity causing the equilibrium in Eq. 6-1to shift to the left. This corresponds to a drive towards creation of neutral surface species causing a reduction in surface charge. Regarding disjoining pressure forces contribution to wettability, this corresponds to weakening of the double layer repulsive forces thereby causing destabilization of the thin wetting water film. Hirasaki

(1991) and Chiquet *et al* (2007) explained that, pH decrease resulted in destabilization of the thin wetting film causing contact angle increases

So far, it can be seen that previous researchers are unanimous with regard to wettability changes being caused by surface charge that develop in response to pH changes. However, while these researchers agree on this none seem to have mentioned any surface energy phenomenon related to surface charge development. In this study, the effect of pH induced surface charge development has been directly linked to changes in solid-liquid interfacial tension. Accordingly, when Young's equation is invoked it explains quite explicitly the cause of wettability decreases with pH decreases.

6.2 Similarities in pH Control

Since the principal cause of wettability evolution in the system silica-CO_2-brine are pH changes, it is necessary to compare the mode of pH control in the present experimental works to those of published works. In this regard, the work of (Jung & Wan, 2012) is worthy of comparison. This is seen in Fig. 6-1. In this study the authors used the drop shape analysis technique where carbon dioxide drop previously equilibrated with brine was established in a high-pressure cell chamber containing brine initially equilibrated with CO_2. The essence of this was to prevent possible dissolution of the gas bubble before the start of experiment. The system was then pressurized and the shape of the drop was digitally monitored. Equilibrium contact angles were measured at each pressure equilibration. The figure shows that at a given salinity contact angle increased to a maximum value. In their work, pressure increases caused dissolution of CO_2 causing pH changes.

In published works dealing with the pH induced wettability change due to the anticipated water rock interaction reactions, contact angles were measured using different approaches. By using imbibing fluids with varying pH this thesis work has used spontaneous imbibition dynamics theory to quantify contact angle changes similar to those of previous researchers and this is with particular regard to observations for Fontainebleau sandstone samples where pH change produced significant contact angle change.

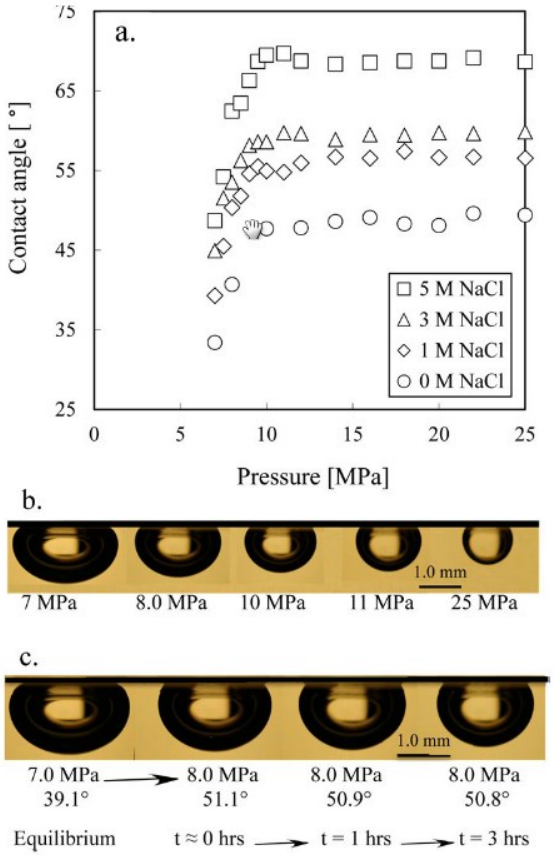

Figure. 6-1: Contact angle changes with pressure (Jung & Wan, 2012)

In the present study, pH control was achieved using dilute nitric acid. In the work of Wang *et al*., (2013) pH controlled was achieved in a similar manner by using acidic solution. The present work also showed decreases in contact angle with pH decreases in both capillary and rock imbibition experiments.

6.3 The Use of Air-Brine-Core System for Wettability/Contact Angle Measurement

In this study, the effect of water rock interaction on wettability was experimentally investigated using acidized water of different pH imbibing spontaneously into an air filled core sample from potential saline aquifer rock samples. In the petroleum literature where the concept of water wettability has a link to residual gas saturation and recovery factors of natural gas reservoirs, air/brine systems have been used to study the wettability. In this regard, Kantzas (2000) carried out spontaneous imbibition tests on core samples from natural gas reservoirs to understand how production rate and wettability impact residual gas saturation using a similar approach.

6.4 Implication for Efficient Carbon Storage in Nova Scotia Continental Shelf

In Nova Scotia, preliminary analyses of available geophysical data reveal that the potential for finding adequate storage capacity related to onshore saline aquifers is small. The work of McIver (1972-Appendix D), shows that the stratigraphic column of the Scotian Shelf has glauconitic sandstones at suitable depths for anthropogenic carbon dioxide storage. These types of sandstones are also target geological repositories for anthropogenic carbon storage in Alberta (Gentzis, 2000) because they underlie large areas of industrial power generation plants. In the Netherlands, there are also potential targets (Xu *et al*., 2001). This means that if anthropogenic carbon storage is to be a viable option for reducing CO_2 concentration in the Scotian environment, then the Scotian shelf is the only last resort for locating potential siliciclastic saline aquifers. The geological facts about this sandstone have already been unveiled by the present study. This thesis work used Wallace sandstone, which is part of the formation that outcrop on shore of the Scotian shelf. This sandstone has been found by X-ray diffraction analysis of powder samples to contain mica (serecite) and glauconite. In addition to this, results of spontaneous imbibition measurements using Wallace sandstone core samples in this thesis work show evidence of formation water pH buffering due to the presence of these diagenetic minerals that are phyllosilicates in origin. Therefore, if the injection of CO_2 into glauconitic sandstones offshore Nova Scotia is to be efficient where water can be easily moved leading to more storage of anthropogenic CO_2, then a strategy must be adopted. This strategy must be to facilitate efficient displacement of formation water. The relative mobility of phases in multiphase flow regimes in porous media depends on relative permeability, which is controlled by a number of factors. They are wettability, interfacial tension, and dynamic viscosity of phases (viscosity ratio) and pore size distribution (McDougall & Sorbie, 1997).

Generally, efficient displacement of resident fluid is obtained where there is favorable mobility ratio defined as the mobility of the displacing fluid to the mobility of the displaced fluid. This parameter must generally be minimized to achieve efficiency in displacement. This is achieved in the petroleum industry by wettability modification from intermediate water wet to water wet for the case of secondary oil recover (Standnes & Austad, 2003). Where, the wettability modification option is not a reality, an ideal option is the viscosification of the injected fluid to achieve favorable mobility ratio for efficient

displacement. The outcome of this is seen in the form of reduced mobility of the injected phase and this prevents injection fluid override of the resident fluid. Figure 6-2 shows a graph of injection sweep efficiency versus mobility ratio and shows consistent increases in sweep efficiencies with decrease in mobility ratios.

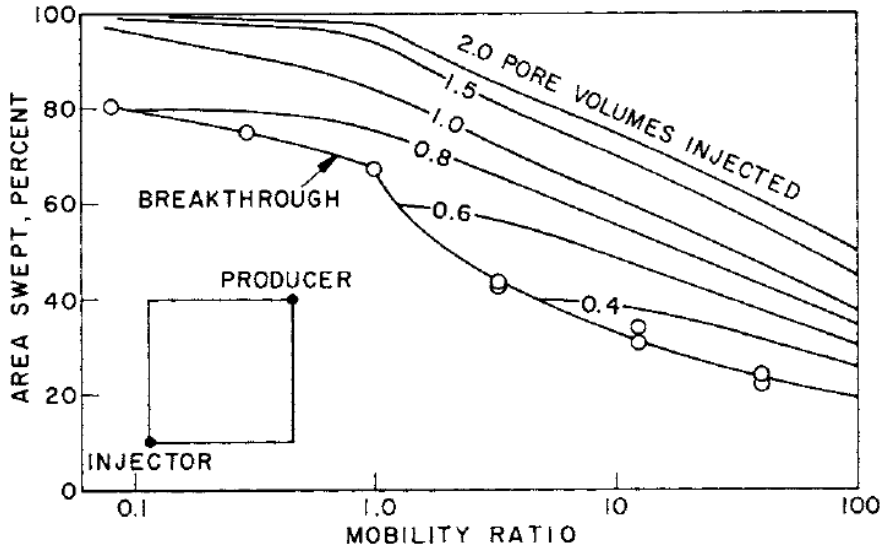

Figure 6-2: Graph of Areal Sweep Efficiency versus mobility ratio (Mahaffey *et al.*, 1966)

For those formations that will show pH buffering the wettability option designed to change the system from water wet to intermediate or gas wet that will enhance favorable mobility ratio is not recommended. Instead, enhancing mobility ratio through modifying viscosity ratio is the best strategy. For gas injection, mobility ratio is the reciprocal of that for water injection in the petroleum industry where the parameter is calculated as the ratio of brine mobility to gas mobility. The objective here is to increase gas viscosity to reduce the mobility ratio. This can be achieved by using viscosified CO_2 similar to that used by the petroleum industry for CO_2 enhanced oil recovery schemes (Bae and Irani, 1993; Heller *et al*., 1985; Enick *et al*., 2012). The essence of this is to dissolve polymers that will increase the dynamic viscosity of injected CO_2. This has the effect of providing favorable mobility ratio in the displacement. It is clear that coupled with the already huge cost of injection well drilling and completion, this strategy will push future geological carbon storage to unaffordable economic limits. However, if the goal of society is to enjoy energy

consumption while keeping global climate safe in order to avoid expected environmental calamities, then the extra cost of geological carbon storage that will be incurred in the light of this proposed strategy must be accepted for the sake of environmental remediation.

6.5 Limitations of this Thesis Work

In all published works so far relating to carbon dioxide induced wettability alteration (Kim *et al*., 2012; and Jun g and Wan 2012) all researchers unanimously agree that the principal mechanism behind the wettability modification is the water-rock interaction phenomenon. This reaction is intimately linked to the surface chemistry characteristics of aquifer/reservoir rock minerals. Generally, the surface functionalities or silanols (Zhuralev, 1987) formed by the dissociation and chemisorption of water molecules (Mahadevan and Garofalini, 2008) on the oxygen ion of oxide minerals are responsible for such reactions due to the amphoteric behavior (Vidal *et al*., 1987). To date, all works on contact angles in the above-cited publications have failed to quantify the effect of the water rock interaction experimentally, although, this effect is lumped into measured contact angles.

The present work has undertaken successful experments to quantify contact angles that also contain water rock interaction effects for two mineralogically distinct potential saline aquifer rock samples. It has also conducted experiments based on cation exchange reactions to quantify formation water pH buffering effects. Like previous workers, the effect of the water rock interaction has not been experimentally accounted for and this is the major limitation.

Based on the experimental results for cap rock materials it is appropriate to admit that expectations of the hypothesis of this thesis work is not met. This is because, for typical geological sequestration conditions where formation brine pH is close to neutral, pH decreases will produce contact angle trends that will typically reflect those of the mineral that compose these rocks. Here, mica is a notable example that can be taken to represent cap rock. This mineral has a point of zero charge pH of 7.6 (Sverjensky, 1994) which is almost the same as that of cap rock or shale rock. In this regard, previous researchers were justified in using mica for experiments. This limitation is probably due to the limitation regarding the procurement of cap rock materials with varied mineralogy as recognized in the geological literature.

6.6 ADVICE FOR EFFICIENT GELOGICAL CARBON SEQUESTRATION

The findings of this thesis work with particular regard to the pH wettability relationship is critical for efficient geological storage of anthropogenic carbon dioxide. In the past, characterization and screening of saline aquifers have centered on traditional approaches that require information about porosity, permeability, rock type, formation brine salinity, thickness and areal extent of potential aquifers. Since wettability controls the mobility of carbon dioxide and formation brine the recommendation of this thesis is that accurate determination of the effective point of zero charge pH of rock samples should be added to the suite of characterization methods. Also, determination of initial formation brine pH is essential. Integrating knowledge of effective point of zero charge pH and initial formation brine pH will provide a firsthand information about trends in wettability change. In other words, if the point of zero charge pH is closer to the initial formation brine pH, then possible wettability increases in accordance with surface charge controlled wettability evolution must be anticipated. In this case, the displacement will be less efficient because of enhanced water wetness. On the contrary, having a significant difference between the effective point of zero charge pH of rock surface and that of initial formation brine is beneficial where initial formation brine pH is above that of the effective point of zero charge pH of rock surface. In this case, decreases in pH caused by carbonic acid dissociation will reduce the surface charge of rock which is the criterion for water wetness reduction leading to efficient displacement of formation brine and maximization of available storage pore volume for a given sequestration project.

Also, since clay or phyllosilicate minerals are known for their cation exchange capacities that have the potential to buffer formation water pH and resist wettability changes, argillaceous formations should be avoided in screening potential saline aquifers for geological carbon storage. Geologically, sandstone is a clastic sedimentary rock (Fralick & Kronberg, 1997) with abundant silica content. However, depending on the degree of sediment diagenesis, modification (Awwiller & Mark, 1991) of these clastic rocks are petrologically recognizable. Therefore, a typical point of zero charge pH close to 3 that could approximate the average value for sandstones is always not possible due to diagenetic

and environmental imprints that cause varied mineralogy. In this regard, a notable example is worth mentioning here in connection with Bentheimer sandstone. This sandstone in Belgium is calcareous and has glauconite (Kock *et al*., 2014). Another type of Bentheimer sandstone occurs along the Dutch-German border with quartz volume fraction between 0.88 and 0.96. It has a point of zero charge pH of 8 (Peksa *et al.,* 2015) found in this reference work (Figure 21 of reference) as the point where the surface charge density verses pH is zero. The implication is that water mobility in this sandstone will be reduced due to expected wettability enhancement. Therefore, determination of the point of zero charge pH of rock samples of potential saline aquifers and the initial pH of formation brine should be considered crucial for planning efficient geological carbon storage.

CHAPTER 7 CONCLUDING STATEMENT

7.1 Summary

In choosing to sequester anthropogenic CO_2 in geologic media for the sake of mitigating global warming due to greenhouse gas effect, the effect of rock fluid interaction on the two-phase flow hydrodynamics is of paramount importance. This is because, the dissolution of CO_2 and its dissociated species results in surface protonation and deprotonation reactions. This has a marked effect on the surface energy of pore surfaces. Viewed from the molecular theory of interfacial tension, water rock interaction will therefore impact solid-liquid interfacial tension or interfacial energy because of the evolution of acid base species that result from protonation and deprotonation reactions. This resulting wettability change affects the relative mobility of water and CO_2 to either enhance efficient carbon storage or reduce water mobility to cause an opposite effect. Also, the effect of rock mineralogy is very important in predicting the overall effect of water rock interaction on wettability. Simply put, wettability decrease will only be possible where pH of aqueous solution is not buffered.

In the petroleum engineering literature, two types of flows can be distinguished. They are spontaneous imbibition and drainage as explained in Chapter 2. If indeed water rock interaction causes surface energy changes to impact wettability, then this effect must be observable for the two types of flows in porous media. In this thesis work, experimental data based on spontaneous imbibition has been used to show the effect of acidity on wettability evolution during CO_2 injection into saline aquifers. The effect of rock mineralogy on wettability evolution has also been established using these data. In Chapter 5, drainage experimental data have also been used to establish the effect of rock mineralogy on wettability and to substantiate the results of Wallace sandstone as observed in Chapter 4.

Accordingly, the following sum up the observations:

1. Although saline aquifers provide promising storage capacities for global anthropogenic carbon storage, the extent to which a given carbon geostorage project can maximise the available subsurface pore volume for storage depends on the mineralogy of the aquifer rock and the salinity of formation.

2. In those saline aquifers where the aquifer rock has authigenic minerals capable of buffering formation water pH as injected CO_2 dissolves, the pH of formation water will remain approximately constant. In these saline aquifers, the aquifer rock will remain predominantly water wet with decreased relative permeability
3. Monomineralic saline aquifer rocks of siliciclastic origin such as sandstones with authigenic and or silica cement are in the class of saline aquifers where the pH of formation water will change significantly due to lack of pH buffering mechanism. This is because, in these aquifers, formation water pH will decrease with increases in hydrogen ion activity following injected CO_2 dissolution, hydration to carbonic acid and subsequent ionization. These decreases in pH will lead to decreases in water wettability and this implies increase water mobility and improved injected gas sweep efficiency
4. For two-phase flow in porous media, involving injected anthropogenic CO_2 and resident formation brine the global saturation balance equation predicts unity for the summation of phase saturations. Similarly, the summation of fractional flow values for the phases at any point leads to unity meaning an increase in the fractional flow of one phase leads to a decrease in the fractional flow of the other phase. This fractional flow increases with phase mobility. Consequently, increases in water fractional flow with pH decreases means decreases in CO_2 relative permeability, mobility and fractional flow and this is the criterion for high sweep efficiency
5. Capillary imbibition experiment conducted in this thesis work that led to a novel method for determining the point of zero charge pH of borosilicate glass and it is comparable to those of previous research works. In the experimental approaches of previous workers pH changes of brine in contact with supercritical CO_2 was achieved by injected gas pressure variation which caused dissolution of gas under isothermal conditions. The result of the current work has established contact angle variation under varying pH conditions similar to those reported by these workers.by pH control

6. The pH dependent wettability equation derived in this thesis has served a number of purposes. In addition to helping to achieve one of the defined tasks it serves two roles. One is the applicability for establishing the hypothesis that different rock systems will respond differently to wettability change due to pH in view of the point of zero charge pH control on wettability. The other role is seen from the fact that the equation contains the point of zero charge pH with specific regard to pH change related to geological carbon storage which is the principal concern of this thesis work.
7. Under typical conditions of formation brine pH (neutral or near neutral) that will be encountered due to carbon dioxide dissolution cap rocks will experience increases in water wetness due to their point of zero charge pH being closer to the initial pH of formation brines.
8. The principal hypothesis of this thesis has been tested from Chapter 3 through Chapter 5

7.2 General Contributions of this Thesis Work

The following are the major contributions to knowledge in the area of anthropogenic CO_2 geologic sequestration that this thesis work has made:

1. This thesis work has shown mathematically the dependence of wettability on formation water pH and this dependence has been experimentally validated.
2. The concept of the point of zero charge pH of a mineral surface is a fundamental surface chemistry parameter used in the colloid industry. In the geological sequestration of CO_2 the system water-CO_2-mineral (rock) surface is the principal focus with regard to physiochemical changes related to wettability evolution due to formation water pH changes. Consequently, the point of zero charge pH is a vital parameter with regard to water rock interaction phenomenon that is central to pH mediated solid-liquid interfacial free energy/tension changes. In the colloid industry, this surface chemistry parameter has been determined using titrimetry or infrared spectrometry technique. In this thesis work the experimental validation of the wettability pH relationship using capillary tubes has made it possible for the determination of the point of zero charge pH of laboratory glass which compares quite well with values found in published literature works. This is a new approach that uses

spontaneous water imbibition quite different from traditional approaches that use titrimetry and atomic force microscopy among others.

3. In all porous media multiphase flow, wettability is intimately linked to relative permeability of phases. In the petroleum literature, relative permeability and wettability or contact angle have been determined separately. The mathematical model presented in this work linked contact angle to drainage relative permeability data. Computation of contact angle from flow test is a notable contribution of this study.
4. Interface thermodynamics is a branch of science that deals with surface and or interface energy changes following molecular interactions at interfaces. In this study the parabolic equation that links pH to contact angle provided the basis for the classification of saline aquifer storage environments with regard to wettability evolution following the injection of CO_2 into these geologic repositories. The bases for this classification are the trend of pH evolution under geologic conditions typical of CO_2 geosequestration and the surface chemistry of saline aquifer rocks with specific regard to the point of zero charge pH of rock mineral surface. Accordingly three storage environments with regard to wettability evolution during carbon dioxide injection into saline aquifers have been identified.
5. Recently the Minerals Resource Engineering Department of Dalhousie provided data on oxide analysis of Wallace Sandstone. In this thesis work, X-Ray Diffraction method has been used to establish the existence of mica and glauconite in this sandstone and this is a contribution to geological literature.

7.3 RECOMMENDATIONS FOR FUTURE STUDIES

Following the outcome of the mathematical modelling of this work one of the experimental objectives was to use the core flooding systems CFS manufacture by Vinci Technologies in order to test some aspect of the theoretical findings. This included determination of the relative permeability of CO_2-brine system at different temperatures using synthetic formation brine salinities. This is because the solubility of CO_2 in formation brine is an explicit function of salinity and temperature. Normally, solubility decrease with temperature and salinity. This obvious solubility trend provides a carefully planned experimental basis where CO_2 can be injected at a constant pressure for relative

permeability experiments at varying synthetic brine salinities. Relative permeabilities obtained under these conditions would simulate different pH conditions if carried out at constant temperature such that the only variable is salinity. By using the concept of fractional flow in petroleum reservoir engineering the fractional flow curves for the different experiments can be plotted for comparison. The result of such an experimental program can be used to further substantiate the theoretical findings of this thesis work that lower pH conditions will enhance higher sweep efficiencies which can be shown by the fractional flow versus water saturation curves at the same temperature but varying salinities and gas solubility. This planned experimental program could not be carried out because of equipment failure. Although optional experimental designs have helped to substantiate the theoretical findings of this study, it is the proposal of this thesis work that the core flooding experiments designed to measure relative permeabilities under varying salinity and pH conditions should be taken up as a future research goal.

The spontaneous imbibition studies in this work were carried out under ambient conditions. We propose that future work on spontaneous imbibition should be carried out in systems where temperature can be varied.

To test the principal hypothesis using drainage relative permeability data, data from sandstones of different petrophysical and random mineralogical compositions were used from literature sources. Generally, contact angles calculated using the mathematical model of this study reflected the siliciclastic nature of the samples where significant contact angle changes are observed under in situ geological carbon storage. Using samples with predetermined authigenic minerals (mica, glauconite, and calcite) composition and of the same porosity and permeability would have provided a more meaningful experimental approach. Therefore, it is the recommendation of this study that future research work should take up this challenge.

In recent times the potential for geological carbon storage in flood basalts has been considered. The reason is that dissolved anthropogenic carbon species in formation water will eventually lead to a thermodynamically stable form of carbon through the formation of carbonates (Oelkers *et al.,* 2008). This will be achieved by dissolution of minerals in this rock to release divalent cations (Golubev *et al*., 2005). This carbonate mineral formation

requires sufficient presence of divalent cations. Normally, formation brine has less of these cations ($F_e^{2+}, Mg^{2+}, Ca^{2+}$). The most significant source of these ions are fosterite (magnesium rich pyroxene) and fayalite (iron rich pyroxene) (Koike, *et al*., 2000), which are found in high proportions in flood basalt. The mathematical model in Chapter 2 of this work arrives at a parabolic relationship between contact angle and the pH of the aqueous medium where the axis of symmetry is the point of zero charge pH of the solid surface. The point of zero charge pH (9.1) found in Appendix 7-1 of these minerals is well above the pH of normal formation or geologic system brine which is 7.4 on the average (Petalas and Diamantis, 1999). This means that as CO_2 dissolves upon injection into flood basalt the pH will decrease away from the the point of zero charge pH meaning an increase in wettability. If this is the case, then increasing water wettability will not enhance sweep efficiency. This study could not investigate this and recommends that future research work takes up the challenge.

REFERENCES

Akbarabadi, M., & Piri, M. (2013, February). Relative permeability hysteresis and capillary trapping characteristics of supercritical CO2/brine systems: An experimental study at reservoir conditions. *Advances in Water Resources*, 52, 190–206.

Aksay, I. A., Hoge, C. E., & Pask, J. A. (1974). Wetting under Chemical Equilibrium and Nonequilibrium Conditions. *The Journal of Physical Chemistry*, 78(12), 1178–1183.

Al Bahlani, A. M., & Babadagli, T. (2008). Heavy-Oil Recovery in Naturally Fractured Reservoirs with Varying Wettability by Steam Solvent Co-Injection. International Thermal Operations and Heavy Oil Symposium, 20-23 October (pp. International Thermal Operations and Heavy Oil Symposium, 20-23 October). Calgary, Alberta, Canada: Society of Petroleum Engineers.

Anderson, W. G. (1987). Wettability Literature Survey Part 5: The Effects of Wettability on Relative Permeability. *Journal of Petroleum Technology*, 39(11), 1453-1468.

Appel, C., Ma, L. Q., & Rhue, R. D. (2003, April). Point of zero charge determination in soils and minerals via traditional methods and detection of electroacoustic mobility. *Geoderma*, 113(1-2), 77–93.

Archer, J., & Wall, C. (1986). Petroleum Engineering Principles and Practice. Boston: *Kluwer Academic Publishers*.

Arrouvel, C., Diawara, B., Costa, D., & Marcus, P. (2007). DFT Periodic Study of the Adsorption of Glycine on the Anhydrous and Hydroxylated (0001) Surfaces of α-Alumina. *The Journal of Physical Chemistry C, 111*(49), 18164-18173.

Ashoori, E., Heigden, T. v., & Rossen, W. (2009). Fractional Flow Theory of Foam Displacements with Oil. SPE International Symposium on Oilfield Chemistry (pp. 260-273). Texas*: Soceity of Petroleum Engineers*.

Atkinson, R. J., Posner, A. M., & Quirk, J. P. (1967). Adsorption of Potential-Determining Ions at the Ferric Oxide-Aqueous Electrolyte Interface. *Journal of Physical Chemistry*, 71(3), 550–558.

Audigane, P., Irina, G., Czernichowski-Lauriol, I., Preuss, K., & Xu, T. (2007, September). Two-dimensional reactive transport modeling of CO2 injection in a saline aquifer at the Sleipner site, North Sea. *American Journal of Science*, 307, 974–1008.

Andre, L., Audigane, P., Azaroual, M., & Menjoz, A. (2007). Numerical modeling of fluid–rock chemical interactions at the supercritical CO2–liquid interface during CO2 injection into a carbonate reservoir, the Dogger aquifer (Paris Basin, France). *Energy Conversion and Management, 48*, 1782–1797.

Awwiller, D., & Mark, L. E. (1991). Diagenetic modification of Sm-Nd model ages in Tertiary sandstones and shales, Texas Gulf Coast. *Geology, 19*(4), 311-314.

Babadagli, T., & Hatiboglu, C. U. (2007, August 15). Analysis of counter-current gas–water capillary imbibition transfer at different temperatures. *Journal of Petroleum Science and Engineering, 55* , 277–293.

Bachu, S. (2000). Sequestration of CO2 in geological media: criteria and approach for site selection in response to climate change. *Energy Conversion & Management, 41*, 953-970.

Bachu, S. (2002). Suitability of the Subsurface in Saskatchewan and Manitoba for Geological Sequestration of Anthropogenic Carbon Dioxide. Geological Survey, *Alberta Energy and Utilities Board. Alberta Geological Survey*

Bachu, S., & Adams, J. (2003, December). Sequestration of CO2 in geological media in response to climate change: capacity of deep saline aquifers to sequester CO2 in solution. *Energy Conversion and Management*, 44(20), 3151–3175.

Bachu, S., Gunter, W., & Perkins, E. (1994). Aquifer Disposal of CO2, Hydrodynamical and Mineral Trapping. *Energy Conversion and Management*, 35(4), 264-279.

Bae, J., & Irani, C. (1993). A Laboratory Investigation of Viscosified CO2 Process. *SPE Advanced Technology Series,* 1(01), 1-6.

Bandara, U. C., Palmer, B. J., & Tartakovsky, A. M. (2016, January 13). Effect of wettability alteration on long-term behavior of fluids in subsurface. *Comp. Part. Mech*.

Banwart, A. B., & Steven, A. (2000, February). Carbon dioxide mediated dissolution of Ca-feldspar: implications for silicate weathering. *Chemical Geology*, 163(1-4), Volume 163, Issues 1–4, February 2000, Pages 25–42.

Barranco Jr., F. T., Dawson, H. E., & Christener, J. M. (1997, February 27). Influence of Aqueous pH and Ionic Strength on the Wettability of Quartz in the Presence of Dense Non-Aqueous-Phase Liquids. *Environ. Sci. Technol*, 31(3), 676-681.

Barthés-Labrousse, M.-G. (2002, September 26). Acid–base characterisation of flat oxide-covered metal surfaces. *Vacuum, 67*(3-4), 385–392.

Barz, D. P., Vogel, M. J., & Steen, P. H. (2009). Determination of the zeta potential of porous substrates by droplet deflection. I. The influence of ionic strength and pH value of an aqueous electrolyte in contact with a borosilicate surface. *Langmuir, 25*(3), 1842-1850.

Bauer, A., & Berger, G. (1998, September). Kaolinite and smectite dissolution rate in high molar KOH solutions at 35° and 80°C. *Applied Geochemistry, 13*(7), 905–916.

Behrens, S. H., & Grier, D. G. (2001). Pair interaction of charged colloidal spheres near a charged wall. *Physical Review E, 64*(5), 050401-1-050401-4.

Bellon-Fontaine, M. (1996, July 31). Microbial adhesion to solvents: a novel method to determine the electron-donor/electron-acceptor or Lewis acid-base properties of microbial cells. Colloids and Surfaces B: *Biointerfaces*, 7(1-2), 47–53.

Benion, B., & Bachu, S. (2006). Dependence on Temperature, Pressure and Salinity of the IFT and Relative Permeability Displacement Characteristics of CO2 Injected in Deep Saline Aquifers. SPE**.** *Annual Technical Conference and Exhibition*. Society of Petroleum Engineers, 2006

Bennion, B., & Bachu, S. (2005). Relative Permeability Characteristics for Supercritical CO2 Displacing Water in a Variety of Potential Sequestration Zones. *SPE Annual Technical Conference and Exhibition,* 9-12 October (pp. 1-15). , Dallas, Texas: Society of Petroleum Engineers.

Bennion, D. B., & Bachu, S. (2007). Permeability and Relative Permeability Measurements at Reservoir Conditions for CO2-Water Systems in Ultra Low Permeability Confining Caprock. *EUROPEC/EAGE Conference and Exhibition*, 11-14, June. London, U.K: Society of Petroleum Engineers.

Bennion, B., & Bachu, S. (2008). Drainage and imbibition relative permeability relationships for supercritical CO2/brine and H2S/brine systems in intergranular sandstone, carbonate, shale, and anhydrite rocks. *SPE Reservoir Evaluation & Engineering, 11*(03), 487-496.

Bennion, S. B. (2008). Effects of in-situ conditions on relative permeability characteristics of CO2-brine systems. *Environ Geol*, 54, 1707–1722.

Benson, B. B., & Krause Jr., D. (1984). The concentration and isotopic fractionation of oxygendissolved in freshwater and seawater inequilibrium with the atmosphere. *Limnol. Oceanogr*, 29(3), 620-632.

Bhatia, M. R. (1983, Novemver). Plate Tectonics and Geochemical Composition of Sandstones. The Journal of Geology, 91(6), 611-627.

Binninga, P., & Celia, M. A. (1999). Practical implementation of the fractional flow approach to multi-phase flow simulation. *Advances in Water Resources*, 22(5), 461–478.

Bjølykke, K. (1998, March Clay Minerals). Clay mineral diagenesis in sedimentary basins — a key to the prediction of rock properties. Examples from the North Sea Basin. *Clay Minerals,* 33(1), 15-34.

Blake, T. D. (2006, July 1). The physics of moving wetting lines. *Journal of Colloid and Interface Science*, 299(1), 1–13.

Blake, T., & Coninck, J. D. (2002, February 25). The influence of solid–liquid interactions on dynamic wetting. *Advances in Colloid and Interface Science*, 96(1-3), 21-36.

Bodhak, S., Bose, S., & Bandyopadhyay, A. (2009). of surface charge and wettability on early stage mineralization and bone cell–materials interactions of polarized hydroxyapatite. *Acta Biomaterialia, 5*(6), 2178-2188.

Boehm, H. P. (1971). Acidic and Basic Properties of Hydroxylated Metal Oxide Surfaces. *Discussion Faraday Society,* 52, 264-275.

Bourikas, K., Vakros, J., & Kordulis, C. (2003, August 1). Potentiometric Mass Titrations: Experimental and Theoretical Establishment of a New Technique for Determining the Point of Zero Charge (PZC) of Metal (Hydr) Oxides. *Journal of Physical Chemistry B*, 107(35), 9441–9451.

Bowden, J. W., Posner, A., & Quirk, J. (1977). *Australian Journal of Soil Research*, 15(2), 121 - 136.

Brandles, J. B., & Schiffrin, D. (1966). Surface tension of dilute acid solutions. *Trans. Faraday Soc.*, 62, 2403-2408.

Brantley, S. L., Kubicki, J. D., & White, A. F. (2008). Kinetics of Water-Rock Interaction. (J. D. Susan L. Brantley, Ed*.) Springer Science Business Media*, LLC.

Brown, C., & . Newstander, E. (1980). The Wettability of Oil/Water/Silica Systems with Reference to Oil Recovery. *Journal of Petroleu Technology,* 100-10

Buckingham, A. D., Fowler, P. W., & Hutson, J. M. (1988). Theoretical studies of van der Waals molecules and intermolecular forces. *Chem. Rev*., 88(6), 963–988.

Butt, H.-J., Graf, K., & Kaplle, M. (2003). *Physics and Chemistry of Interfaces.* Wiley-VCH.

Cacace, M. G., Landau, E. M., & Ramsden, J. J. (1997, August). The Hofmeister series: salt and solvent effects on interfacial phenomena. *Quarterly Reviews of Biophysics, 30* (30), 241-277.

Calvert, S. E., & Pedersen, T. F. (1992). Organic carbon accumulation and preservation in marine sediments how important is anoxia." Organic matter. *: productivity, accumulation, and preservation in recent and ancient sediments, 533* , 231-263.

Carré, A., Lacarrière, V., & Birch, W. (2003). Molecular interactions between DNA and an aminated glass substrate. Journal of Colloid and Science, 260(1), 49–55.

Carrigy, M. A., & Mellon, G. B. (1964, September). Authigenic Clay Mineral Cements in Cretaceous and Tertiary Sandstones of Alberta. *Journal of Sedimentary Research (SEPM),* 34(3), 461-472.

Carrol, D. (1959). Ion Echange in Clays and Other Minerals. *Journal of American Soceity Bulletin*, 70(6), 749-779.

Chalbaud, C., Robin, M., Lombard, J., Martin, F., Egermann. P., & Bertin, H. (2009, January). Interfacial tension measurements and wettability evaluation for geological. *Advances in Water Resources*, 31(1), 98–109.

Chan, D., Perram, W. J., White, R. L., & Healy, T. W. (1975). Regulation of surface potential at amphoteric surfaces during particle–particle interaction. *Journal of the Chemical Society, Faraday Transactions 1: Physical Chemistry in Condensed Phases, 71*, 1046-1057.

Chapelle, F. H., & Knoble, L. L. (1983). Aqueous Geochemistry and the Exchangeable Cation Composition of Glauconite in the Aquia Aquifer, Maryland. *Ground water*. 21(3), 343–352.

Chatelier, R. C., Drummond, C. J., Chan, D. Y., Vasic, Z. R., Gengenbach, T. R., & Griesser, H. J. (1995). Theory of Contact Angles and the Free Energy of Formation of Ionizable Surfaces: Application to Heptylamine Radio-Frequency Plasma-Deposited Films. *Langmuir, 11*(10), 4122–4128.

Checco, A., Guenoun, P., & Daillant, J. (2003, October 31). Nonlinear Dependence of the Contact Angle of Nanodroplets on Contact Line Curvature. *Pysical Review Letters*, 91(18-31).

Chibowski, E., & Perea-Carpio, R. (2002). Problems of contact angle and solid surface free energy determination. *Advances in Colloid and Interface Science*, 98, 245-264

Chiquet, P., Broseta, D., & Thibeau, S. (2007). Wettability alteration of caprock minerals by carbon dioxide. *Geofluids*, 2, 112-122.

Christian, A. C. (1973, August). Offshore Fracture Gradients. *Journal of Petroleum Technology*, 25(08).

Connors, K. A. (1990). Chemical kinetics: the study of reaction rates in solution. John Wiley & Sons.

Cuddy, M. F., Poda, A. R., & Brantley, L. N. (2013). Determination of Isoelectric Points and the Role of pH for Common Quartz Crystal Microbalance Sensors. *Applied Materiala and Interface, 5*(9), pp 3514–3518.

Davidson, T. A., & Vickers, A. F. (1972). The optical properties of mica in the vacuum ultraviolet. *J. Phys. C: Solid State Phys., 5*, 879-887.

Debecker, B., & Vervoort, A. (2013). Two-dimensional discrete element simulations of the fracture behaviour of slate. *International Journal of Rock Mechanics and Mining Sciences, 61*, 161-170.

Detournay, E. (2004, March). Propagation Regimes of Fluid-Driven Fractures in Impermeable Rocks. *Int. J. Geomech, 4*(1), 35-45.

Doster, F., & Hilfer, R. (2011, December). Generalized Buckley–Leverett theory for two-phase flow in porous media. *New Journal of Physics*, 13.

Doughty, C., Freifeld, B. M., & Trautz, R. C. (2008). Site characterization for CO2 geologic storage and vice versa: the Frio brine pilot, Texas, USA as a case study. *Environ Geology*, 54, 1635–1656.

Edie, R. W., & Andrichuk, J. M. (2005, July 28). Meander Belt Entrapment of Hydrocarbons, Campbell-Namao Field, Alberta. *Search and Discovery Article #20027.*

Elwing, H., Welin, S., & Nilsson, U. a. (1987, September). A wettability gradient method for studies of macromolecular interactions at the liquid/solid interface. *Journal of Colloid and Interface Science,* 119(1), 203–210.

Emberley, S., Hutcheon, I., Shevalier, M., Durocher, K., & Gunter, W. (2004, July-August). Geochemical monitoring of fluid-rock interaction and CO2 storage at the

Weyburn CO2-injection enhanced oil recovery site, Saskatchewan, Canada. *Energy*, 29(9-10), 1393-1401.

Enick, R. M., Olsen, D. K., Ammer, J. R., & Schuller, W. (2012). Mobility and Conformance Control for CO2 EOR via Thickeners, Foams, and Gels -- A Literature Review of 40 Years of Research and Pilot Tests. SPE Improved Oil Recovery Symposium, 14-18 April. Tulsa, Oklahoma, USA: *Society of Petroleum Engineers*.

Erslev, E. A. (1998). Limited, localized nonvolatile element flux and volume change in Appalachian slates By Eric A. Erslev. *The Geological Soceity of America, 110*(7), 900-915.

Espinoza, D. N., & Santamaria, J. C. (2010). Water-CO2-mineral systems: Interfacial tension, contact angle, and diffusion Implications to CO2 geological storage. *Water Resources Research*, 47(7), 1-10.

Esteban, M., & Taberner, C. (2003, May). Secondary porosity development during late burial in carbonate reservoirs as a result of mixing and/or cooling of brines. *Journal of Geochemical Exploration,* (78-79) 355–359.

Fatt, I., & Klikoff JR, W. A. (1959, October). Effect of Fractional Wettability on Multiphase Flow through Porous Media. *Journal of Petroleum Technology*, 10(11), 71-76.

Flett, M., Gurton, R., & Taggart, I. (2004). The function of gas-Water Relative Permeability Hysteresis in the Sequestration of carbon Dioxide in saline Aquifers. *Socrity of Petroleum Engineers*, 1-11..

Fralick, P., & Kronberg, B. (1997, October). Geochemical discrimination of clastic sedimentary rock sources. *Sedimentary Geology, 113*(1-2), Volume 113, Issues 1–2, October 1997, Pages 111–124.

Frenkel, J. (1946). Kinetic Theory of Liquids. *Oxford University Press.*

Fritz, J., Baller, M. K., Lang, H. P., Strunz, T., Meyer, E., Güntherodt, H.-J., . . . Gimzewski, J. K. (2000, November 10). Stress at the Solid−Liquid Interface of Self-

Assembled Monolayers on Gold Investigated with a Nanomechanical Sensor. *Langmuir, 16*(25), 9694–9696.

Garcia, J. E., & Pruess, K. (2003). Flow Instabilities during Injection of CO2 into Saline Aquifers. Proceedings, TOUGH Symposium 2003. Berkeley, California: *Lawrence Berkeley National Laboratory.*

Grahame, D. C. (1947). The electrical double layer and the theory of electrocapillarity. Chemical reviews. *Chemical reviews, 3*, 441-501.

Gentzis, T. (2000). Subsurface sequestration of carbon dioxide — an overview from an Alberta (Canada) perspective. *International Journal of Coal Geology*, 43 (1-4), 287-305.

Gislason, S. R.-B. (2010). Mineral sequestration of carbon dioxide in basalt: A pre-injection overview of the CarbFix project. *International Journal of Greenhouse Gas Control*, 4, 537–545.

Glastone, S. K. (1941). The Theory of Rate Processes. *Ind. Eng. Chem*, 33, 430.

Glover, P. W., Meredith, P. G., & Sammonds, P. R. (1994, November 10). Ionic surface electrical conductivity in sandstone. *Journal Of Geophysical Research*, Ages 21,635-21,650, November 10, 1994, Vol. 99, (NO. Bll, P), 21,635-21,650.

Gray, W. G. (1991). Unsaturated Flow Theory Including Interfacial Phenomena. *Water Resources Research,* 27(8), 1855-1863.

Golubev, S. V., Pokrovsky, O. S., & Schott, J. (2005, April 25). Experimental determination of the effect of dissolved CO2 on the dissolution kinetics of Mg and Ca silicates at 25 °C. *Chemical Geology*, 217(3-4), 227–238.

Gunter, W. D., Bachu, S., & Benson, S. (2004). The role of hydrogeological and geochemical trapping in sedimentary basins for secure geological storage of carbon dioxide. *Geological Society, London, Special Publications*, 233, 129-145.

Gunter, W., Perkinsa. E., & Hutcheon, I. (2000). Aquifer disposal of acid gases: modelling of water-rock reactions for trapping of acid wastes. *Applied Geochemistry*, 15, 1085-1095.

Guntera, W., Perkinsa, E., & Hutcheon, I. (2000, September 1). Aquifer disposal of acid gases: modelling of water–rock reactions for trapping of acid wastes. *Applied Geochemistry*, 15(8), 1085-1095.

Haddad, S. C., Prior, D. J., & Smalley, P. C. (2006, February). Quartz Cement in the Fontainebleau Sandstone, Paris Basin, France: Crystallography and Implications for Mechanisms of Cement Growth. *Journal of Sedimentary Research* 76(2), 244-256.

Hanor, J. S. (1994). Origin of saline fluids in sedimentary basins. *Geological Society, London, Special Publications*, 78, 151-174.

Hassanizadeh, S. M., & Gray, W. G. (1993). Thermodynamics Basis of Capillary Pressure in Porous Media. *Water Resources Research*, 29(10), 3389-3405.

Hassanzadeh, H., Pooladi-Darvish, M., & Elsharkawy, A. M. (2008). Predicting PVT data for CO2–brine mixtures for black-oil simulation of CO2 geological storage. *International journal of greenhouse gas control, 2*(1), 6 5 – 77.

Haven, H. L., Peakman, T. M., & Rullkötter, J. (2001). "Early diagenetic transformation of higher-plant triterpenoids in deep-sea sediments from Baffin Bay. *Geochimica et Cosmochimica ActaVolume*, 56(5), 2001-2024.

Helgeson, H. C. (1969). Thermodynamics of hydrothermal systems at elevated temperatures and pressures. *American Journal of Science, 267*, 729-804.

Heller, J., Dandge, D., Card, R., & Donaruma, L. (1985). Direct Thickeners for Mobility Control of CO2 Floods. *Society of Petroleum Engineers Journal*, 25(5), 679-685.

Herminghaus, S. (2000, October 15). *Europhys. Lett., 2000, 52*(2), 165–170.

Hicks, R. J., Jamieson, R. A., & Reynolds, P. H. (1999). Detrital and metamorphic 40Ar/39Ar ages from muscovite and whole-rock samples, Meguma Supergroup, southern Nova Scotia. *Canadian Journal of Earth Sciences, 36*(1), 23-32.

Hinkley, R., & Davis, L. (1986). Capillary pressure discontinuities and end effects in homogeneous composite cores: Effect of flow rate and wettability. Conference: Society of

Petroleum Engineers annual technical conference and exhibition, New Orleans, LA, USA, 5 Oct 1986. New Orleans*: Society of Petroleum Engineers*, Richardson, TX.

Hirasaki, G. (1991, June). Wettability: Fundamentals and Surface Forces. (2. 226, Ed.) *Society of Petroleum Engineers*, 6(2), 217-226.

Holm, L. W., & Josendal, V. A. (1974). Mechanisms of oil displacement by carbon dioxide. *Journal of petroleum Technology, 26*(12), 1-427.

Holloway, S. (2001). Storage of Fossil Fuel-Derived Carbon Dioxide beneath the Surface of the Earth. *Annual Review of Energy and the Environment*, 26, 145-166.

Hopkins, J. C. (1981, March). Sedimentology of Quartzose Sandstones of Lower Mannville and Associated Units, Medicine River Area, Central Alberta. *Bulletin of Canadian Petroleum Geology*, 29(1), 12-41.

Hower, J., Elsinger, E. V., Hower, M. E., & Perry, E. A. (1976). Mechanism of burial metamorphism of argillaceous sediment: 1. Mineralogical and chemical evidence. *The Geological Soceity of America, 85*(5), 725-737.

Huang, W. T. (1962). Petrology. *McGraw-Hill Book Company.*

Ide, S. T., Jessen, K., & Orr Jr., F. M. (2007). Storage of CO2 in saline aquifers: Effects of gravity, viscous, and capillary forces on amount and timing of trapping. *International Journal of Green House Gas Control, 1*, 48 1 – 49 1.

Iglauer, S. (2011). Dissolution Trapping of Carbon Dioxide in Reservoir Formation Brine – A Carbon Storage Mechanism. In *Mass Transfer - Advanced Aspects* (pp. 234-262). Publisher InTech. Retrieved from www.intechopen.com.

Iglauer, S., Pentland, H. C., & Busch, A. (2015). CO2 wettability of seal and reservoir rocks and the implications for carbon geo-sequestration. *Water Resources Research, 51*(1), 729-774.

Ihmels, E. C., & Gmehling, J. (2001). Densities of Toluene, Carbon Dioxide, Carbonyl Sulfide, and Hydrogen Sulfide over a Wide Temperature and Pressure Range in the Sub- and Supercritical State. *Ind. Eng. Chem. Res*., 40, 4470-4477.

Illés, E., & Tombácz, E. (2006). The effect of humic acid adsorption on pH-dependent surface charging and aggregation of magnetite nanoparticles. *Journal of Colloid and Interface Science*, 295(1), 115–123.

Janczuk, B., Białopiotrowicz, T., & Zdziennicka.Anna. (1999). Some Remarks on the Components of the Liquid Surface Free Energy. *Journal of Colloid and Interface Science*, 211, 96–103.

James H Jr, C., & David, R. (1972). *United States Patent No. US 3666506 A*.

Jansson, C., Wullschleger, S. D., Kalluri, U. C., & Tuskan, G. A. (2010). Phytosequestration: Carbon Biosequestration by Plants and the Prospects of Genetic Engineering. *BioScience,* 60(9), 685-696.

Jasper, L. (2006, February). Wetting phenomena at the CO2/Water/Glass interface. *Langmuir*, 22(5), 2161–2170.

Jindal, R., Swallow, & Kerr, J. (2008). Forestry-based carbon sequestration projects in Africa: Potential benefits and challenges. *Natural Resources Forum*, 32 (2), 116-130.

Joanny, J., & de Gennes, P. (1984). A model for contact angle hysteresis. The Journal of *Chemical Physics*, 81(552), 1-12.

Jung, J.-W., & Wan, J. (2012, July 27). Supercritical CO2 and Ionic Strength Effects on Wettability of Silica Surfaces: Equilibrium Contact Angle Measurements. *Energy Fuels*, 26(9), 6053–6059.

Kantzas, A. (200). Residual Gas Saturation Revisited. SPE/CERI Gas Technology Symposium, 3-5 April, Calgary, Alberta, Canada. Alberta: Society of Petroleum Engineers.

Karim, Sani Abdul:"The effect of disproportionate permeability reducers on spontaneous imbibition of water into Wallace Sandstone" MEg Petroleum Engineering gruation project report-*Dalhouie University*, 2013

Karimia, E., Ahmad, A., Hamid, R. S., & Arash, A. (2012). The potential of glauconitic sandstone as a potassium fertilizer for olive plants. *Archives of Agronomy and Soil Science, 58*(9), 983–993

Kemp, A. I., Hawkesworth, C. J., Foster, G., Paterson, B. A., Woodhead, J., Hergt, J. M., Whitehouse, M. J. (2007, February 16). Magmatic and Crustal Differentiation History of Granitic Rocks from Hf-O Isotopes in Zircon. *Science, 315*, 980-983.

Kewen, L. (2004). Theoretical Development of the Brooks-Corey Capillary Pressure Model from Fractal Modeling of Porous Media. SPE/DOE Symposium on Improved Oil Recovery (pp. 1-6). Tulsa, Oklahoma: *Society of Petroleum Engineers*.

Kharaka, Y., Cole, D., & Thordsen, J. K. (2006a). Gas–water–rock interactions in sedimentary basins: CO2 sequestration in the Frio Formation, Texas, USA. *Journal of Geochemical Exploration* 89 (2006), 89, 183–186.

Kharaka, Y., Cole, D., Hovorka, S., Gunter, W., Knauss, K., & Freifeld, B. (2006b). Gas-water-rock interactions in Frio Formation following CO2 injection: Implications for the storage of greenhouse gases in sedimentary basins. *Geology*, 34(7), 577-580.

Kharaka, Y. K., Thordsen, J. J., Kakouros, E., Ambats, G., Herkelrath, W. N., Beers, S. R., Zheng, L. (2010). Changes in the chemistry of shallow groundwater related to the 2008 injection of CO2 at the ZERT field site, Bozeman Montana. *Environ Earth Sci, 60*, 273–284.

Kim, Y., Wan, J., Kneafsey, T. J., & Tokunaga, T. K. (2012). "Dewetting of Silica Surfaces upon Reactions with Supercritical CO2 and Brine: Pore-Scale Studies in Micromodels. *Environment Science and Technology*, 46(7), 4228–4235.

King, H. (2005-2016). Retrieved from Geology.com: http://geology.com/rocks/slate.shtml

Knauss, K. G., & Wolery, T. J. (1998). The dissolution kinetics of quartz as a function of pH and time at 70°C. *Geochimica et Cosmochimica Acta, 52*(1), 43-53.

Kock, T. D., Boone, M., & Schutter, G. D. (2014). Replacement stones for Lede stone in Belgian historical monuments. *Geological Society, London, Special Publication, 391*, 31-46.

Koide, H., Tazaki, Y., Noguchi, Y., Nakayama, S., Ijima, M., Ito, K., & Shindo, Y. 3. (1992). Subterranean Containment and Long Term Storage of Carbon Dioxide in Unused Aquifers and Depleted Natural Gas Reservoir. *Energy Conservation and Management*, 33(5-8), 619-626.

Koike, C., Tsuchiyama, A., Shibai, H., Suto, H., Tanabe, T., Chihara, H.; Okada, K. (2000). Absorption Spectra of Mg-rich Mg-Fe and Ca Pyroxenes in the mid and far-infrared regions. *Astronomy and Astrophysics*, 1115-1122.

Koretsky, C. (2000, May 8). The significance of surface complexation reactions in hydrologic systems: a geochemist's perspective. *Journal of Hydrology*, 230(3-4), 127–171.

Kosmulski, M. (2002, September 1). The pH-Dependent Surface Charging and the Points of Zero Charge. *Journal of Colloid and Interface Science*, 253(1), 77–87.

Kosmulski, M. (2004). pH-dependent surface charging and points of zero charge II. Update. *Journal of Colloid and Interface Science, 275(1)*, 214–224.

Kossen, N., & Heertjss, P. (1965, June). The determination of the contact angle for systems with a powder. *Chemical Engineering Science*, 20(6), 593–599.

Kosmulski, M. (2009, September 15). pH-dependent surface charging and points of zero charge. IV. Update and new approach. *Journal of Colloid and Interface Science, 337*(2), 439–448.

Krause, M., Pperin, J., & Benson, S. (2009). Modelling Permeability Distribution in Sandstone Core Sample for History Matching Water Core Flood Experiments. SPE International Conference on CO2 Capture, Storage and Utilization. 16, pp. 768-777. San Diego California usa: *Society of Petroleum Engineers*.

Kwok, D., & Neumann, A. (1999). Contact angle measurement and contact angle interpretation. *Advances in Colloid and Interface Science*, 81, 167-249.

Labajos-Broncano, L., Antequera-Barroso, J., & Gonzalez-Martın, M. (2004).On the constancy of the free energy reduction caused by imbibition in porous media. *Powder Technology* 148 (2004, 148) 48–52.

Lanson, B., Beaufort, D., & Berger, G. A. (2002). Authigenic kaolin and illitic minerals during burial diagenesis of sandstones: a review. *Clay Minerals* (2002) 37, 37, 1–22.

Laudelout, H., Bladel, R. v., Bolt, G. H., & Page, A. L. (1968). Thermodynamics of heterovalent cation exchange reactions in a montmorillonite clay. *Trans. Faraday Soc*., 64, 1477-1488.

Lee, H., Reis, J., Dohner, J., & Lightfoot, E. (1974, July). Single-phase chromatography: Solute retardation by ultrafiltration and electrophoresis. *AIChE Journal*, 20(4), 776–784.

Leea, J., Moon, H., Fowler, J., Schoellhammer, T., & Kim, C.-J. (2002, January 1). Electrowetting and electrowetting-on-dielectric for microscale liquid handling. *Sensors and Actuators A: Physical*, 95(2-3), 259–268.

Leij, S. A. (1997). Estimating interfacial areas for multi-fluid soil systems. *Journal of Contaminant Hydrology*, 27(1-2), 83–105.

Li, K., & Horne, R. N. (2002, January). Experimental verification of methods to calculate relative permeability using capillary pressure data. *In SPE Western Regional/AAPG Pacific Section Joint Meeting. Society of Petroleum Engineers* (pp. 1-10). Soceity of Petroleum Engineers.

Lin, H., Takashi, F., Takisawa, T. T., & Hashida, T. (2008). Experimental evaluation of interactions in supercritical CO2/water/rock minerals system under geologic CO2 sequestration conditions. J Mater Sci, 43, 2307–2315.

Lindquist, W. B., & Venkatarangan, A. (2000, September 10). Pore and throat size distributions measured from synchrotron X-ray tomographic images of Fontainebleau sandstones. *Journal of Geophysical Research*, 105(B 59), 21509-21527.

Liu, L., Suto, Y., Bignall, G., Yamasaki, N., & Hashida, T. (2003). CO2 injection to granite and sandstone in experimental rock/hot water systems. *Energy Conversion and Management 44 (2003), 44*, 1399–1410.

Liu, K., Yao, X., & Jiang, L. (2010). Recent developments in bio-inspired special wettability. *Chem. Soc. Rev., 39*, 3240-3255.

Ma, S., Zhang, X., & Morrow, N. (1999). Characterization of Wettability from Spontaneous Imbibition Measurements. *Journal of Canadian Petroleum Technology*, 38(13).

Machemer, S. D., & Hutcheon, I. (1988, January). Geochemistry of Early Carbonate Cements in the Cardium Formation, Central Alberta. *Journal of Sedimentary Petrology*, 58(1), 136-147.

Magot, M., Ollivier, B., & Patel, B. K. (2000). Microbiology of petroleum reservoirs. Antonie van Leeuwenhoek, 77, 103–116.

Mahadevan, T. S., & Garofalini, S. H. (2008). Dissociative chemisorption of water onto silica surfaces and formation of hydronium ions. *The Journal of Physical Chemistry C, 112*(5), 1507-1515.

Mahaffey, C. J., Rutherford, W., & Development, C. M. (1966). Sweep Efficiency by Miscible Displacement in a Five-Spot. *Soceity of Petroleum Engineers*, 6(1), 73-80.

Marek, K. (2002). The pH-Dependent Surface Charging and the Points of Zero Charge. *Journal of Colloid and Interface Science*, 253, 77–87.

Marmur, A. (2004). Adhesion and Wetting in an Aqueous Environment: Theoretical Assessment of Sensitivity to the Solid Surface Energy. *Langmuir*, 20, 1317-1320.

Martel, A., Gibling, M., & Nguyen, M. (2001). Brines in the Carboniferous Sydney Coalfield, Atlantic Canada. *Applied Geochemistry*, 16, 35-55.

Matter, J. M., & Takahashi, T. (2007, February). Experimental evaluation of in situ CO2-water-rock reactions during CO2 injection in basaltic rocks: Implications for geological CO2 sequestration. *Geochemistry, Geophysics, Geosystems, 8*(2), 1-19.

Mcbride, E. F. (1963, September). A Classification of Common Sandstones. *Journal of Sedimentary Petrology,* 33(3), 664-669.

McCafferty, E., & Wightman, J. P. (1997). Determination of the surface isoelectric point of oxide films on metals by contact angle titration. *Journal of colloid and interface science, 194*(2), 344-355.

McDougall, S., & Sorbie, K. (1997). The Effect of Interfacial Tension Upon Gas-Oil Relative Permeability Measurements: Interpretation Using Pore-Scale Models. *SPE Annual Technical Conference and Exhibition, 5-8 October, San Antonio, Texas* (pp. 791-803). Society of Petroleum Engineers.

McGrail, B. P., Todd, S. H., Ho, A. M., Chien, Y.-J., Dooley, J. J., & Davidson, L. C. (2006). Potential for carbon dioxide sequestration in flood basalts. *JOURNAL OF GEOPHYSICAL RESEARCH, 111*(B12201).

McIver, N. L. (1972). Cenozoic and Mesozoic Stratigraphy of the Nova Scotia Shelf. *Canadian Journal of Earth Sciences*, 9(1), 54-70.

Miller Jr., D. (1966). Diagenesis of Sedimentary Rocks. *WGA, 2005* - Symposium on Recently Developed Geologic Principles and Sedimentation of the Permo-Pennsylvanian of the Rocky. *American Association of Petroleum Geologists (AAPG).*

Muhammad, F., Guo, M., Qi, W., Sun, F., Wang, A., Yingjie Guo, & Zhu, G. (2011, May 17). pH-Triggered Controlled Drug Release from Mesoporous Silica Nanoparticles via Intracelluar Dissolution of ZnO Nanolids. *J. Am. Chem. Soc., 133*(23), 8778–8781.

Naidu, R., Bolan, N.S., Kookana, R.S. & Tiller, K.G. (1994). Ionic-strength and pH effects on the sorption of calcium and the surface charge of soils. *European Journal of Soil Science*, 45(4), 419-429

Nam, J. H., & Kaviany, M. (2003). Effective diffusivity and water-saturation distribution in single- and two-layer PEMFC diffusion medium. *International Journal of Heat and Mass Transfer,* 46(24), 4595–4611.

Netz, R. R., & Andelman, D. (1997, January 1). Roughness-induced wetting. *Phys. Rev., E 55*, 687

Newell, D. L., Kaszuba, J. P., & Viswanathan, H. S. (2008, December 11). Significance of carbonate buffers in natural waters reacting with supercritical CO2: Implications for monitoring, measuring and verification (MMV) of geologic carbon sequestration. *Geophysical Research Letters*, 35(23).

Nguyen, T., & John, W. (1978). Ploar and Dispersion Force Contribution to Total Surface Free Energy of Wood. *Wood Sci. Technol*, 12, 63-74.

Noh, M. H., Lak, L. W., & Araque-Martinez, A. N. (2007). Implications of Coupling Fractional Flow and Geochemistry for CO2 Injection in Aquifers. *Society of Petroleum Engineers.*

Noiriel, C., Made, B., & Gouze, P. (2007). Impact of coating development on the hydraulic and transport. *Water Resources, 43*, 1-16.

Nuh, J.S. & Schwarz, J.A. (1989). Estimation of the point of zero charge of simple oxide by mass titration. *Journal of Colloid and Interface Science*, 130(1), 157-164

Nwajiaku, T. G. (2011). Geological Sequestration of Carbon Dioxide: The Effcet of Temperature on on the Relative Permeability of Supercritical Carbon Dioxide/Brine in Deep Saline Aquifers. Halifax: *Dalhousie University Library.*

Oberthur, S., & Ott, H. E. (1999). The Kyoto Protocol: International Climate Policy for the 21 St Century. *Berlin Heidelberg: Springer Verlag Berlin Heidelberg* 359.

Oelkers, E. H., Gislason, S. R., & Matter, J. (2008). Mineral Carbonation of CO2. *Element*, 4(5), 333-337.

O'Brien, B. H., & Charles, D. A. (1985). Concretionary Green Beds between Halifax and Goldenville Formations: Local Dopecenters on a Continental Margin. *Atlantic Geology, 21*(2)

Oostrom, M., & Lenhard, R. J. (1998). Comparison of relative permeability-saturation pressure parametric models for infiltration and redistribution of a light nonaqueous-phase liquid in sandy porous media. *Advances in Water Resources, 21*(2), 145-157.

Oss, C. J. (2006). Interfacial Forces in Aqueous Media-Second Edition. New York: *Taylor and Fracncis.*

Osman, M. A., & Suter, U. W. (2000). Determination of the cation-exchange capacity of muscovite mica. *Journal of colloid and interface science, 224*(1), 112-115.

Oss, C. J., Chaudhury, M. K., & Good, R. J. (1988a). Interfacial Lifshitz-van der Waals and polar interactions in macroscopic systems. *Chem. Rev*., 88(6), 927–941.

Oss, C. J., Good, R. J., & Chaudhury, M. K. (1988b). Additive and Nonadditive Surface Tension Components and the Interpretation of Contact Angles. *Langmuir*, 4(4), 884–891.

Pande, K., Ramey Jr, H., & Brigham, W. (1987). Frontal Advance Theory for Flow in Heterogeneous Porous Media. SPE California Regional Meeting, 8-10 April. Ventura, California: *Society of Petroleum Engineers*.

Parks, G. A., & de Bruyn, P. L. (1962). The Zero Point oF Charge oF Oxides. *J. Phys. Chem.*, 66(6), 967–973.

Pease, D. C. (1945). The Significance of the Contact Angle in Relation to the Solid Surface. *Journal of Physical Chemistry*, 49(2), 107–110.

Peksa, A. E., Wolf, K.-H. A., & Zitha, P. L. (2015, November). Bentheimer sandstone revisited for experimental purposes. *Marine and Petroleum Geology, 67*, 701–719.

Petalas, C. P., & Diamantis, I. B. (1999). Origin and distribution of saline ground waters in the upper Miocene aquifer system, coastal Rhodope area, northeastern Greece. *Hydrogeology Journal*, 7, 305–316.

Perrin, J., & Benson, S. (2010). An Experimental Study on the Influence of Sub-Core Scale Heterogeneities on CO2 Distribution in Reservoir Rocks. *Transp Porous Media*, 82, 93-109.

Petalas, C. P., & Diamantis, I. B. (1999, C. P. Petalas 7 I. B. Diamantis). Origin and distribution of saline groundwaters in the upper Miocene aquifer system, coastal Rhodope area, northeastern Greece. *Hydrogeology Journal*, 7, 305–316.

Petrov, P., & Petrov, I. (1992). A combined molecular-hydrodynamic approach to wetting kinetics. *Langmuir*, 8(7), 1762–1767.

Pope, G. A. (1980, June). The Application of Fractional Flow Theory to Enhanced Oil Recovery. *Soceity of Petroleum Engineering.*

Porrenga, D. H. (1968, April 15). Non-Marine Glauconitic Illite in the Lower Oligocene of Aardebrug, Belgium. *Clay Minerals*, 7(421).

Pikaray, S., Banerjee, S., & Mukherji, S. (2005). Sorption of arsenic onto Vindhyan shales: role of pyrite and organic carbon. *Current Science, 88*(10), 1580-1585.

Portier, S., & Rochelle, C. (2005, December 10). Modelling CO2 solubility in pure water and NaCl-type waters from 0 to 300 8C and from 1 to 300 bar Application to the Utsira Formation at Sleipner. *Chemical Geology* 217 (2005), 217, 187– 199.

Poston, Ysrael, S., Hossain, A., & Montgomery, E. (1970). The Effect of Temperature on Irreducible Water Saturation and Relative Permeability of Unconsolidated Sands. *Society of Petroleum Engineers Journal, 10*(02), 170-180.

Puah, L. S., Sedev, R., Fornasiero, D., Ralston, J., & & Blake. (2010, October 14). Influence of Surface Charge on Wetting Kinetics. *Langmuir*, 26(22), 7218–17224.

Qasem, F. H., Nashawi, I., & Sami, R. G. (2008, Jnauary). Recovery performance of partially fractured reservoirs by capillary imbibition. *Journal of Petroleum Science and Engineering*, 60(1), 39–50.

Quarry, W. (2001). Retrieved from Wallace Sandstone Test Results: http://www.wallacequarries.com/

Ramanan, R. K. (2009). Bio-sequestration of carbon dioxide using carbonic anhydraseenzyme purified from Citrobacter freundi. *World J Microbiol Biotechnol*, 25, 981-987.

Reimer, P. (1996). Greenhouse Gas Mitigation Technologies, an Overview of the CO2 Capture, Storage and Future Activities-The IEA Greenhouse Gas R&D Programme. *Energy Conversion and Management*, 37 (6-8), 665-670.

Reymond, J. P., & Kolenda, (1999). Estimation of the point of zero charge of simple and mixed oxides by mass titration. *Powder Technology*, 103(1), 30-36.

Riebesell, U., Wolf-Gladrow, D. A., & Smetacek, V. (1963). Carbon dioxide limitation of marine phytoplankton growth rate. *Nature*, 361(6409), 249 - 251.

Rosen, M. J., & Kunjappu, J. T. (2012). Surfactants and Interfacial Phenomena-Fourth Edition. New Jersy: John Wiley and Sons.

Rogers, J. D., & Grigg, R. B. (2000). Literature Analysis of the WAG Injection Abnormalities in the Carbon Dioxide Process. *Soceity of Petroleum Engineers*, 1-21.

Ross, G. D., Todd, A. C., Tweedie, J. A., & Will, A. G. (1982). The Dissolution Effects of CO2-Brine Systems on the Permeability of U.K. and North Sea Calcareous Sandstones. SPE Enhanced Oil Recovery Symposium (pp. 1-14). SPE/DOE

Ruffet, C., Gueguen, Y., & Darot, M. (1991). Complex conductivity measurements and fractal nature of porosity. *Geophysics*, 56(6), 758-768.

Rupp, F., Scheideler, L., Rehbein, D., Axmann, D., & Geis-Gerstorfer, J. (2004). Roughness induced dynamic changes of wettability of acid etched titanium implant modifications. *Biomaterials, 25*(7-8), March–April 2004, Pages 1429–1438.

Saleem Akhtar, M. (1993). Potassium Availability as Affected by Soil. Proceedings of the Regional Symposium held in Tehran, Iran June. Tehran: Research Institute (SWRI) and the *International Potash Institute* (IPI).

Salem, H. S., & Chilingarian, G. V. (1999). Determination of specific surface area and mean grain size from well-log data and their influence on the physical behavior of offshore reservoirs. Journal of Petroleum Science and Engineering, 22, 241–252.

Sally, B. M., Oldenburg, C., Hoversten, M., & Imbus, S. (2005). :" Carbon dioxide Capture for Storage in Deep Geologic Formations-Results from CO2 Capture Projects-Volume 2. New York: Elsevier.

Sasowsky, I. D., Foos, A., & Miller, C. M. (2000). Lithic Controls on the Removal of Iron and Remediation of Acid Mine Drainage. *Wat. Res. Vol., 34*(10), 2742-2746.

Sater, A., Iqbal, G. M., & Buchwalter, J. L. (2008). Parctical Enhanced Reservoir Engineering. PennWell Corporation.

Scales, P., Grieser, F., & Healy, T. (1992). Langmuir. 8, 965–974.

Shen, J., Ebner, A. D., & Ritter, J. A. (1999). 4.4.6 Determing the Effective Point of Zero Charge pH of Wallace Sanstone of Silica–Magnetite Composite Oxides. *Journal of Colloid and Interface Science, 214*, 333–343

Schwarz, J., Driscoll, C., & Bhanot, A. K. (1984, January). The zero point of charge of silica—alumina oxide suspensions. *Journal of Colloid and Interface Science, 97*(1), 55–61.

Schwarz, J. S., & James, A. (1989). Estimation of the point of zero charge of simple oxides by mass titration. *Journal of Colloid and Interface Science*, 130(1), 157–164.

Shao, L.-H., Ju¨rgen, B., Dominik, K., Raghavan, N. V., Theodore, F. B., & Alex, V. H. (2010). Electrocapillary maximum and potential of zero charge of carbon aerogel. Phy.Chem. *Chem. Phys*, 7580-7587.

Sherwin, M. D. (1996, September). Channel Trends in the Glauconitic Member, Southern Alberta. *Bulletin of Canadian Petroleum Geology*, 44(3), 530-540.

Silin, D., Patzek, T., & Sally, B. M. (2009). A Model of Buoyancy-Driven Two-Phase Countercurrent Fluid Flow. *Transp Porous Media*, 76, 449–469.

Smith, C. R., Tracy, G., & Farrar, R. L. (1992). Applied Reservoir Engineering Volume 1. Oklahoma*: Oil and Gas Consultant International*.

Sposito, G., Skipper, N. T., Sutton, R., Park, S.-H., Soper, A. K., & Greathouse, J. A. (1999, March). Surface geochemistry of the clay minerals. *Proc. Natl. Acad. Sci., 96*, 3358–3364.

Spycher, N., & Pruess, K. (2010). A Phase-Partitioning Model for CO2–Brine Mixtures at Elevated Temperatures and Pressures: Application to CO2-Enhanced Geothermal Systems. *Transp Porous Med*, 82, 173–196.

Spycher, N., Pruess, K., & Ennis-king, J. (2003). CO2-H2O mixtures in the geological sequestration of CO2. I. Assessment and calculation of mutual solubilities from 12 to 100°C and up to 600 bar. *Geochimica et Cosmochimica Acta*, 63(16), 3015–303.

Srasra, E., & Trabelsi-Ayedi, M. (2000, July). Textural properties of acid activated glauconite. *Applied Clay Science* Volume, 17(1-2), 71–84.

Standnes, D. C., & Austad, T. (2003, April 15). Wettability alteration in carbonates: Interaction between cationic surfactant and carboxylates as a key factor in wettability alteration from oil-wet to water-wet conditions. Colloids and Surfaces A: *Physicochemical and Engineering Aspects*, 216(1-3), 243–259.

Stenina, N., Bazarov, L., & Shcherbakova, M. a. (1984). Structural State and Diffusion of Impurities in Natural Quartz of Different Genesis. *Phys Chem Minerals* (1984) 10: 10, 180-186.

Stevens, S. H., Kuuskraa, V. A., Gale, J., & Beecy, D. (2001, September). CO2 Injection and Sequestration in Depleted Oil and Gas Fields and Deep Coal Seams: Worldwide Potential and Costs. *Environmental Geosciences, 8*(3), 200–209.

Somasundaran, P., & Agar, G. (1967). The zero point of charge of calcite. *Journal of Colloid and Interface Science, 24*(4), 433-440.

Stillinger, F. H., & Rahman, A. (1972, April 13). Molecular Dynamics Study of Temperature Effects on Water Structure and Kinetics. *The Journal of Chemical Physics*, 57, 1281-1292.

Sulpizi, M. G.-P. (2012, February 27). The Silica–Water Interface: How the Silanols Determine the Surface Acidity and Modulate the Water Properties. *J. Chem. Theory Comput*, 2012, 8 (3), pp, 1037–1047.

Suter, M. A. (1, April). Determination of the Cation-Exchange Capacity of Muscovite Mica. *Journal of Colloid and Interface Science*, 224(1), 112–115.

Suttner, L. J., Basu, A., & Mack, G. H. (1981, Decfember). Climate and the Origin of Quartz Arenites. *Journal of Sedimentary Petrology*, 51(4), 1235-1246.

Sverjensky, D. A., & Sahai, N. (1996). Theoretical Prediction of Single Site Surface Protonation equilibrium Constant for Oxides and Silicates in Water. *Geochimica et Cosmochimica Acta*, 60(20), 3773-3797.

Sverjensky, D. A. (1994, July). Zero-point-of-charge prediction from crystal chemistry and solvation theory. *Geochimica et Cosmochimica Acta, 58*(14), 3123-3129.

Takahashi, S., & Anthony, K. R. (2010). Wettability estimation of low-permeability, siliceous shale using surface forces. *Journal of Petroleum Science and Engineering*, 75(1-2), 33–43.

Timothy, W. D., James, A. T., Sven, V., Thomas, Proffena, Katie, P., Erik, E. (2006). Localizing Nonclassical Nonlinearity in Geological Materials with Neutron Scattering Experiments. *AIP Conference Proceedings* #383. *Innovations in Nonlinear Acoustics: ISNA 1.*

Tomita, K., Takahashi, H., & Watanabe, T. (1988). Quantification Curves for Mica/Smectite Interstratifications by X-Ray Powder Diffraction. *Clays and Clay Minerals*, 36(3), 258-262.

Trevino, K. J., Shearer, J. C., McCurdy, P. R., Pease-Dodson, S. E., Okegbe, C. C., & Fisher, E. R. (2011, September). Isoelectric points of plasma-modified and aged silicon oxynitride surfaces measured using contact angle titrations. *Surfaces and Interfaces Analysis, 43*(9).

Tripp, C. P., & Combes, J. R. (1998, Deccember 4). Chemical modification of metal oxide surfaces in supercritical CO2: The interaction of supercritical CO2 with the adsorbed water layer and the surface hydroxyl groups of a silica surface. *Langmuir*, 14(26).

Vezenov, D. V., Noy, A., Rozsnyai, L. F., & Lieber, C. M. (1997). Force Titrations and Ionization State Sensitive Imaging of Functional Groups in Aqueous Solutions by Chemical Force Microscop. *Journal of American Chemical Soceity*, 119(18), 2006-2015.

Vidal, A., Papirer, E., Jiao, W. M., & Donnet, J. B. (1987). Modification of silica surfaces by grafting of alkyl chains. I—Characterization of silica surfaces by inverse gas-solid chromatography at zero surface coverage. *Chromatographia, 23*(2), 121-128.

Vishnyakov, A., Shen, Y., & Tomassone, M. S. (2008, October). Solvation Forces between Silica Bodies in Supercritical Carbon Dioxide. *Langmuir*, 24(3), 13420–13425.

Walderhaug, O., Bjørkum, P. A., Nadeau, P. H., & Langnes, O. (2001). Quantitative modelling of basin subsidence caused by temperature-driven silica dissolution and reprecipitation. *Petroleum Geoscience, 7*, 107-113.

Wang, N. F., & Shengche, J. (1997). Modeling Sorption of Trace Metals on Natural Sediments by Surface Complexation Model. *Environmental Science & Technology*, 31(2).

Wang, S., Edwards, I. M., & Clarens, A. F. (2013). Wettability Phenomena at the CO2−Brine−Mineral Interface:. *Environ. Sci. Techno, 47*, 234−241.

Wang, R., & Wang, L. (1995). Adsorption Behavior of Radium in Carbonaceous Slate. *Journal of Rdaioanlytical and Nuclear Chmemistry, 189*(2), 269-276.

Wangab, Y. M., Zhu, M., & Bai, M. (2010, Jannuary 22). Wettability and Nanotribological Property of Multiply Alkylated Cyclopentanes (MACs) on Silicon Substrates. *Tribology Transactions,* 53(2), 219-223.

Washburn, E. (1921). The dynamics of capillary flow. *Phys. Rev*, 17, 273–283.

Weides, S., M. I., & Majorowicz, J. a. (2014). The Cambrian Basal Sandstone Unit in central Alberta — an investigation of temperature distribution, petrography, and hydraulic and geomechanical properties of a deep saline aquifer. *Can. J. Earth Sci*., 51, 783–796.

Weissenborn, P. K., & Pugh, R. J. (1996). Surface tension of aqueous solutions of electrolytes: relationship with ion hydration, oxygen solubility, and bubble coalescence. *Journal of Colloid and Interface Science, 184*(2), 550-563.

Whyman, G., Bormashenko, E., & Stein, T. (2008, January 4). The rigorous derivation of Young, Cassie–Baxter and Wenzel equations and the analysis of the contact angle hysteresis phenomenon. *Chemical Physics Letters*, 450(4-6), 355–359.

Xu, T., Apps, J. A., & Pruess, K. (2001, July 20). Analysis of mineral trapping for CO2 disposal in deep aquifers. *Lawrence Berkeley National Laboratory*.

Xu, T., Apps, J. A., & Pruess, K. (2005). Mineral sequestration of carbon dioxide in a sandstone–shale system-Geochemical Aspects of CO2 sequestering. *Chemical Geology*, 217(3-4), 295-318.

Xu, T., Sonnenthal, E., Spycher, N., & Pruess, K. (2006). TOUGHREACT—a simulation program for non-isothermal multiphase reactive geochemical transport in variably saturated geologic media: applications to geothermal injectivity and CO 2 geological sequestration. *Computers & Geosciences, 32*(2), 145-165.

Yadav, P. V., Sharma, T., & Saxena, V. (2000, August). Dissolution kinetics of potassium from glauconitic sandstone in acid lixiviant. *International Journal of Mineral Processing*, 60(1), 15–36.

Ẑalac, S., & Kallay, N. (1992, March 1). Application of mass titration to the point of zero charge determination. *Journal of Colloid and Interface Science*, 149, 233-240.

Zhmud, B. V., Tiberg, F., & Hallstensson, K. (2000). Dynamics of Capillary Rise. *Journal of Colloid and Interface Science*, 228, 263–269.

Zhuravlev, L. T. (1987). Concentration of hydroxyl groups on the surface of amorphous silicas. *Langmuir*, 3(3), 316–318.

Zhuravlev, L. T., & Potapov, V. V. (2006). Density of Silanol Groups on the Surface of Silica Precipitated. *Russian Journal of Physical Chemistry*, 2006 80(7), 1119–1128.

Appendix 3-1: Interfacial tension of carbon dioxide-brine system versus pressure and salinity

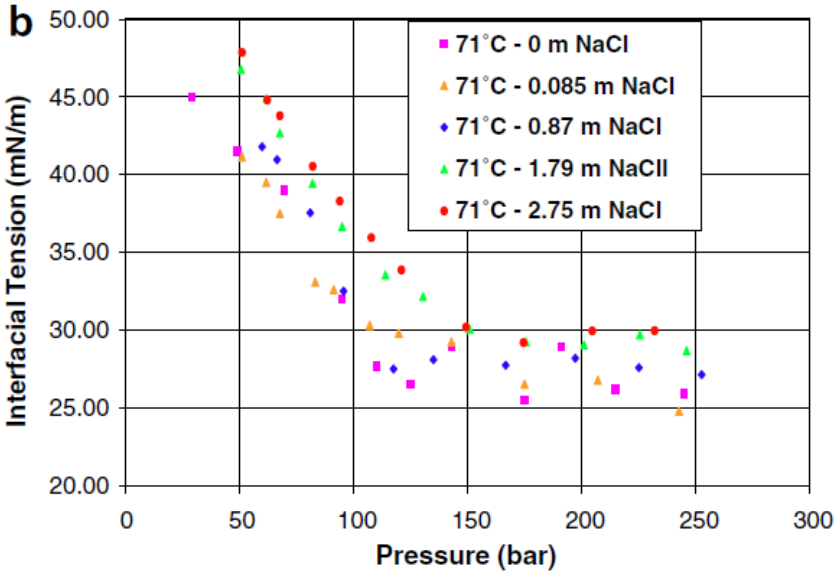

Ref: Chalbaud *et al.*, 2009

Appendix 3-2: Carbon dioxide pressure versus formation water pH

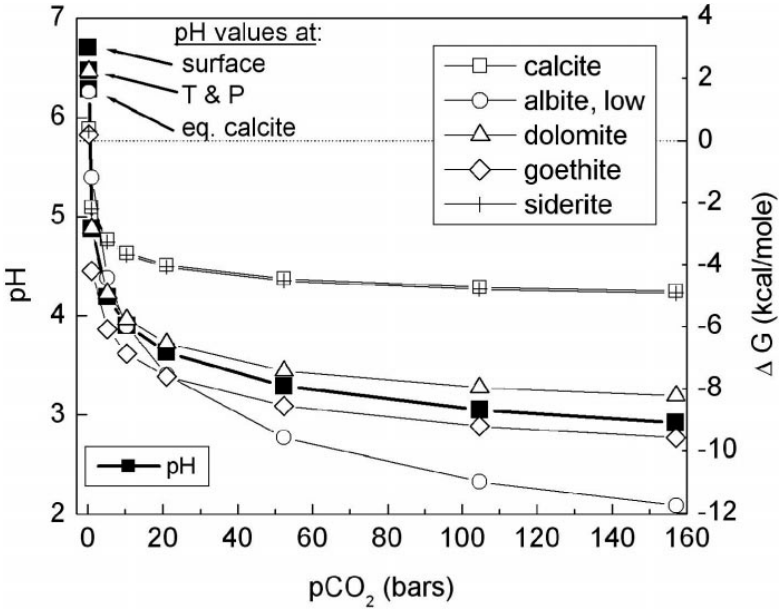

Ref: Kharakas *et al.*, 2006b

Appendix 4A: Density of carbon dioxide versus depth

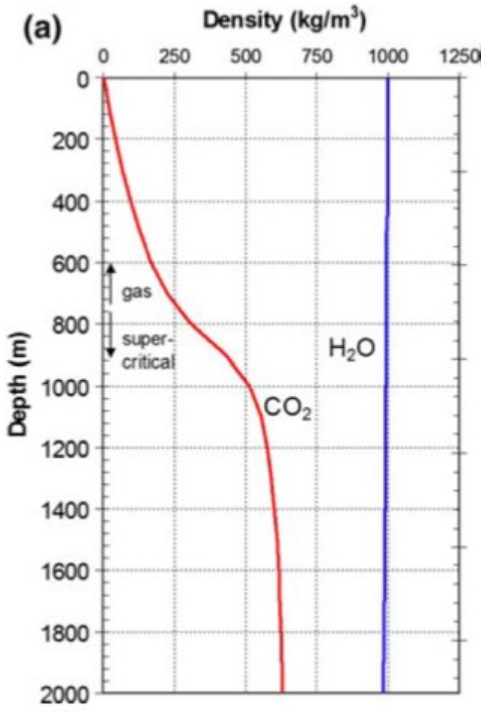

Ref: Doughty *et al*., 2008

Appendix 4B Density of carbon dioxide versus depth

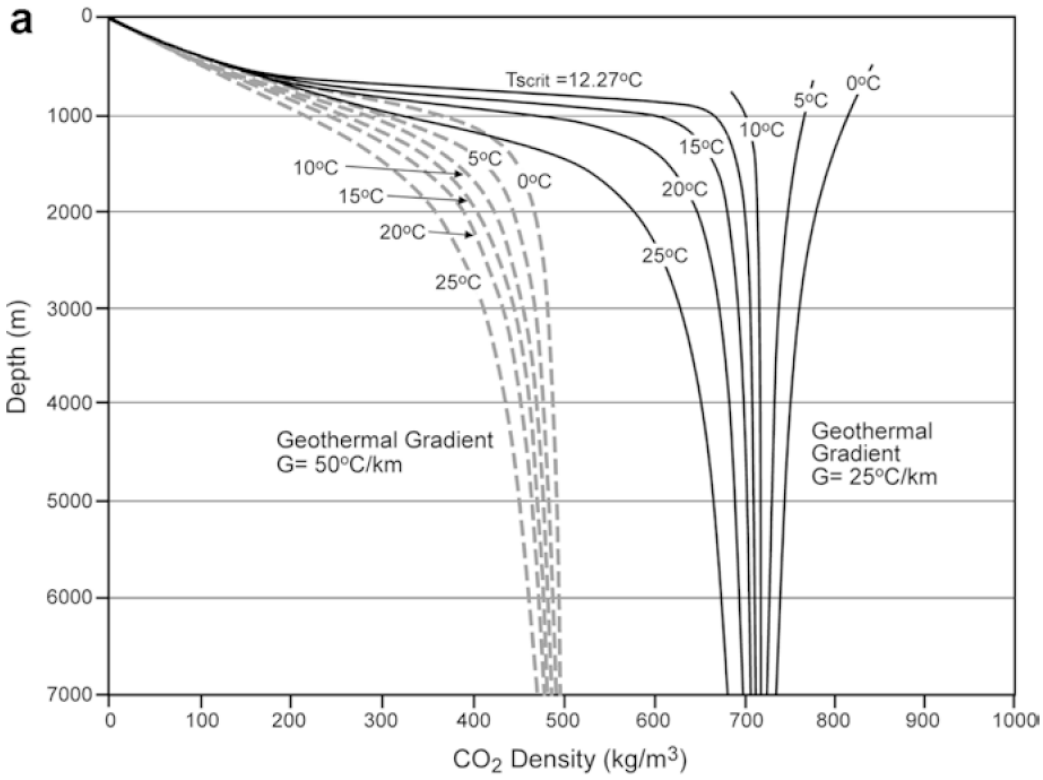

Ref: (Bachu & Adams, 2003)

Appendix 4C: Interfacial tension between carbon dioxide and water at varying pressure

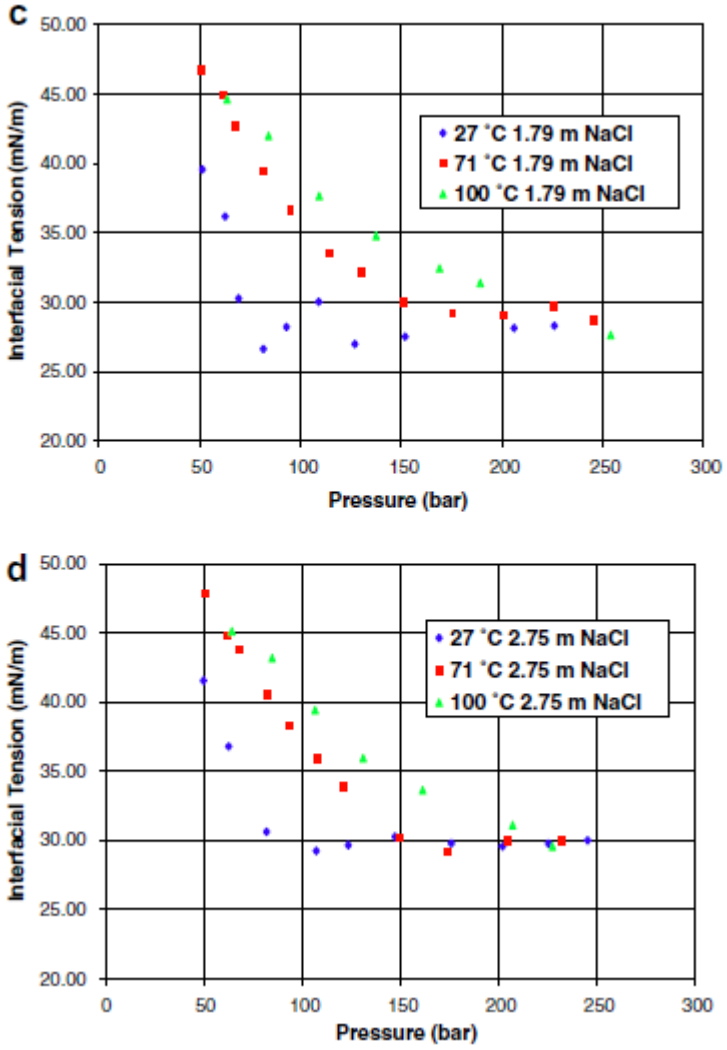

Ref: Chalbaud *et al* (2009)

Appendix 4D: Stratigraphic terminology proposed for the Jurassic-Cretaceous sediments of the Nova Scotia shelf

GROUP	FORMATION	MEMBER	DOMINANT LITH.	MAXIMUM THICKNESS
QUATERNARY	* SABLE ISLAND		SAND AND GRAVEL	
	* LA HAVE		CLAY	
	* SAMBRO		SAND	
	* EMERALD		SILT	
	* SCOTIAN SHELF		GLACIAL DRIFT	
THE GULLY GROUP	BANQUEREAU		MUDSTONE	4000'
	WYANDOT		CHALK	750'
	DAWSON CANYON	LST. MARKER	SHALE	3000'
NOVA SCOTIA GROUP	LOGAN CANYON		SANDSTONE & SHALE	800'
		SABLE SHALE	SHALE	500'
			SANDSTONE & SHALE	2000'
	NASKAPI		SHALE	750'
	MISSISAUGA	LST. MARKER	SANDSTONE	3700'
WESTERN BANK GROUP	MIC MAC		CALCAREOUS SHALE	4000'
	VERRILL CANYON		SHALE	> 2000'
	ABENAKI	BACCARO	LIMESTONE	2500'
		MISAINE	CALCAREOUS SHALE	300'
		SCATARIE	LIMESTONE	400'
	MOHAWK		SANDSTONE & SHALE	3500'
	IROQUOIS		DOLOMITE	650'
	ARGO		SALT	> 3000'

* Informal Map Units From KING, 1971.

Ref: (McIver, 1972)

Appendix 4E: Chemical composition of Wallace sandstone (http://www.wallacequarries.com/)

Results of mineral analysis carried out by Dalhousie University (Mineral Engineering Center) Halifax, Nova Scotia. February 19th, 2001.

- **SiO2** Silicon Dioxide "Silica" **82.00 %**
- **AI2O3** Aluminium Oxide "Alumina" **8.12 %**
- **Fe2O3** Ferric Oxide "Hematile" **3.19 %**
- **Na2O** Sodium Oxide **1.67 %**
- **K2O** Potassium Oxide **1.13 %**
- **MgO** Magnesium Oxide **0.72 %**
- **CaO** Calcium Oxide **0.81 %**
- **TiO** Titanium Oxide "Titania" **0.29 %**
- **MnO** Manganese Oxide "Magnesia" **0.10 %**
- **L.O.I.** Loss on Ignition **2.59 %**

Appendix 4F: Results of monophasic permeability test

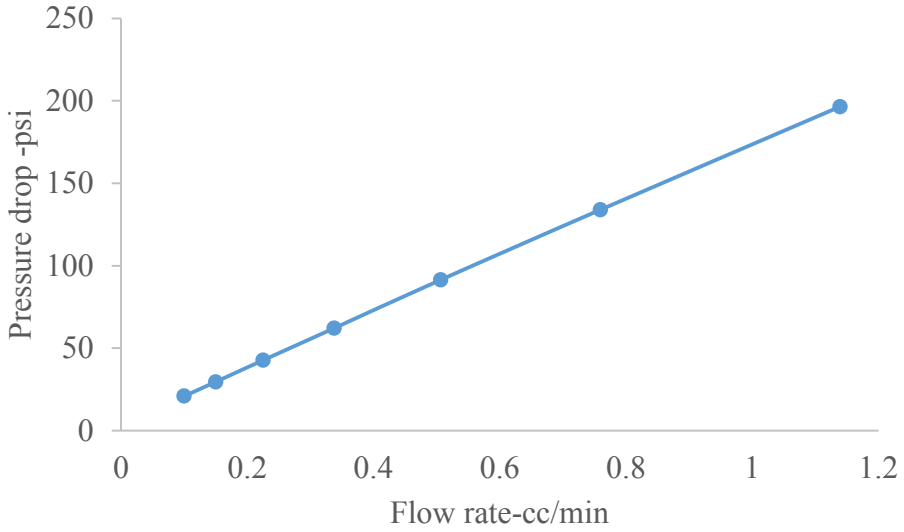

Appendix 4G: Point of zero charge pH of some oxides (Parks and de Bruyn, 1962)

Solid	pH: Z.p.c.	pH: Min. solubility	pH: I.e.p. (calcd.)	Comment	Ref.
			1		35
WO_3	0.43	0.43		*a,e*	36
SiO_2	<2			*b,e,f*	37, 38, 16
SnO_2	4.5			*a,e*	16
	(5.5–7.3)			*b,e*	16
TiO_2	6.7			*b,f*	39
	6			*a,e*	16
	(4.7)			*b,c,e*	16
ZrO_2	~4			*b,g*	38
Al_2O_3	6.94 ± 0.37			*a,e*	40
	(8.4)			*b,e*	16
	(9.45)			*b,f*	41
		7.7			42

Appendix 4H: Point of zero charge of oxides (Kosmulski M. , The pH-Dependent Surface Charging and the Points of Zero Charge, 2002)

Material	Description	Salt	T	Method	pH_0
SiO_2	Aerosil OX 50 Degussa	10^{-3}–0.1 mol dm^{-3} NaCl	25	pH iep	<4 if any 2.4
SiO_2	Polysciences	10^{-4}–0.1 mol dm^{-3} KNO_3		iep	<3 if any
SiO_2	Aerosil 380	10^{-2} mol dm^{-3} NaCl, $NaNO_3$	25	iep Acusto	2–4 (if any)
SiO_2	Quartz	10^{-2} mol dm^{-3} NaCl, $NaNO_3$	25	iep Acusto	2–4 (if any)
SiO_2	Duke	10^{-3}–10^{-2} mol dm^{-3} NaCl		iep	2.5–4.5
SiO_2	Quartz, Alfa Aesar	$KOH + HNO_3$		Acusto	2.3
SiO_2	Stöber	10^{-3} mol dm^{-3} KBr		iep	2
SiO_2	Aerosil 380	10^{-3}–0.1 mol dm^{-3} $NaClO_4$	25	iep pH	$\zeta = 0$ at pH <5 <3 if any
SiO_2	Geltech	10^{-3} mol dm^{-3} NaCl, KCl, LiCl, CsCl		Acusto	$\zeta = 0$ at pH 2
SiO_2	Quartz, Sigma	0.1 mol dm^{-3} NaCl, KCl, LiCl, CsCl		Acusto	<2 if any
SnO_2	Cassiterite, natural	None		iep	<3 if any

Appendix 4I: Albite + NaCl Brine + Supercritical CO2, 75 °C and 200 bar for nonmineral buffering saline aquifer system (Newell, *et al*., 2008)

Sample	Hours	Bars	T °C	Al^{3+}	Na^{+}	$SiO_2(aq)$	HCO_3^{-}	CO_2 Total	Cl^{-}	$SO4^{2-}$	Ca^{2+}	Fe^{2+}	K^{+}	Mg^{2+}	pH Bench	pH *In Situ*[b]
start	0.0	1	21	0.01	23614	0.75	1.8	1.8	35626	19.7	0.0	0.0	0.0	0.0	7.99	7.99
1	9050.9	194	75	0.14	23934	9.57	6.0	6.0	39238	26.6	0.0	0.0	0.0	0.0	8.95	8.21
2	626.8	191	75	0.19	23906	9.89	5.4	5.4	35654	1.80	26.4	0.07	12.8	2.33	7.65	7.25
3	1128.8	199	74	0.11	24213	10.37	5.2	5.2	35311	2.18	12.1	0.02	11.0	2.31	7.31	7.05
4	2953.5	202	76	0.12	21245	9.85	17.0	17.0	36442	8.15	10.8	0.05	6.21	0.63	6.31	6.35
5	2976.8	350	76	3.54	20730	35.42	nd[c]	41866	36145	8.44	36.3	8.10	10.3	1.46	4.80	3.11
6	3096.9	335	75	4.90	20874	35.55	nd[c]	nd	36417	0.20	53.8	0.93	11.7	1.32	4.57	nd
7	4944.6	330	75	5.05	21309	44.70	nd[c]	58325	36069	5.02	9.12	3.75	14.6	0.86	4.63	3.04

[a]All concentrations in ppm; nd, not determined.

[b]*In situ* pH calculated using The Geochemist Workbench by reacting degassed fluid chemistry from 25 to 75°C and then titrating in the CO_2 total less the dissolved HCO_3^{-} (~17 ppm).

[c]CO_2 injected after sample –04; HCO_3^{-} not determined on post injection samples - only total system CO_2; the pre-inject value of 17 ppm HCO_3^{-} is assumed; The water rock ratio at the start of the experiment was 118:1. We injected 15.4 grams of CO_2 with water: rock ratio at 77:1 after sample –04.

Appendix (4J)-: X-Ray powder diffraction analysis of Wallace sandstone powder

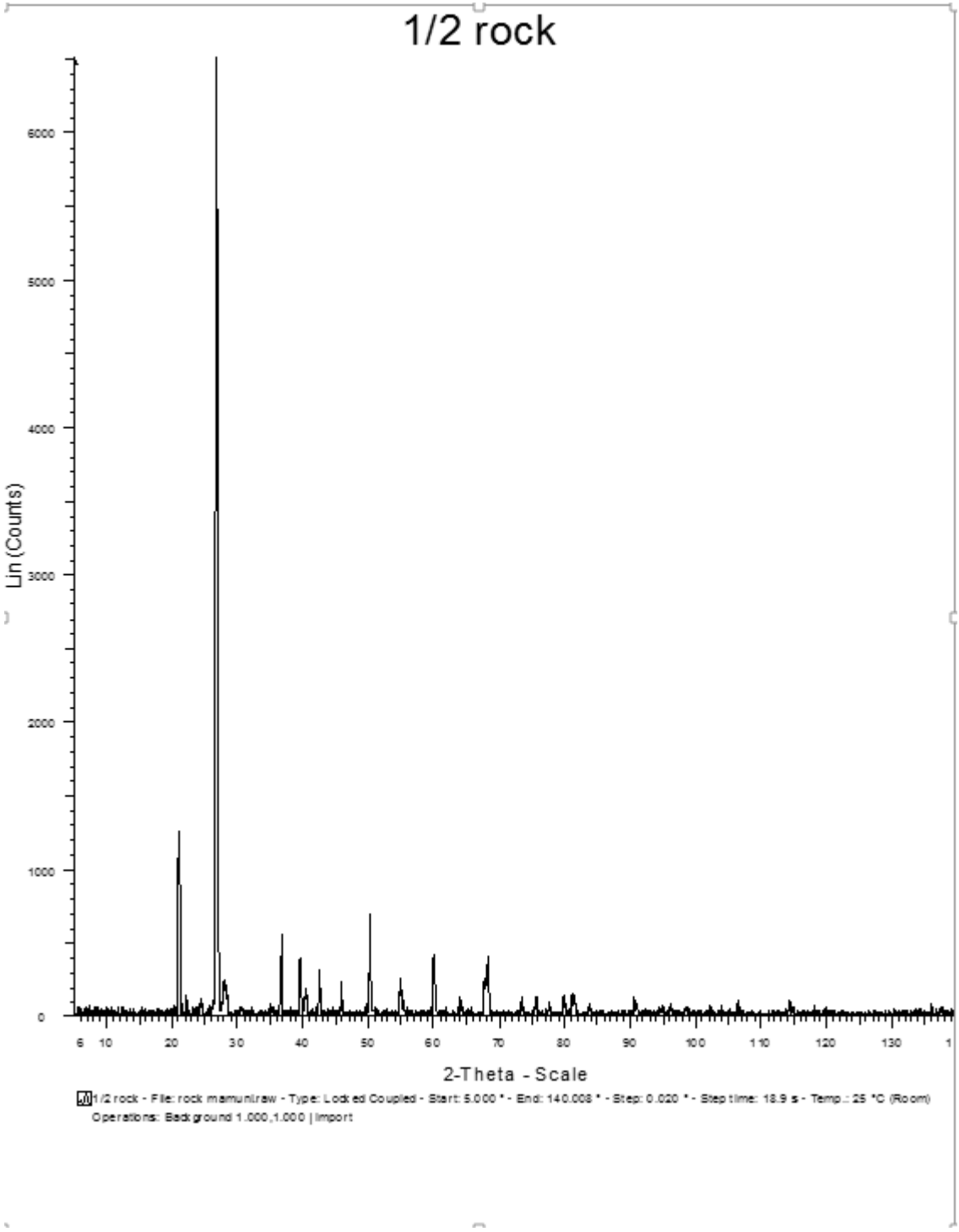

Appendix 4K: X-ray powder diffraction analysis of mica (Tomita *et al*., 1988)

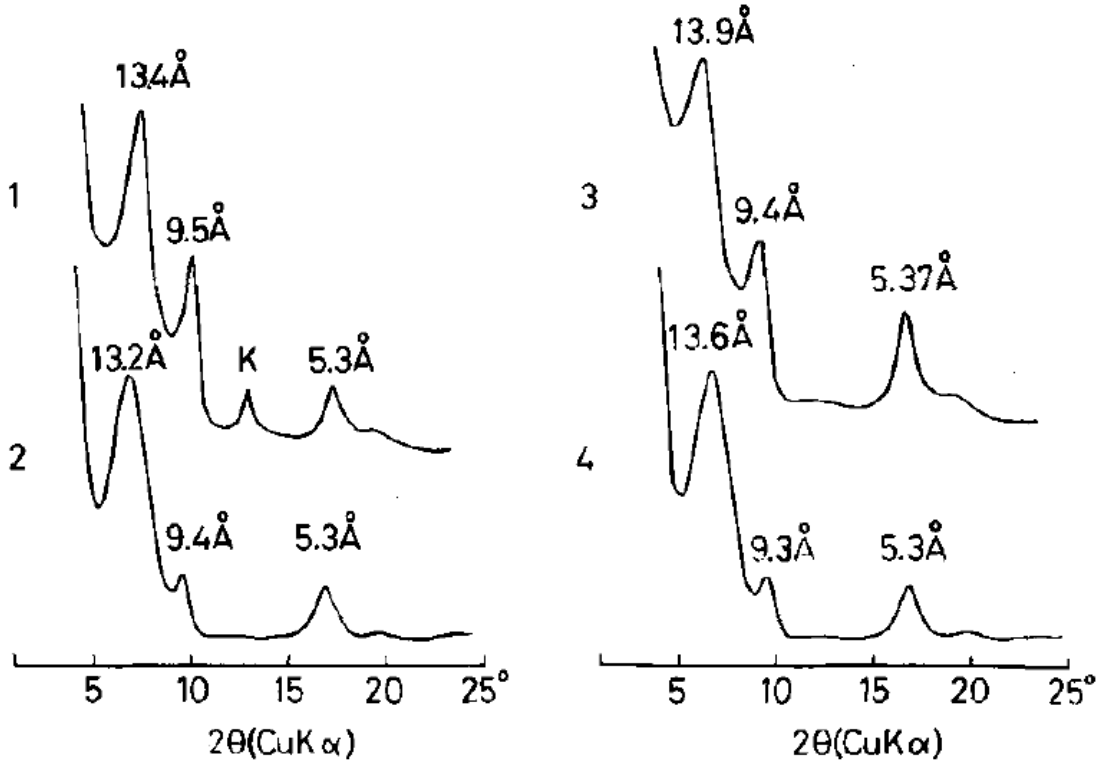

Appendix 4L: X-ray powder diffraction analysis of non-marine glauconite (Porrenga, 1968)

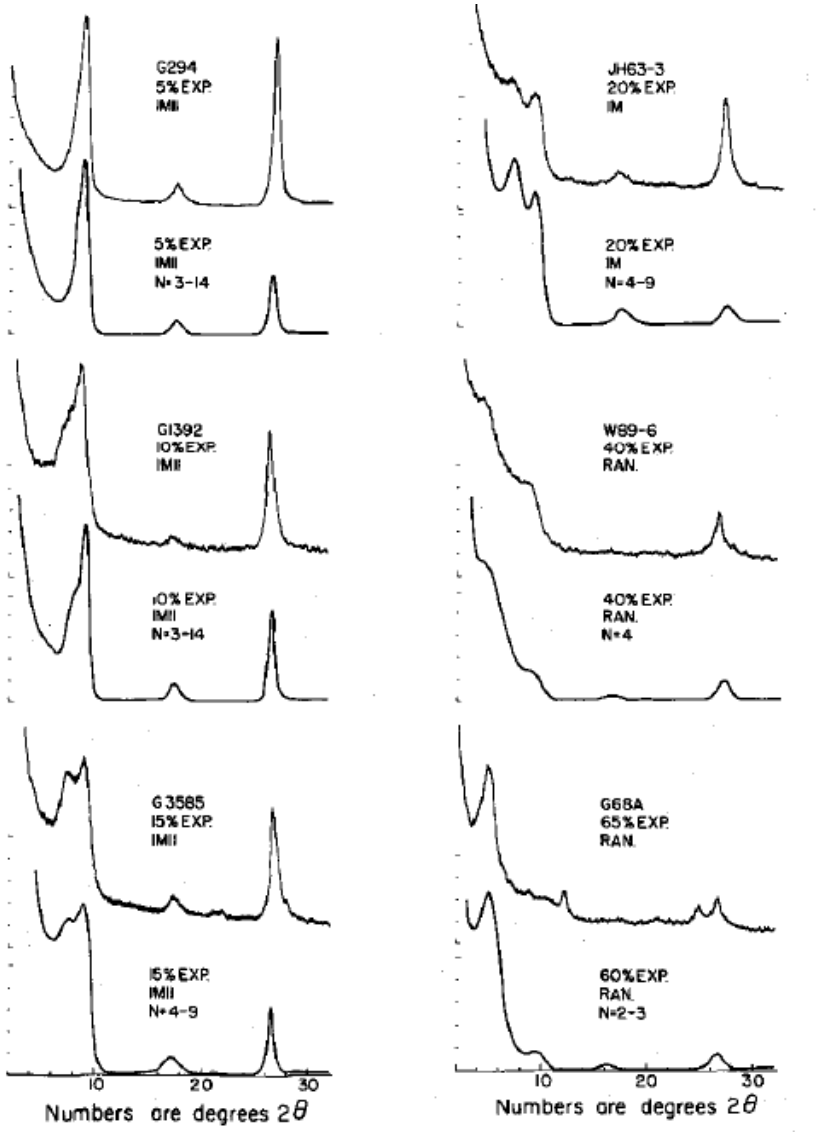

Appendix 4M: Surface tension increment for aqueous HCL against concentration

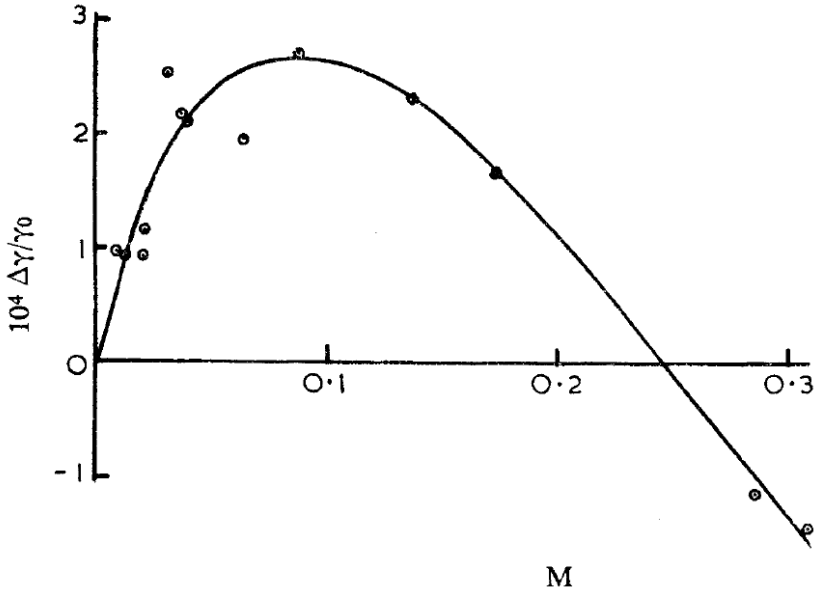

Ref: (Brandles & Schiffrin, 1966)

Appendix 4N: wettability pH parabolic relationship

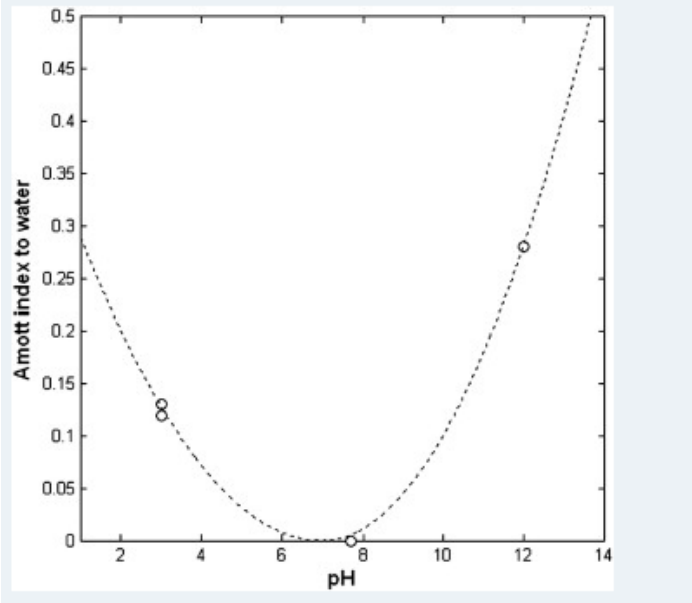

Ref: Takahashi and Anthony, 2010

Appendix 4O: Porosity and permeability of Wallace sandstone Core samples

Core	PV (cm^3)	φ (%)
W-4	10.54	12.2
W-5	10.54	12.2
W-6	11.12	12.9
W-7	11.9	13.7
W-22	11.12	12.9

Ref: Karim, 2013 MEng project report, Dalhousie University

Where k permeability, PV is pore volume, phi is porosity, Sm is specific surface area per unit mass

APPENDICES FOR CAPILLARY IMBIBITION EXPERIEMNTS

Appendix 4.3.1: Experiment 1

pH	Capillary rise	Capillary rise	Cos (theta)
	mm	m	
8.41	49	0.049	0.87
4.99	40	0.04	0.686
3.84	38	0.038	0.645
3.58	37	0.037	0.624
3.23	37	0.037	0.624
3.08	32	0.032	0.655
2.74	38	0.038	0.645
2.41	39	0.039	0.665

Appendix 4.3.2: Experiment 2

pH	capillary rise	capillary rise mm	cosine of contact angle
6.4	30	0.03	0.614178082
3.07	24	0.024	0.491342466
2.88	22.5	0.0225	0.460633562
2.58	23.5	0.0235	0.481106164
2.27	23	0.023	0.470869863
2.06	23	0.023	0.470869863
1.96	24	0.024	0.491342466
1.58	24.5	0.0245	0.501578767
1.461	25	0.025	0.511815068
1.17	26	0.026	0.532287671

Appendix 4.3.3: Experiment 3

pH	capillary rise mm	capillary rise m	cosine of contact angle
7.05	4	0.004	0.081890411
5.89	3.5	0.0035	0.07165411
3.95	2	0.002	0.040945205
3.39	1.5	0.0015	0.030708904
3.07	1.4	0.0014	0.028661644
1.09	2	0.002	0.040945205
0.87	2.5	0.0025	0.051181507

Appendix 4.3.3.1

pH	Cap rise-mm		
1.29	19	0.019	67.11
4.55	21	0.021	64.54
6.23	25	0.025	59.23
9.18	29	0.029	53.58
12	35	0.035	44.23

Appendix 4.3: Graph of contact angle versus pH from published work (Barranco Jr., Dawson, & Christener, 1997)

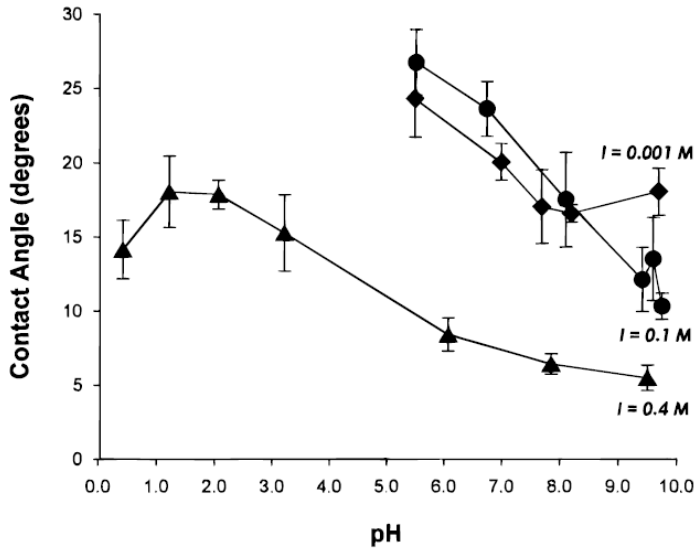

Appendix 4.4.1: Detailed calculations for equation validation

The wettability pH equations is given as:

$$cos(\theta) = cos(\theta)_o + \zeta[0.5pH^2 - pH_{PZC}pH + (pH_{PZC}pH_o - 0.5pH_o^2)] \quad (2\text{-}70)$$

Where:

$$\zeta = \frac{2.303}{F\gamma_{LV}}\left(\frac{2\pi}{\epsilon n k_B T}\right)^{-0.5} \quad (2\text{-}71)$$

To see if the coefficients of the quadratic fits of experiment 1 and experiment can be obtained using parameters of Table 4-1. The following procedure was followed.

- Calculation of the parameter defined by Eq. (2-71)
- Substitution of initial pH of experimental brine for each experiment into E. (2-70)
- Substitution of average value of the point of zero charge pH of borosilicate glass (3.1) deduced in this study
- Multiplication through by the value of the parameter defined by Eq. (2-71)

- Comparison of the resulting coefficients with those of quadratic fit

The following parameters were used for the calculation of the coefficient of Eq. (2-70)

R=8300 J/K
kB=3.8*10^-27
T=273
F=96485 C/mol
F=96485 C/mol
From brine salinity permittivity is =75.45
interfacial tension = 0.070 N/m
ni =Na and Cl
zi=1for Na and Cl

The value of the parameter is calculated as: 0.01180758

For experiment 1 the initial pH is 8.41

The coefficient of the square of pH^2 is given by= 0.5*0.01180758

This gives: 0.00708455

The third term is calculated as: -9.29305

The product of this and the coefficient of the quadratic equation gives: -0.10972843

The wettability at the point of zero charge pH is: 0.624

Addition of this to the previous figure (-0.10973) gives: 0.51427

Experiments 2

The coefficient of the square of pH^2 is given by= 0.5*0.01180758

This gives: 0.00708455

From the plot the average value of the square of pH^2 is = (0.0108+0.0081)/2 = 0.01015

From the plots the average value of point of zero charge pH is: 3.1

The product of 0.01180758 and 3.1 gives: 0.0366035

The average of the coefficient of pH gives: 0.05365

The wettability ant the point of zero charge pH is: 0.35

The initial pH of the solution is: 6.4

The third term of the equation on the RHS is calculated as:-0.64

The product of the coefficient and this value gives: -0.03434

The addition of the wettability value at the point of zero charge pH to this value gives: 0.315664

For experiment 1(Figure 4-12) substitutions of coefficients gives the quadratic equation as:

$$y = 0.010x^2 - 0.04x + 0.32 \tag{4-1}$$

From the parabolic fit to experimental data (Figure 4-12) the experimental equation gives:

$$y = 0.0088x^2 - 0.0581x + 0.87012 \tag{4-2}$$

The coefficients of these equations are appreciably closer

For Figure 4-13, substitution of coefficients gives the quadratic equation as

$$y = 0.010x^2 - 0.04x + 0.51 \tag{4-3}$$

Parabolic fit to experimental data gives:

$$y = 0.0137x^2 - 0.086x + 0.6057 \tag{4-4}$$

The coefficients of these equations are appreciably closer

Appendix 4.4.2 (iso): Determination of isoelectric point from polynomial plots

(Trevino *et al*., 2010)

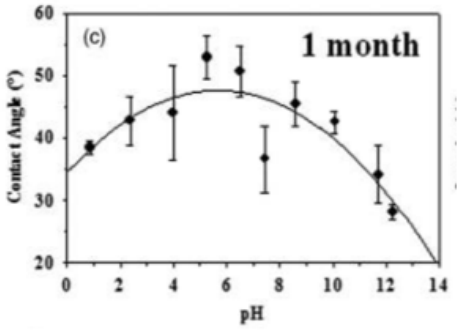

Trevino *et al*., (2010)

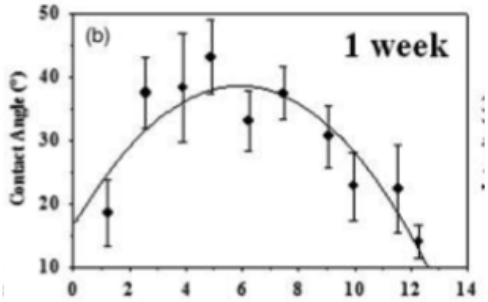

(McCafferty and Wightman, 1997)

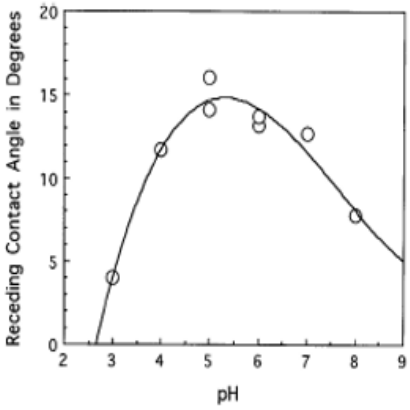

(McCafferty and Wightman, 1997)

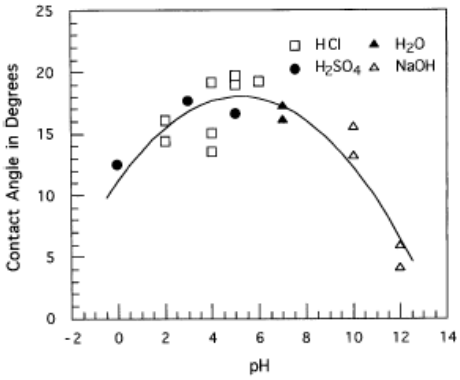

Appendix 4.5 Zeta potential of borosilicate glass versus pH (Barz *et al.*, 2009)

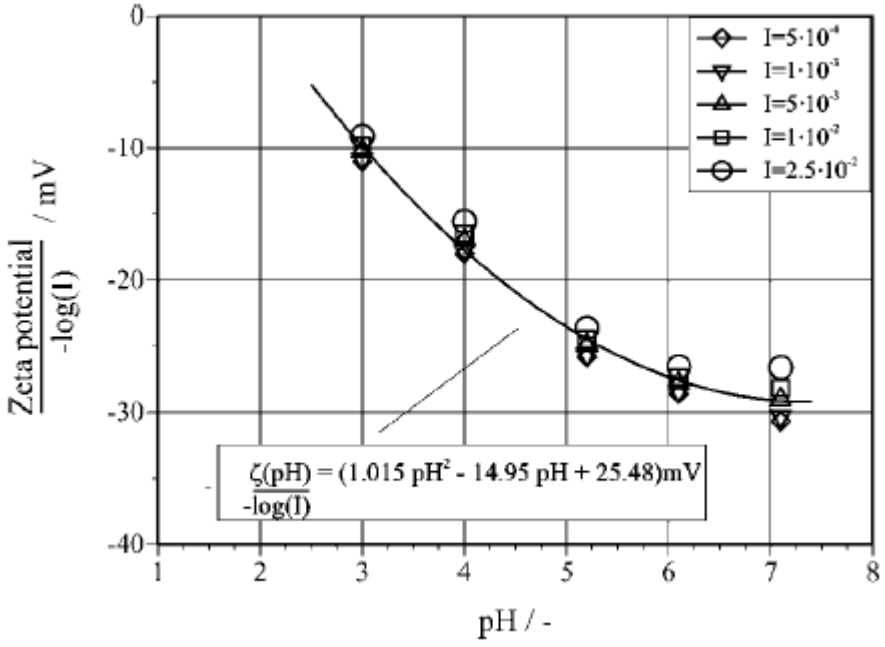

Appendix 4-6: Point of zero charge pH a mixture of silica and alumina mixture (Reymond & Kolenda, 1999)

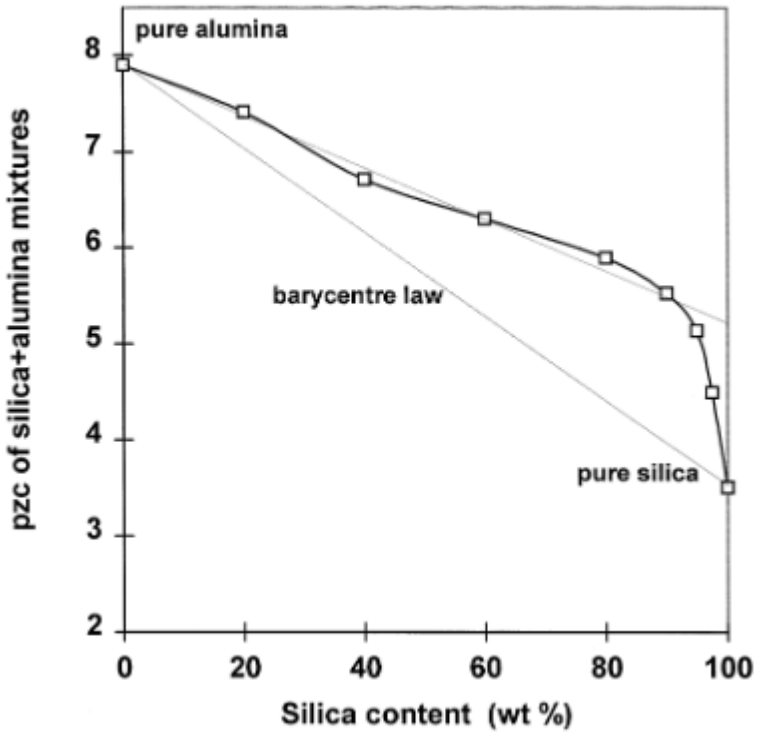

Appendix4-7: Point of zero charge pH of silica as function of magnetite impurity Shen *et al*., (1999)

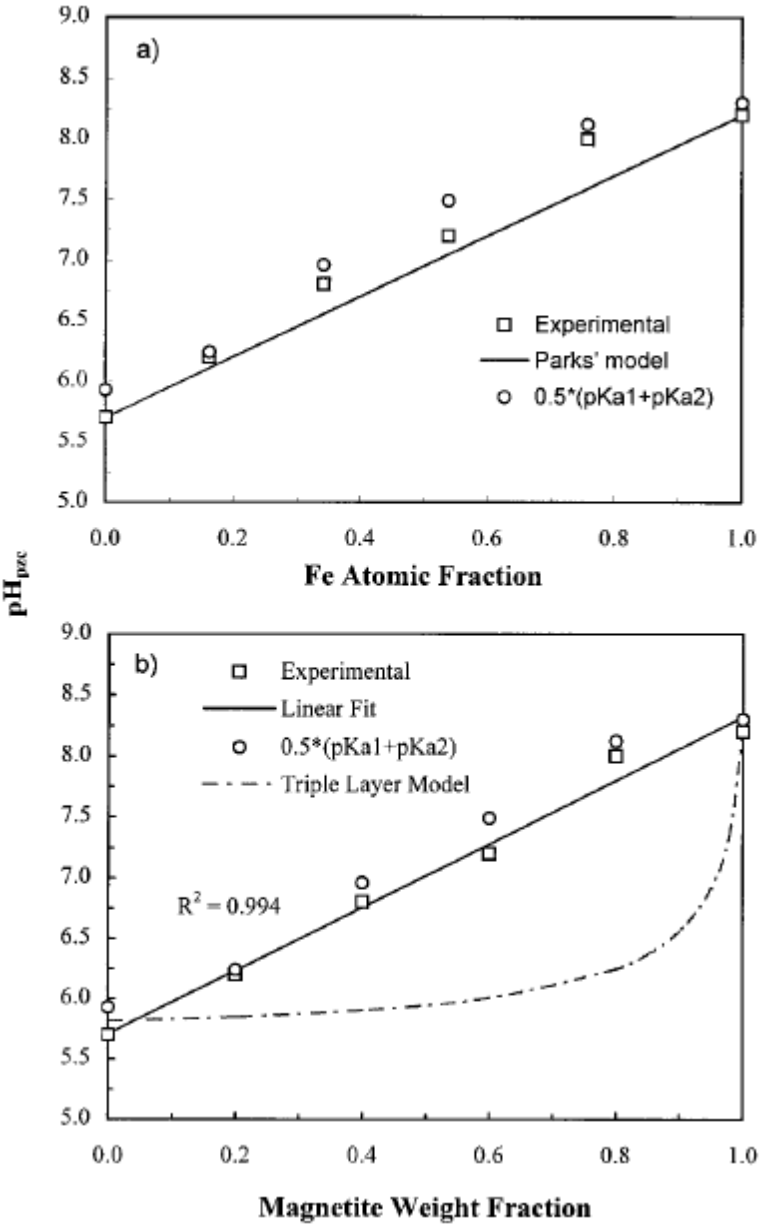

APPENDICES FOR SPONTANEOUS IMBIBITION

Synthetic Brine Experiment with Wallace Sandstone

Appendix 4.4.1.1: Experimental data for imbibition for pH 1.79 (Wallace sandstone)

time-min	time - sec	height-mm	height-m
1	60	1.5	0.0015
3	180	3.5	0.0035
6	360	4	0.004
10	600	7	0.007
15	900	8	0.008
34	2040	10	0.01
60	3600	13	0.013
80	4800	15	0.015
103	6180	16	0.016
141	8460	18	0.018
194	11640	23	0.023
240	14400	25	0.025
260	15600	27	0.027
287	17220	28	0.028
350	21000	30	0.03
390	23400	32.5	0.0325
420	25200	34	0.034
507	30420	37	0.037

Appendix 4.4.1.2: Experimental data for imbibition rise for pH 3.03 9Wallace sandstone

time mm	height mm	height m	time – sec	h sq
9	4.5	0.0045	540	2E-05
15	6	0.006	900	3.6E-05
21	8.5	0.0085	1260	7.2E-05
30	8.5	0.0085	1800	7.2E-05
45	10	0.01	2700	0.0001
60	10.5	0.0105	3600	0.00011
92	14	0.014	5520	0.0002
120	15	0.015	7200	0.00023
150	17.5	0.0175	9000	0.00031
170	19	0.019	10200	0.00036
190	20	0.02	11400	0.0004
213	21	0.021	12780	0.00044
270	23	0.023	16200	0.00053
305	24	0.024	18300	0.00058
347	26	0.026	20820	0.00068
423	28.5	0.0285	25380	0.00081
472	31	0.031	28320	0.00096
1273	50	0.05	76380	0.0025

Appendix 4.4.1.3: Experimental data for imbibition rise for pH 5.11 (Wallace sandstone)

time-min	height-mm	Height m	time sec	height sq-m2
1	0.5	0.0005	60	0.00000025
3	1	0.001	180	0.000001
9	2	0.002	540	0.000004
25	7.5	0.0075	1500	0.00005625
60	10	0.01	3600	0.0001
80	10.5	0.0105	4800	0.00011025
100	11.5	0.0115	6000	0.00013225
126	12	0.012	7560	0.000144
150	14	0.014	9000	0.000196
190	15	0.015	11400	0.000225
220	15.5	0.0155	13200	0.00024025
360	20	0.02	21600	0.0004
403	21	0.021	24180	0.000441
441	22	0.022	26460	0.000484
496	23.5	0.0235	29760	0.00055225
1288	41	0.041	77280	0.001681

Appendix 4.4.1.4: Experimental data for imbibition rise for pH 6.77 (Wallace sandstone)

time-min	height-mm	height-m	times-s	height sq-m2
9	5	0.005	540	0.000025
13	9	0.009	780	0.000081
27	10	0.01	1620	0.0001
52	11	0.011	3120	0.000121
100	13	0.013	6000	0.000169
126	16	0.016	7560	0.000256
210	21	0.021	12600	0.000441
273	27.5	0.0275	16380	0.00075625
346	30	0.03	20760	0.0009
432	32	0.032	25920	0.001024
493	35	0.035	29580	0.001225
521	36.5	0.0365	31260	0.00133225
1040	55	0.055	62400	0.003025
1182	57	0.057	70920	0.003249
1300	60	0.06	78000	0.0036

Appendix 4.4.1.5: Experimental data for imbibition rise for pH 9.77 (Wallace sandstone)

time-min	height-mm	height m	time sec	height sq
1	0.5	0.0005	60	2.5E-07
3	1	0.001	180	1E-06
9	2	0.002	540	4E-06
25	7.5	0.0075	1500	5.6E-05
60	10	0.01	3600	0.0001
80	10.5	0.0105	4800	0.00011
100	11.5	0.0115	6000	0.00013
126	12	0.012	7560	0.00014
150	14	0.014	9000	0.0002
190	15	0.015	11400	0.00023
220	15.5	0.0155	13200	0.00024
360	20	0.02	21600	0.0004
403	21	0.021	24180	0.00044
441	22	0.022	26460	0.00048
496	23.5	0.0235	29760	0.00055
1288	41	0.041	77280	0.00168

Appendix 4.4.1.6: Wallace sandstone experiments results with tap water

pH =1.97

Tine-s,	Height sq-m^2
540	0.000025
780	0.000081
1620	0.0001
3120	0.000121
6000	0.000169
7560	0.000256
12600	0.000441
16380	0.000756
20760	0.0009
25920	0.001024
29580	0.001225
31260	0.001332
62400	0.003025
70920	0.003249
78000	0.0036

pH =3.02

Time-s	Ht. sq. m^2
540	2.00E-05
780	4.00E-05
1260	7.00E-05
1620	8.00E-05
5400	0.0003
7560	0.0004
12600	0.0007
16380	0.001
21120	0.0013
25200	0.0014
31260	0.0018

pH=7.66

Time-s	Ht. sq. m^2
540	0.000009
780	0.000016
1260	0.000025
1620	0.000036
4800	0.000081
7560	0.000196
12600	0.000324
16380	0.0004
20760	0.000506

APPENDICES FOR FONTAINEBLEAU SANDSTONE EXPERIMENTS

Appendix 4.4.1 for pH 5.34

time-sec	Height-m	height sq-m^2
20	0.004	0.000016
48	0.005	0.000025
63	0.006	0.000036
100	0.007	0.000049
139	0.008	0.000064
90	0.008	0.000064
290	0.012	0.000144
375	0.014	0.000196
465	0.016	0.000256
540	0.02	0.0004
840	0.025	0.000625
1080	0.027	0.000729
1260	0.03	0.0009
1500	0.032	0.001024
1800	0.035	0.001225
2100	0.039	0.001521
2400	0.042	0.001764

Appendix 4.4.2 for pH 2.8

time-sec	height-m	height sq m
130	0.0035	0.00001225
180	0.005	0.000025
268	0.007	0.000049
300	0.009	0.000081
348	0.01	0.0001
410	0.011	0.000121
535	0.012	0.000144
798	0.015	0.000225
1000	0.016	0.000256
1650	0.02	0.0004
1846	0.0215	0.00046225
2658	0.024	0.000576
3300	0.026	0.000676
3600	0.027	0.000729

Appendix 4.4.2a: Baseline experimental data for Wallace sandstone experiments using tap water

time-s	height-m	height squared-m^2
50	0.003	0.000009
200	0.006	0.000039
260	0.007	0.000049
344	0.008	0.000064
456	0.009	0.000081

Appendix 4.4.2b. Appendix for baseline experiments with Wallace sandstone core sample using kerosene

time-s	heigh-mm	height-m	height squared-m^2
8	1	0.001	0.000001
16	1.5	0.0015	0.00000225
39	2.5	0.0025	0.00000625
70	4	0.004	0.000016
280	5.5	0.0055	0.00003025
207	7	0.007	0.000049
312	8	0.008	0.000064
465	9.5	0.0095	0.00009025
640	12	0.012	0.000144
860	13	0.013	0.000169

APPENDICES FOR SAND PACK EXPERIMENTS

Appendix 4.7.1 for pH 6.95

time -s	height-mm	height sq-m2
8	36	0.001296
13	45	0.002025
31	63	0.003969
70	68.4	0.00467856
111	81	0.006561
220	90	0.0081

Appendix 4.7.2 for pH 4.56

time-sec	height-mm	height sq-m2
6	40	0.0016
16	60	0.0036
35	80	0.0064
60	90	0.0081
97	100	0.01

Appendix 4.7.3 for pH 3.34

time-sec	height-mm	height sq-m2
7	54	0.002916
19	90	0.0081
26	108	0.011664
60	135	0.018225
131	180	0.0324
170	189	0.035721

Appendix 4.7.4 for pH 1.96

time sec	height-mm	height sq-m2
9	36	0.001296
16	45	0.002025
25	54	0.002916
40	63	0.003969
50	72	0.005184
135	90	0.0081
187	95.4	0.00910116

APPENDICES FOR CATION EXCHNAGE REACTIONS

Appendix 4.6.1: Experiment for initial pH 5.37 (Wallace sandstone) 10 gm in 100 cc

initial hydrogen ion concentration: 0.0000043 mol/l

Time minutes	pH	Hydrogen ion concentration at time t	log of adsorbed hydrogen ion concentration
0	6.14	7.24436E-07	-5.446655439
1	6.4	3.98107E-07	-5.408724663
3	6.49	3.23594E-07	-5.400509242
4	6.58	2.63027E-07	-5.393944134
5	6.64	2.29087E-07	-5.390308154
6	6.68	2.0893E-07	-5.388163048
7	6.71	1.94984E-07	-5.386685194
8	6.74	1.8197E-07	-5.385310503
9	6.76	1.7378E-07	-5.384447629
10	6.78	1.65959E-07	-5.383625188
11	6.79	1.62181E-07	-5.383228512
12	6.82	1.51356E-07	-5.382093844
13	6.83	1.47911E-07	-5.381733329
14	6.84	1.44544E-07	-5.381381309
15	6.86	1.38038E-07	-5.380701934
16	6.86	1.38038E-07	-5.380701934
17	6.87	1.34896E-07	-5.38037418
18	6.88	1.31826E-07	-5.380054126
19	6.89	1.28825E-07	-5.379741584
25	6.92	1.20226E-07	-5.378847246
27	6.93	1.1749E-07	-5.378562987
30	6.94	1.14815E-07	-5.378285377
57	6.89	1.28825E-07	-5.379741584
90	7.01	9.77237E-08	-5.376515398
107	7.03	9.33254E-08	-5.376061084

Appendix 4.6.2 for initial pH 5.37 for Fontainebleau sandstone
10 gm in 100 cc

initial hydrogen ion concentration: 0.0000042 mol/l

Time minutes	pH	Hydrogen ion concentration at time t	log of adsorbed hydrogen ion concentration
0	6.09	8.12831E-07	0.629408786
1	5.11	7.76247E-06	0.629401837
2	5.13	7.4131E-06	0.629402186
4	5.18	6.60693E-06	0.629402992
6	5.21	6.16595E-06	0.629403433
8	5.24	5.7544E-06	0.629403845
10	5.27	5.37032E-06	0.629404229
12	5.3	5.01187E-06	0.629404587
14	5.32	4.7863E-06	0.629404813
16	5.32	4.7863E-06	0.629404813
18	5.37	4.2658E-06	0.629405333
20	5.4	3.98107E-06	0.629405618
22	5.42	3.80189E-06	0.629405797
24	5.44	3.63078E-06	0.629405968
26	5.46	3.46737E-06	0.629406132
28	5.49	3.23594E-06	0.629406363
30	5.51	3.0903E-06	0.629406509
32	5.52	3.01995E-06	0.629406579
34	5.54	2.88403E-06	0.629406715
36	5.55	2.81838E-06	0.629406781
38	5.57	2.69153E-06	0.629406908
40	5.58	2.63027E-06	0.629406969
45	5.62	2.39883E-06	0.6294072
50	5.64	2.29087E-06	0.629407308
60	5.67	2.13796E-06	0.629407461
70	5.72	1.90546E-06	0.629407694
80	5.74	1.8197E-06	0.629407779

continuation

Time-minutes	pH	Hydroegn ion concentration at time t	Log of adsorbed hydrogen ion concentation
	5.77	1.69824E-06	0.629407901
127	5.83	1.47911E-06	0.62940812
242	6.15	7.07946E-07	0.629408891

Appendix 4.6.3 for an initial pH of 1.76 (Wallace sandstone)

10 gm in 100 cc, Initial pH: 6.9initial hydrogen ion concentration: 0.0173 mol/l

Time minutes	pH	Hydrogen ion concentration at time t	log of adsorbed hydrogen ion
0	2.1	0.007943282	concentration
1	2.24	0.005754399	-0.774624337
2	2.27	0.005370318	-0.773632738
3	2.3	0.005011872	-0.772709362
4	2.35	0.004466836	-0.771309069
5	2.4	0.003981072	-0.770064851
6	2.44	0.003630781	-0.769169835
7	2.5	0.003162278	-0.767975656
8	2.57	0.002691535	-0.766779067
9	2.6	0.002511886	-0.766323283
10	2.64	0.002290868	-0.765763194
11	2.69	0.002041738	-0.765132734
12	2.74	0.001819701	-0.764571606
13	2.78	0.001659587	-0.764167418
14	2.83	0.001479108	-0.763712274

Continuation

Time - minutes	pH	Hydrogen ion concentration at time t	Log of adsorbed hydrogen ion concentration
15	2.87	0.001348963	-0.763384358
16	2.91	0.001230269	-0.763085511
17	2.95	0.001122018	-0.762813139
18	2.99	0.001023293	-0.762564882
19	3.03	0.000933254	-0.762338592
20	3.06	0.000870964	-0.762182109
22	3.12	0.000758578	-0.761899921
23	3.15	0.000707946	-0.761772851
24	3.19	0.000645654	-0.761616569
25	3.22	0.00060256	-0.761508483
26	3.24	0.00057544	-0.761440478
27	3.26	0.000549541	-0.761375543
28	3.29	0.000512861	-0.761283596
29	3.29	0.000512861	-0.761283596
30	3.33	0.000467735	-0.761170502
35	3.39	0.00040738	-0.761019288
40	3.43	0.000371535	-0.760929506
50	3.49	0.000323594	-0.760809455
60	3.54	0.000288403	-0.760721355
75	3.57	0.000269153	-0.760673171

Appendix 4.6.4 for an initial pH of 1.78 for Fontainebleau sandstone
10 gm in 100 cc

Initial pH: 4.85

initial hydrogen ion concentration: 0.01659 mol/l

		Hydrogen ion	log of
Time	pH	concentration	adsorbed hydrogen
minutes		at time t	ion concentration
0	1.84	0.014454398	-2.670479622
1	1.86	0.013803843	-2.55499436
2	1.87	0.013489629	-2.50858631
3	1.88	0.013182567	-2.467572724
5	1.89	0.012882496	-2.430918315
6	1.9	0.012589254	-2.397859033
7	1.91	0.012302688	-2.367814881
9	1.92	0.012022644	-2.340335169
10	1.93	0.011748976	-2.315062724
13	1.94	0.011481536	-2.291709681
15	1.95	0.011220185	-2.270040639
18	1.96	0.010964782	-2.249860639
22	1.97	0.010715193	-2.2310064
26	1.98	0.010471285	-2.213339809
30	1.99	0.01023293	-2.196743001
32	2	0.01	-2.181114585
35	2.01	0.009772372	-2.166366713
41	2.02	0.009549926	-2.152422767
52	2.04	0.009120108	-2.1266857
79	2.08	0.008317638	-2.082370454

Appendix 4.6.5 for an initial pH of 1.75 for Wallace sandstone 2.2 gm in 100 cc

initial hydrogen ion concentration: 0.01778 mol/l

Time minutes	pH	Hydrogen ion concentration at time t	log of adsorbed hydrogen ion
0	1.85	0.014125375	-2.437157232
4	1.88	0.013182567	-2.337484628
8	1.91	0.012302688	-2.261432497
16	1.94	0.011481536	-2.200765363
20	1.95	0.011220185	-2.183108378
28	1.96	0.010964782	-2.166520245
38	1.97	0.010715193	-2.150899701
74	1.98	0.010471285	-2.136159001
100	1.98	0.010471285	-2.136159001
243	1.98	0.010471285	-2.136159001

Appendix 4.6.6 for an initial pH of 1.81 for Fontainebleau sandstone 2.2 gm in 100 cc

initial hydrogen ion concentration: 0.01549 mol/l

Time minutes	pH	hydrogen ion concentration at time t	log of adsorbed hydrogen ion concentration
60	1.9	0.012589254	-2.537789855
123	1.9	0.012589254	-2.537789855
212	1.91	0.012302688	-2.496847982
246	1.92	0.012022644	-2.460252187
396	1.93	0.011748976	-2.427241695

APPENDICES FOR REPEATED WALLACE SANDSTONE EXPERIMENTS

Appendix 4.8.5 for pH 3.5

time-s	ht-mm	ht-m	ht sq
60	2	0.002	0.000004
520	6	0.006	0.000036
1500		0.00906	0.000082
2000		0.0102	0.000104
2705	12	0.012	0.000144

Appendix 4.8.6 for pH 4.5

time-s	ht-mm	ht-m	ht sq-m2
60	1.5	0.0015	2.3E-06
518	5.5	0.0055	3E-05
1200	8	0.008	6.4E-05
1930	11	0.011	0.00012
2630	13	0.013	0.00017
3188	14	0.014	0.0002

Appendix 4.8.7 for pH 6.6

time sec	ht-mm	ht-m	ht sq-m2
60	2	0.002	4E-06
510	5	0.005	2.5E-05
1500		0.01072	0.00012
2000		0.01225	0.00015
3000		0.01449	0.00021
3580	16	0.016	0.00026

Appendix 4.9.1: Compsotion of shale and Slates (Erslev, 1998)

Rock types	Shales								Shales and slates		Slates		
Source	Clarke (1924)			NASC*									
	(1)	(2)	(3)	(4)	(5)	(6)	(7)	(8)	(9)	(10)	(11)	(12)	(13)
n	78	27	51	40	n/a	n/a	136	105	50	36	79	69	13
SiO_2 (wt%[n])	63.75	62.25	64.66	64.49	61.07	63.70	68.56	63.46	65.37	64.59	63.66	62.57	62.34
TiO_2	0.71	0.56	0.86	0.78	0.99	1.01	0.69	0.80	1.14	0.78	0.77	0.86	0.69
Al_2O_3	16.90	15.51	17.62	16.81	18.14	19.17	17.19	17.93	17.55	18.45	18.48	18.50	18.34
Fe_2O_3	7.39	6.63	7.73	6.24	8.15	7.32	5.70	7.75	7.95	6.73	8.26	8.45	7.97
MnO	0.00	0.00	0.00	0.06	0.13	0.11	0.05	0.09	0.04	N.D.	N.D.	0.11	0.17
MgO	2.68	3.03	2.47	2.84	2.68	2.23	2.20	2.83	2.86	2.77	2.64	2.78	3.12
CaO	3.40	6.74	1.50	3.60	4.16	1.32	1.42	1.53	0.13	1.64	1.32	1.39	1.57
Na_2O	1.43	2.02	1.07	1.13	1.09	1.22	1.25	1.63	0.39	1.27	1.39	1.28	1.68
K_2O	3.55	3.03	3.87	3.91	3.37	3.75	2.83	3.83	4.26	3.78	3.48	3.96	3.93
P_2O_5	0.19	0.22	0.21	0.14	0.22	0.16	0.16	0.15	0.31	N.D.	N.D.	0.11	0.20
Zr (ppm)	176	N.D.	N.D.	200	200	210	206	N.D.	199	N.D.	N.D.	N.D.	N.D.
Total	100.0	100.0	100.0	100.0	100.0	100.0	100.0	100.0	100.0	100.0	100.0	100.0	100.0

Appendix 4.9.2: Composition of carbonaceous slate (Wang & Wang, 1995)

Component	Concentration, %
SiO_2	64.31
Fe_2O_3	4.20
CaO	0.49
Al_2O_3	16.52
FeO	1.04
CO_2	0.26
K_2O	6.56
TiO_2	0.48
Na_2O	0.19

Appendix 4.9.3 Experiment for size range 300-335 micrometer pH 6.95

Time sec	Height mm	Height sq. m^2
13	35	0.001225
19	40	0.0016
38	45	0.002025
69	60	0.0036
90	65	0.004225
125	85	0.007225
150	90	0.0081

Appendix 4.9.4 Repeated experiments for pH 6.95 for size range 300-335 micrometer

Time sec	Height mm	Height sq. m^2
11	15	0.00023
25	25	0.00063
42	30	0.0009
60	34	0.00116

Appendix 4.9.5 Experiment for size range 300-335 micrometer pH 5.05

Time sec	Height mm	Height m^2
4	30	0.0009
9	34	0.00116
23	45	0.00203
36	53	0.00281
41	58	0.00336
50	65	0.00423
60	75	0.00563
78	80	0.0064
90	85	0.00723

Appendix 4.9.6 Repeated experiment for size range 300-335 micrometer for pH 5.05

Time sec	Height mm	Height m^2
3	30	0.0009
6	40	0.0016
15	60	0.0036
24	70	0.0049
34	85	0.00723

Appendix 4.9.7 Experiment for size range 106-163 micrometers
pH 6.95

Time sec	Height mm	Height sq. m^2
30	5	0.000025
43	10	0.0001
70	15	0.000225
90	18	0.000324
160	25	0.000625
200	27	0.000729
220	30	0.0009
300	35	0.001225
310	36	0.001296

Appendix 4.9.8 Repeated experiment for size range 106-163 micrometers
pH 6.95

Time sec	Height mm	Height sq. m^2
20	5	2.5E-05
33	10	0.0001
58	15	0.00023
80	20	0.0004
140	27	0.00073
157	30	0.0009

Appendix 4.9.9 Experiment for size range 106-163 micrometers pH 5.12

Time sec	Height mm	Height sq. m^2
6	5	0.000025
70	15	0.000225
90	18	0.000324
100	21	0.000441
124	23	0.000529
140	25	0.000625
160	27	0.000729
180	30	0.0009

Appendix 4.9.10 Repeated experiment for size range 106-163 micrometers pH 5.12

Time sec	Height mm	Height sq. m^2
11	5	0.000025
18	8	0.000064
27	10	0.0001
63	22	0.000484
76	24	0.000576
86	25	0.000625
95	26	0.000676
108	30	0.0009

Appendix 5-1: Relative permeability data for experiment at 55 °C

Sw	krw	krCO2	FW	SCO2	FCO2
0.992	0.94	0	0.94	0.008	0.06
0.947	0.637	0.016	0.473227	0.053	0.526773
0.899	0.38	0.057	0.123911	0.101	0.876089
0.865	0.235	0.103	0.033386	0.135	0.966614
0.801	0.059	0.222	0.001117	0.199	0.998883
0.791	0.041	0.247	0.000488	0.209	0.999512
0.759	0.007	0.327	1.09E-05	0.241	0.9999891
0.753	0.004	0.342	3.39E-06	0.247	0.99999661
0.751	0.003	0.349	1.87E-06	0.249	0.99999813
0.748	0.002	0.357	8.13E-07	0.252	0.99999919
0.745	0.001	0.364	1.99E-07	0.255	0.9999998

Appendix 5-2: Relative permeability data for experiment at 65 °C

Sw	krw	krCO2	Fractional flow of water	Sg	FCO2
0.997	0.98	0.002	0.953197	0.003	0.046803
0.991	0.94	0.007	0.852528	0.009	0.147472
0.953	0.703	0.04	0.394066	0.047	0.605934
0.907	0.458	0.079	0.13564	0.093	0.86436
0.854	0.245	0.124	0.030727	0.146	0.969273
0.837	0.189	0.139	0.016976	0.163	0.983024
0.802	0.098	0.168	0.003981	0.198	0.996019
0.773	0.045	0.193	0.000749	0.227	0.999251
0.752	0.02	0.21	0.000137	0.248	0.999863
0.723	0.002	0.235	1.23E-06	0.277	0.99999877
0.72	0.001	0.238	3.05E-07	0.28	0.9999997

Appendix 5-3: Relative permeability data for experiment at 75 C

Sw	krw	krCO2	Fractional flow of water	Sg	FCO2
0.988	0.96	0.001	0.946417	0.012	0.053583
0.903	0.703	0.025	0.471819	0.097	0.528181
0.855	0.574	0.046	0.272791	0.145	0.727209
0.801	0.444	0.076	0.132205	0.199	0.867795
0.752	0.343	0.108	0.064252	0.248	0.935748
0.704	0.255	0.146	0.028688	0.296	0.971312
0.656	0.18	0.19	0.01158	0.344	0.98842
0.553	0.064	0.305	0.00096	0.447	0.99904
0.451	0.007	0.452	7.86E-06	0.549	0.99999214
0.42	0.001	0.503	1.44E-07	0.58	0.99999986

APPENDICES FOR LITERATURE SOURCE DATA AND RESULTS OF COMPUTATIONS BASED ON CURRENT STUDY

Ellerslie sandstone

Appendix 5-4: Carbon dioxide brine data for Ellersely sandstone (Bennion & Bachu, Relative Permeability Characteristics for Supercritical CO2 Displacing Water in a Variety of Potential Sequestration Zones, 2005)

Sg	krg	krw	Sw	Se	Pc	krw/krg
0.034	0.0008	0.8052	0.966	0.945513	58617.58	1006.5
0.051	0.0018	0.7159	0.949	0.918269	59864.58	397.7222
0.068	0.0034	0.632	0.932	0.891026	61176.9	185.8824
0.085	0.0055	0.5535	0.915	0.863782	62560.09	100.6364
0.102	0.0082	0.4127	0.898	0.836538	64020.42	50.32927
0.119	0.0115	0.4127	0.881	0.809295	65564.92	35.88696
0.136	0.0153	0.4127	0.864	0.782051	67201.51	26.97386
0.153	0.0199	0.293	0.847	0.754808	68939.2	14.72362
0.17	0.025	0.2411	0.83	0.727564	70788.24	9.644
0.188	0.0309	0.1943	0.812	0.698718	72880.45	6.288026
0.205	0.0374	0.1528	0.795	0.671474	74997.57	4.085561
0.222	0.0446	0.1164	0.778	0.644231	77267.8	2.609865
0.239	0.0525	0.0851	0.761	0.616987	79709.41	1.620952
0.256	0.0612	0.0588	0.744	0.589744	82343.79	0.960784
0.273	0.0706	0.0375	0.727	0.5625	85196.19	0.531161
0.29	0.0807	0.0211	0.71	0.535256	88296.57	0.261462
0.307	0.0916	0.0095	0.693	0.508013	91680.85	0.103712
0.324	0.1032	0.0025	0.676	0.480769	95392.45	0.024225
0.341	0.1156	0	0.659	0.453526	99484.42	0

Ellerslie sandstone continued

FFC	Jsw	sigmacosthe	theta	logkrw	logSe	lamda
0.013995	0.21547	0.014764	0.454981	-0.0941	-0.024332578	2.30657
0.034673	0.230968	0.014066	0.433481	-0.14515	-0.037029968	2.174541
0.071369	0.242082	0.013715	0.422647	-0.19928	-0.050109798	2.04724
0.124308	0.250679	0.013544	0.41738	-0.25688	-0.063595824	1.924379
0.22109	0.257661	0.013485	0.415549	-0.38437	-0.077514087	1.021109
0.284731	0.263546	0.013502	0.416071	-0.38437	-0.091893212	1.690987
0.34624	0.268675	0.013574	0.418316	-0.38437	-0.106764768	3.33269
0.492452	0.273294	0.01369	0.421879	-0.53313	-0.122163683	1.466187
0.596986	0.277602	0.013839	0.426473	-0.6178	-0.138128737	1.358087
0.694366	0.282013	0.014025	0.43221	-0.71153	-0.1556981	1.273954
0.777611	0.286211	0.014221	0.438241	-0.81588	-0.172970567	1.164922
0.84553	0.290617	0.014429	0.444662	-0.93405	-0.190958537	1.05744
0.898096	0.295424	0.014643	0.451249	-1.07007	-0.20972386	0.951347
0.936983	0.300864	0.014853	0.457734	-1.23062	-0.229336771	0.845306
0.964152	0.307229	0.01505	0.463779	-1.42597	-0.249877473	0.738915
0.982027	0.314899	0.015217	0.468949	-1.67572	-0.271438123	0.630223
0.992792	0.324387	0.015338	0.47268	-2.02228	-0.294125327	0.516054
0.998307	0.336408	0.015389	0.474242	-2.60206	-0.318063335	0.38603
1	0.351977	0.015339	0.472709		sum	24.88598
	sum	0.272685	8.403232		ave	1.382554
	ave	0.013634	0.420162		1/lamda	0.723299
	costheta	0.420162				
	theta	65.17 deg	deg			

Cardium sandstone

Appendix 5-5: Carbon dioxide brine data for Cardium sandstone (Bennion & Bachu, 2006)

Sw	Sg	krg	krw	krg/krw	FFC	FFW
1	0	0	1	------	------	-----
0.969	0.031	0.0002	0.9715	4857.5	0.001784	0.998216
0.938	0.062	0.0008	0.7539	942.375	0.009127	0.990873
0.907	0.093	0.0019	0.6468	340.4211	0.024864	0.975136
0.876	0.124	0.0038	0.5499	144.7105	0.056588	0.943412
0.845	0.155	0.0068	0.4628	68.05882	0.113111	0.886889
0.814	0.186	0.011	0.3849	34.99091	0.198759	0.801241
0.783	0.217	0.0166	0.3159	19.03012	0.313243	0.686757
0.752	0.248	0.0239	0.2552	10.67782	0.448397	0.551603
0.72	0.28	0.0329	0.2025	6.155015	0.585102	0.414898
0.689	0.311	0.0438	0.1573	3.591324	0.70734	0.29266
0.658	0.342	0.0569	0.1191	2.093146	0.805707	0.194293
0.627	0.373	0.0723	0.0874	1.208852	0.877756	0.122244
0.596	0.404	0.0902	0.0616	0.682927	0.927061	0.072939
0.565	0.435	0.1107	0.0413	0.37308	0.95879	0.04121
0.534	0.466	0.134	0.0259	0.193284	0.978217	0.021783
0.503	0.497	0.1602	0.0148	0.092385	0.989469	0.010531
0.472	0.528	0.1896	0.0074	0.03903	0.995524	0.004476
0.401	0.599	0.2222	0.003	0.013501	0.998447	0.001553
0.41	0.59	0.2582	0.0008	0.003098	0.999643	0.000357
0.379	0.621	0.2978	0	0	1	0

Cardium sandstone continued

Se	logSe	logkrw	lamda	Pc	Jsw	costhe *sigma	costhe
1	0	0	----!	31800	0	-----	-----
0.950081	-0.02224	-0.01256	0.615719	33062.01	0.212177	0.007279509	0.367652
0.900161	-0.04568	-0.12269	0.777929	34446.39	0.238699	0.006741623	0.340486
0.850242	-0.07046	-0.18923	0.777926	35972.86	0.254313	0.006608104	0.333743
0.800322	-0.09674	-0.25972	0.777882	37665.69	0.265305	0.006632401	0.33497
0.750403	-0.12471	-0.33461	0.777801	39555.19	0.274007	0.006743913	0.340602
0.700483	-0.1546	-0.41465	0.777746	41679.73	0.281744	0.006911005	0.349041
0.650564	-0.18671	-0.50045	0.777663	44088.66	0.289565	0.007112985	0.359242
0.600644	-0.22138	-0.59312	0.777604	46846.59	0.298594	0.007329379	0.370171
0.549114	-0.26034	-0.69357	0.776867	50151.44	0.310806	0.007538148	0.380715
0.499195	-0.30173	-0.80327	0.776773	53919	0.327959	0.007680552	0.387907
0.449275	-0.34749	-0.92409	0.776631	58414.08	0.354814	0.007691089	0.388439
0.399356	-0.39864	-1.05849	0.776429	63884.2	0.400074	0.007459738	0.376754
0.349436	-0.45663	-1.21042	0.776208	70707.8	0.482497	0.006846098	0.345763
0.299517	-0.52358	-1.38405	0.775846	79496.3	0.647102	0.00573911	0.289854
0.249597	-0.60276	-1.5867	0.775299	91311.33	1.017933	0.004190601	0.211647
0.199678	-0.69967	-1.82974	0.774442	108187.3	2.008113	0.002516858	0.127114
0.149758	-0.82461	-2.13077	0.772884	134626.2	5.443887	0.001155291	0.058348
0.035427	-1.45067	-2.52288	0.724724	402657.2	1237.15	1.52049E-05	0.000768
0.049919	-1.30173	-3.09691	0.762314	310271.5	336.2901	4.31021E-05	0.002177

continuation

		ave	0.764668		Average of	0.005591301	
		1/lamda	1.307758		cos theta	0.282388914	
					theta	73.6	deg

Basal Cambrian sandstone

Appendix 5-6: Carbon dioxide-brine drainage data for Basal Cambrian sandstone (Bennion & Bachu, Relative Permeability Characteristics for Supercritical CO2 Displacing Water in a Variety of Potential Sequestration Zones, 2005)

krg	Sco2	Sw	krw	Se	logSe	logkrw)	lamda
0.0003	0.035	0.965	0.9105	0.950425	-0.02208	-0.04072	-1.73013826
0.00005	0.071	0.929	0.9105	0.899433	-0.04603	-0.04072	-0.94545785
0.0008	0.106	0.894	0.8248	0.849858	-0.07065	-0.08365	-1.10130152
0.0012	0.106	0.894	0.743	0.849858	-0.07065	-0.12901	-1.70353614
0.0019	0.141	0.859	0.665	0.800283	-0.09676	-0.17718	-1.71113108
0.0029	0.177	0.823	0.5911	0.749292	-0.12535	-0.22834	1.6972539
0.0047	0.212	0.788	0.5211	0.699717	-0.15508	-0.28308	-1.70270729
0.0076	0.247	0.753	0.4552	0.650142	-0.18699	-0.3418	-1.70630045
0.0123	0.282	0.718	0.3933	0.600567	-0.22144	-0.40528	-1.70968526
0.0194	0.318	0.682	0.3356	0.549575	-0.25997	-0.47418	-1.70060985
0.0299	0.353	0.647	0.2821	0.5	-0.30103	-0.5496	-1.70317338
0.0449	0.388	0.612	0.2328	0.450425	-0.34638	-0.63302	-1.70580731
0.0657	0.424	0.576	0.1879	0.399433	-0.39856	-0.72607	-1.69744915
0.094	0.459	0.541	0.1474	0.349858	-0.45611	-0.8315	-1.69929261
0.1315	0.494	0.506	0.1114	0.300283	-0.52247	-0.95311	-1.70104473

Continuation

krg	Sco2	Sw	krw	Se	logSe	logkrw)	lamda
0.1805	0.529	0.471	0.08	0.250708	-0.60083	-1.09691	-1.70307486
0.1805	0.565	0.435	0.0535	0.199717	-0.69959	-1.27165	-1.69163745
0.2433	0.6	0.4	0.0318	0.150142	-0.8235	-1.49757	-1.69283346
0.3228	0.635	0.365	0.0154	0.100567	-0.99755	-1.81248	-1.69052762
0.4221	0.671	0.329	0.0045	0.049575	-1.30474	-2.34679	-1.66481809
0.5554	0.706	0.294	0	7.86E-17	-16.1044	----	-----
						sum	-32.6577803
						ave	-1.63288901
						1/lamd	-0.61241149

continuation

Jsw	WF	costheta	krw/krg	FFG
0.211917	0.001406781	0.052083721	3035	0.003879
0.238979	0.001290296	0.047771058	18210	0.000649
0.254411	0.001254824	0.046457765	1031	0.011335
0.254411	0.001254824	0.046457765	619.1667	0.018733
0.265313	0.001248348	0.046217991	350	0.032668
0.274186	0.001257614	0.046561049	203.8276	0.054812
0.281861	0.00127571	0.047231032	110.8723	0.096339
0.289634	0.001298578	0.048077674	59.89474	0.16482
0.29861	0.001322194	0.048952001	31.97561	0.26989
0.310677	0.001341754	0.049676207	17.29897	0.405921
0.327622	0.001348145	0.049912818	9.434783	0.55611
0.354034	0.001329893	0.049237068	5.184855	0.695096
0.399982	0.001266935	0.046906146	2.85997	0.805179
0.481551	0.001141234	0.042252265	1.568085	0.882875
0.643516	0.000937714	0.034717304	0.847148	0.933122
1.00552	0.000670188	0.024812599	0.443213	0.963858
2.006835	0.000385934	0.014288571	0.296399	0.975537
5.393948	0.000170983	0.006330364	0.130703	0.989063
23.74332	4.96405E-05	0.001837855	0.047708	0.99598
345.2474	5.26317E-06	0.00019486	0.010661	0.999099
5.98E+58	3.46889E-53	1.2843E-51	---!	-----!
	sum	0.749976113		
	ave	0.035713148		
	theta	87.94	deg	

WF:= wetting force measured as the product of interfacial tenstion and cosine of contact.

It is the same as sigma cost theta

FFC= Fractional flow of carbon dioxide

Sigmacostheta = prodiuct of interfacial tension and contact angle

Lamda: exponent of the capillary pressure equation

Appendix 5-7: Maple work sheet for CO_2 molar density calculation

$$> f := x > \frac{328}{11.03}\cdot 0.008314472\cdot x - \frac{328\cdot 0.000846344}{11.03}\cdot x^2 - \frac{328\cdot 3\cdot 76587\cdot 10^{-6}}{11.03}\,x^4 - 1;$$

$$0.2472481248\,x - 0.02516779982\,x^2 - 6.832421396\,x^4 - 1 < x$$

$$solve(f(x) = 0, x);$$

$$RootOf\left(\left(0.2623242299\,x - 0.02670242176\,x^2 - 7.249032457\,x^4 - 1 < x\right)(\_Z)\right)$$

$$solve\left(\frac{328}{11.03}\cdot 0.008314472\cdot x - \frac{328\cdot 0.000846344}{11.03}\cdot x^2 - \frac{328\cdot 3\cdot 76587\cdot 10^{-6}}{11.03}\,x^4 - 1 = 0, x\right);$$

$$0.4366293840 + 0.4144480886\,I,\ -0.4366293840 + 0.4617432231\,I,\ -0.4366293840 - 0.4617432231\,I,\ 0.4366293840 - 0.4144480886\,I$$

$$> f := x > \frac{338}{11.03}\cdot 0.008314472\cdot x - \frac{338\cdot 0.000846344}{11.03}\cdot x^2 - \frac{338\cdot 3\cdot 76587\cdot 10^{-6}}{11.03}\,x^4 - 1;$$

$$0.2547861773\,x - 0.02593511079\,x^2 - 7.040726927\,x^4 - 1 < x$$

$$solve(f(x) = 0, x);$$

$$RootOf\left(\left(0.2547861773\,x - 0.02593511079\,x^2 - 7.040726927\,x^4 - 1 < x\right)(\_Z)\right)$$

continuation

$$solve\left(\frac{338}{11.03}\cdot 0.008314472\cdot x - \frac{338\cdot 0.000846344}{11.03}\cdot x^2 - \frac{338\cdot 3\cdot 76587\cdot 10^{-6}}{11.03}\,x^4 - 1 = 0, x\right);$$

$$0.4333622519 + 0.4108145973\,I,\ -0.4333622519 + 0.4588252758\,I,\ -0.4333622519 - 0.4588252758\,I,\ 0.4333622519 - 0.4108145973\,I$$

$$f := x > \frac{348}{11.03}\cdot 0.008314472\cdot x - \frac{348\cdot 0.000846344}{11.03}\cdot x^2 - \frac{348\cdot 3\cdot 76587\cdot 10^{-6}}{11.03}\,x^4 - 1;$$

$$0.2623242299\,x - 0.02670242176\,x^2 - 7.249032457\,x^4 - 1 < x$$

Continuation

$solve(f(x) = 0, x);$

$$RootOf\left(\left(0.2623242299\,x - 0.02670242176\,x^2 - 7.249032457\,x^4 - 1 < x\right)(\_Z)\right)$$

$$solve\left(\frac{348}{11.03}\cdot 0.008314472\cdot x - \frac{348\cdot 0.000846344}{11.03}\cdot x^2 - \frac{348\cdot 3\cdot 76587\cdot 10^{-6}}{11.03}\,x^4 - 1 = 0, x\right);$$

$$0.4302141875 + 0.4073048984\,I,\ -0.4302141875 + 0.4560206116\,I,\ -0.4302141875 - 0.4560206116\,I,\ 0.4302141875 - 0.4073048984\,I$$

Appendix 5-8 Virial Equation of state constants (virial eqn. of state for co2 density) (Ihmels & Gmehling, 2001)

Constants for Carbon dioxide	Value
a1	0.0006477
a2	0.32395218
a3	52.05474
a4	-794.87556
a5	-84.209265
a6	1.10*10^-6
a7	-0.00546645
a8	4.2676144
a9	-0.000000732
a10	0.00099511
a11	1.55*10^-7
a12	-0.00012445
a12	2.15*10^-6

Appendix 5-9 (Spycher *et al.*, 2003)

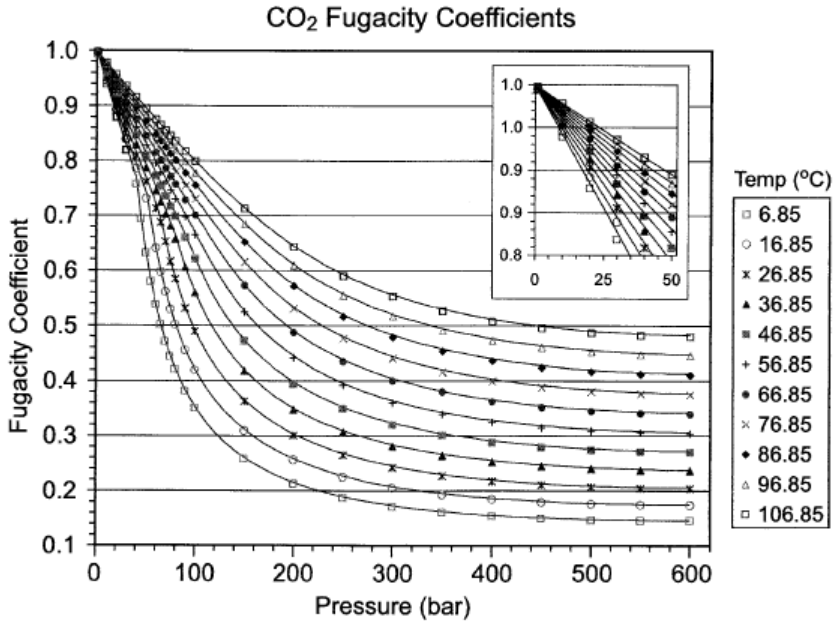

Appendix 5-10: Equivalent sodium chloride concentration correction chart (Al Bahlani & Babadagli, 2008)

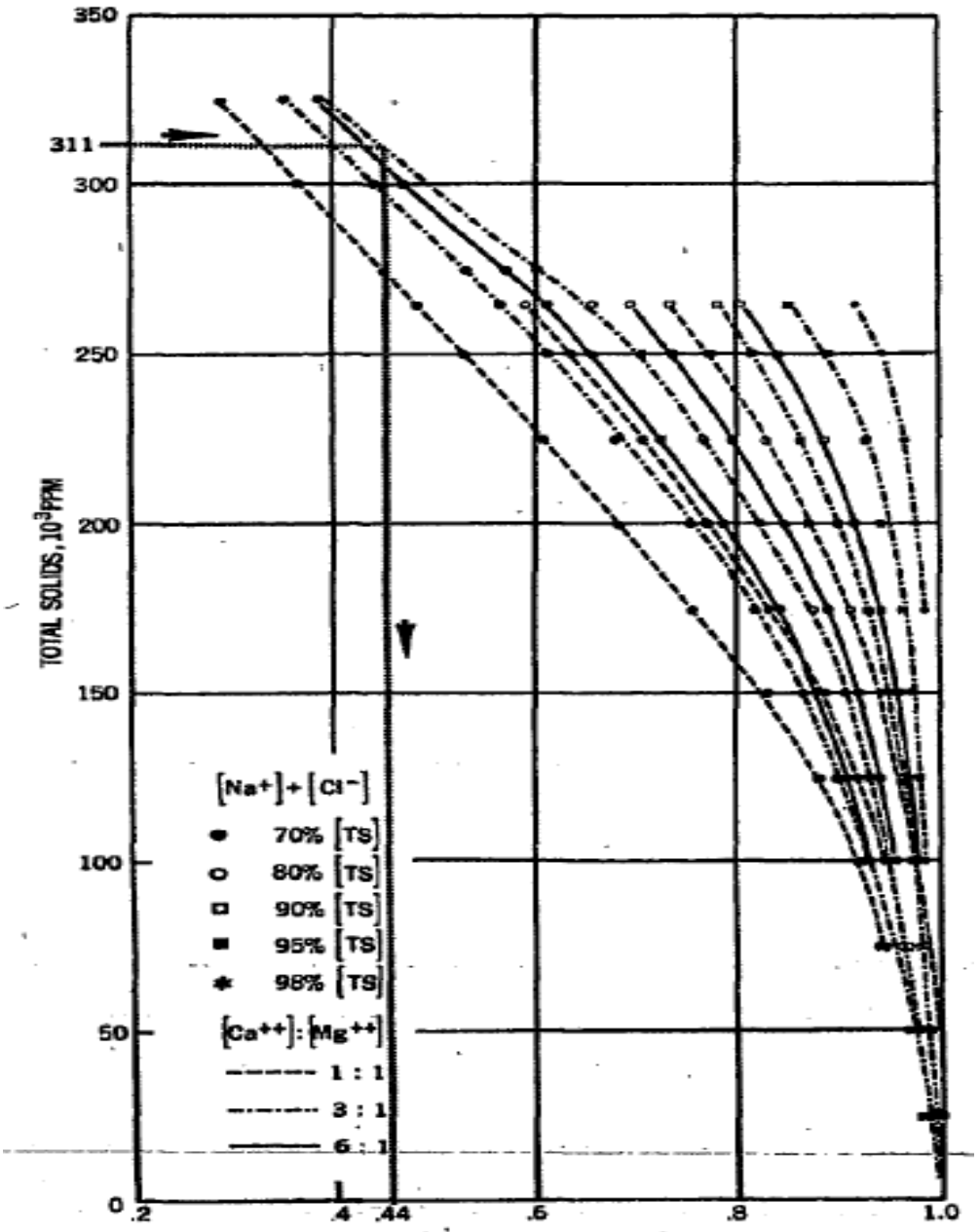

FIG. 2—CATION CORRECTION FACTOR FOR $(NaCl)_e$

Appendix 5-11: Literature sources for drainage experiments

	Relative permeability test	
	Data type	Reference
Cardium sandstone	Drainage	(Benion & Bachu, 2006)
Ellerslie sandstone	Drainage	(Bennion & Bachu, Relative Permeability Characteristics for Supercritical CO2 Displacing Water in a Variety of Potential Sequestration Zones, 2005)
Basal Cambrian sandstone	Drainage	(Bennion & Bachu, Relative Permeability Characteristics for Supercritical CO2 Displacing Water in a Variety of Potential Sequestration Zones, 2005)

Appendix 5-12: Literature sources of references for fluid and interfacial properties

	Data type			
	Brine/water viscosity ratio	tension-N/m	Temperature -C	Ref.
C S	8.68	19.8	43	Benion and Bachu, 2006
E S	14.52	32.5	40	Benion and Bachu, 2008
BCS	11.82	27	75	Benion and Bacu, 2008

CS: Cardium sandstone

ES: Ellersely sandstone

BCS: Basal Cambrian sandstone

Appendix 5-13: Wettability of oil-silica-water systems (Brown & . Newstadter, 1980)

Oil	θ°	Reference
Benzene	30	Present work
	0	
Toluene	20	
	0	
n-Nonane	0	
n-Heptane	22	
	0	
Toluene	35	(23) on standing, θ → 0°
Benzene	29	
Hexane	25	
Benzene	43	(24)

Appendix 5-14

The relationship between water relative permeability and effective saturation and pore size distribution index is give as (Oostrom & Lenhard, 1998):

$$k_{rw} = S_e^{\left(\frac{2+3\lambda}{\lambda}\right)} \qquad 1$$

In which k_{rw} is wetting phase relative permeability, S_e is effective saturation and λ is the pore size distribution index

Taking the logarithm of Eq. 1 and solving for the pore size distribution index gives:

$$\lambda = \frac{3\log S_e}{3\log S_e - \log k_{rw}} \qquad 2$$

Or

$$\lambda = \frac{2\log S_e}{\log k_{rw} - 3\log S_2}$$

Petrophysically, the pore size distribution index is a macroscopic porous medium parameter that depends on pore structure. It must therefore be the same for all data points. Eq. 2 is therefore used to calculate pore size distribution index for all relative permeabilities and effective saturations. The results are summed up and the average is calculated. The reciprocal of this parameter is then calculated.

The equation (3-21) for drainage capillary pressure is then used with the reciprocal of the pore size distribution index to calculate drainage capillary pressure. Information about breakthrough capillary pressure is taken from cited literature work.

In the case of Wallace sandstone the product of interfacial tension and cosine of contact angle is calculated using Eq. 3-20. In the case of Rock samples from literatures sources the contact angle is deduced by diving the product of the cosine of the contact angle and interfacial tension by interfacial tension Details calculations are found in appendices 5-4 to 5-6 extracts are found in Table 10 to Table 12 for literature source data and from Tables 5-7 to 5-9 for Wallace sandstone.

Extracted breakthrough capillary pressure data from the cited literatures sources were as follow:

Ellersely sandstone: 56300 Pa

Cardium sandstone: 31800 Pa

Basal Cambrian sandstone: 31900 Pa

Porosities were as follow:

Cardium sandstone: 15.3 %

Ellersely sandstone: 12.6%

Basal Cambrian sandstone: 11.7%

Brine saturated permeabilities were as follow:

Cardium sandstone: 0.356 mD

Ellersely: 0.376 mD

Basal Cambrian sandstone: 0.81 mD

$$J(S_w) = A\left(\frac{1}{S_e^{c_1}} - 1\right) + B\left(\frac{1}{S_e^{c_2}} - 1\right)^{1/c_2} \quad \text{(3-18a)}$$

In which

$$S_e = \frac{S_w - S_{iw}}{1 - S_{iw}} \quad \text{(3-18b)}$$

In which the following $A, B, c_1 c_2$ are fitting parameters, S_w is water saturation and S_{iw} irreducible water saturation

This equation is written with the curve fitting parameters as (Nam & Kaviany, 2003):

$$J(S_w) = 0.0038\left(\frac{1}{S^{c_1}} - 1\right) + 0.28\left(\frac{1}{S^{c_2}} - 1\right)^{1/c_2} \quad \text{.....(3-19)}$$

$$\sigma_{gl}\cos\theta = \frac{P_c}{\sqrt{\frac{\phi}{K}}J(S_w)} \quad (3\text{-}20)$$

The relationship between capillary pressure, breakthrough capillary pressure and effective saturation is given as (Kewen, 2004):

$$P_{dc} = P_b\left(\frac{S_w - Siw}{1 - S_{iw}}\right)^{-1/\lambda} \quad (3\text{-}21)$$

Appendix: 7-1: Point of Zero charge pH of minerals phases (Sverjensky, 1994)

PHASE	ε_k[a]	$s/r_{M\text{-}OH}$[b]	Exptl. pH_{zpc}[c]	Calc. pH_{pzc}
BeO	7.16	0.1890	10.2	9.5
CaO	11.95	0.0976		12.3
NiO	11.9	0.1077	9.85-11.3	11.8
CuO	18.1	0.1686	9.5	8.6
ZnO	8.49	0.1676	8.7-9.3	10.0
FeO(OH)	11.7	0.165	9.0-9.7	9.4
amorphous SiO_2	3.807	0.3818	3.5	3.9
β-MnO_2	10000	0.2301	4.6-7.3	4.8
SnO_2	9.0	0.2177	7.3	7.7
ZrO_2	22.0	0.1803		7.9
ThO_2	18.9	0.1456	9.0-9.3	9.6
UO_2	24.0	0.1480		9.2
$CaTiO_3$	165.0	0.1409		8.8
$MgAl_2O_4$	8.3	0.1703		9.9
$FeAl_2O_4$	40.0	0.1693		7.9
$ZrSiO_4$	11.5	0.1559		9.8
Zn_2SiO_4	12.99	0.2389	7.4	6.1
ANDALUSITE	6.9	0.2531	5.2-7.8	6.9
KYANITE	7.8	0.2402	5.2-7.9	7.1
SILLIMANITE	11.0	0.2736	5.6-6.8	4.9
FORSTERITE	7.26	0.1972	10.5	9.1
GROSSULAR	8.53	0.2113		8.1
ALMANDINE	4.3	0.2135		10.4

Appendix J Series (Graphical Approach to Error analysis)
Fontainebleau

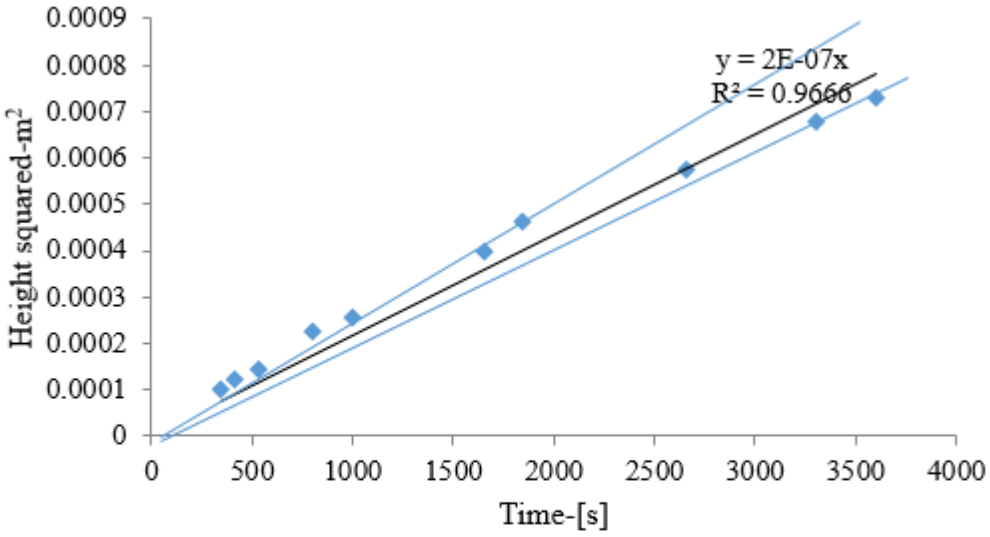

Figure 4-22: A plot of height rise squared versus time for early spontaneous imbibition dynamics for pH equal to 2.80 (from appendix 4.4.1) (Fontainebleau Sandstone)

Sand pack

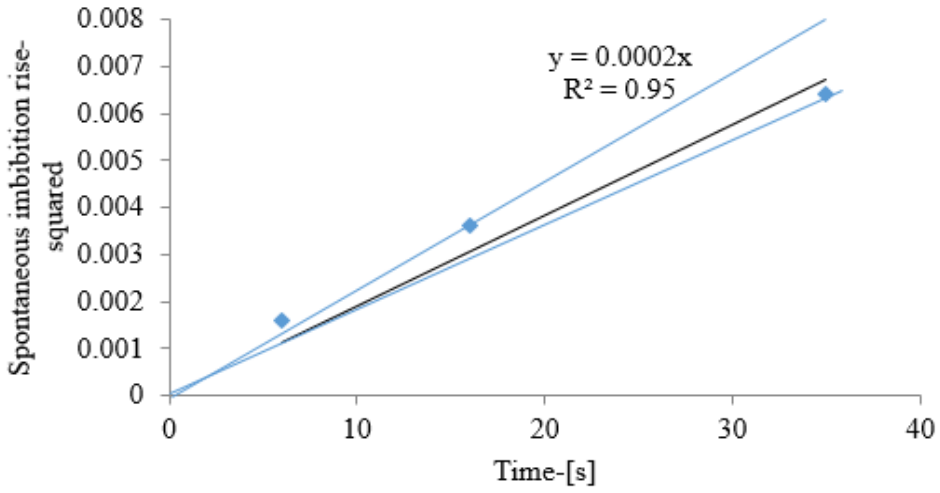

Figure 4-26: Spontaneous imbibition rise squared versus pH for pH equal to 4.56 plotted for the linear section of the data (from appendix 4.7.2)

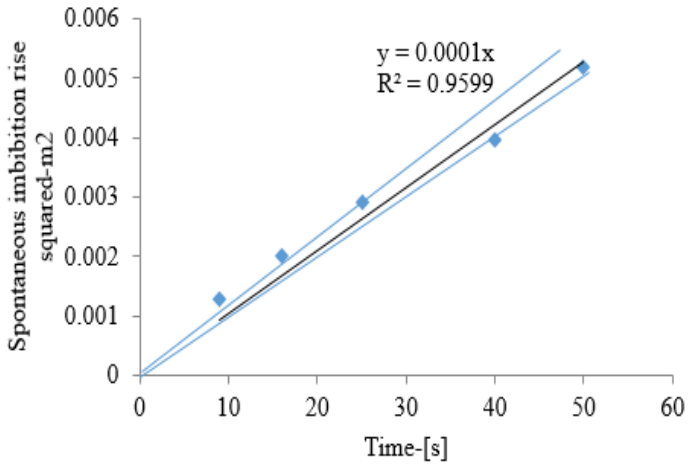

Figure 4-29: Spontaneous imbibition rise squared versus pH for pH equal to 1.96 (from appendix 4.7.4)

4.4.6 Error Analysis

Cap rock

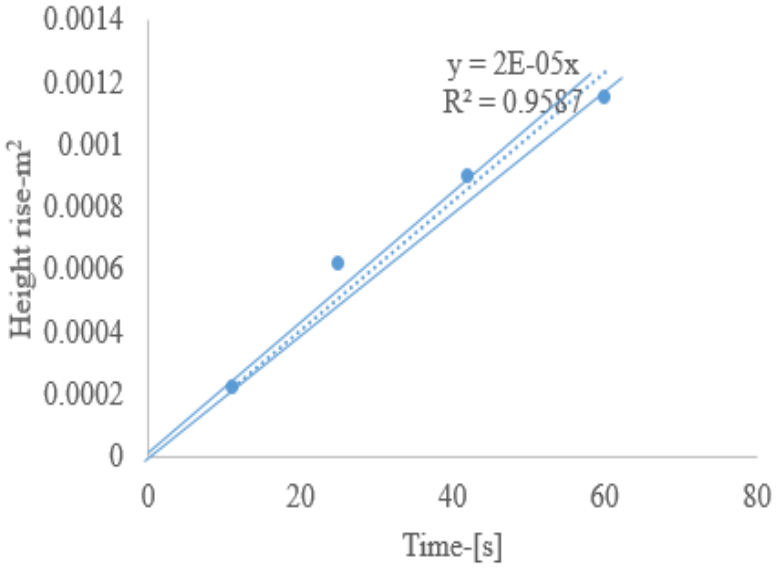

Figure 4.9.4: Experimental plot for pH equal to 6.95 repeated

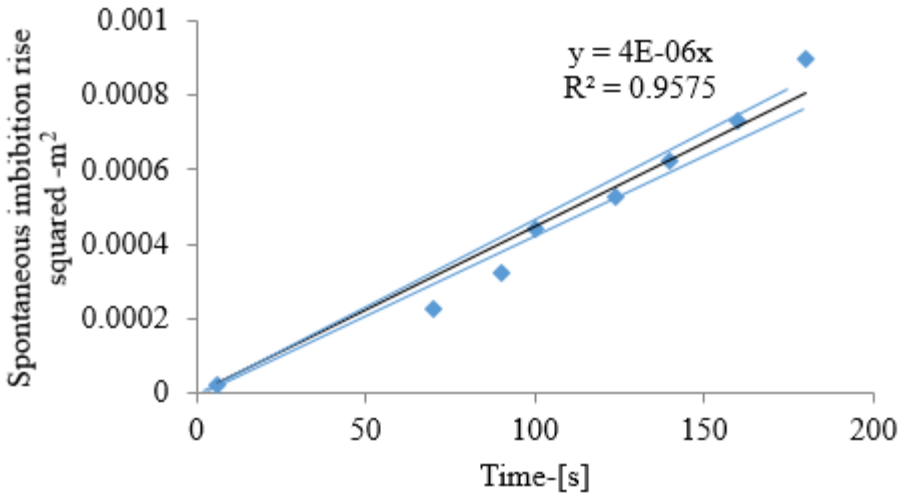

Figure 4.9.9: Experimental plot for pH equal to 5.12

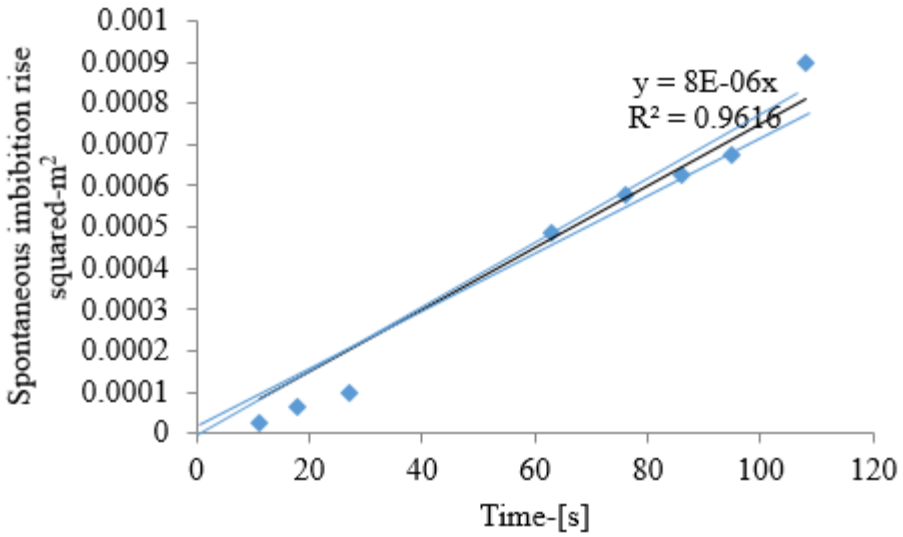

Figure 4.9.10: Experimental plot for pH equal to 5.12 repeated

Appendix K Series (Derivation of Relative Error)

Ref: http://www3.nd.edu/~amoukasi/CBE358_Lab1/Data_Error_analysis.pdf

All units except reactive errors are in m^2/s

Fontainebleau Sandstone

Figure 4-22

In this analysis excel was used to fit the best straight line

Gradient of bets fit line: $2*10^{-7}$

Minimum gradient of imposed straight line: 0.00043/2500 = 0.00000172

Maximum gradient of impose straight line: 0.0006/2500 = 0.00000024

Difference between bets fit line and minimum gradient: 0.0000008

Difference between bets fit line and maximum straight line gradient: -0.00000004

Summation of absolute differences: 0.000000068

Error: 0.000000068/2: 0.000000034

Relative error: 0.000000024/0.0000002 = 0.17

Sand Pack Porous Sample

Figure 4-26

Gradient of bets fit line: 0.0002

Minimum gradient of imposed straight line: 0.005/30 = 0.000167

Maximum gradient of impose straight line: 0.0063/300 = 0.00217

Difference between bets fit line and minimum gradient: $3.33*10^{-5}$

Difference between bets fit line and maximum straight line gradient: $-1.66*10^{-5}$

Summation of absolute differences: $4.99*10^{-5}$

Error: $4.99*10^{-5}/2 = 2.5*10^{-5}$

Relative error: $2.5*10^{-5}/0.0002 = 0.17$

Figure 4-29

Gradient of bets fit line: 0.0001

Minimum gradient of imposed straight line: 0.0038/40 = 0.000095

Maximum gradient of impose straight line: 0.0044/40 = 0.00011

Difference between bets fit line and minimum gradient: 0.000005

Difference between bets fit line and maximum straight line gradient: -0.00001

Summation of absolute differences: 0.000015

Error: 0.0000075/2 = 0.0000075

Relative error: 0.0000075/0.0001 = 0.08

Cap Rock Porous Samples

Figure 4.9.4

Gradient of bets fit line: 0.00002

Minimum gradient of imposed straight line: 0.000025

Maximum gradient of impose straight line: = 0.000213

Difference between bets fit line and minimum gradient: $1.6*10^{-6}$

Difference between bets fit line and maximum straight line gradient: -0.000195

Summation of absolute differences: 0.000195

Error: $1.96*10^{-6}$

Relative error: $1.96*10^{-6}/0.00002 = 0.098$

Figure 4.9.9

Gradient of bets fit line: $4*10^{-6}$

Minimum gradient of imposed straight line: $0.0006/150 = 3.866*10^{-6}$

Maximum gradient of impose straight line: $0.00065/150 = 4.33*10^{-6}$

Difference between bets fit line and minimum gradient: $1.33*10^{-7}$

Difference between bets fit line and maximum straight line gradient: $-3.33*10^{-7}$

Summation of absolute differences: $4.66*10^{-7}$

Error: $4.44*10^{-7}/2 = 2.33*10^{-7}$

Relative error: $2.33*10^{-7}/0.000004 = 0.06$

Figure 4.9.10

Gradient of bets fit line: $8*10^{-6}$

Minimum gradient of imposed straight line: 0.0006/100 = 0.0000062

Maximum gradient of impose straight line: 0.00075/100 = 0.0000084

Difference between bets fit line and minimum gradient: 0.0000018

Difference between bets fit line and maximum straight line gradient: -0.0000004

Summation of absolute differences: 0.0000022

Error: 0.0000022/2 = 0.0000011

Relative error: 0.0000011/0.000008 = 0.12